A High-Resolution Study of Local Calcium Signalling in Heart Muscle

Cherrie Hei Ting Kong

A thesis submitted in fulfilment of the requirements for the degree of Doctor of Philosophy

Department of Physiology
Faculty of Medical and Health Sciences
University of Auckland
2012

Declaration

I, Cherrie Hei Ting Kong, confirm that the work presented in this thesis is my own. Where information has been derived from other sources, I confirm that this has been indicated in the thesis.

Communications

Papers

Kong, CHT and Cannell, MB. Relationship between L-type Ca channel opening and activation of local SR Ca release. (*In preparation*)

Kong, CHT and Cannell, MB. Extraction of sub-microscopic Ca fluxes from blurred and noisy fluorescent indicator images with a detailed model fitting approach. (*In review*)

Cannell, MB and Kong, CHT. Local control in cardiac E-C coupling. *J Mol Cell Cardiol.* 2012;**52**(2):298-303.

Kong, CHT, Soeller, C and Cannell, MB. Increasing sensitivity of Ca^{2+} spark detection in noisy images by application of a matched-object detection algorithm. *Biophys J.* 2008;**95**(12):6016-24.

Presentations

Kong, CHT and Cannell. MB. EC coupling latency in rat ventricular myocytes. *Biophysical Society Annual Meeting*; Philadelphia, United States of America; Feb, 2013. (*Symposium pending*)

Kong, CHT and Cannell, MB. Latency of CICR during rat action potentials. *Physiology 2012*; Edinburgh, United Kingdom; Jul, 2012. (*Symposium*)

Kong, CHT and Cannell, MB. Looking at the trigger for CICR during rat cardiac action potentials. Biophysical Society Annual Meeting; San Francisco, United States of America; Feb, 2010. (*Poster*)

Kong, CHT and Cannell, MB. An improved calcium spark detector. Biophysical Society Annual Meeting; Long Beach, United States of America. Feb, 2008. (*Poster*)

Related papers and presentations

Laver, DR, Kong, CHT, Imtiaz, MS and Cannell, MB. Termination of calcium-induced calcium release: An emergent property of stochastic channel gating and molecular scale architecture. *J Mol Cell Cardiol. 2012 (Published online)*

Gadeberg, HC, Kong CHT, Cannell, MB and James, AF. Properties of Ca^{2+} transients in rabbit atrial myocytes. *Biophysical Society Annual Meeting*; Philadelphia, United States of America; Feb, 2013. (*Submitted*)

Gadeberg, HC, Kong CHT, Cannell, MB and James, AF. Wheat germ agglutinin staining of rabbit cardiac myocytes. *Physiology 2012*; Edinburgh, United Kingdom; Jul, 2012. (*Poster*)

Jayasinghe, ID, Baddeley, D, Kong, CHT, Wehrens, XH, Cannell, MB and Soeller, C. Nanoscale organization of junctophilin-2 and ryanodine receptors within peripheral couplings of rat ventricular cardiomyocytes. Biophys J. 2012;**102**(5):L19-21.

Kaur, S, Kong, CHT, Cannell MB and Ward, M-L. EPAC activation of cardiac muscle. Biophysical Society Annual Meeting; San Diego, United States of America, Feb, 2012. (*Poster*)

Laver, DR, Kong, CHT, Imtiaz, MS and Cannell, MB. SR calcium release channel mechanisms for cardiac arrhythmias and their drug-based therapy. Australian Physiological Society Meeting; Perth, Australia; Dec, 2011. (*Symposium*)

Kaur, S, Kong, CHT, Cannell, MB and Ward, M-L. The role of EPAC in excitation-contraction (E-C) coupling in cardiac muscle. Medical Sciences Congress; Queenstown, New Zealand; Dec, 2010. (*Poster*)

Ward, M-L, Kaur, S, Kong, CHT and Cannell, MB. The role of EPAC during cAMP-dependent activation of isolated rat ventricular muscle. World Congress of the International Society for Heart Research (ISHR); Kyoto, Japan; May, 2010. (*Poster*)

Abstract

Ca^{2+}-induced Ca^{2+} release (CICR) is fundamental to cardiac function. Ca^{2+} sparks reflect microscopic CICR originating in clusters of Ca^{2+} release units (CRU) located at junctions of the SR and surface membrane (JSR). Approximately 10^4 Ca^{2+} sparks evoked by an action potential (AP) give rise to the cell-wide increased in Ca^{2+} that activates contraction. However, the ability of surface membrane Ca^{2+} channels (LTCCs), which are activated during the AP, to trigger Ca^{2+} sparks remains an area of uncertainty. A second area of uncertainty resides in our understanding of the mechanism that terminates regenerative CICR.

This study examined the activation and termination of Ca^{2+} sparks and hence, gating properties of the CRU. Using voltage-clamp to control the activation of LTCCs and high resolution Ca^{2+} spark recording, the voltage-dependence of Ca^{2+} spark latency was investigated to probe the underlying relationship between LTCC gating and CICR. The results show that latency had a complex voltage-dependence due to the interaction of LTCC gating and LTCC unitary current leading to CRU activation. Using computer modelling, the data could be explained by 1 - 2 LTCC openings at 0 *mV* being required to trigger a Ca^{2+} spark, with approximately equal contributions from LTCC and CRU activation delays.

Tetracaine was used to investigate the relationship between release flux and the number of channels available in the CRU. The results show that CICR termination is consistent with a component arising from JSR Ca^{2+} depletion. To investigate why previous studies have not detected a profound JSR Ca^{2+} depletion, a computer model of local Ca^{2+} release was constructed. Dye signals were simulated by incorporating measured microscope blurring and the parameters in the model to fit experimental data. The model calculations show that previous experimental studies have severely under-estimated local JSR depletion due to problems arising from microscope blurring and dye properties - even when the signal origin is perfectly in-focus. This analysis showed that in order to reproduce observed Ca^{2+} spark morphology, JSR Ca^{2+} depletion (and subsequent reduction in release flux) had to precede CRU closure.

Acknowledgements

I hereby express my sincere gratitude to those who have made substantial contributions to my 'Doctor of Philosophy'. There is no doubt in my mind that I needed these people to reach this point: ~ 50,000 words, countless thoughts (one would hope so!) and ~ 18,000 *km* from where it first began. It has been a real privilege to have had this opportunity to explore and see things made possible by Science! I wish to thank:

My supervisor, **Prof. Mark B. Cannell**: for demonstrating and inspiring rigorous critique, an integrative approach to problem-solving and a phenomenal passion to understand; for encouraging me to reach higher and continuing to help me despite recurring bouts of self-doubt; for his immense intelligence and technical skill.

The cardiac research group at the University of Auckland: **Assoc. Prof. Christian Soeller**, **Dr. Marie-Louise Ward**, **Dr. Patricia J. Cooper**, **Dr. David Crossman**, **Dr. David Baddeley**, **Dr. Isuru D. Jayasinghe**, **Michelle Munro**, **Sarbjot Kaur**, **Xin Shen** and **Smitha Ravi**, for being warm, intelligent, helpful and humorous workmates and friends. Particular thanks to **CS**, *my co-supervisor*, for clear-headed trouble-shooting and advice, especially during the last few months I was in New Zealand and **PJC**, *my advisor*, for giving me solid foundations for isolating and patching cells.

Other University of Auckland staff: **Arthur Frankcom-Burgess** and **Louey Bosanac** for help in the workshop and **Dr. Raj Subramanian** for encouraging me into various teaching roles, which were good for both my confidence and humility.

Other research colleagues: **Prof. Clive Orchard** (*University of Bristol*), for giving me time to finish writing my thesis, and along with **MBC**, the opportunity to have this challenging, but rewarding experience and **Assoc. Prof. Derek R. Laver** (*University of Newcastle*) for providing the RyR single-channel data.

Auckland Medical Research Foundation and **University of Auckland** for my Ph.D. scholarships.

My other friends and family who have kept me going: **Irene Vorontsova**, **Kieran Veale**, **Dr. Lin-Chien Huang**, **Anna Zhou** and my sister, **Tiffany Kong** for encouraging me without prompt and reminding me of 'outside'; **Karyn Floyd**, for listening and being steadfast with lessons on 'assertiveness' and 'self-compassion'; and my parents, **Nestor and Monica Kong** for giving me the freedom and support to undertake challenges of my choosing, even if it has meant seeing each other only once per year for almost a decade!

Table of Contents

List of Figures

List of Tables

List of Abbreviations and Terminology

ΔL	Difference in latencies between the depolarising and repolarising step protocols
$[A]_b$	free concentration of *A* in compartment *b*
AP	action potential
ATP	adenosine 3’,5’-triphosphate
Ca^{2+}	calcium ion
Ca^{2+} blink	local SR Ca^{2+} depletion signal
Ca^{2+} scrap	global SR Ca^{2+} depletion signal
Ca^{2+} spark	cytosolic signal of local SR Ca^{2+} release, mediated by RyR channel clusters
Ca^{2+} sparklet	fluorescent measurement of Ca^{2+} influx via LTCCs
Ca^{2+} spike	global SR Ca^{2+} release measured by using a combination of a low-affinity Ca^{2+} dye and high-affinity Ca^{2+} buffer
Ca^{2+} quark	local SR Ca^{2+} release event that is smaller than a Ca^{2+} spark and may be from a single RyR channel
CaM	calmodulin
CICR	Ca^{2+}-induced Ca^{2+} release
couplon	functional coupling of LTCCs and RyRs in a micro-domain
corbular SR	disc-like protrusions of the sarcoplasmic reticulum that contain RyR channels
CSQ	calsequestrin
CRU	calcium release unit, consisting of RyR channels at a junction
DHP	dihydropyridine
DM-nitrophen	dimethoxy nitrophenyl EDTA, also known as DMNP-EDTA (1-(4,5-dimethoxy-2-nitrophenyl)-1,2-diaminoethane-N,N,N',N'-tetraacetic acid)

EC coupling	excitation-contraction coupling
EDTA	ethylene-diamine-tetra-acetic acid
EGTA	ethylene glycol tetraacetic acid (glycol-bis(2-aminoethylether)-N,N,N',N'-tetraacetic acid)
EM	electron microscope/microscopy
extended SR	a subset of corbular SR that are not proximal to surface sarcolemmal or transverse-tubular membranes
F	Faraday's constant: 96485.35 *C/mol*
FACSIMILE	Flow and Cytometry Simulator
FKBP	FK506 binding protein
FWHM	full-width at half maximum amplitude
G_{CPL}	LTCC-RyR macroscopic coupling gain
γ_{CPL}	LTCC-RyR microscopic coupling gain
K_D	dissociation constant
$_i$	(subscript) denoting intracellular compartment, namely, the cytosolic space
I_{Ca}	whole-cell inward Ca^{2+} current delivered by LTCCs
i_{Ca}	LTCC single-channel current
IDL	Interactive Data Language
I_{event}	current associated with an event, for example, a Ca^{2+} spark or Ca^{2+} transient
i_{RyR}	RyR single-channel current
I_{spark}	current associated with a Ca^{2+} spark
JSR	junctional sarcoplasmic reticulum, a subset of corbular sarcoplasmic reticulum
LLE	long-lasting local SR Ca^{2+} release event
LSCM	laser-scanning confocal microscope/microscopy

LTCC	L-type calcium channel
NCX	sodium-calcium exchanger
n_X	number of x per cell or per couplon, depending on context
$_O$	(subscript) denoting extracellular space
P_{CPL}	LTCC-RyR coupling fidelity, the probability that an LTCC opening activates a Ca^{2+} spark
P_O	open probability
PSF	point spread function, the response of an acquisition system in the spatial domain
P_{spark}	probability of Ca^{2+} spark occurrence
RyR	ryanodine receptor channel subtype 2, also known as the sarcoplasmic reticulum Ca^{2+} release channel
rogue RyR	ryanodine receptor channels that are on extended sarcoplasmic reticulum
SERCA	sarco-endoplasmic reticulum calcium ATPase
SL	sarcolemma, including surface membrane and transverse tubules
SOICR	store overload-induced calcium release
SR	sarco-endoplasmic reticulum
τ_C	mean closed time
TnC	troponin-C
τ_O	mean open time
TT	transverse-tubular network
z	valence

1. Introduction

1.1. Calcium in cardiac excitation-contraction (EC) coupling

The calcium cation (Ca^{2+}) is an important biological messenger that participates in numerous functions within an organism. It acts as an intracellular signal for a range of cellular processes, including muscle contraction, neurotransmitter or hormone secretion and cell death (for reviews, see Berridge, *et al.*, 1998; Brown and Macleod, 2001; Saris and Carafoli, 2005). To achieve specificity, Ca^{2+} is spatially and temporally compartmentalised. By actively maintaining a low free cytosolic Ca^{2+} concentration ($[Ca^{2+}]_i$), steep Ca^{2+} gradients are established and release of Ca^{2+} can be targeted to organise the vast array of Ca^{2+}-regulated cellular events.

A.V. Hill recognised early on (1949) that a mechanism must exist to relay electrical excitation at the muscle cell surface to force development in the myoplasm. This 'excitation-contraction (EC) coupling' (Sandow, 1952) now refers to a specific sequence of events that transforms an action potential (AP, see Schuetze, 1983, for a brief review on their discovery) stimulus to a contractile response. Though it is now well-established that Ca^{2+} is crucial in this process, it took Ringer's discovery (published in 1883) and subsequently, over a century of experiments, to understand the necessity of extracellular Ca^{2+} ($[Ca^{2+}]_O$) in the early steps of cardiac EC coupling, as well as bring about a consensus that Ca^{2+} is the activator of muscle contraction.

As an activator of muscle contraction

Though S. Ringer (1883) had shown that $[Ca^{2+}]_O$ was required for cardiac muscle contraction, the details of its involvement in EC coupling were unclear. In 1913, G.R. Mines showed that APs could be activated without $[Ca^{2+}]_O$, which suggested that $[Ca^{2+}]_O$ was not important in the initiation of electrical excitation. For many years, adenosine 3',5'-triphosphate (ATP, which had been discovered by K. Lohmann in 1931) was thought to activate contraction because it was a substrate for actomyosin (*e.g.* Engelhardt and Ljubimowa, 1939; Szent-Gyorgi, 1942a). However, application of ATP caused isolated actomyosin to both contract *and* relax ('swell', Szent-Gyorgi, 1942b). It was later clarified that ATP dissociates actomyosin (Erdös, 1943), as well as stimulate a non-dialyzable factor that relaxed intact muscle (Marsh, 1951). Closer examination of this 'relaxing factor'

identified it as previously-described myocyte fraction whose lipid content well-correlated with ATPase activity (Kielley and Meyerhof, 1948). Around this period, Heilbrunn and Wiercinski (1947) were able to inject Ca^{2+} directly into the myoplasm to cause contraction, while Bozler (1954) showed that metal chelator, EDTA (ethylene-diamine-tetra-acetic acid) caused muscle relaxation. However, the idea that Ca^{2+} was the physiological activator of muscle contraction was not established until Weber (1959) showed acto-myosin activity was Ca^{2+}-dependent and S. Ebashi and colleagues recognised the strong correlation between the ability of an agent to chelate Ca^{2+} and its ability to relax muscle and also showed that in the presence of ATP, the relaxing factor increased Ca^{2+} binding (see Ebashi, 1980). Shortly after, it was shown that Ca^{2+} cycling was closely associated with contraction and relaxation in cardiac muscle (Fanburg, *et al.*, 1964).

As an activator of calcium release in cardiac muscle

Though it had been accepted by the early 1960's that Ca^{2+} could activate muscle contraction, the mechanism that increased $[Ca^{2+}]_i$ following electrical activation had not been described. It was known that in cardiac muscle, electrical stimulation was associated with a Ca^{2+} influx (*e.g.* Langer and Brady, 1963), whose role remained unclear until voltage-clamp techniques were developed. Using a sucrose-gap voltage-clamp, Beeler and Reuter (1970b; 1970a; 1970c) were able to show that the magnitude of this inward current was proportional to developed tension in the range of voltages they studied. A subsequent series of experiments by Fabiato and Fabiato (*e.g.* 1973; 1977; 1983; 1985b) showed that the Ca^{2+} influx activated a much larger Ca^{2+} release from sarco-endoplasmic reticulum (SR), the primary intracellular Ca^{2+} store (Hasselbach, 1966; Maclennan, 1970; MacLennan and Wong, 1971; Ebashi, 1980). Though this 'Ca^{2+}-induced Ca^{2+} release' (CICR) was first proposed for skeletal muscle (Endo, *et al.*, 1970; Ford and Podolsky, 1970), it is of primary importance in cardiac muscle. It is now known that the inward Ca^{2+} current (I_{Ca}) is carried predominantly by the voltage-gated L-type Ca^{2+} channel (LTCC, Reuter, *et al.*, 1982; Cavalie, *et al.*, 1983), named for its large and long-lasting conductance in chick dorsal root ganglia (Nowycky, *et al.*, 1985). The LTCC has also been identified as a dihydropyridine (DHP) receptor (Curtis and Catterall, 1984). Similarly, the molecular target of CICR is the cardiac SR Ca^{2+} release channel, whose open probability (P_O) increases with $[Ca^{2+}]_i$ and is also a ryanodine receptor (RyR, subtype 2, Inui, *et al.*, 1987; Rousseau, *et al.*, 1987; Lai, *et al.*, 1988).

The current scheme of cardiac EC coupling proceeds as follows: *(1)* An AP rapidly depolarises the cell membrane from a resting potential of – 80 mV to a peak of ~ + 50 mV. This excitation *(2)* activates LTCCs that generate I_{Ca}, which is then able to *(3)* trigger SR Ca^{2+} release by CICR. *(4)* Together, I_{Ca} and Ca^{2+} released from the SR produce the whole-cell Ca^{2+} transient, which increases $[Ca^{2+}]_i$ from ~ 100 nM to 1 µM (Allen and Kurihara, 1982; Cannell, *et al.*, 1987a). *(5)* This Ca^{2+} enables cross-bridge cycling and sliding of the thick and thin filaments to cause cell shortening and force production (Huxley, 1971). *(6)* During relaxation, resting $[Ca^{2+}]_i$ is restored to the SR and extracellular space by the sarco-endoplasmic reticulum ATPase (SERCA, the relaxing factor described above) and surface membrane Na^+-Ca^{2+} exchange (NCX, Reuter and Seitz, 1968), respectively.

Calcium-induced calcium release and local control

Several lines of evidence support CICR as the primary mechanism for triggering SR Ca^{2+} release in cardiac muscle. These include the requirement for Ca^{2+} as the LTCC charge carrier to evoke SR Ca^{2+} release (Näbauer, *et al.*, 1989) and the ability to evoke SR Ca^{2+} release with 'tail' Ca^{2+} currents that occur during repolarising steps (Cannell, *et al.*, 1987a; Beuckelmann and Wier, 1988) and in the absence of an electrical stimulus (Niggli and Lederer, 1990). However, a major criticism was that CICR is an inherently regenerative, high-gain, positive-feedback system. These qualities are inconsistent with the observation that Ca^{2+} transients could be graded with I_{Ca} (Cannell, *et al.*, 1987b; Sipido and Wier, 1991; Wier, *et al.*, 1994). It was proposed that this problem could be solved through 'local control' of RyR channel gating, wherein the RyR channel(s) are activated by nearby LTCC(s), but not by Ca^{2+} flux from relatively distant activated RyR channels (Lederer, *et al.*, 1990; Niggli and Lederer, 1990; Stern, 1992b; Wier, *et al.*, 1994). Unlike previous 'common-pool' models of CICR, local control spatio-temporally confines regenerative behaviour to sub-cellular micro-domains. This *functional coupling* between LTCCs and RyRs have led to them being collectively called a 'couplon' (Stern, *et al.*, 1997).

Strong evidence in support of local control came from the discovery (Cheng, *et al.*, 1993) and subsequent functional characterisation (Cannell, *et al.*, 1994; López-López, *et al.*, 1994; Cannell, *et al.*, 1995) of 'Ca^{2+} sparks' in cardiac muscle. These local SR Ca^{2+} release events had small amplitudes and were spatio-temporally restricted, involving a mere doubling in the fluorescence of a Ca^{2+}-sensitive fluorochrome (Fluo-3) in ~ 10 *ms* over ~ 2 *µm* and which dissipated in ~ 20 *ms* (Cheng, *et al.*, 1993; Cannell, *et al.*, 1994). During EC

coupling, I_{Ca} controls SR Ca^{2+} release by coordinating a rapid activation of ~ 10^4 Ca^{2+} sparks. The cell-wide Ca^{2+} transient results from this near-synchronous recruitment of discrete elementary events (Cannell, *et al.*, 1994; Cannell, *et al.*, 1995), an idea that is distinct from grading the amplitudes of individual Ca^{2+} sparks (López-López, *et al.*, 1994).

Spontaneous calcium release

Ca^{2+} sparks are able to occur without I_{Ca}, for example, in the absence of $[Ca^{2+}]_o$ (Cheng, *et al.*, 1993), at resting membrane potential (Cannell, *et al.*, 1994) and in saponin-permeabilised myocytes (Lukyanenko and Gyorke, 1999). These 'spontaneous' events show similar characteristics to that of evoked Ca^{2+} sparks and are therefore thought to be of the same origin and fundamental mechanism (Cannell, *et al.*, 1994). Occurrence of spontaneous Ca^{2+} sparks is increased with $[Ca^{2+}]_{SR}$ (Bassani and Bers, 1995; Lukyanenko, *et al.*, 1996; Díaz, *et al.*, 1997; Satoh, *et al.*, 1997).

Occasionally, individual spontaneous Ca^{2+} sparks are able to activate a neighbouring event to form a 'macro-spark' (Cheng, *et al.*, 1996; Parker, *et al.*, 1996). This larger Ca^{2+} gradient can then activate other sites and cause propagating SR Ca^{2+} release, or a 'Ca^{2+} wave' (Wier, *et al.*, 1987; Berlin, *et al.*, 1989; Takamatsu and Wier, 1990; Lipp and Niggli, 1993; Cheng, *et al.*, 1996; Satoh, *et al.*, 1997). Ca^{2+} waves demonstrate that under certain circumstances (*e.g.* increased $[Ca^{2+}]_{SR}$, when Ca^{2+} spark frequency, P_{spark}, is increased, Díaz, *et al.*, 1997, see also Song, *et al.*, 1997 over a smaller $[Ca^{2+}]_{SR}$ range), CICR can be regenerative at a cell-wide level. This aberrant SR Ca^{2+} release can be arrhythmogenic due to activation of NCX, which is electrogenic (Lederer and Tsien, 1976; Kass, *et al.*, 1978; Cannell and Lederer, 1986a; Berlin, *et al.*, 1989).

Other activators of calcium release

Though I_{Ca} is considered the primary trigger for CICR during EC coupling (Fabiato, 1983; Näbauer, *et al.*, 1989; Cleemann and Morad, 1991; Sipido and Wier, 1991), other mechanisms have been proposed and may serve to augment the trigger current or be dominant in other conditions. These other sources of trigger Ca^{2+} include: *(1)* the T-type Ca^{2+} channel (Nilius, *et al.*, 1985; Balke, *et al.*, 1992), although its contribution during normal EC coupling in adult animals may be low (Sipido, 1998; Sipido, *et al.*, 1998); *(2)* troponin C of the myofilaments (Ter Keurs, *et al.*, 2005), though this may only be a

small effect during Ca^{2+} waves; *(3)* Ca^{2+} flux through Na^{+} channels (Santana, *et al.*, 1998, although see Piacentino, *et al.*, 2002); *(4)* direct depolarisation of the SR membrane, although there is not thought to be a potential difference across the SR (Somlyo, *et al.*, 1981; Meissner and McKinley, 1982); *(5)* NCX in reverse mode, and *(6)* direct coupling between the LTCC and RyR channel.

Ca^{2+} entry through NCX has been shown to evoke SR Ca^{2+} release under some circumstances (Leblanc and Hume, 1990; Levi, *et al.*, 1994; Lipp and Niggli, 1994; Hancox and Levi, 1995; Sham, *et al.*, 1995b). The idea is that during the AP upstroke, the large Na^{+} influx via Na^{+} channels and subsequent large local increase in $[Na^{+}]$ is able to reverse NCX. However, it has been argued that this is implausible because Ca^{2+} influx via NCX is slow and only significant at very positive potentials, is less effective than LTCCs in triggering SR Ca^{2+} release and that any effect of NCX on CICR may be due to an indirect effect through $[Ca^{2+}]_{SR}$ and/or loss of voltage control during large Na^{+} currents, leading to I_{Ca} activation (Crespo, *et al.*, 1990; Sham, *et al.*, 1992; Sham, *et al.*, 1995a; Sipido, *et al.*, 1995; Evans and Cannell, 1997). Nevertheless, recent studies have suggested that reverse-mode NCX may augment local I_{Ca} and thereby enhance the ability of I_{Ca} to trigger release (Goldhaber, *et al.*, 1999; Sobie, *et al.*, 2008; Larbig, *et al.*, 2010; Neco, *et al.*, 2010; Torres, *et al.*, 2010) during CICR.

Physical coupling between LTCCs and RyR channels is the primary mechanism by which SR Ca^{2+} release is triggered in skeletal muscle and has also been proposed as an additional mechanism for the myocardium (Hobai, *et al.*, 1997; Ferrier and Howlett, 2001). However, the low LTCC:RyR channel ratio (*e.g.* Bers and Stiffel, 1993) means this mechanism is not feasible for most RyR channels. The observed voltage-dependence of SR Ca^{2+} release may be explained by incomplete removal of CICR (e.g. Balke and Goldman, 2003; Griffiths and MacLeod, 2003; Trafford and Eisner, 2003). Thus, CICR remains the predominant activation mechanism for SR Ca^{2+} release.

1.2. Structures in local excitation-contraction coupling

A typical ventricular cardiac myocyte can be likened to a flattended cylinder with a high surface area to volume ratio (~ 150 *pF/cell* at ~ 30 – 40 *pL*, Bers, 2001). The cell is abundant with mitochondria for energy homeostasis and myofilament bundles that are structured into repeating contractile units called sarcomeres. As in all striated muscle, these

sarcomeres are demarcated by *z*-lines, which in cardiac ventricular myocytes are typically ~ 1.8 *μm* apart under zero load and ~ 20 % shorter during contraction. A tubular SR network wraps around the myofilament bundles. During EC coupling, information is transduced across both the sarcolemma (SL) and SR. These lipid membranes allow the establishment and maintenance of important electrochemical gradients, as well as localisation of the key channels and transporters required for this fundamental process. Local control theory requires small distances between RyRs and LTCCs for activation of SR Ca^{2+} release, but relatively large distances between the RyR clusters themselves (see below) to prevent propagation of CICR (Ca^{2+} waves). Thus, high-resolution structural information has been important in determining the physical constraints of CICR and helped refine the physiological scheme.

Surface sarcolemma and transverse-tubular network

The SL defines the myocyte and is comprised of a lipophilic bilayer surrounded by an external glycocalyx matrix. The SL can be divided into two regions, the surface sarcolemma and transverse-tubular (TT) network (though up to 60 % are not necessarily transverse and may be oblique or axial, Sommer and Waugh, 1976; Soeller and Cannell, 1999). TTs are invaginations of the SL that extend from the surface into the cell and assist in rapid delivery of electrical excitation. In mammals, TTs occur at the z-lines, are ~ 60 - 300 *nm* in diameter and may be 21 - 64 % of the SL (in rat, Page and Surdyk-Droske, 1979; Kawai, *et al.*, 1999; Soeller and Cannell, 1999). For reviews of TT function, see Brette and Orchard, 2003; Ibrahim, *et al.*, 2011.

LTCCs are located in the SL, although their density and precise location are unclear. An early binding study suggested that LTCC density was ~ 15 DHP sites $/\mu m^2$ (Lew, *et al.*, 1991), which is much higher (assuming one DHP binding site per LTCC) than that predicted by electrophysiology data (*e.g.* ~ 3 LTCCs $/\mu m^2$, Josephson, *et al.*, 2010b). An early study of radio-DHP binding of light and heavy membrane fractions suggested that LTCCs are ~ 3-fold more densely populated in TTs compared to the surface SL (Wibo, *et al.*, 1991). This observation is supported by a later functional study that used formamide to measure whole-cell I_{Ca} in the presence and absence of TTs (Kawai, *et al.*, 1999). Detubulation by osmotic shock was associated with a 26 % decrease in cell capacitance and a 76 % decrease in I_{Ca}, which equates to ~ 9-fold larger LTCC density in the TTs (Kawai, *et al.*, 1999), assuming this method had no other effects on I_{Ca} and cell integrity. High-

resolution scanning patch-clamping could not detect LTCC current at the surface and only ~ 2 LTCCs $/\mu m^2$ at TT openings (Gu, *et al.*, 2002). Interestingly, a recent study has suggested that TT LTCCs may be more active than those at the surface SL (Chase, *et al.*, 2010).

The surface and TT membranes also contain NCX. Its location appears to be anti-correlated with that of LTCCs (*i.e.* NCX occur where LTCCs do not, Scriven, *et al.*, 2000, although see Jayasinghe, *et al.*, 2009), which may be important when considering the role(s) of NCX during EC coupling.

Sarcoplasmic reticulum

The SR is another tubular membrane system that is distinct from the SL and continuous with the nucleo-plasmic envelope (Porter and Palade, 1957; Sommer and Waugh, 1976; Ogata and Yamasaki, 1990; Wu and Bers, 2006). It occupies ~ 3.5 % of total cell volume (Page, *et al.*, 1971) and is the principal internal Ca^{2+} store. The tubules of the SR network (~ 25 - 40 *nm* in diameter, Sommer and Waugh, 1976) form a hexagonal-like lattice around the contractile machinery (Porter and Palade, 1957; Sommer and Waugh, 1976) and contain SERCA (Maclennan, 1970; MacLennan and Wong, 1971) and its inhibitory regulator, phospholamban, tethered to the cytosolic leaflet (see Simmerman and Jones, 1998).

'Corbular' SR are distinct disc-like protrusions (100 - 400 *nm* in diameter, Porter and Palade, 1957) of the SR that contain electron-dense structures (Sommer and Waugh, 1976) identified as RyR channels (Meissner and Henderson, 1987; Rousseau, *et al.*, 1987; Rardon, *et al.*, 1989). It has been estimated that only 4 - 10 % of total SR is corbular (Page, *et al.*, 1971; Page and Surdyk-Droske, 1979), but most of them (*e.g.* ~ 85 % in rat, Jayasinghe, *et al.*, 2009) are associated with SL membranes at 'junctions' (or 'dyads' to distinguish them from 'triads' in skeletal muscle). It has been suggested that LTCCs on the SL are also aggregated near junctions (Carl, *et al.*, 1995; Sun, *et al.*, 1995; Scriven, *et al.*, 2000; Sedarat, *et al.*, 2000, although see Crossman, *et al.*, 2011). Corbular SR that are not junctional SR (JSR) have also been called 'extended' JSR (Jorgensen, *et al.*, 1993; Junker, *et al.*, 1994; Franzini-Armstrong, *et al.*, 1999) that contain 'rogue' RyR channels that are not part of a couplon (Sobie, *et al.*, 2006). Corbular SR are continuous with the remaining SR network via one or two thin tubules (Peachey, 1965) and is the primary location of a low affinity, high capacity Ca^{2+} buffer, calsequestrin (CSQ, MacLennan and Wong, 1971;

Campbell, *et al.*, 1983b; Jorgensen and Campbell, 1984; Jorgensen, *et al.*, 1985; Jorgensen, *et al.*, 1993). JSR that are proximal to surface SL are termed 'peripheral' junctions, while those proximal to TTs are 'internal' junctions (Jewett, *et al.*, 1973; Sommer and Waugh, 1976) and are not thought to be different from one another (Franzini-Armstrong, *et al.*, 1999), although this is largely unclear.

Measurement of interjunctional distance using RyR channels as a marker have yielded a separation of ~ 0.4 – 1 μm in rat using electron microscopy (Franzini-Armstrong, *et al.*, 1999), immuno-fluorescence (Chen-Izu, *et al.*, 2006; Soeller, *et al.*, 2007) and Ca^{2+} spark measurements (Parker, *et al.*, 1996; Cleemann, *et al.*, 1998). This equates to ~ 30,000 SR Ca^{2+} release sites per cell, which agrees with the estimated number of Ca^{2+} sparks required for a Ca^{2+} transient (~ 10^4, Cannell, *et al.*, 1994). For internal junctions, ~ 6 JSR surround a myofilament bundle at each *z*-line and are therefore more closely associated across the *z*-disc than along the cell (Chen-Izu, *et al.*, 2006; Soeller, *et al.*, 2007). Peripheral junctions occur at the invagination of the TT from the SL and so appear as doublets that flank *z*-line staining (Chen-Izu, *et al.*, 2006; Soeller, *et al.*, 2007). Each JSR is thought to contain a cluster of RyR channels to form a 'Ca^{2+} release unit' (CRU, *e.g.* Franzini-Armstrong, *et al.*, 2005).

Calcium release unit

Immuno-fluorescence and electron microscopy studies suggest a CRU consists of ~ 200 RyRs in rat (Franzini-Armstrong, *et al.*, 1999; Chen-Izu, *et al.*, 2006; Soeller, *et al.*, 2007). However, a recent study of peripheral couplings using single-molecule detection suggests that the number of RyRs per CRU may be as low as ~ 14 (Baddeley, *et al.*, 2009). Though the reason for this discrepancy is unknown, there may be true differences between peripheral and internal CRU. Another possibility is that confocal microscopy has relatively poor spatial resolution (that cannot be fully corrected for by de-convolution), which would over-estimate CRU size. Similarly, the thin sections used for electron microscopy would also create a selection bias for large CRUs. At the same time, single-molecule detection may under-estimate CRU size due to incomplete (probabilistic binding and/or exclusion from a restricted space leading to missed labels) and/or non-specific (leading to false positives and reduction in signal-to-noise) antibody labelling. Binding studies appear to agree with larger CRU sizes (Bers and Stiffel, 1993), however, Ca^{2+} spark analyses suggest that only 6 - 20 RyR channels are required to generate the underlying release flux (Soeller

and Cannell, 2004). Thus, further data are required to determine the size of a CRU and whether peripheral and internal couplings are fundamentally different.

RyR channels within a CRU are organised in an array, whose arrangement has been shown to form spontaneously in vitro (Yin and Lai, 2000). This lattice-like grid at an *en face* view displays quatrefoil RyR channels arranged ~ 31 *nm* (centre-to-centre) apart, at a ~ 61 ° angle so that the channels are staggered and each channel is in physical contact with 4 others (Franzini-Armstrong, *et al.*, 1999; Yin and Lai, 2000).

The single RyR channel is a large (~ 2.3 *MDa*) homo-tetramer (Inui, *et al.*, 1987; Lai, *et al.*, 1988) that is associated with four small (12 *kDa*) FK-506 binding proteins (*e.g.* FKBP12.6, see Fill and Copello, 2002 for a review). The RyR protein contains a large central pore, with a large cytoplasmic NH_2 domain (29 x 29 *nm*, Radermacher, *et al.*, 1994; Yin, *et al.*, 2005) that protrudes 12 *nm* into the junctional space (Franzini-Armstrong, *et al.*, 1999). Though RyR2 has yet to be crystallised and many of these structural studies have been performed on skeletal RyR1, the genetic variants (including RyR3) are thought to share similar topology (Wagenknecht and Samsó, 2002).

Junctional space and cytoplasm

The junctional space between JSR and SL membranes is narrow (~ 15 *nm*, Fawcett and McNutt, 1969; Forbes and Sperelakis, 1973; Franzini-Armstrong, *et al.*, 1999) and contains many interesting properties that are likely important for local control, but not well understood (*e.g.* Tan, *et al.*, 2007). The characterisation of these properties is important when analysing fluxes responsible for Ca^{2+} sparks.

Ca^{2+} diffusion within the junction is not well characterised, but is likely to be limited by the large RyRs acting as barriers, buffering and electrostatic effects (Soeller and Cannell, 1997). Computer modelling studies suggest that fast and slow Ca^{2+} buffers including ATP, calmodulin and the cytosolic leaflets of the SL and JSR membranes effectively prolong the duration of Ca^{2+} in the junction, but do not control [Ca^{2+}] near the channel pore (Stern, 1992a; Langer and Peskoff, 1996; Soeller and Cannell, 1997; Soeller and Cannell, 2004). Further, the negatively-charged phospholipid heads of the bilayer give rise to electrostatic effects on cation movement, which increases [Ca^{2+}] in a region several nanometers near the lipid bilayer (Soeller and Cannell, 2004). Details of the Ca^{2+}, Mg^{2+} and ATP gradients are

likely to be important in the regulation of RyR gating during a Ca^{2+} spark (Valent, *et al.*, 2007).

The junctional space is continuous with the cytoplasm, where other Ca^{2+} buffers and the majority of Ca^{2+}-sensitive fluorescent dyes are located (Stern, 1992a; Soeller and Cannell, 2004). Examples of immobile buffers include troponin-C (Holroyde, *et al.*, 1980; Fabiato, 1983) and mitochondria (see Saris and Carafoli, 2005 for a review). The buffering power of the cytosol is thought to be high, such that during a Ca^{2+} transient (where free $[Ca^{2+}]_i$ increases to ~ 1 *μM*, Cannell, *et al.*, 1987a), 50 – 100 *μM* $[Ca^{2+}]$ needs to be released from the SR (Berlin, *et al.*, 1994; Delbridge, *et al.*, 1996; Shannon, 1997). Further, diffusion of Ca^{2+} (and ATP, Vendelin and Birkedal, 2008) in the cytosol is thought to be asymmetric, where Ca^{2+} sparks are more narrow along the short axis of the myocyte (Parker, *et al.*, 1996, although see Banyasz, *et al.*, 2007; Shkryl, *et al.*, 2012). The reason for this is unknown, but is thought to involve the spatial distribution of SERCA activity (Gómez, *et al.*, 1996) and mitochondria. The anisotropy in diffusion is thought to explain the circularity of Ca^{2+} wave-fronts despite an anisotropic distribution of CRUs (Ishide, *et al.*, 1990; Takamatsu and Wier, 1990; Engel, *et al.*, 1994; Subramanian, *et al.*, 2001).

1.3. I_{Ca}, the primary trigger for CICR

Understanding LTCC properties is important in identifying how it activates and/or controls SR Ca^{2+} release. Its gating behaviour has complex dependencies on voltage and local $[Ca^{2+}]_i$ (for a review, see McDonald, *et al.*, 1994). LTCCs are activated and inactivated by depolarisation, which give rise to a bell-shaped current-voltage relationship. I_{Ca} activates, peaks and reverses at ~ - 40, 0 and + 55 *mV*, respectively. At very positive potentials, a net outward current is carried by monovalent cations, although Ca^{2+} influx is still appreciable (Zhou and Bers, 2000). During a step pulse, whole-cell I_{Ca} reaches its maximum in ~ 2 *ms* and declines with a fast and slow component (Reuter and Scholz, 1977; Lee and Tsien, 1984; McDonald, *et al.*, 1986). As might be expected of a Hodgkin-Huxley gating scheme (1952), the rate of activation increases with depolarisation (Isenberg and Han, 1994).

Modal gating

At the single-channel level, an activated LTCC can exhibit a range of gating behaviours from periods of quiescence to long-lasting openings. These behaviours tend to cluster and

have been described as modal (McDonald, *et al.*, 1994). Modes 0, 1 and 2 describe periods of non-conductance (*i.e.* a blank sweep), typical openings and rare long openings (> 5 *ms*, Hess, *et al.*, 1984, Cavalié, *et al.*, 1986; Yue, *et al.*, 1990; Imredy and Yue, 1994), respectively. However, it is unclear whether discrete modes or a continuum of behaviour exists (Lacerda and Brown, 1989). Different conditions appear to favour certain types of behaviour, for example, DHP agonists (*e.g.* s(-)-Bay-K-8644, Hess, *et al.*, 1984), β-adrenergic stimulation (Yue, *et al.*, 1990) and pulsing to positive potentials favour long openings, while DHP antagonists (*e.g.* nifedipine) favour non-conductance (*i.e.* decrease channel availability, rather than change open or closed times during conducting sweeps, McDonald, *et al.*, 1994).

During 'typical' gating, LTCCs exhibit a mean closed time ($\tau_{C,LTCC}$) of ~ 3.3 – 4.7 *ms* (Rose, *et al.*, 1992; Takeda, *et al.*, 1995; Josephson, *et al.*, 2010b) and a mean open time ($\tau_{O,LTCC}$) of ~ 0.27 – 1.1 *ms* (Rose, *et al.*, 1992; Josephson, *et al.*, 2010b). The variability in these parameters have led to estimates of open probability ($P_{O,LTCC}$) that differ by an order of magnitude (0.02 – 0.25 at 0 *mV*, Rose, *et al.*, 1992; Josephson, *et al.*, 2002b; Inoue and Bridge, 2003; Josephson, *et al.*, 2010b). Eqn. 1.1 shows the general formula for calculating channel open probability (P_O) from the mean closed (τ_C) and open (τ_O) times:

$$P_O = \frac{\tau_O}{\tau_O + \tau_C} \qquad \textbf{Eqn. 1.1}$$

Facilitation

When held at a physiological resting membrane potential, I_{Ca} exhibits a positive staircase upon repeated electrical stimulation to ≥ 0 *mV*. Interestingly, this 'facilitation' or restitution of I_{Ca} is reversed at a more positive holding potential (*e.g.* – 50 *mV*, Pietrobon and Hess, 1990). Facilitation appears to occur at a single-channel level, where conductance, frequency and duration of openings are increased (Josephson, *et al.*, 2002b; Josephson, *et al.*, 2002a).

Inactivation

The transition of LTCCs into a non-conducting state ('inactivate') is Ca^{2+}-, voltage- and time-dependent (for a review, see Eckert and Chad, 1984). In both whole-cell and single-channel studies, voltage-dependent inactivation is observed even when LTCCs are depolarised only to a sub-threshold potential, which suggests that activation is not required

for inactivation (McDonald, *et al.*, 1994). Voltage-dependent inactivation of LTCCs is thought to be slow compared to Ca^{2+}-dependent inactivation, which occurs due to its own Ca^{2+} current, as well as SR Ca^{2+} release (*e.g.* Tseng, 1988). When the latter is removed, I_{Ca} declines at approximately half the rate (Hadley and Hume, 1987; Sham, *et al.*, 1995a; Puglisi, *et al.*, 1999). Following voltage-dependent inactivation, LTCCs can be made available again by repolarisation to negative potentials. Recovery from inactivation occurs at a rate that increases with decreasing membrane potential. A putative mechanism for Ca^{2+}-inactivation involves calmodulin (Altamirano and Bers, 2007a), though this is disputed (Imredy and Yue, 1994), while a 'ball and chain' mechanism similar to that of Na^{+} channels has been proposed for LTCC voltage-dependent inactivation (McDonald, *et al.*, 1994).

Unitary and whole-cell flux

Typical whole-cell peak I_{Ca} has been measured to be ~ 0.7 - 2 *nA* in guinea-pig or rat ventricular myocytes (Rose, *et al.*, 1992; Cannell, *et al.*, 1995), while single-channel current (i_{Ca}) at 0 *mV* has been measured to be 0.12 and 0.17 *pA* (Rose, *et al.*, 1992; Guia, *et al.*, 2001 in 2 and 10 mM $[Ca^{2+}]_O$, respectively, where conductance saturates at ~ 20 *mM*, see also Hess and Tsien, 1984; Shorofsky and January, 1992).

Eqn. 1.2 can be used to estimate the number of available channels in a cell (*n*) given the ensemble current (*e.g.* whole-cell, *I*), unitary current (*i*) and the maximum P_O are known. The actual number of channels present (*N*) can be obtained if the fraction available (f_A, measured in single-channel recordings as the proportion of sweeps that show no openings) is known (McDonald, *et al.*, 1994).

$$I = i \cdot n \cdot P_O \qquad \textbf{Eqn. 1.2}$$

where,

$$n = N \cdot f_A$$

Assuming a maximum steady-state I_{Ca} of 1 *nA*, i_{Ca} of 0.06 *pA* and $P_{O,LTCC}$ of 0.25 (Josephson, *et al.*, 2010b), LTCC density would be ~ 67,000 LTCCs */cell* or ~ 4 LTCCs $/\mu m^2$, assuming a cell capacitance of 150 *pF* and 1 $\mu F/cm^2$ (Bers, 2001). As stated previously, this LTCC density is only ~ 30 % of the DHP binding site density

(250,000 */cell*, Lew, *et al.*, 1991). This discrepancy could be reconciled if $P_{O,LTCC}$ is 10-fold smaller (Rose, *et al.*, 1992), as in Bers (2001), or if f_A was ~ 0.3 (*i.e.* a large fraction of LTCCs are unable to be activated). However, single-channel studies have shown that f_A at 0 *mV* can be as high as 90 % (using Ca^{2+} as the charge carrier, Rose, *et al.*, 1992) or as low as 10 *%* (using Ba^{2+} as the charge carrier, Tsien, *et al.*, 1986; Inoue and Bridge, 2003, although Yue, *et al.*, 1990 obtained variable f_A of 20 – 90 *%*, with a mean of 50 *%*). There is also the possibility that LTCC function under physiological conditions may be more complex than that discernable by single-channel recordings (*e.g.* coupled-gating, Navedo, *et al.*, 2010; different phosphorylation status depending on LTCC location, Chase, *et al.*, 2010).

Trigger calcium in the junction

Ca^{2+} influx through the LTCCs during each heart beat contributes to CICR, as well as the cell's Ca^{2+} load (Fabiato, 1983; Eisner and Trafford, 2009). For CICR, the amount (and rate) of Ca^{2+} entering the junction and sensed by the CRU is crucial, but has not been measured at this time. The factors that need to be taken into consideration include Ca^{2+} diffusion, Ca^{2+} buffering and junction geometry.

The spatio-temporal profile of $[Ca^{2+}]$ in the junction ($[Ca^{2+}]_{junction}$) due to Ca^{2+} influx has been simulated in computer models that incorporated known properties of the small cytosolic space (*e.g.* Langer and Peskoff, 1996; Cannell and Soeller, 1997; Soeller and Cannell, 1997; Valent, *et al.*, 2007). With SL Ca^{2+} binding sites and electrostatic effects taken into consideration, Soeller and Cannell (1997) estimated that $[Ca^{2+}]_{junction}$ (4 *nm* from SL, 2.5 *nm* radially from LTCC) reached 65 - 70 *μM* within ~ 0.3 *ms* of a 0.2 *pA* LTCC opening. This large gradient dissipated to 50 *%* in < 0.1 *ms* upon LTCC closure. However, interaction with Ca^{2+} buffers meant that the remaining phase of $[Ca^{2+}]_{junction}$ decline was slow, so that ~ 1 *ms* after LTCC closure, $[Ca^{2+}]_{junction}$ was still 2 *μM* and at 5 *ms*, $[Ca^{2+}]_{junction}$ was 200 *nM*. This long tail may have important consequences for RyR channel (and LTCC) gating. The spatial $[Ca^{2+}]_{junction}$ gradient was also steep and developed a shape more radially-confined than a hemisphere ('omega' shape, Soeller and Cannell, 1997), which suggested that an LTCC can only serve one or a few RyR channels.

1.4. Efficiency of calcium-induced calcium release

Quantification of the functional coupling between LTCCs and RyRs during EC coupling remains a controversial issue. Many measures of how well LTCC current triggers a CRU have been introduced, creating some confusion over their definitions and relevance. One common theme appears to be that EC coupling is impaired in disease and may be restored by β-adrenergic signalling (Gómez, *et al.*, 1997, although see Zhou, *et al.*, 1999). However, these ideas appear uncertain as EC coupling 'efficiency' under physiological conditions remains unclear.

A. Fabiato suggested that only the initial phase of I_{Ca} is important for CICR, while the remainder serves to potentiate $[Ca^{2+}]_{SR}$ (see Fig. 1 in Fabiato, 1985a). By interrupting I_{Ca} at various delays following activation, subsequent studies have been able to show that the rate of rise of Ca^{2+} transients did not increase further beyond a delay of ~ 6 *ms* (Wier, *et al.*, 1994; Cannell, *et al.*, 1995). Though this macroscopic level of control has been attributed to the recruitment of CRUs, the role of I_{Ca} within a junction is less well-defined. It is unclear how many LTCC openings are required to trigger a CRU and how this relates to the actual number of LTCCs available within a junction (n_{LTCC}). These details are important because as the number of LTCCs required increases, the more likely that LTCC properties will dominate the latency and uniformity of SR Ca^{2+} release. To activate a large number of LTCCs with short delay (*i.e.* during EC coupling), the number of available LTCCs would have to increase, which might render more I_{Ca} redundant with respect to CICR and reduce the effective amplification.

Definitions of efficiency

$$\begin{aligned} P_{CPL} &= \frac{\text{no. successful openings}}{\text{total no. LTCC openings}} \\ &= P(\text{success}|\text{opening}) \\ &= \frac{P(\text{success} \cap \text{opening})}{P(\text{opening})} \end{aligned} \qquad \textbf{Eqn. 1.3}$$

EC coupling 'fidelity' (P_{CPL}) measures the probability that a single LTCC opening will trigger a Ca^{2+} spark (Wang, *et al.*, 2001; Cheng and Lederer, 2008). Eqn. 1.3 shows how P_{CPL} can be calculated, where success is defined by an observed Ca^{2+} spark. Experimentally, P_{CPL} is difficult to determine and has been commonly estimated by

measuring P_{spark} for a given local or whole-cell trigger. Eqn. 1.4 describes how P_{spark} is the product of the probability that at least one LTCC opens in a junction (using the Binomial theorem) and P_{CPL}, where P_{CPL} is some (unknown) function of i_{Ca} and $\tau_{O,LTCC}$ (Santana, *et al.*, 1996; Gómez, *et al.*, 1997; Inoue and Bridge, 2003). Since P_{spark} is too high during normal EC coupling to be counted, various techniques have been used to decrease P_{spark} and improve signal contrast, for example: *(1)* selective activation a single CRU by loose-seal patch clamp (Wang, *et al.*, 2001), *(2)* reduction of I_{Ca} through $n{\cdot}P_O$ by pharmacological blockade (*e.g.* nifedipine, Santana, *et al.*, 1996; Collier, *et al.*, 1999; verapamil, López-López, *et al.*, 1995; or D600/methoxyverapamil, Cheng, *et al.*, 1995) or through i_{Ca} by reducing $[Ca^{2+}]_O$ (*e.g.* Bridge, *et al.*, 1999).

$$P_{spark} = P_{CPL} \cdot \left(1 - (1 - P_{O,LTCC})^{n_{LTCC}}\right) \qquad \textbf{Eqn. 1.4}$$

where,

$$P_{CPL} = g(i_{Ca}) \cdot h(\tau_{O,LTCC})$$

While coupling fidelity measures CICR efficiency in terms of the success or failure of a given trigger to activate SR Ca^{2+} release, coupling gain (G_{CPL}) quantifies the amount of SR Ca^{2+} released for a given trigger, also known as the amplification factor of CICR. Eqn. 1.5 describes one type of calculation, where G_{CPL} is ratio of release to trigger current magnitude (Cannell, *et al.*, 1994; Wier, *et al.*, 1994). For macroscopic gain, the event is usually the Ca^{2+} transient, while for microscopic gain, the event is a Ca^{2+} spark. Flux integrals have also been used introduced by Gomez, *et al.* (1997) because G_{CPL} is dependent on the relative size (analogue) and duration (digital) of the currents (Cannell, *et al.*, 1995).

$$G_{CPL} = \frac{I_{event}}{I_{Ca}} \qquad \textbf{Eqn. 1.5}$$

Measuring G_{CPL} is difficult due to the inability to directly measure SR Ca^{2+} release flux. Ca^{2+} dyes and imaging only measure (relatively) bulk $[Ca^{2+}]_i$, which should be slower than the true time-course of release. Different techniques have been used to correct for these effects, for example: *(1)* using the rate of decline of a Ca^{2+} transient to take into account Ca^{2+} removal by SERCA and diffusion, although this assumes this effect is constant throughout release (Sipido and Wier, 1991; Wier, *et al.*, 1994) and *(2)* using 'Ca^{2+} spikes',

which aim to measure the approximate global release flux by combining a fast, low-affinity Ca^{2+} dye with a slow Ca^{2+} buffer (Sham, *et al.*, 1998; Altamirano and Bers, 2007b). However, this method likely underestimates the true time course of SR Ca^{2+} release (Soeller and Cannell, 1999), so the estimated microscopic coupling gains may represent a lower limit. Alternatively, since P_{spark} is proportional to I_{event} (Eqn. 1.2), P_{spark}/I_{Ca} can be used as a measure of G_{CPL} (e.g. Santana, *et al.*, 1996; Gómez, *et al.*, 1997). Whole-cell G_{CPL} has been measured to be 3 – 16 at 0 *mV* (Beuckelmann and Wier, 1988; Sipido and Wier, 1991; Cannell, *et al.*, 1994; Cheng, *et al.*, 1994; Wier, *et al.*, 1994; López-López, *et al.*, 1995).

As expected, G_{CPL} is sensitive to $[Ca^{2+}]_{SR}$, which affects I_{event} and P_{CPL} (*e.g.* Janczewski, *et al.*, 1995; Díaz, *et al.*, 1997). Further, as implied in Eqn. 1.4, P_{CPL} and G_{CPL} are sensitive to membrane potential and time, primarily due to i_{Ca} and LTCC gating kinetics. In order to encapsulate these time-dependent changes, EC coupling efficiency is also measured by the delay between LTCC and Ca^{2+} spark activation, also known as the latency of EC coupling.

LTCCs may be redundant at negative potentials

Under a condition of reduced P_{spark}, studies have shown that both P_{spark} and I_{Ca} have a bell-shaped voltage-dependence (López-López, *et al.*, 1995; Santana, *et al.*, 1996; Gómez, *et al.*, 1997). A slight leftward shift in the voltage-dependence of P_{spark} gives rise to a P_{spark}/I_{Ca} ratio (or G_{CPL}) that declines monotonically with increasing step voltage (Santana, *et al.*, 1996). Comparison of this relationship with the voltage-dependence of i_{Ca} suggests that P_{spark} increases with the square of i_{Ca} (Santana, *et al.*, 1996), so that at negative potentials (*e.g.* - 30 *mV*), one LTCC opening is sufficient to trigger a Ca^{2+} spark (*i.e.* P_{CPL} is near 1, López-López, *et al.*, 1995; Santana, *et al.*, 1996). Evidence in support of this idea can be found in earlier studies that showed a wide, bell-shaped voltage-dependence of Ca^{2+} transient amplitude or maximum rate of rise (Barcenas-Ruiz and Wier, 1987; Cannell, *et al.*, 1987a; Callewaert, 1992), which suggests that the ability of a single LTCC opening to trigger SR Ca^{2+} release was not fundamentally changed when ~ 90 % of LTCCs were blocked, as in the study by Santana, *et al.* (1996). Altamirano and Bers (2007b) also showed high coupling fidelity from Ca^{2+} spike measurements. They suggested that at 0 *mV*, only one LTCC opening was required to trigger CICR and that below this potential, i_{Ca} increases so that extra LTCC openings become redundant. At + 50 *mV*, in the absence of an

LTCC blocker, Collier, *et al.* (1999) was able to show that I_{Ca} could trigger Ca^{2+} sparks at low P_{spark}, although coupling fidelity was not quantified.

Although only one LTCC opening may be required to trigger CICR at 0 *mV*, the waiting time to this opening may be too long (and variable) due to stochastic gating. It has been suggested that 2 – 3 LTCCs in a junction can ensure a Ca^{2+} spark is activated at 0 *mV* (Inoue and Bridge, 2003). However, not all studies have agreed with these interpretations of high coupling fidelity and gain. Depolarisations to ~ 70 *mV* above resting potential (the actual voltage was unknown due to the loose-seal patch clamp method, but can be assumed to be near ~ 0 *mV*) yielded P_{CPL} ~ 0.7 in the presence of high $[Ca^{2+}]_O$ and a LTCC agonist, FPL-64176 (Wang, *et al.*, 2001). When extrapolated to more physiological conditions, these authors concluded that only one in 60 LTCC openings trigger a Ca^{2+} spark (Cheng and Lederer, 2008). Measurement of CICR at very negative potentials have also led Poláková, *et al.* (2008) to conclude that P_{CPL} is low. The rationale behind their approach was that during repolarisation to negative potentials (- 40 to - 120 *mV*), LTCC re-openings would not occur and measured CICR delays would be the result of I_{Ca} influx from first openings and CRU activation. Extrapolation to 0 *mV* yielded a $P_{CPL} < 0.05$, although the authors assumed that $\tau_{O,LTCC}$ was *not* voltage-dependent (in contrast to Josephson, *et al.*, 2010b) and it is unclear how well whole-cell tail currents can be used to measure $\tau_{O,LTCC}$ at very negative potentials due to problems associated with voltage-clamp speed.

EC coupling latency

The latency of Ca^{2+} transients in voltage-clamped and field-stimulated myocyes have been measured at 2 - 5 *ms* from the stimulus pulse (Cannell, *et al.*, 1987b; Wier, *et al.*, 1987; Beuckelmann and Wier, 1988; Cheng, *et al.*, 1994; Isenberg and Han, 1994; Wier, *et al.*, 1994; Cannell, *et al.*, 1995). When SR Ca^{2+} release was inhibited, the delay to the appearance of the trigger fluorescence was the same, suggesting that SR Ca^{2+} release followed the Ca^{2+} trigger closely (Cannell, *et al.*, 1994). Ca^{2+} spike latencies during AP-clamp were between 2 – 6 *ms* (Inoue and Bridge, 2003), which supports the idea that the majority of SR Ca^{2+} release occurs during the early repolarising phase of the AP (Sah, *et al.*, 2001; Sah, *et al.*, 2002; Inoue and Bridge, 2003; Cooper, *et al.*, 2010).

When Ca^{2+} transients were evoked at increasing step potentials, latency decreased (Isenberg and Han, 1994), which shows that the delay in CICR qualitatively follows the increase in

rate of LTCC activation (and open probability), rather than i_{Ca}, which decreases with membrane potential. When Ca^{2+} spikes were evoked with step pulses to 0 *mV*, latency increased with holding potential (*Altamirano and Bers, 2007b*), which suggests that CICR is sensitive to the number of LTCCs available. In contrast, Ca^{2+} spike latency was relatively insensitive to reduced $[Ca^{2+}]_O$ (0.25 *mM*) during depolarisations to 0 *mV*, which implies that I_{Ca} is normally more than sufficient to trigger SR Ca^{2+} release (Altamirano and Bers, 2007b). However, the latencies reported by Altamirano, *et al.* were much longer than those reported elsewhere (~ 15 – 40 *ms*), although the analysis method was not described. When Ca^{2+} spikes were evoked using tail currents (– 120 to – 40 *mV*), Ca^{2+} spikes occurred with a delay of ~ 1 *ms* from the repolarising step (Poláková, *et al.*, 2008). This value is close to the maximum activation rate constant of RyR channels measured in lipid bilayers (Laver and Honen, 2008), although it is possible that problems associated with voltage-clamp settling time and image resolution (0.5 *ms/line*) may make this an upper estimate. By recording Ca^{2+} sparklets using loose-seal patch-clamp, Wang, *et al.* (2004) measured a mean Ca^{2+} sparklet to Ca^{2+} spark latency of 6.7 *ms*, which is slow compared to the other studies since i_{Ca} had been augmented by FPL-64176 and 20 *mM* $[Ca^{2+}]_O$. In fact, the loose-seal patch clamp technique may have some significant disadvantages for such analyses (see below in section 1.5).

1.5. Ryanodine receptor, the SR calcium release channel

The RyR channel is the primary protein target for CICR in cardiac muscle (Meissner and Henderson, 1987; Lai, *et al.*, 1988). Unfortunately, direct measurement of RyR channel characteristics *in situ* is difficult because the channels are located in the SR and not easily subjected to conventional on-cell patch-clamping. While purification and reconstitution into lipid bilayers or use of lipid vesicles have been useful in obtaining single RyR channel properties, these techniques do not examine the function of a CRU array, nor can they examine any RyR regulation that results from junction geometry. On the other hand, while live-cell imaging of Ca^{2+} sparks can record the activity of an intact CRU, this technique does not record current directly. Therefore, gating properties obtained from a range of techniques must be evaluated together to gain insight into the function and regulation of RyR channel clusters in the living myocyte (for a review, see Fill and Copello, 2002).

Activation by cytosolic calcium

The most notable characteristic of an RyR channel is its ability to open in response to $[Ca^{2+}]_i$. Studies in cardiac vesicles and reconstituted bilayers have revealed that RyR open probability ($P_{O,RyR}$) increases with $[Ca^{2+}]_i$ to a maximum of ~ 0.5 – 0.9 (K_D ~ 0.6 – 1.6 μM), depending on $[Mg^{2+}]$ and [ATP] (Schiefer, *et al.*, 1995; Xu, *et al.*, 1996; Copello, *et al.*, 1997; Zahradníková, *et al.*, 1999; Laver and Honen, 2008). Though the RyR homo-tetramer contains four Ca^{2+} binding sites, it is unclear how many of these need to be occupied for the channel to activate. Some studies have suggested that the Ca^{2+}-dependence of RyR activation kinetics is variable (*e.g.* Schiefer, *et al.*, 1995; Copello, *et al.*, 1997), while others have suggested that three or more sites need to be occupied (Zahradníková, *et al.*, 1999; Laver and Honen, 2008). At the whole-cell level, the amplitude of Ca^{2+} transients evoked by LTCC tail currents displayed a linear relationship with current amplitude, which suggested that only one Ca^{2+} was sufficient to open an RyR (Fan and Palade, 1999). Another study measuring Ca^{2+} sparks revealed a square relationship between i_{Ca} and Ca^{2+} spark activation, suggesting 2 Ca^{2+} ions are required (Santana, *et al.*, 1996). This non-linearity may have been revealed by the reduced I_{Ca} density. In skinned Purkinje fibres, Fabiato (1985b) showed that Ca^{2+} transient amplitude increased by the 1.5 – 2.1th power of $[Ca^{2+}]_i$, although it was clear to him that the rate of solution change was important and this may have limited the apparent $[Ca^{2+}]_i$-dependence of CICR.

Inactivation and adaptation

$[Ca^{2+}]_i$ may also have an inhibitory effect on RyR gating, as suggested by a reduction in the amplitude of Ca^{2+} transients in skinned fibres at high $[Ca^{2+}]_i$ (> 3 μM, Fabiato, 1985b) and in $P_{O,RyR}$ in single-channel studies at $[Ca^{2+}]_i$ above 200 μM (Meissner and Henderson, 1987; Laver, *et al.*, 1995; Schiefer, *et al.*, 1995; Copello, *et al.*, 1997; Györke and Györke, 1998; Laver and Honen, 2008, although see Chu, *et al.*, 1993). Single-channel recordings suggest that $[Ca^{2+}]_i$-dependent inactivation (sometimes referred to as 'desensitisation' in earlier literature to differentiate this mechanism from voltage-dependent inactivation) is due to a disproportionately large decrease in open time ($\tau_{O,RyR}$) at high $[Ca^{2+}]_i$ (Laver and Honen, 2008). It has been suggested that one inhibitory site is located in the cytosolic domain of the RyR and that it had slow kinetics, with a high affinity for Ca^{2+} (Fabiato, 1985b), although a more recent study suggests there may be another inhibitory site that is predominantly occupied by Mg^{2+} (Laver and Honen, 2008).

Like $[Ca^{2+}]_i$-dependent inactivation, 'adaptation' was originally described as a reduction in $P_{O,RyR}$ during elevated $[Ca^{2+}]_i$ (Gyorke and Fill, 1993). However, unlike inactivation, adaptation followed a much slower time-course (seconds) and these RyRs could be re-activated by a larger Ca^{2+} stimulus (Gyorke and Fill, 1993). The idea was that this slow mechanism could be involved in regulating Ca^{2+} homeostasis when $[Ca^{2+}]_i$ is increased for sustained period. A subsequent study appeared to show that the rate of adaptation was sensitive to Mg^{2+} and the phosphorylation state of the RyR channels (Valdivia, *et al.*, 1995). However in both of these studies, adaptation was observed using photolysis of caged Ca^{2+} (DM-nitrophen) to activate single RyR channels in bilayers. This technique has since been heavily scrutinised (see Lamb, 1997; Gyorke, 1999; Zahradníková, *et al.*, 1999; Lamb, *et al.*, 2000; Sitsapesan and Williams, 2000). Originally, Gyorke and colleagues had thought that the photolysis of DM-nitrophen produced a step increase in $[Ca^{2+}]_i$ (to 200 *nM*), which caused the average RyR to open rapidly (~ 1.1 *ms*), then close slowly (~ 1.3 *s*) despite a maintained agonist concentration. While $P_{O,RyR}$ was declining, a larger $[Ca^{2+}]$ stimulus could be un-caged to re-activate the RyR. However, the initial opening rate was suspiciously high (~ 5×10^9 */M/s*), which caused a re-evaluation of the un-caging behaviour. It was shown that flash photolysis of DM-nitrophen produced a large over-shoot of $[Ca^{2+}]_i$ (as high as ~ 60 *μM* in conditions similar to the original experiments, Zucker, 1993; Ellis-Davies, *et al.*, 1996; Lamb, 1997), which could cause $[Ca^{2+}]_i$-inactivation, rather than a new phenomenon. On the other hand, it was argued that although the high $[Ca^{2+}]_i$ might explain the fast opening rate and long opening (*e.g.* Zahradnikova and Zahradnik, 1995), the brevity (< *ms*) of the pulse could not have caused $[Ca^{2+}]_i$-dependent inactivation. In any case, inactivation would not have allowed the channel re-activate. Further investigation revealed that $P_{O,RyR}$ was well correlated with the duration of the flash pulse, rather than steady-state $[Ca^{2+}]_i$, suggesting that the 'adaptation' behaviour was a phenomenon related to extremely high $[Ca^{2+}]_i$ (Lamb, *et al.*, 2000). Finally, experiments using a different method to produce step changes in $[Ca^{2+}]_i$ (fast solution changers) showed a lower RyR activation rate, a more moderate open time and could not be activated by a large stimulus (Schiefer, *et al.*, 1995; Sitsapesan, *et al.*, 1995), consistent with $[Ca^{2+}]_i$-dependent inactivation. Presently, there appears to be agreement that adaptation and $[Ca^{2+}]_i$-inactivation are the same mechanism (Gyorke, 1999).

Around the same time that adaptation was being postulated in isolated RyRs, Yasui, *et al.* (1994) showed in isolated myocytes that further Ca^{2+} release could be elicited by a larger

stimulus ~ 50 *ms* following a previously evoked Ca^{2+} transient. Though the original authors attributed this observation phenomenon to adaptation, it has since been shown that following maximal SR Ca^{2+} release (*i.e.* at ~0 *mV*), a substantial fraction of $[Ca^{2+}]_{SR}$ is still available (accessed by application of caffeine, Sham, *et al.*, 1998). When Ca^{2+} spikes were evoked at short delay, it was discovered that the pattern of release was complementary. That is, CRUs were only activated by the second stimulus if they had failed in the first stimulus (Sham, *et al.*, 1998; DelPrincipe, *et al.*, 1999). This is consistent with previous results, which had shown that secondary release amplitudes that were negatively-correlated with that of the primary event (Fabiato, 1985b; Cheng, *et al.*, 1996).

Regulation by SR calcium

RyR channels also appear to be sensitive to $[Ca^{2+}]_{SR}$, although it is unclear whether the effect is direct. An early lipid bilayer study showed that when activated by (sub-maximal) 10 μM $[Ca^{2+}]_i$, $P_{O,RyR}$ was insensitive to $[Ca^{2+}]_{SR}$ even when it was increased to 4 mM (Sitsapesan and Williams, 1994). This observation led the authors to reject the possibility that Ca^{2+} flux through the RyR channel could access its own cytosolic activation sites: a 'feed-through' activation mechanism that was first suggested for skeletal (Tripathy and Meissner, 1996) then also cardiac (Xu and Meissner, 1998) RyRs. However, when sulmazole was added (which increases $[Ca^{2+}]_i$-sensitivity of RyR by interacting with the caffeine binding site), $P_{O,RyR}$ became sensitive to $[Ca^{2+}]_{SR}$ (Sitsapesan and Williams, 1994; Sitsapesan and Williams, 1997). Subsequent studies found similar effects using ATP (Lukyanenko, *et al.*, 1996; Györke and Györke, 1998) and use of trypsin in the luminal bath appeared to abolish this $[Ca^{2+}]_{SR}$-sensitivity (Ching, *et al.*, 2000), suggesting that CSQ may play an important role as the luminal 'Ca^{2+} sensor' (Gyorke, *et al.*, 2004; Qin, *et al.*, 2008), although it is unclear how trypsin affected channel integrity. In the intact myocyte, increased $[Ca^{2+}]_{SR}$ was associated with steep increases in evoked (*e.g.* Han, *et al.*, 1994; Bassani, *et al.*, 1995) and spontaneous SR Ca^{2+} release (Cheng, *et al.*, 1996; Lukyanenko, *et al.*, 1996; Díaz, *et al.*, 1997; Satoh, *et al.*, 1997). The prevalence of increased $[Ca^{2+}]_{SR}$ and an associated increase in SR Ca^{2+} release in some disease states has led to the coinage of term 'store overload-induced Ca^{2+} release' (SOICR, *e.g.* Jiang, *et al.*, 2004), though it does not appear to be a distinct mechanism from the $[Ca^{2+}]_{SR}$-sensitivity described above.

Recent single-channel studies and complementary computer modelling have re-kindled support for the 'luminal triggered feed-through' mechanism for RyR channel activation

(Laver, 2007; Laver and Honen, 2008). By examining only the closed durations, it was shown that the RyR channel had limited sensitivity to $[Ca^{2+}]_{SR}$ (only when < 300 *nM*) even in the presence of ATP. The concept behind this analysis is that in the closed state, any effect of feed-through and associated CICR would be absent (unlike previous studies, which examined $P_{O,RyR}$), thus allowing the true $[Ca^{2+}]_i$-sensitivity to be examined at various $[Ca^{2+}]_{SR}$. Computer modelling of this work suggested that the luminal Ca^{2+} activation sites are predominantly occupied by Mg^{2+} (Laver, 2007; Laver and Honen, 2008). However, a recent paper has suggested that the cytosolic activation sites of an RyR are shielded from its own release flux (Liu, *et al.*, 2010). This was based on the observation that $P_{O,RyR}$ only increased moderately even when release flux was larger than that expected under physiological conditions (Liu, *et al.*, 2010). To explain this, a simple calculation of diffusion from a pore was used to show that this flux would be too low to produce enough Ca^{2+} to reach the activation sites (Liu, *et al.*, 2010). However, the (non-trivial) calculation from flux to $[Ca^{2+}]$ near the Ca^{2+} sensor in this study is unclear (*e.g.* the equation supplied does not include time-dependence of Ca^{2+} accumulation near the pore). Such flux 'shielding' seems even more problematic when the same study also showed that when two RyRs were incorporated into the bilayer, the Ca^{2+} flux from one channel could increase the ensemble P_O, even though the separation distance between the channels would be larger than the distance between a channel's pore and its own activation sites. The authors explain that this discrepancy could be due to 'Ca^{2+} occupancy', wherein an active RyR channel would have its activation sites already occupied and therefore, insensitive to the local Ca^{2+} and/or 'fateful inactivation', wherein channel inactivation fatefully follows activation, rendering the RyR channel insensitive to further Ca^{2+} stimulation, although this has not been shown for RyRs (Fill and Copello, 2002).

Closure of the calcium release unit

Robust Ca^{2+} spark termination (*e.g.* ~ 20 *ms*, Cheng, *et al.*, 1993) despite a sustained trigger (Sham, *et al.*, 1998) suggests that reliable mechanism(s) must exist to inhibit the positive-feedback of local CICR. Several mechanisms have been proposed to explain CICR termination (see Fill and Copello, 2002 for a review). These include intrinsic RyR gating mechanisms (described above), as well as phenomena that result from the RyR channel cluster arrangement and/or location in a spatially-restricted junction. They are: *(1)* $[Ca^{2+}]_i$-dependent inactivation (see above), *(2)* stochastic attrition and *(3)* SR Ca^{2+} depletion.

Stochastic attrition arises from a finite probability that all of the independently-gating RyRs within a CRU can be closed simultaneously (Stern, 1992b). The average time for stochastic attrition to occur increases steeply with the number of RyR channels in a CRU (Stern, 1992b; Stern and Cheng, 2004, see Eqn. 3.1), such that it becomes highly unlikely for reported CRUs containing ~ 200 (Franzini-Armstrong, *et al.*, 1999; Chen-Izu, *et al.*, 2006; Soeller, *et al.*, 2007) or 14 RyRs (Baddeley, *et al.*, 2009; Cannell and Kong, 2012). The rate of stochastic attrition can be increased if RyR channels within a CRU are allosterically coupled, so that the gating properties of one RyR are dependent on that of its neighbour due to conformational change, likely transduced via FKBP-12.5. 'Coupled gating' was first suggested for skeletal RyR, when isolated RyR channel clusters exhibited multiples of the recorded unitary current without intermediary steps (*i.e.* no multiples of the single-channel current, Marx, *et al.*, 1998). The application of this mechanism to cardiac RyR was supported by computer modelling at the time (Stern, *et al.*, 1999) and seemed to be observed in single-channel studies (Marx, *et al.*, 2001). Application of rapamycin, which was known to remove FKBP-12.6 from the RyR channels (Kaftan, *et al.*, 1996) revealed the expected intermediate steps, suggesting that FKBP-12.6 played a role in coupling the RyRs (Marx, *et al.*, 2001). However, rapamycin is also known to decrease RyR channel conductance, which potentially confounds the interpretation of the results in the context of likely functional coupling mediated by Ca^{2+}. FKBP-12.6 over-expression studies showed that $P_{O,RyR}$ was reduced, but that the synchronicity of SR Ca^{2+} release was improved (Gomez, *et al.*, 2004; Loughrey, *et al.*, 2004). Some computer models have suggested that coupled gating is insufficient to terminate release (*e.g.* Jafri, *et al.*, 1998) and may require an additional mechanism (*e.g.* $[Ca^{2+}]_{SR}$-sensitivity, Sobie, *et al.*, 2002).

The extent of $[Ca^{2+}]_{SR}$ depletion and its effect on CRU gating remains controversial. It was initially thought that Ca^{2+} transients only released a fraction of the SR content as assessed by caffeine (Bassani, *et al.*, 1995; Sham, *et al.*, 1998; Shannon, *et al.*, 2000; Shannon, *et al.*, 2003a). This might imply that additional $[Ca^{2+}]_{SR}$ remains available to be released again. However, closer examination revealed that regions that had initially released Ca^{2+} could not be activated again within ~ 50 *ms*, even with a larger stimulus (Yasui, *et al.*, 1994; Sham, *et al.*, 1998). Similarly, measurement of Ca^{2+} spark interval at highly active release sites revealed that P_{spark} was dramatically reduced below an interval of ~ 50 *ms* (Sobie, *et al.*, 2005, see also Tanaka, *et al.*, 1998; Wang, *et al.*, 2001). Although it is unclear what causes this apparent 'refractory period' (see Cheng, *et al.*, 1996; DelPrincipe, *et al.*, 1999),

measurement of Ca^{2+} spark amplitude restitution suggests ~ 100 - 200 *ms* is required to refill junctional SR Ca^{2+} ($[Ca^{2+}]_{JSR}$) (Brochet, *et al.*, 2005; Sobie, *et al.*, 2005; Ramay, *et al.*, 2011). This slow time-course is consistent with more recent measurements of local $[Ca^{2+}]_{SR}$ with a fluorescent indicator ('Ca^{2+} blink', Brochet, *et al.*, 2005), which show a time constant of recovery of ~ 180 *ms (*Zima, *et al.*, 2008b; Picht, *et al.*, 2011), as well as 'Ca^{2+} scrap' recovery (cell-wide $[Ca^{2+}]_{SR}$ fluorescence signals that recovered in ~ 150 *ms*, Shannon, *et al.*, 2003a). However, Ca^{2+} blink amplitude (relative to the caffeine-insensitive 'background' fluorescence) is small, dropping consistently by ~ 40 *%* (Zima, *et al.*, 2008b), similar to that measured from Ca^{2+} scraps (~ 60 %, Shannon, *et al.*, 2003a). From this result, the authors concluded that local $[Ca^{2+}]_{SR}$ depletion could not be solely responsible for the termination of Ca^{2+} sparks. Instead, another factor (*e.g.* CSQ) must exist to steepen and shift the relationship between $P_{O,RyR}$ and $[Ca^{2+}]_{SR}$. However, the measurement of $[Ca^{2+}]_{JSR}$ depletion may be severely hindered by the optical resolution and contamination of the depletion signal by neighbouring structures.

RyR channel (Ca^{2+} quark) and couplon (Ca^{2+} spark) fluxes

Early measurements of single RyR channel current in bilayers held at 0 *mV* yielded i_{RyR} ~ 4 *pA* using either 53 *mM* Ca^{2+} (Marx, *et al.*, 1998) or Ba^{2+} (Kaftan, *et al.*, 1996) as the charge carrier. This large unitary flux led researchers to suggest various mechanisms that would provide such a large conductance, including multiple pores and/or dielectric focussing of Ca^{2+} near the pore by a charged domain/fixed surface charges (for reviews, see Williams, *et al.*, 2001; Fill and Copello, 2002). However, later studies in more physiological conditions supported more modest unitary currents and therefore, more simple conductance schemes. For example, Mejia-Alvarez, *et al.* (1999) obtained i_{RyR} ~ 0.6 *pA* in 2 *mM* $[Ca^{2+}]_{SR}$.

Initial measurements of Ca^{2+} spark amplitude (~ 270 *nM*) gave rise to an estimated CRU flux of ~ 4 *pA* for 10 *ms*, which made it unclear (at the time) whether one or more RyR channels were responsible for a Ca^{2+} spark (Cheng, *et al.*, 1993, see also Eqn. 1.2). However, the result of Mejia-Alvarez, *et al.* (1999) and subsequent measurements of Ca^{2+} sparks fluxes suggest more than one RyR channel is almost certainly involved. Although Ca^{2+} spark amplitudes vary across studies (*e.g.* as large as ~ 20 *pA*, Izu, *et al.*, 2001), they appear to have a monotonically decaying distribution due to sampling by confocal microscope (*e.g.* Pratusevich and Balke, 1996; Song, *et al.*, 1997; Izu, *et al.*, 1998; Cheng,

et al., 1999). However, imaging of Ca^{2+} sparks at a single release site have led to varied conclusions. Some studies suggest that the amplitude distribution is modal (Bridge, *et al.*, 1999; Inoue and Bridge, 2003) and is associated with an average of 6 – 20 active RyRs (Soeller and Cannell, 2004), while others suggest that CRUs exhibit quantal release fluxes (Wang, *et al.*, 2004). The amplitude of one quantum was calibrated to be 1.2 *pA*, which is larger than the measured i_{RyR}, but smaller than a typical Ca^{2+} spark. One possibility is that each CRU is comprised of sub-clusters, as observed in peripheral couplings (Baddeley, *et al.*, 2009; Jayasinghe, *et al.*, 2012), which are able to be activated independently of each other, with a reduced probability of cross-activation (Xie, *et al.*, 2010). However, the concept of quantal release in cardiac CRUs is controversial (*e.g.* see Zahradnikova, *et al.*, 2010) because it has only been observed using the loose-seal patch clamp technique (Wang, *et al.*, 2001; Shen, *et al.*, 2004; Wang, *et al.*, 2004). This method was employed based on the assumption that it did not distort the local membrane system, while allowing activation of the LTCCs beneath the pipette (Wang, *et al.*, 2001). However, it is likely that membrane is distorted during loose-seal formation, which would alter the geometry of the local junction and the physical distances between LTCCs and RyRs and perhaps between RyRs (to allow quantal release, see below). On the other hand, if the seal was sufficiently 'loose', then voltage-control would be compromised (see discussion of loose-seal patch clamp by Roberts and Almers, 1992), which may have important effects on CICR efficiency due to the voltage-dependent LTCC gating kinetics and unitary current. Thus, gating behaviour of the CRU remains to be clarified.

The initial description of Ca^{2+} sparks as an 'elementary' event of EC coupling (Cheng, *et al.*, 1993) prompted a search for a smaller quantum. 'Ca^{2+} quarks' were proposed by Lipp and Niggli (1996) from the observation that Ca^{2+} transients evoked by photo-activation of DM-nitrophen did not show the wave-front spatial non-uniformities that should reflect Ca^{2+} sparks (Cannell, *et al.*, 1994). Furthermore, apparently 'sub-threshold' 2-photon activation of DM-nitrophen evoked SR Ca^{2+} release events that appeared smaller than Ca^{2+} sparks (Lipp and Niggli, 1998). However, the Ca^{2+} spark used in this study for comparison was ~ 6-fold more long-lasting than previously-reported events, which suggests that the comparison may have been made between a 'macro-spark' (Cheng, *et al.*, 1993) and small, out-of-focus Ca^{2+} sparks. It is difficult to interpret these studies due to: *(1)* the relatively large size and shape of the 2-photon photolysis spot (~ 60 *fL*, Lipp and Niggli, 1998; Denk, 1994) compared to a single RyR channel or even CRU (~ 5 *aL* junction, Brochet, *et al.*,

2005); *(2)* DM-nitrophen's substantial binding affinity for Mg^{2+} ($K_{D,Ca}$ = 5 *nM*, $K_{D,Mg}$ = 2.5 *μM*, Ellis-Davies and Barsotti, 2006; Faas, *et al.*, 2005), meaning 0 Mg^{2+} was used, which directly affects RyR channel gating (*e.g.* Xu, *et al.*, 1996); and *(3)* uncertainties over effects on EC coupling due to the introduction of 1 mM high-affinity buffer, though authors used 'loaded' DM-nitrophen (*i.e.* Ca^{2+}-DM-nitrophen), which should likely equilibrate *in situ* with Mg^{2+} and increase $[Ca^{2+}]_i$. Similar to quantal release, Ca^{2+} quarks can only occur if the RyR channels within a CRU are not well-coupled to their own or adjacent release flux (*e.g.* very insensitive to Ca^{2+} or increased separation distances, Baddeley, *et al.*, 2009; Xie, *et al.*, 2010, and/or reduced $i_{RyR}/[Ca^{2+}]_i$-sensitivity, see Zima, *et al.*, 2010; Porta, *et al.*, 2011; Sato and Bers, 2011). Nevertheless, the opening of single or few rogue RyR channels (Junker, *et al.*, 1994; Franzini-Armstrong, *et al.*, 1999), perhaps in the form of Ca^{2+} quarks, may occur and be responsible for diastolic SR Ca^{2+} 'leak' during diastole. However, the extent of this phenomenon is highly controversial (Bassani and Bers, 1995; Shannon, *et al.*, 2002; Santiago, *et al.*, 2010; Zima, *et al.*, 2010).

1.6. Aims of Study

This study seeks to clarify the importance of various biological and experimental factors that initiate and shape the Ca^{2+} spark. This involved examination of the activation and termination kinetics of Ca^{2+} sparks, as well as the effect of intracellular buffers and microscope blurring on the fluorescent signal. The focus of this work and its relevance to EC coupling is portrayed in Fig. 1.1 (modified from Cannell and Kong, 2011).

As described in section 1.4, data from recent studies have questioned the reliability of LTCC-RyR coupling during CICR. In particular, 'dyssynchronous' Ca^{2+} release in a disease model has highlighted the lack of clarity on the determinants of Ca^{2+} spark latency. This problem is addressed in Chapter 2 of this thesis, where the ability of an LTCC opening to trigger a CRU (P_{CPL}) was examined by measuring the latency of Ca^{2+} transients and Ca^{2+} sparks (Fig. 1.1, marked by red). The relative contributions of LTCC and CRU kinetics to the latency of Ca^{2+} spark production was estimated by using different voltage step protocols, tested using a simple computer model that incorporated channel parameters obtained from the literature and compared to latencies recorded during a recorded rat action potential.

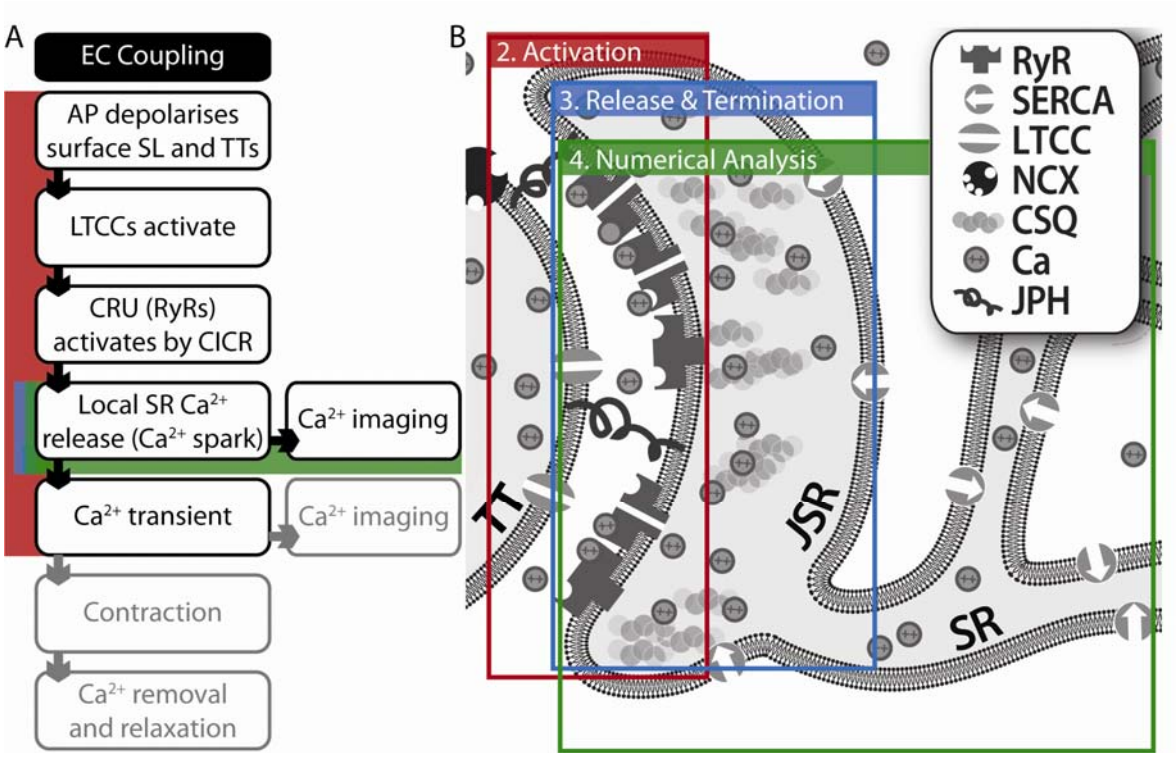

Figure 1.1 Schematic of CICR and local control (focus of study). (A) shows a linear representation of the processes that occur during cardiac EC coupling, starting from top to bottom. **(B)** shows a schematic of a dyad, through a cross-section of a transverse tubule (TT). The junctional sarcoplasmic reticulum (JSR) wraps around the tubule, where their membranes are separated by a small gap (not to scale). The relevant proteins are shown, including the ryanodine receptor (RyR), sarco-endoplasmic reticulum ATPase (SERCA), L-type Ca^{2+} channel (LTCC), Na^{+}-Ca^{2+} exchanger (NCX), calsequestrin (CSQ) and junctophillin (JPH). The focus of each the following results chapters (numbered 2 – 4, marked by red, blue and green, respectively) are indicated in both panels. See text for details. This figure has been modified and used with permission from Cannell and Kong, 2012.

Measurement of Ca^{2+} spark properties have suggested that a robust mechanism(s) terminates regenerative CICR, although the details of this is unclear (see section 1.5, Closure of the calcium release unit'). In Chapter 3, Ca^{2+} spark termination is investigated by examining the relationship between the amplitude and duration of release flux during spontaneous Ca^{2+} sparks, as well as long-lasting local events that occur when RyR open probability is reduced by tetracaine (Fig. 1.1, marked by blue). Characteristics that distinguish between the various termination mechanisms (*e.g.* Ca^{2+}-sensitivity, the presence of a refractory period) are used to determine the most likely candidate.

Finally, the effects of various buffers (including diffusible fluorescent Ca^{2+} dyes such as, Fluo-4 in the cytosol, or Fluo-5N in the SR) and microscope blurring on the recorded Ca^{2+} spark and Ca^{2+} blink were investigated (Fig. 1.1, marked by green). In Chapter 4, a new computer model containing a single junctional SR and adjacent junctional space is described. This model incorporated microscope blurring functions that were measured in experimental conditions, as well as a deformable CRU gating function that was altered to reproduce experimental Ca^{2+} sparks.

2. Activation of Local SR Ca^{2+} Release during Action Potentials

2.1. Background

Cardiac EC coupling (Sandow, 1952) begins with an AP that propagates across and into the cell via TTs. The AP activates I_{Ca} (Beeler and Reuter, 1970b), which then recruits Ca^{2+} sparks (Cheng, *et al.*, 1993) by CICR (Fabiato, 1983) to give rise to the whole-cell Ca^{2+} transient (Cannell, *et al.*, 1994; López-López, *et al.*, 1994; López-López, *et al.*, 1995). CICR occurs due to RyR channels (Inui, *et al.*, 1987; Rousseau, *et al.*, 1987; Lai, *et al.*, 1988), which are predominantly arranged in clusters or CRUs (Franzini-Armstrong, *et al.*, 1998; Franzini-Armstrong, *et al.*, 1999). It is thought that the activation of each CRU is triggered by local I_{Ca} (Stern, 1992b) to produce a Ca^{2+} spark. During EC coupling, it is likely that most (Sham, *et al.*, 1998), if not all, CRUs within the cell are activated by I_{Ca} to produce the Ca^{2+} transient (Cannell, *et al.*, 1994; Cannell, *et al.*, 1995). Since the Ca^{2+} transient results from spatio-temporal summation of Ca^{2+} sparks, its amplitude and time-course are determined by the variability in delay, extent and duration of Ca^{2+} spark activation.

Though the triggering of Ca^{2+} sparks is relatively synchronous under physiological conditions, (Cannell, *et al.*, 1994), their co-ordination may be compromised in heart failure, wherein cells isolated from animal models have exhibited ‘dyssynchronous’ evoked SR Ca^{2+} release (*e.g.* Litwin, *et al.*, 2000). Although this observation may be (partly) due to other changes associated with heart failure (*e.g.* T-tubule (re)-organisation and/or AP prolongation, Louch, *et al.*, 2004; Cannell, *et al.*, 2006; Cooper, *et al.*, 2010), it highlights the need to clarify the *physiological* time-course of SR Ca^{2+} release activation during an AP and the principle factor(s) that is responsible for this delay. Any latency in CICR from the time of electrical stimulation likely arises from the kinetics of: *(1)* LTCC activation; *(2)* Ca^{2+} diffusion from I_{Ca} to RyR channels; *(3)* RyR activation; *(4)* diffusion of Ca^{2+} from the release site; and *(5)* dye-binding, though their relative contributions are unknown and will be the subject of this study.

Previous studies using fluorescent indicators to measure $[Ca^{2+}]_i$ have shown that during an AP, Ca^{2+} transients in rat myocytes occur $2 - 4$ *ms* after application of the field stimulus and at no detectable delay from the Ca^{2+} trigger (Cannell, *et al.*, 1994). This suggests that processes *(2)* to *(5)* occur rapidly (within the time resolution of the records, which was

~ 2 *ms*) and that LTCC activation required an upper limit of 2 – 4 *ms* due to the unknown delay caused by using field electrodes to excite the cell to the threshold potential (Cannell, *et al.*, 1994). Similarly, Ca^{2+} spikes in rabbit myocytes were shown to occur 2 - 6 *ms* after the peak of the AP (+ 50 *mV*, Inoue and Bridge, 2003).

However, I_{Ca} during an AP is complex due to the changes in LTCC gating kinetics and the driving force for Ca^{2+} entry. The whole-cell current is given by Eqn. 2.1 (modified from Eqns 1.1 and 1.2), where n_{LTCC} is number of available LTCCs, which is the product of the total number of LTCCs and the fraction available as experimentally determined in single-channel studies by the proportion of sweeps where no openings are observed (McDonald, *et al.*, 1994), $P_{O,LTCC}$ is determined by the mean open ($\tau_{O,LTCC}$) and closed times ($\tau_{C,LTCC}$) and i_{Ca} is LTCC unitary current.

$$I_{Ca} = n_{LTCC} \cdot P_{O,LTCC} \cdot i_{Ca} \qquad \textbf{Eqn. 2.1}$$

where,

$$P_{O,LTCC} = \frac{\tau_{O,LTCC}}{\tau_{O,LTCC} + \tau_{C,LTCC}}$$

LTCC unitary current is important as the trigger for CICR and dependent on the electrochemical gradient of Ca^{2+} across the sarcolemma and described by the Goldman-Hodgkin-Katz flux equation (Eqn. 2.2, Hille, 2001), where *P* is permeability, *z* is valence (2), V_m is membrane potential in *V*, *R* is the Universal Gas constant (8.314 *J/mol/K*), *F* is Faraday's constant (96485 *C/mol*) and *T* is temperature in *K*.

$$i_{Ca} = Pz^2 \cdot \frac{V_m F^2}{RT} \cdot \frac{[Ca^{2+}]_i - [Ca^{2+}]_o \cdot e^{-\frac{zFV_m}{RT}}}{1 - e^{-\frac{zFV_m}{RT}}} \qquad \textbf{Eqn. 2.2}$$

The single-channel Ca^{2+} current diminishes upon depolarisation to the peak of the AP (typically > + 40 *mV*), which is far more positive than the voltage range over which CICR is maximal during voltage-clamp steps (~ 0 *mV*, Cannell, *et al.*, 1987b; Wier, *et al.*, 1987; Beuckelmann and Wier, 1988; Isenberg and Han, 1994). On the other hand, LTCC gating kinetics are voltage-, $[Ca^{2+}]_i$- and time-dependent (McDonald, *et al.*, 1994). Faster activation occurs at more positive potentials (McDonald, *et al.*, 1994; Josephson, *et al.*,

2010b) and is associated with shorter SR Ca^{2+} release latencies (Isenberg and Han, 1994; Inoue and Bridge, 2005). It has been shown that the rate of *repolarisation* during the AP has a strong influence on the Ca^{2+} transient (Sah, *et al.*, 2002) which suggests there may be a complex interplay of variables that determine CICR latency. A possible explanation for this phenomenon is that it takes time for LTCCs to open so that during early repolarisation, the driving force for Ca^{2+} entry is increased while the majority of LTCCs are open. It has been suggested that this reduced impact of the stochastic delay in LTCC opening by synchronous increase in driving force for Ca^{2+} entry is an important factor for producing a more synchronised recruitment of Ca^{2+} sparks and a uniform Ca^{2+} transient (Inoue and Bridge, 2003; Cooper, *et al.*, 2010).

At a given potential, the stochastic delay of LTCC activation ($\tau_{act,LTCC}$) is determined by $\tau_{C,LTCC}$ and n_{LTCC} (Eqn. 2.3). Assuming independent gating, the apparent rate constant for leaving the closed state is the sum of all rate constants for leaving that state (Colquhoun and Hawkes, 1983), which would place a lower limit for the mean latency for a Ca^{2+} spark to be evoked if a single LTCC can trigger a spark (*e.g.* Santana, *et al.*, 1996; Altamirano and Bers, 2007b).

$$\tau_{act,LTCC} = \frac{\tau_{C,LTCC}}{n_{LTCC}} \qquad \textbf{Eqn. 2.3}$$

Santana, *et al.* (1996) showed that at negative potentials (- 40 to - 30 *mV*), a single LTCC was sufficient to activate a Ca^{2+} spark. However, at more positive potentials where i_{Ca} is reduced, P_{spark} and the probability of a single LTCC opening triggering a Ca^{2+} spark (‘coupling fidelity’, Wang, *et al.*, 2001) may be reduced. This effect could be potentially offset by the increase in $\tau_{O,LTCC}$ at positive potentials (Josephson, *et al.*, 2010b), although this has not been shown. Certainly, it has been suggested that CICR requires few (one at 0 *mV*, Altamirano and Bers, 2007b and three at + 50 *mV*, Inoue and Bridge, 2003) to ~ 60 LTCCs (at 0 *mV*, Wang, *et al.*, 2001; Cheng and Lederer, 2008; Poláková, *et al.*, 2008) to ensure a sufficient number of LTCC openings occur rapidly to trigger a Ca^{2+} spark. However these latter studies did not measure SR Ca^{2+} release latencies and probabilities under physiological conditions and CICR fidelities were extrapolated to the physiological case (Wang, *et al.*, 2001; Cheng and Lederer, 2008; Poláková, *et al.*, 2008). On the other hand, Inoue and Bridge (2003) compared Ca^{2+} spike latencies during APs in intact cells to

LTCC kinetics measured from single channels incorporated into lipid bilayers. Similarly, Altamirano and Bers (2007b) altered I_{Ca} in intact myocytes, however they only examined its effect on SR Ca^{2+} release at 0 *mV*, which may not reflect the situation during the AP.

To clarify the distribution of Ca^{2+} spark latency during EC coupling, Ca^{2+} transients and sparks evoked by AP-clamp were examined at high temporal resolution and signal-to-noise. The relative contributions of LTCC (process *1*, see above) and RyR channel (process *3*) activation kinetics were determined by comparing Ca^{2+} transient and Ca^{2+} spark latencies when SR Ca^{2+} release was evoked by depolarising and repolarising steps. The strategy used to reduce P_{spark} involved reducing LTCC availability by nifedipine, which also allowed investigation of how a reduced I_{Ca} current density affects its ability to trigger SR Ca^{2+} release, as well as an estimate of n_{LTCC} during an AP.

2.2. Methods

Preparation of isolated myocytes

Single cardiac ventricular myocytes were obtained by enzymatic dissociation (Powell and Twist, 1976; Hohl, *et al.*, 1982; Bkaily, *et al.*, 1984; Mitra and Morad, 1985). Male Wistar rats (200 – 300 *g*, 6 – 9 weeks old) were anaesthetised with pentobarbital (140 *mg/kg*, i.p.) as approved by the University of Auckland Animal Ethics Committee (R330/1, R649/1). When surgical anaesthesia was achieved (~ 2 *min*), the chest cavity was opened by one cut through the rib-cage on the right side of the sternum, a second cut across the thorax just anterior of the diaphragm and a third cut through the left rib-cage, parallel to the sternum. The heart was lifted gently and removed by cutting the aorta several *mm* from the base of the heart and quickly washed in modified Ca^{2+}-free Tyrode's solution (in *mM*: 140 NaCl, 4 KCl, 1 $MgCl_2$, 10 HEPES, 10 D-glucose, *pH* = 7.4 at room temperature, ~ 22 *ºC*). The aorta was cannulated on a Langendorff perfusion system (37 *ºC*) and perfused with 50 *mL* oxygenated Ca^{2+}-free Tyrode's solution for 5 *min.* The time from when surgical anaesthesia was achieved to the start of perfusion was maintained to within 30 – 60 *s*. The heart was then perfused with Ca^{2+}-Tyrode's solution that also contained 200 *µM* $CaCl_2$, collagenase II (1 *mg/mL*, Worthington Biochemical Corp., New Jersey, U.S.A.) and protease I (0.1 *mg/mL*, Sigma-Aldrich, Missouri, U.S.A.) for 10 – 20 *min* until the heart developed a glassy appearance and rapid drip rate. The ventricles were then excised and placed into low Ca^{2+}-Tyrode's solution (100 or 150 µM, 37 *ºC*) and minced finely with dissecting scissors.

The resulting cell suspension was separated from the tissue pieces by decanting into a tube, which was then allowed to sediment and the supernatant removed. The sedimented pellet of cells was re-suspended in 0.5 or 1 *mM* Ca^{2+}-Tyrode's solution with 0.5 *mM* sodium pyruvate in petri dishes for storage at room temperature. The minced tissue pieces were repeatedly re-suspended in fresh low Ca^{2+}-Tyrode's solution, triturated with a wide-bore Pasteur pipette if necessary, sedimented and re-suspended in storage solution to yield several dishes of myocytes. All cells were used within ~ 6 *hrs*.

Myocytes were incubated for 25 *min* (room temperature, in a darkened environment) with 5 *μM* Fluo-4/*AM* or Fluo-5F/*AM* (acetoxymethyl ester, Gee, *et al.*, 2000, Invitrogen, California, U.S.A.) by adding 2.5 *μL* of a 2 *mM* stock (2.5 % Pluronic® F-127 in dimethyl sulfoxide, Invitrogen and Sigma-Aldrich, respectively) to 1 *mL* of cell suspension. Dye-loaded cells were allowed to sediment for 5 min, then the incubation solution was removed and the cells suspended in ~ 2 *mL* of storage solution.

Electrophysiology of cardiac myocytes

Two main perfusion systems were used in these studies, which were used interchangeably on the imaging systems described, depending on the functionality required. Both systems used rectangular Perspex chambers with number 1.5 glass cover-slip bottoms (glued on with silicone rubber), which were served by gravity-fed reservoirs selected by an electronic valve system (VC-6, Warner Instruments, Connecticut, U.S.A.). Solution flow was along the long-axis of the rectangular chamber.

The first chamber was designed for field stimulation, with lengths of platinum wire placed along each longitudinal side of the rectangular chamber to act as electrodes. These were connected to a signal generator (*e.g.* SD9 stimulator, Grass Technologies, Rhode Island, U.S.A.). The solution was removed by suction pump system. This was comprised of a modified plastic pipette tip (bent slightly after heating and bevelled) dipped into one end of the chamber and was connected through plastic tubing to a closed glass jar. A suction pump was used to create negative pressure in the glass jar, which could then remove solution from the chamber. The plastic pipette tip was attached to an extra piece of Perspex whose height could be adjusted with a screw, which allowed the height of the solution in the chamber to be adjusted by changing the height of the pipette tip.

The second chamber was designed for electrical recordings and contained a chloride-coated silver wire along one longitudinal side to act as ground. The solution level was controlled by a servo-motor system as described by Cannell and Lederer (1986b). The solution was removed from one end of the bath by a gear pump (through plastic tubing with its opening fixed near the bottom of the bath). The solution level nearby was detected by a brass float that was coated with adhesive (Photomount™, 3M Technologies, Minnesota, U.S.A.) to make it hydrophobic. This was attached via a bent stainless steel tube (25G) to a force transducer (SensorOne Technologies Corp., California, U.S.A.), which was then connected to an electrical circuit (see Cannell and Lederer, 1986b) that altered the voltage across the pump (and therefore, pump rate) depending on the voltage across the force transducer. Thus, an increase from a set solution level (where pump rate equalled inflow rate) caused an increase in the pump rate and vice versa. The time-constant of solution application in this chamber was measured by detecting the appearance of fluorescein at different locations within the bath. The time constant for solution change was ~ 30 *s* for central regions of the chamber (data not shown). The edges were not used due to inaccessibility by the patch-pipette. During experiments, ~ 2 – 5 *min* was allowed for equilibration during drug application and ~ 15 *min* for drug wash-out.

For whole-cell voltage-clamp (Lee, *et al.*, 1980; Hamill, *et al.*, 1981) experiments, pipettes were pulled from boroscillicate glass capillaries (1.5 *mm* O.D., 0.86 *mm* I.D., Harvard Instruments, Massachusetts, U.S.A.) on a Flaming Brown Pipette Puller (P-87, Sutter Instrument Co., California, U.S.A.) and filled with (in *mM*): 100 CsAsp, 30 CsCl, 5 MgATP, 10 HEPES, 100 *μM* Fluo-4 (or 5F) pentapotassium salt (*pH* = 7.2 at room temperature with CsOH) to result in pipette resistances of ~ 2 - 3 *MΩ*. The pipette solution was made fresh daily and stored on ice. The pipette solution usually contained no Na^+ to reduce the possibility of the NCX in contributing to trigger Ca^{2+} during EC coupling, although preliminary data in 5 and 10 *mM* [Na^+] suggest that the general conclusions of this study are unchanged (not shown). During recording, cells were superfused with Tyrode's solution (see above) that contained 1 *mM* $CaCl_2$ and 10 *mM* tetraethylammonium chloride. Unless otherwise stated, a VE-2 amplifier and headstage (Alembic Instruments Inc., Montreal, Canada) was used with series resistance compensation enabled. In these experiments, AP-clamp was employed to reduce cell to cell variability in AP time-course. The AP used as the command profile for AP-clamp experiments was measured using an Axopatch 200B amplifier and CV201A headstage (Molecular Devices, California, U.S.A.)

in current-clamp mode. The pipette solution was 140 *mM* KCl, *pH* = 7.2 at room temperature with KOH. For nifedipine dose-response curves, the pipette solution also contained 10 *mM* NaCl.

Cells were stimulated at 0.2 *Hz*. For depolarising steps, membrane potential (V_m) was ramped from a holding potential of - 80 to -40 *mV* in 550 *ms* to inactivate the fast Na^+ current and then stepped to a test potential (-30 to +50 *mV*) for 200 *ms*. For repolarising steps, V_m was stepped from - 80 to + 100 *mV* for 5 *ms* and stepped to a test potential (- 120 to + 20 *mV*) for 21 *ms*. A pre-conditioning train of 4 step pulses to 0 *mV* for 200 *ms* were used. The pre-pulse to + 100 *mV* meant that LTCCs were activated, but could not conduct Ca^{2+} until the membrane was repolarised to a potential that increased the driving force for Ca^{2+} entry. Longer pre-pulses of 10, 20, 30 *ms* were tested and showed no difference in the latency of Ca^{2+} transients (data not shown). Both of these protocols were performed immediately following the AP-clamp protocol. Junction potential was estimated to be 14 *mV* (Barry, 1994) and corrected for during analysis. The amplitude of I_{Ca} was taken as the difference between the measured peak current and the value at the end of the test pulse (Shorofsky and January, 1992).

Ca^{2+} transient and Ca^{2+} spark imaging

For nifedipine dose-response measurements, fluorescence was recorded using an inverted Nikon Diaphot 200 microscope with a 1.3 numerical aperture (*N.A.*), 40 x oil immersion objective. Excitation light was provided by a Xenon arc lamp (L.T.I. A1020) and the photomultiplier tube signal was converted at 10 *nA/V* and low-pass filtered at 3.15 *kHz* (Ithaco 4392 dual 24 *dB/octave* filter) prior to digitisation by Digidata 1200 for viewing in PClamp *v*9.2 (Molecular Devices). A shutter system (SD-10 shutter drive/timer, Uniblitz, New York, U.S.A.) triggered by PClamp was used to limit illumination of the cell to the period of the test pulse.

For all other experiments, an inverted LSM 710 (Zeiss, Oberkochen, Germany) confocal microscope was used with a 1.1 *N.A.*, 40 x water-immersion objective. The microscope pinhole and scan motors were checked and calibrated using the Zeiss software every-day ~ 2 *hrs* prior to the start of experiments. Line-scan images were triggered by PClamp using a custom-written macro for Zen 2008 software (*Zeiss*). PClamp controlled the voltage-clamp and at the start of the test pulse, also activated an LED that was detected by a

transmitted-light PMT and stored in the second channel of the image. Images were recorded at 16-bit, ~ 0.35 *ms/line* and 0.083 *µm/px*, for ~ 50 *ms* per stimulus, with the line-scan placed parallel to the long-axis of the cell. Recording of spontaneous Ca^{2+} sparks used similar systems.

Drugs

15 *µM* nifedipine (Sigma-Aldrich) was used to reduce LTCC availability (McDonald, *et al.*, 1994) and therefore reduce P_{spark} so individual Ca^{2+} sparks could be measured. 10 *µM* FPL-64176 (FPL, Tocris Bioscience, Bristol, U.K.) was used to prolong $\tau_{O,LTCC}$, without altering $\tau_{C,LTCC}$ (Rampe and Lacerda, 1991). Nifedipine was made as a 10 *mM* stock solution in methanol, while the FPL stock was made to 10 *mM* in Milli-Q water (Millipore Corp., Massachusetts, U.S.A.). Both were stored at 4 *ºC*. All reagents were purchased from Sigma-Aldrich or Scharlau (Barcelona, Spain).

Image analysis and programming

Image processing and Ca^{2+} spark analysis were performed using custom programs written in Interactive Data Language (IDL v6.3, ITT Visual Information Solutions, Colorado, U.S.A.). Ca^{2+} transient and spark images were normalised to F/F_0 by dividing by an averaged spatial fluorescence profile over the pre-stimulus period, where defined. For detection of spontaneous events, images were divided by a preceding region that did not contain Ca^{2+} sparks (judged by eye) for spontaneous events.

Line-scan images were analysed in 1000-line segments to automatically detect Ca^{2+} sparks. They were normalised to F/F_0, then passed to the 'Matched Filter Detection Algorithm' (Kong, *et al.*, 2008) to detect and locate Ca^{2+} sparks. The user-defined '*sigp*' parameter was set to 1×10^{-9} so that very few false positives would be detected. The matched filter was set to a typical Ca^{2+} spark of $\Delta F/F_0$ 1.0, full width at half maximum (FWHM) 1.5 *µm*, time to peak of 10 - 15 *ms* and time to half decay of 25 *ms*. Results that included overlapping events or were in areas of increased Ca^{2+} (*e.g.* spontaneous Ca^{2+} waves) were discarded.

Unless otherwise stated, curve-fitting was performed with a Levenberg-Marquardt least squares algorithm (Moré, 1978) implemented in IDL (Markwardt, 2009) in IDL. Error bars

indicate one S.E.M., although one standard deviation (S.D.) may be shown (when stated) to display data variation that is smaller than the symbol size.

Measurement of SR Ca^{2+} release latency

Ca^{2+} transient time profiles were obtained by averaging across the spatial dimension of the image, while that of Ca^{2+} sparks were obtained by locating the centroid manually, averaging over 0.7 μm. For Ca^{2+} sparks, the amplitude time profile of a neighbouring non-sparking region was subtracted to minimise contribution from out-of-focus fluorescence. Latency of SR Ca^{2+} release was measured by fitting a sigmoid curve (Eqn. 2.4, where A is amplitude, t_0 is shift in time, τ is time constant of rise and $C \approx 1$) to the rising phase of the release event.

$$\frac{F}{F_0} = \frac{A}{1 + e^{-\frac{t - t_0}{\tau}}} + C \qquad \textbf{Eqn. 2.4}$$

The start of SR Ca^{2+} release was defined as where the fitted curve exceeded a threshold. This threshold was calculated as a proportion of the maximum rate of rise (Eqn. 2.5) calculated from Eqn. 2.4. This method of determining threshold (green lines, Fig. 2.1) was chosen over a basic amplitude threshold (red lines, Fig. 2.1) because the latter does not correctly measure the start of events that have different rates of rise (black lines, Fig. 2.1). Similarly, calculation of the threshold as a proportion of event amplitude leads to different start times for events of different rates of rise (blue lines, Fig. 2.1). Although a threshold approach always produces an error from the 'true' start (arrow, Fig. 2.1), the rate of rise method ensures this error is the same between events with different rates of rise (*e.g.* Ca^{2+} transients and Ca^{2+} sparks). Using the time of the maximum rates of rise would also provide this advantage; however, the offset from true start would be relatively large.

$$\text{Threshold} = 0.1 \cdot \text{maximum rate of rise} + C \qquad \textbf{Eqn. 2.5}$$

The time of a reference point to the start of release was used as SR Ca^{2+} release latency. For AP-clamp experiments, this reference point was the time at which the AP reached - 40 mV during the AP upstroke. This value was chosen because it was never contaminated by the stimulus artefact during current-clamp recordings and it is also at the foot of the activation curve for I_{Ca} (McDonald, *et al.*, 1994). For depolarising steps, the reference point

was at the start of the depolarising pulse and for repolarising steps, the reference point was the start of the repolarising pulse.

The latency during depolarisation steps includes the waiting time for LTCCs to open, while latency measured during repolarising steps does not because the LTCCs are already activated during the pre-pulse. In this approximation, the difference in latency between depolarising and repolarising steps at each potential (*ΔL*) should reflect the waiting time for the first LTCC in a junction to open. Should this first LTCC opening be insufficient to trigger CICR, then the latency measured during repolarising steps should also depend on

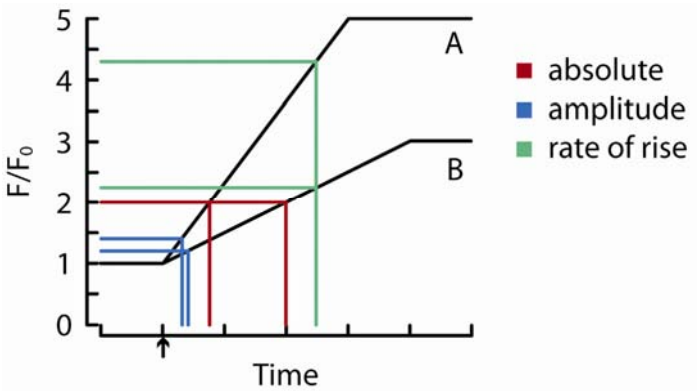

Figure 2.1 Using the maximum rate of rise to determine the start of an event. This illustration shows two signals, **A** and **B** that increase at different rates and for durations (*e.g.* Ca^{2+} transients and Ca^{2+} sparks). The black arrow indicates the 'true' start of fluorescence increase, which is the same for both functions and unknown in an experiment. The different colours indicate the results of three different methods for estimating this start. For example, an absolute threshold of 2 (red lines) yields different start times for each event, at an error that depends on the rate of rise. If the threshold is weighted by the signal peak amplitude (*e.g.* $0.1 \cdot \Delta F/F_0 + 1$, which would be 1.4 and 1.2 for A and B, respectively), the resulting start times would also be different for the two events (blue lines). If the threshold is weighted by the maximum rate of rise ($2.5 \cdot \Delta F/F_0/dt + 1$, which would be 4.3 and 2.25 for A and B, respectively), then the resulting start estimates would be the same (green lines). In other words, the rate of rise threshold method allows the comparison of the latencies of events with different rates of rise and amplitudes because they should have the same error from 'true' start.

the voltage-dependence of LTCC activation kinetics, rather than CRU activation kinetics alone.

The observation time for Ca^{2+} sparks was finite, which potentially missed late events (*i.e.* low frequency information is limited by the length of the recording) and would reduce the observed mean latency. To estimate the extent of this bias, the underlying latency distribution was assumed to be a declining mono-exponential function, where the true mean (*i.e.* an infinite observation period) is τ and the observed mean due a finite observation period (T_{obs}) is τ_{obs} (Eqn. 2.6). Note that as τ_{obs} approaches ~ $T_{obs}/2$, τ approaches infinity and cannot be back-calculated.

$$\tau_{obs} = \frac{(\tau + T_{obs}) \cdot e^{-\frac{T_{obs}}{\tau}} - \tau}{e^{-\frac{T_{obs}}{\tau}} - 1}$$ **Eqn. 2.6**

Estimating latency of SR Ca^{2+} release during AP-clamp

The contribution of LTCC waiting time to the latency of Ca^{2+} spark production during an AP was estimated from *ΔL(V)*. The AP-clamp profile, *V(t)* was used to obtain ΔL(t). The probability of SR Ca^{2+} release event occurrence, *P(t)* was estimated using the whole-cell nifedipine-sensitive current during an AP-clamp, using Eqn. 2.2 to estimate i_{Ca} and Eqn. 2.1. Once a CRU had activated, it was assumed not to activate again over the observation period. The effect of this was calculated by multiplying the latency histogram by the probability that the CRU did not fire (*i.e.* 1 – the cumulative latency histogram).

Monte Carlo simulations of SR Ca^{2+} release latency

To examine how CICR latency could be produced by LTCC and RyR gating in a junction, a simple computer model incorporating reported LTCC, $[Ca^{2+}]_{junction}$ response to I_{Ca} and RyR channel parameters was constructed (for a summary of parameters, see Table 2.1). The simulated latencies were compared to those recorded during depolarising and repolarising steps to various potentials. Stochastic LTCC openings were simulated using exponentially-distributed open and closed times, with means $\tau_{O,LTCC}$ and $\tau_{C,LTCC}$, respectively. These kinetic parameters are described by Eqn. 2.7 (Rose, *et al.*, 1992; Takeda, *et al.*, 1995; Josephson, *et al.*, 2010b), where no re-openings were allowed at – 120 *mV* (Poláková, *et al.*,

2008). For $\tau_{O,LTCC}$, τ_{max} = 1.3, slope = 18 and V_0 = -17. For $\tau_{C,LTCC}$, τ_{max} = 10, slope = -10 and V_0 = - 5. The fraction of LTCCs available was taken from Rose, *et al.* (1992). The number of LTCCs available in the couplon (n_{LTCC}/couplon) was also varied. The LTCCs were initially closed or open to reflect their state at the beginning of the depolarising or repolarising pulse, respectively.

$$\tau_{x,LTCC} = \frac{\tau_{max}}{1 + e^{\left(\frac{V_m - V_0}{slope}\right)}} \qquad \textbf{Eqn. 2.7}$$

$[Ca^{2+}]_{junction}$ was computed following the results of Soeller and Cannell (1997), who numerically-determined the effects of various Ca^{2+} buffers and a two-dimensional junction

Parameter	Value	Notes and References
Number of trials	500	
Time step, dt (μs)	1	
Record duration, T_{obs} (*ms*)	21, 45	For repolarising and depolarising steps, respectively
LTCC mean open times, $\tau_{O,LTCC}$ (*ms*)	Eqn. 2.7	Rose, et al., 1992; Takeda, et al., 1995; Josephson, et al., 2010b
LTCC mean closed times, $\tau_{C,LTCC}$ (*ms*)	Eqn. 2.7	*Ibid*
i_{Ca} (proportion of i_{Ca} at 0 *mV*)	Eqn. 2.2	Using P = 0.00018, $[Ca^{2+}]_i$ = 100 *nM*, $[Ca^{2+}]_o$ = 1 *mM*, and T = 22 *ºC* to obtain 0.1 *pA* at 0 *mV* (Guia, et al., 2001)
$[Ca^{2+}]_{junction}$	Eqn. 2.8	Function of i_{Ca} and time, approximated to Soeller and Cannell, 1997
RyR mean closed time, $\tau_{C,RyR}$ (*ms*)	Fig. 2.2*B*	Data from single-channel lipid bilayer studies (Laver, D., personal communication; Laver and Honen, 2008)
RyR mean open time, $\tau_{O,RyR}$ (*ms*)	2	0.9 ± 0.1 *ms* (n = 25, pCa = 3.3 to 5, 1 *mM* Mg^{2+}; Laver, D., personal communication) and ~ 3 *ms* in 0.22 *mM* Mg^{2+} (Laver and Honen, 2008).

Table 2.1 Simulation parameters for estimating the latency to SR Ca^{2+} release in simple Monte Carlo model. See text for details.

geometry on the amplitude and time-course of $[Ca^{2+}]_{junction}$ as a result of Ca^{2+} influx. They showed that for one LTCC opening of 0.2 *pA*, $[Ca^{2+}]_{junction}$ increased to ~ 70 *μM* in (essentially) the steady-state and following LTCC closure, $[Ca^{2+}]_{junction}$ decayed with a rapid initial phase (~ 0.1 *ms*) and more slowly at later times (~ 2.5 *ms*).

This was emulated in the model by a piece-wise approximation, as defined by Eqn. 2.8 and shown in Fig. 2.2A (solid line). The rate constants of $[Ca^{2+}]_{junction}$ production and dissipation were more rapid immediately following LTCC state transitions. The default values were $\tau_{C,junction}$ = 1.08 *μs*, $\tau_{O,junction}$ = 70 *μs* and $[Ca^{2+}]_{rest}$ = 100 *nM*.

$$\Delta[Ca^{2+}]_{junction,t} = \frac{S \cdot k_{t-1}}{\tau_{C,junction}} - \frac{([Ca^{2+}]_{junction,t-1} - [Ca^{2+}]_{rest})}{\tau_{O,junction}} \qquad \textbf{Eqn. 2.8}$$

where,

$[Ca^{2+}]_{junction,t-1} = S \cdot i_{Ca}$ *μM;*	$\tau_{O,LTCC} = dt$
$\tau_{C,junction}$ = 5.56 *μs*, $\tau_{O,junction}$ = 0;	$\tau_{O,LTCC} \leq$ 4 *μs*
$\tau_{O,junction}$ = 285.71 *μs*;	0.1 < $\tau_{C,LTCC} \leq$ 1.2 *ms*
$\tau_{O,junction}$ = 2 *ms*;	1.2 < $\tau_{C,LTCC} \leq$ 3 *ms*
$\tau_{O,junction}$ = 5 *ms*;	$\tau_{C,LTCC} \geq$ 3 *ms*

S was set to 0.6 at 0 *mV* to give a steady-state $[Ca^{2+}]_{junction}$ ~ 35 *μM*, which corresponds to an i_{Ca} of ~ 0.12 *pA* since Soeller and Cannell (1997) modelled a 0.2 *pA* unitary flux, while i_{Ca} under physiological conditions is likely to be much smaller (*e.g.* Guia, *et al.*, 2001). This scaling factor is reasonable since steady-state $[Ca^{2+}]_{junction}$ should be linearly proportional to i_{Ca} (Soeller and Cannell, 1997). Since the model presented here is non-spatial, it follows that steady-state $[Ca^{2+}]_{junction}$ is also proportional to the number of LTCCs that are open.

The RyR channel response to $[Ca^{2+}]_{junction}$ was estimated from RyRs reconstituted into lipid bilayers in the presence of 0 (Copello, *et al.*, 1997; Laver and Honen, 2008), 0.22 (Laver and Honen, 2008) and 1 *mM* Mg^{2+} (D. Laver, personal communication). The RyR channel opening rates from these data-sets were fitted by eye to Hill equations of the form shown by Eqn. 2.9, where K_D is the dissociation constant for $[Ca^{2+}]_{junction}$ and H is the Hill coefficient. The RyR opening rate in more physiological $[Mg^{2+}]$ (~ 0.5 *mM*, Gupta, *et al.*, 1984; Blatter and McGuigan, 1986; Quamme, 1990) was estimated (dashed line, Fig. 2.2B).

$$\frac{1}{\tau_{C,RyR}} = \left(\frac{\text{maxrate} \cdot [Ca^{2+}]_{junction}{}^{H}}{[Ca^{2+}]_{junction}{}^{H} + K_D{}^{H}}\right) \qquad \textbf{Eqn. 2.9}$$

The number of RyR channels within a CRU that were able to detect $[Ca^{2+}]_{junction}$ (n_{RyR}) was also varied.

$$P_{O,CRU}(t) = 1 - \left[1 - P_{O,RyR}(t)\right]^{n_{RyR}} \qquad \textbf{Eqn. 2.10}$$

The open probability of the CRU ($P_{O,CRU}$) was calculated as a function of time and was the probability that at least one RyR channel opened (from the Binomial Distribution, Eqn.

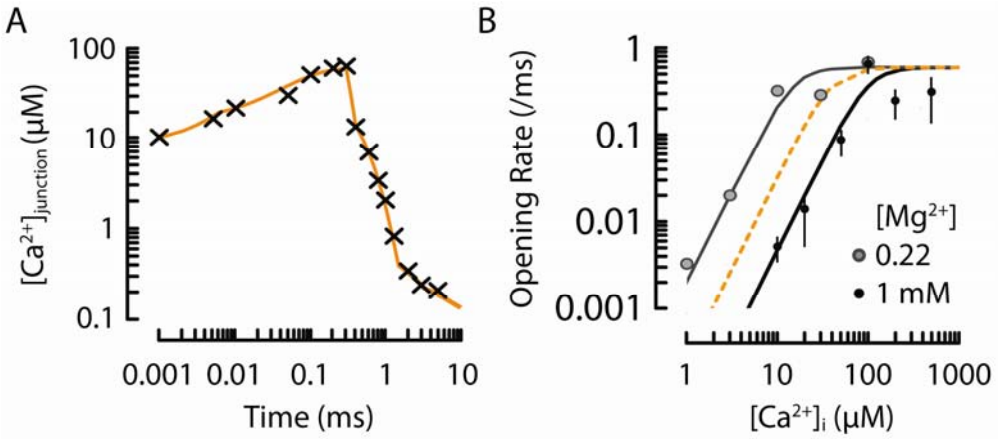

Figure 2.2 Ca^{2+} in the junction and RyR channel opening rate used in Monte Carlo simulations. (A) shows the piece-wise function (orange line, Eqn. 2.8) used to calculate the appearance of $[Ca^{2+}]_{junction}$ in response to an LTCC opening of 0.3 ms and 0.2 *pA*, as shown by Soeller and Cannell (1997) for $[Ca^{2+}]$ at 4 *nm* below and 2.5 *nm* radial distance from the mouth of the LTCC. At LTCC open durations that were longer than ~ 0.3 *ms*, $[Ca^{2+}]_{junction}$ reached a steady-state level that is proportional to i_{Ca}. Once the LTCC closed $[Ca^{2+}]_{junction}$ decayed rapidly to half of its maximal value in 0.1 *ms*, then decreased more slowly at later times. **(B)** shows the opening rates of single RyR channels as observed in lipid bilayers in the presence of (in *mM*): 2 ATP, 0.22 $[Mg^{2+}]_i$ and 0.1 $[Ca^{2+}]_{SR}$ (grey circles, Laver and Honen, 2008) or 2 ATP, 1 $[Mg^{2+}]_i$ and 1 $[Ca^{2+}]_{SR}$ (black circles, D. Laver, personal communication). These were fitted by Hill equations (Eqn. 2.9) with parameters, H = 2.8 and maximum opening rate = 0.5 */ms*. In 0.22 *mM* Mg^{2+}, K_D = 15 *μM* (*grey line*) and in 1 *mM* Mg^{2+}, K_D = 100 *μM* (black line). On the basis that physiological $[Mg^{2+}]$ is ~ 0.5 *mM* (Gupta, et al., 1984; Blatter and McGuigan, 1986; Quamme, 1990), the opening rate was estimated as an intermediate (orange line), where K_D = 40 *μM*.

2.10), where the probability of each RyR opening ($P_{O,RyR}$) is independent. The mean SR Ca^{2+} release latency was measured from the start of the simulation to the time when $P_{O,CRU}$ reached 0.5 (arithmetic mean).

Estimating whole-cell release flux by deconvolution

Even though the measurement error is theoretically consistent between events (see Fig. 2.1), the mean Ca^{2+} transient latency at a fixed threshold reflects the time of activation of *early* Ca^{2+} sparks, while the mean Ca^{2+} spark latency corresponds to the time of *most probable* Ca^{2+} spark activation. Even the time of the maximum rate of rise during a Ca^{2+} transient likely under-estimates average Ca^{2+} spark latency due to missed late events (loss of signal contrast as the Ca^{2+} transient proceeds). To estimate the time-course of Ca^{2+} spark production in the nifedipine-free case, a Ca^{2+} spark was used to de-convolve a Ca^{2+} transient by a Richardson-Lucy algorithm. The signal-to-noise ratio of the Ca^{2+} spark image was improved by spatial averaging assuming spatial symmetry. Both the Ca^{2+} transient and spark images were baseline-subtracted and convolved with a 3 pixel wide Savitzy-Golay filter first in the spatial, then time dimensions. The total energy of the Ca^{2+} spark image was set to unity. The Ca^{2+} transient image was padded with zeros, so that the image width and length were doubled.

2.3. Results

Latency of SR Ca^{2+} release during AP-clamp

The latencies of Ca^{2+} transients evoked by AP-clamp were measured. The AP profile used (Fig. 2.3Ai) was recorded from a rat ventricular myocyte and was chosen for its stable resting V_m at – 80 *mV* and which rapidly reached a peak potential of ~ + 50 *mV* (see Kim, *et al.*, 2010). This AP evoked a nifedipine-sensitive current (I_{Ca}, Fig. 2.3Aii) and Ca^{2+} transient (Fig. 2.3Aiii). Spatially-averaged fluorescence began to increase ~ 4 *ms* after the AP depolarised to - 40 *mV* and reached a peak in ~ 12 *ms* (Fig. 2.3Aiii), which can be seen more clearly in the time derivative (Fig. 2.3Aiv). Although the time to peak of this Ca^{2+} transient is typical and suggests a relatively synchronous cell-wide activation of Ca^{2+} sparks, non-uniformities are apparent in the line-scan image (Fig. 2.3Av). These non-uniformities can be better appreciated at high time-resolution (Fig. 2.3Bv), where Ca^{2+} appears with stochastic delay at a spatial periodicity of ~ 1.8 *μm* and then diffuses and/or

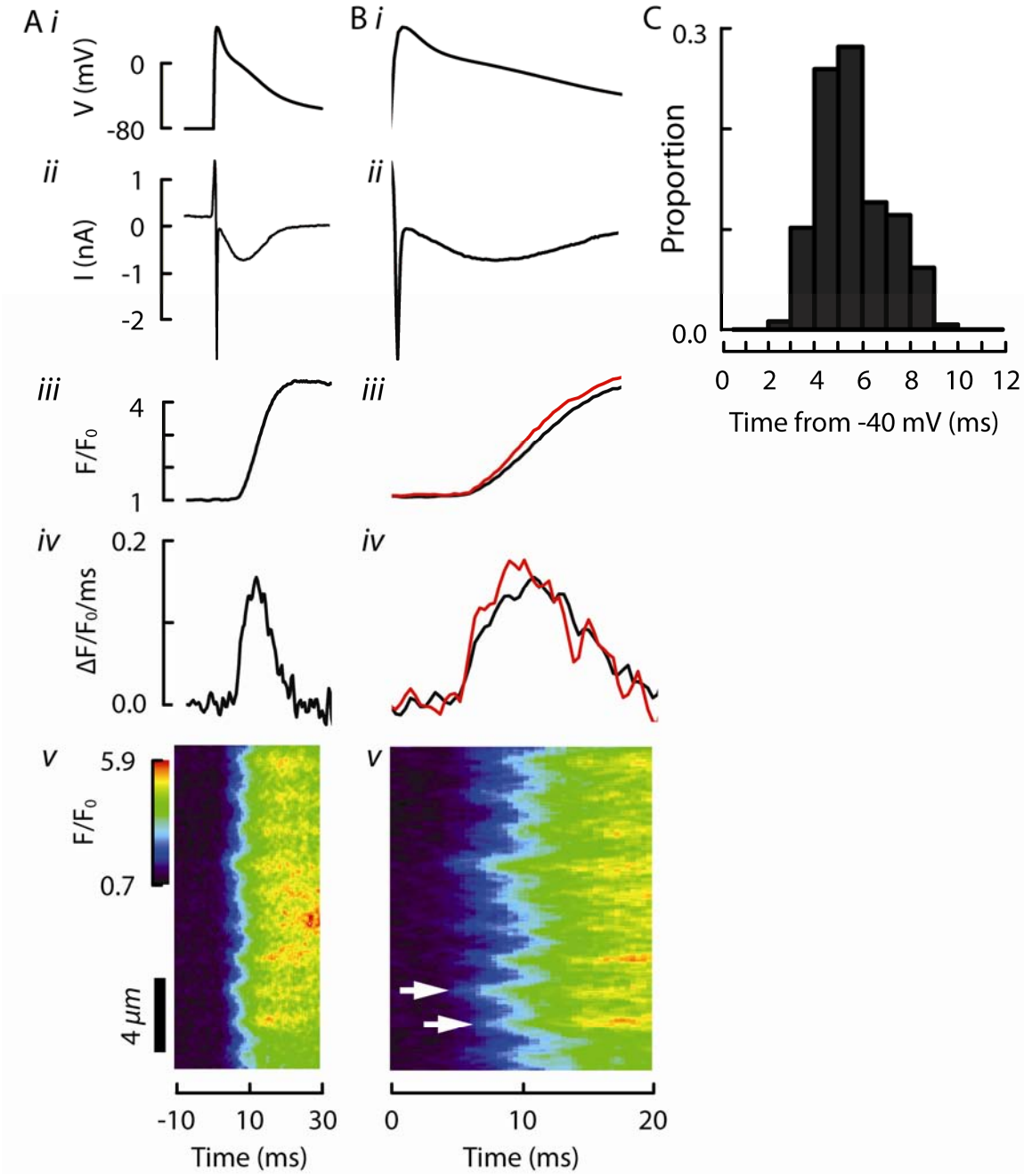

Figure 2.3 Latency of Ca^{2+} transients during AP-clamp. (Ai) shows the AP-clamp profile, that elicited a **(ii)** nifedipine-sensitive current and **(iii)** Ca^{2+} transient (spatial average). The fluorescence begins to increase at ~ 4 *ms*, as shown in the time derivative **(iv)**. Examination of the ***(v)*** fluorescence image reveals that during a normal Ca^{2+} transient, non-uniformities at the wave-front are present. At high time-resolution **(Bv)**, it is clear that they occur every ~ 1.8 *μm* (*e.g.* white arrows). Fluorescence at these local regions (averaged across 0.25 *μm*) increased more rapidly **(**red lines, **Biii** and **iv)** than the spatial average **(**black lines, from **Aiii** and **iv)**. Compared to the time-course of I_{Ca} **(ii)**, the maximum rate of the rise of the Ca^{2+} transient occurs near the peak of I_{Ca}. **(C)** shows a normalised histogram of Ca^{2+} transient latencies, as measured to the start of the Ca^{2+} transient at ~ 1.8 *μm* intervals (*n* = 721 intervals, 7 cells).

superimposes with other/late release events. When fluorescence profiles from only these early gradients were averaged, the resulting time-course (red line, Fig. 2.3Biv) is faster than the initial estimate from the spatial average (black line, Fig. 2.3Biv) with an earlier (~ 2 *ms*) maximum rate of rise, but with little difference in the start time. A summary of latencies measured from these regions are shown in Fig. 2.3C. The shortest and mean latencies were ~ 2 and 5.4 *ms*, respectively (Fig. 2.3C), which corresponds to + 15 and ~ -10 *mV* during the repolarising phase of the AP. Note that this range of potenails is within the LTCC window current (McDonald, *et al.*, 1994).

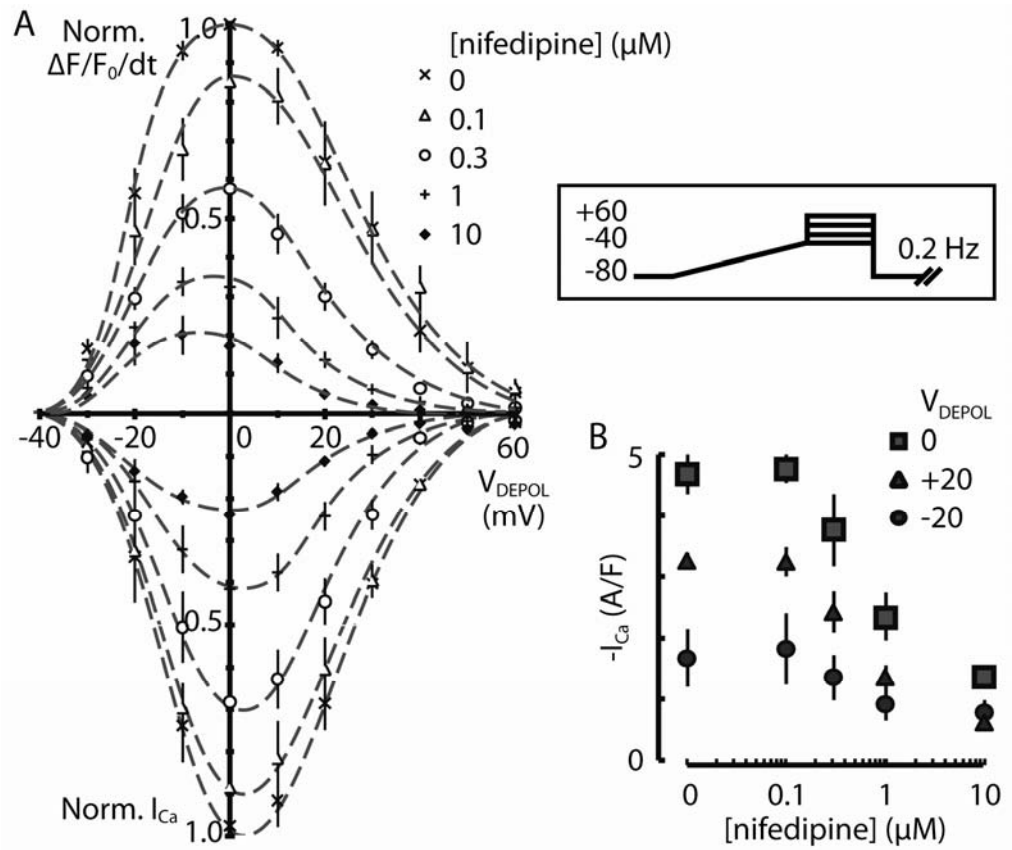

Figure 2.4 Effect of nifedipine on peak I_{Ca} and maximum rate of rise of Ca^{2+} transients. (A) shows the current-voltage relationship for peak I_{Ca} (bottom panel, normalised to maximum peak I_{Ca} for each cell) and maximum rate of rise of Ca^{2+} transients (top panel, normalised to the maximum for each cell) in response to different concentrations of nifedipine. (*n* = 2 cells, with 3 or 4 sweeps for each data-point). The potentials here have not been corrected. If maximum rate of rise of the Ca^{2+} transient is proportional to P_{spark}, this data suggests that in 10 *μM* nifedipine, P_{spark} has reduced by ~ 76 %. **(B)** shows the effect of nifedipine on I_{Ca} at - 20, 0 and + 20 *mV* in one cell.

The problem with measuring SR Ca^{2+} release latency from Ca^{2+} transients is that it measures only the latency of early Ca^{2+} sparks, while later events are not resolved due to loss of signal contrast at high P_{spark}. The time of peak during a Ca^{2+} transient is not a good indicator of global SR Ca^{2+} release termination, but shows the time to which Ca^{2+} release and uptake fluxes are equal (assuming the Ca^{2+} dye is at steady-state). To measure Ca^{2+} spark latency directly, nifedipine was used to decrease P_{spark} and enhance signal contrast. Nifedipine reduced P_{spark} because it reduced I_{Ca} density (bottom panel, Fig. 2.4A), with no apparent shift in voltage-dependence. At 10 μM nifedipine, peak I_{Ca} (~ 0 mV) was reduced by 76 %. At this level of I_{Ca} inhibition, a similar reduction in the maximum rate of rise of the associated Ca^{2+} transients was also observed (top panel, Fig. 2.4A). The actual current density from one cell is shown in Fig. 2.4B.

Line-scan images of AP-clamp evoked SR Ca^{2+} release in the presence of 15 μM nifedipine revealed discrete Ca^{2+} sparks (Fig. 2.5A). Ca^{2+} sparks occurred with variable probability and delay during a given stimulus, as shown by the changing pattern of release between subsequent stimuli (Fig. 2.5A). Time-profiles of Ca^{2+} sparks (marked by white dashes, Fig. 2.5A) are shown. A summary of the time-course of Ca^{2+} spark production during the AP-clamp is shown in Fig. 2.5B. The mode and mean latencies were 7.5 and 9.6 ms, respectively, which correspond to potentials between -15 and -25 mV during the repolarisation phase of the AP.

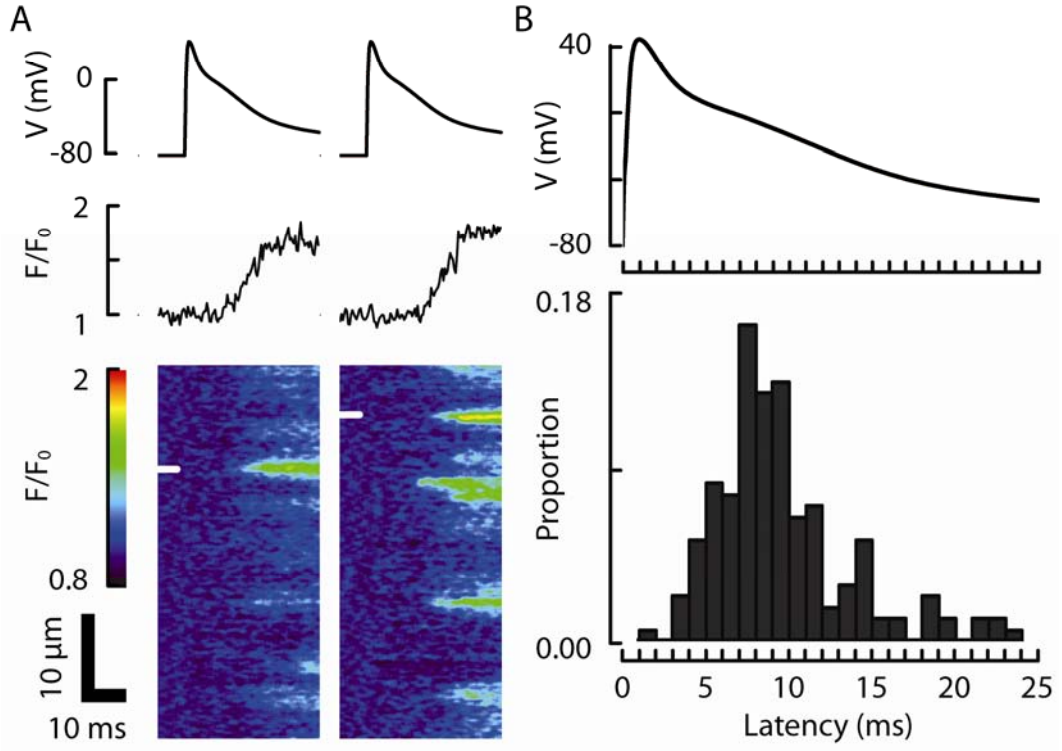

Figure 2.5 Ca^{2+} spark latency when evoked under AP-clamp. (A) shows examples of Ca^{2+} sparks evoked during an AP-clamp in the presence of 15 μM nifedipine. Time profiles of the Ca^{2+} sparks marked by white dashes on the line-scan images are also shown. **(B)** shows a summary histogram of Ca^{2+} sparks (n = 170 events, 6 cells) evoked under AP-clamp and the corresponding time-course of command potential. The mode and mean latencies were 7.5 and 9.6 $\pm$ 4.2 *ms* (S.D.), respectively.

Latency of SR Ca^{2+} release during depolarising and repolarising steps

Since Ca^{2+} sparks occur at some delay following the initiation of the AP, it was of interest to determine whether the rate of LTCC activation is a primary contributor. To do this, SR Ca^{2+} release was evoked by depolarising and repolarising steps to various potentials and the measured latencies were compared. During depolarising steps, P_{spark} and Ca^{2+} spark latency changed depending on the test potential. The dependence of P_{spark} on step potential was already shown in Fig. 2.5A, but are now visualised in the line-scan images and spatial time-profiles of Fig. 2.6A. As test potential increased, Ca^{2+} transient and Ca^{2+} spark latency decreased (Fig. 2.6B). At potentials below - 30 *mV*, P_{spark} was extremely low and the few latencies measured were highly variable. The correction for limited observation duration (T_{obs} = 45 *ms*, Eqn. 2.6) was applied to these measured latencies and an estimate of the mean detection error was subtracted (the shortest mean latency observed during repolarising steps, which was 1.45 *ms* at – 100 *mV*, Fig. 2.7B). The corrected latencies are shown in Fig. 2.6C. Note that the negative relationship between of SR Ca^{2+} latency and test potential is not as steep as the reported voltage-depence of $\tau_{C,LTCC}$ (Josephson, *et al.*, 2010b). However, i_{Ca} decreases with increasing test potential (Eqn. 2.2), which would slow RyR activation kinetics and prolong CICR latency.

To estimate the effect of test potential on the activation of RyR channel clusters, the repolarising step protocol was used to first activate, but prevent Ca^{2+} influx through LTCCs, then increase the driving force for Ca^{2+} entry with repolarisation to activate SR Ca^{2+} release (e.g. Fig. 2.7A). The latency of SR Ca^{2+} release from repolarising steps (Fig. 2.7B) was shorter than that measured during depolarising steps (Fig. 2.6B), as expected if the delay due to LTCC activation was removed. Further, unlike the voltage-dependence of latency during depolarising steps, latency increased with V_{REPOL} (Fig. 2.7B), as would be expected due to a decrease in i_{Ca} (Eqn. 2.2). Following the correction for observation bias (T_{obs} = 21 *ms*, Eqn. 2.6) and detection error using the same method as applied to depolarising step latencies, repolarising step latencies showed a relatively shallow dependence on estimated i_{Ca} (~ inversely proportional, see Fig. 2.7C), compared to reported [Ca^{2+}]-dependence of isolated RyR channels (*e.g.* Meissner and Henderson, 1987; Copello, *et al.*, 1997; Laver and Honen, 2008). This could be explained if CICR is operating in the near-saturation range of RyR activation kinetics (see Fig. 2.2B) and/or the voltage-dependence of latency includes waiting time for subsequent LTCC openings.

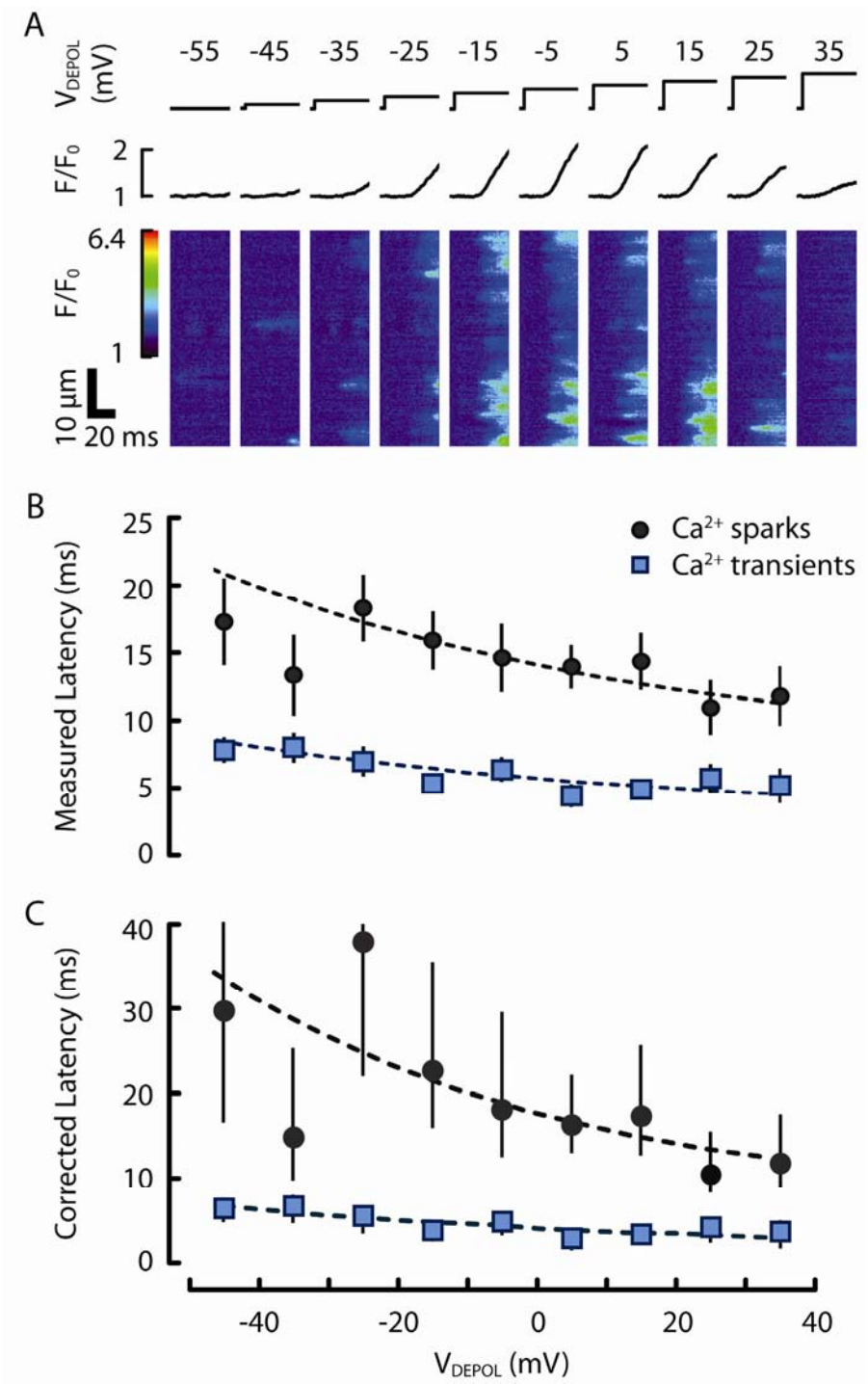

Figure 2.6 Ca^{2+} transients and Ca^{2+} sparks elicited by depolarising steps. **(A)** Time profiles (spatial average of whole image) and line-scan images of Ca^{2+} sparks evoked at increasing step potentials in 15 *µM* nifedipine (same cell). **(B)** Latencies of Ca^{2+} transients (blue squares, n = 74) and Ca^{2+} sparks (black circles, n = 62). The trend lines were fitted by eye: $\text{latency} = A \cdot e^{-\frac{V_{DEPOL}}{\tau}} + C$, where $\tau = 40\ mV$. For Ca^{2+} transients, A = 1.5 *ms*, C = 4.2 *ms* and for Ca^{2+} sparks, A = 3.75 *ms* and C = 10.5 *ms*. **(C)** shows latencies corrected for T_{obs} bias (Eqn. 2.6) and detection error (see text). Trend lines were the same as above, except for Ca^{2+} transients, C = 2.75 *ms* and for Ca^{2+} sparks, A = 15 *ms*, τ = 60 *mV* and C = 3 *ms*.

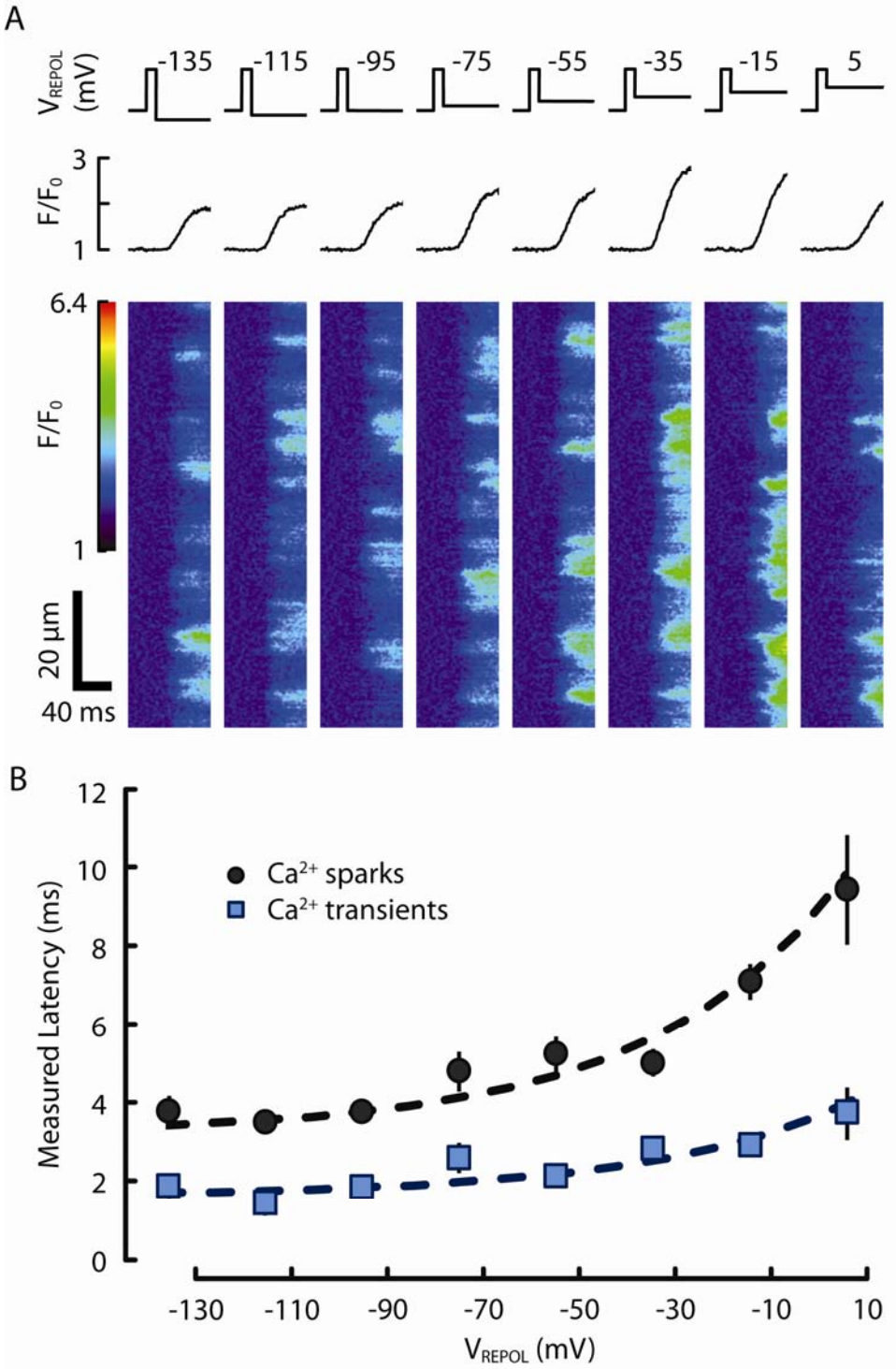
A
V_{REPOL} (mV)
-135
-115
-95
-75
-55
-35
-15
5
F/F0
3
1
6.4
F/F0
1
20 µm
40 ms
B
Measured Latency (ms)
12
10
8
6
4
2
0
Ca2+ sparks
Ca2+ transients
-130
-110
-90
-70
-50
-30
-10
10
V_{REPOL} (mV)

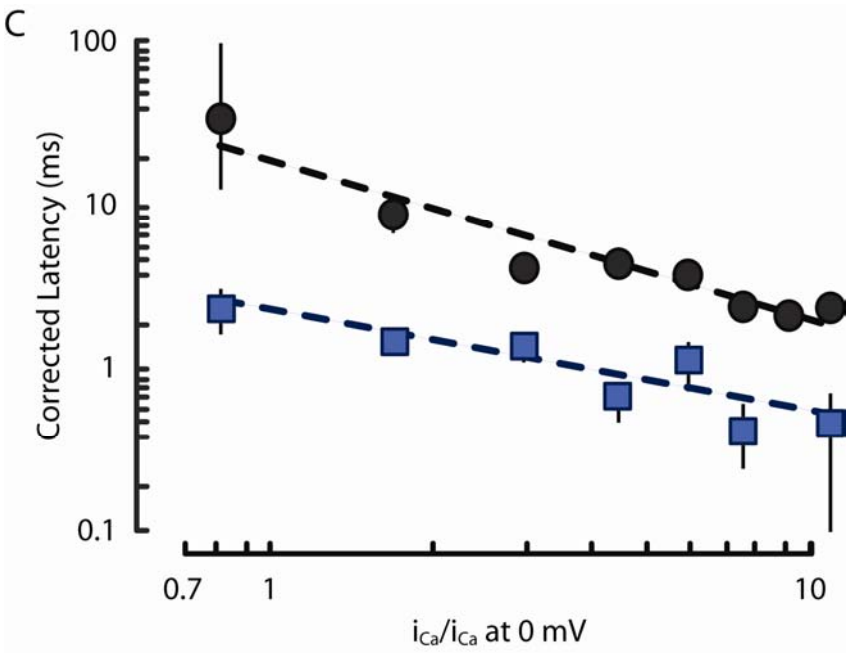

Figure 2.7 Ca^{2+} transients and Ca^{2+} sparks evoked by repolarising steps. **(A)** Time profiles (spatial average of whole image) and line-scan images of Ca^{2+} sparks evoked by repolarising steps in 15 μM nifedipine (same cell). **(B)** shows Ca^{2+} transient (*blue squares*; n = 88) and Ca^{2+} spark (black circles, n = 122) latencies as a function of repolarising step potential. Data obtained from 5 cells. The trend lines were fitted by eye: latency $= A \cdot e^{-\frac{V_{REPOL}}{\tau}} + C$. For Ca^{2+} sparks, $A = 5.5\ ms$, $\tau = 40\ mV$ and $C = 3.2\ ms$ and for Ca^{2+} transients, $A = 2\ ms$, $\tau = 40\ mV$ and $C = 1.6\ ms$. **(C)** shows corrected mean latencies against i_{Ca} at each V_{REPOL} (estimated by Eqn. 2.2). Mean latencies were corrected for observation bias (Eqn. 2.6) and detection error (see text). The fitted trend lines for Ca^{2+} transients and Ca^{2+} spark corrected latencies were: $2.3 \cdot (\frac{i_{Ca}}{i_{Ca}\text{at 0mV}})^{-0.7}$ and $18.5 \cdot (\frac{i_{Ca}}{i_{Ca}\text{at0mV}})^{-1.0}$, respectively.

Another important measure of CICR function is P_{spark}, which appeared to be voltage-dependent during repolarising steps. Though SR Ca^{2+} release occurred with very short delay at very negative V_{REPOL}, P_{spark} was very much reduced. Ca^{2+} transients evoked at very negative V_{REPOL} showed smaller amplitudes and maximum rates of rise (Fig. 2.8A,B). The first derivatives of these Ca^{2+} transients suggests that the initial rate of Ca^{2+} spark production was similar across different potentials, but that the duration of SR Ca^{2+} release at very negative potentials was relatively short (Fig. 2.8B). Overall, as V_{REPOL} decreased (and i_{Ca} increased, Eqn. 2.2), the maximum rate of rise of Ca^{2+} transients increased initially, but then decreased again as i_{Ca} increased further (blue squares, Fig. 2.8C). This phenomenon can be explained by the voltage-dependence of $\tau_{O,LTCC}$, which decreases at decreasing potentials to limit the activation of Ca^{2+} sparks. To test this idea, FPL was used to prolong $\tau_{O,LTCC}$. Preliminary data appears to show that maximum rate of rise did not decrease at negative potentials (white squares, Fig. 2.8C). Thus, it would seem that under normal circumstances, CICR may be limited by decreasing $\tau_{O,LTCC}$ at potentials below approximately - 35 *mV*, with maximal release occurring at more positive potentials, to approximately - 10 *mV*.

Comparison of Ca^{2+} spark latencies during depolarising and repolarising steps within this range should provide some insight into LTCC waiting times in the intact myocyte. Calculation of ΔL at - 15 *mV* suggests that the time spent waiting for a sufficient number of LTCCs to open were ~ 2 and 9 *ms* for Ca^{2+} transients and sparks, respectively (Fig. 2.9A). At a more positive potential (5 *mV*), ΔL was reduced ~ 1 and 4.5 *ms* for Ca^{2+} transients and sparks, respectively. Thus, waiting time for LTCC openings would comprise ~ 62 % of the observed latency during depolarisation to – 15 *mV*, but only ~ 36 % when depolarising to 5 *mV*, as i_{Ca} is reduced and RyR activation is slowed.

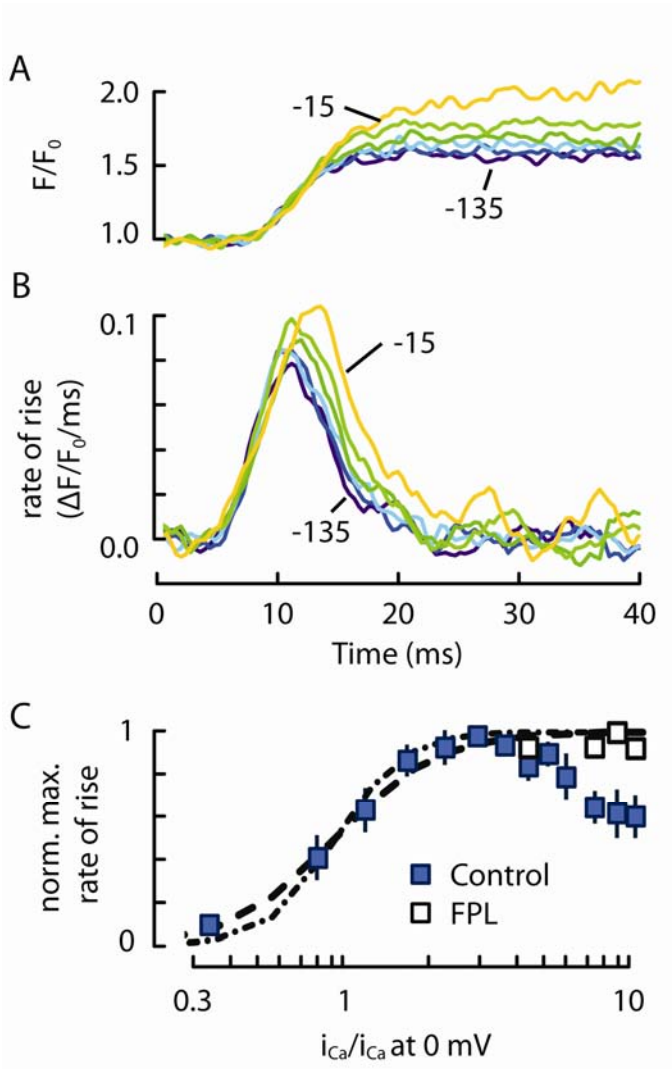

Figure 2.8 Maximum rate of rise of Ca^{2+} transients elicited by repolarising steps. Ca^{2+} transient amplitude **(A)** and rate of rise **(B)** from one cell at different V_{REPOL} (indicated). Traces were aligned by their start time. Release duration appeared longer at more positive potentials. **(C)** shows the dependence of max. rate of rise (normalised to the maximum for each cell) on i_{Ca} (estimated using Eqn. 2.2). Under normal conditions (blue squares, *n* = 164 sweeps, 3 cells, error bars show one S.D.), the maximum rate of rise shows a biphasic relationship. Curves are Hill equations of the form: $\text{norm. max. rate of rise} = \frac{i_{Ca}/i_{Ca at 0mV}{}^{H}}{K_D{}^{H}+i_{Ca}/i_{Ca at 0mV}{}^{H}}$, where K_D = 0.095 and H = 2 (dashed line) and 3 (dash-dotted line). Preliminary data shows FPL-64167 (white squares, 1 cell) appeared to counteract the reduction in maximum rate of rise at negative potentials.

Latencies during AP-clamp

When ΔL was used as the basis for $\tau_{C,LTCC}(V)$ in the nifedipine (Ca^{2+} sparks, black line, Fig. 2.9A) and nifedipine-free (Ca^{2+} transients, blue line, Fig. 2.9A), the time-course of SR Ca^{2+} release for Ca^{2+} sparks could be reproduced reasonably well (compare Fig. 2.9B to Fig.s 2.5 and 2.3).

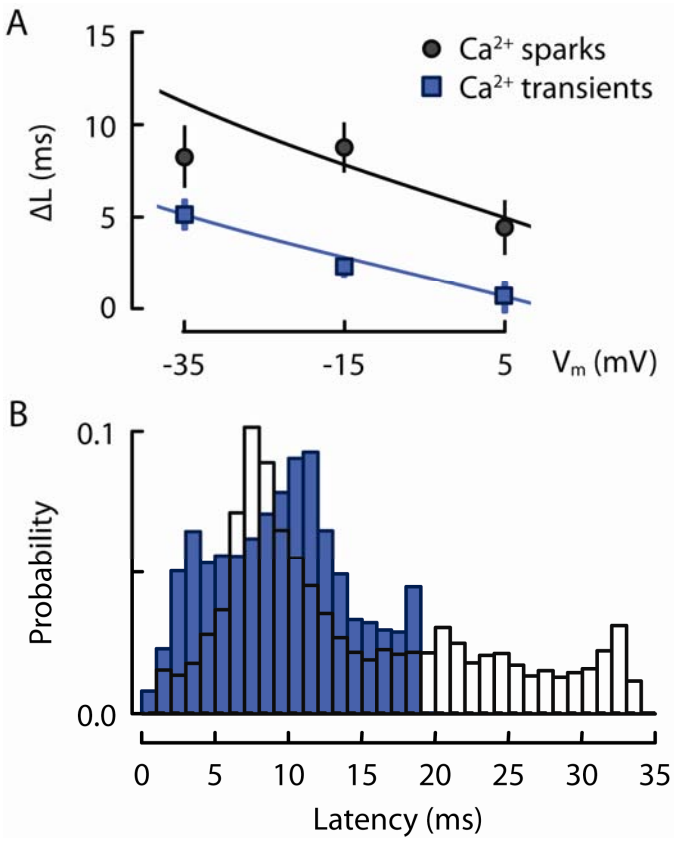

Figure 2.9 Prediction of AP-clamp evoked Ca^{2+} spark latency from ΔL. (A) Estimate of waiting time for LTCCs from the difference in latencies between depolarising and repolarising steps (ΔL). The curves that were used to estimate corresponding waiting times during an AP were for Ca^{2+} transients, $\Delta L = 2.5 \cdot e^{-\frac{V}{40}} - 1.8 \cdot e^{\frac{V}{40}} + 2.1$ and for Ca^{2+} sparks, $\Delta L = 4 \cdot e^{-\frac{V}{40}} - 2 \cdot e^{\frac{V}{40}} + 5.8$, where V was the membrane voltage during the AP-clamp in *mV*. **(B)** The predicted latencies of Ca^{2+} sparks (black) during the AP-clamp protocol, with a mode at 7.5 *ms* and the mean at 10.5 *ms*. For Ca^{2+} transients (blue), the modes occurred at 3.5 and 11.5 *ms*, while the mean occurred at 12 *ms*.

Monte Carlo simulations of SR Ca^{2+} release activation

Though the voltage-dependence of repolarising step latencies is consistent with a $[Ca^{2+}]$-dependence of RyR activation that is near-linear (see Fig. 2.2 and Fig. 2.7C) and the voltage-dependence of *ΔL* (Fig. 2.9A) is consistent with the general voltage-dependence of LTCC activation (McDonald, *et al.*, 1994; Josephson, *et al.*, 2010b), numerical analysis was performed usingknown kinetic parameters of LTCCs, junction $[Ca^{2+}]_i$ response to Ca^{2+} influx and RyR channels. Fig. 2.10 illustrates the principles of the computer simulations. Fig. 2.10A panels show the stochastic opening and closing of LTCCs that resulted from exponentially-distributed open and closed times. Note that when n_{LTCC}/couplon was four, the occurrence of four concurrent openings was rare, with an expected mean duration of all four being open being $\tau_{O,LTCC}/4$ (Colquhoun and Hawkes, 1983). The number of LTCCs open was assumed to be proportional to I_{Ca} flowing into the junction, which was in turn

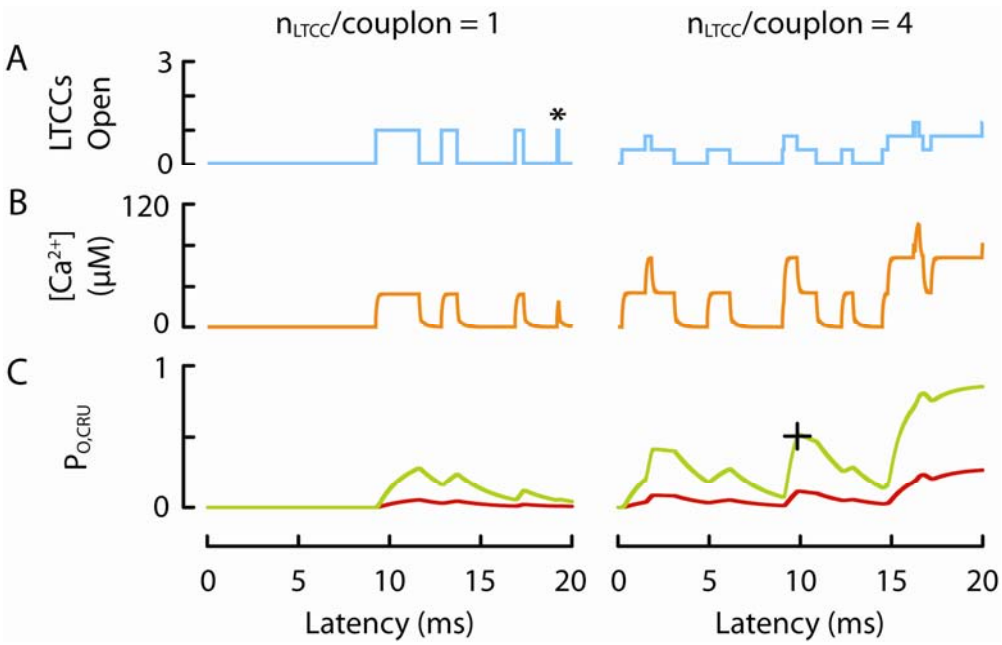

Figure 2.10 Monte Carlo simulation of CRU activation. LTCC parameters, $\tau_{O,LTCC}$ = 1 *ms*, $\tau_{C,LTCC}$ = 4 *ms*, i_{Ca} = 0.2 *pA*, with one (left panels) or four (right panels) n_{LTCC}/couplon. RyR channel parameters as stated in Methods. **(A)** shows the stochastic behaviour of LTCC gating and **(B)** shows the resulting $[Ca^{2+}]_{junction}$ response. Note that very short openings (asterisks) do not raise $[Ca^{2+}]_{junction}$ to the steady-state level. **(C)** shows the response of a CRU with n_{RyR} of one (red line) and three (green line) that are able to sense the influx of Ca^{2+}. The times of CRU activation ($P_{O,CRU}$ = 0.5) are indicated by crosses.

proportional to $[Ca^{2+}]_{junction}$ at steady-state, as shown by Soeller and Cannell (1997). Notice that for short openings (asterisks in left panel, Fig. 2.10A), $[Ca^{2+}]_{junction}$ substantially under-estimated Ca^{2+} influx. This is because when an LTCC opens, $[Ca^{2+}]_{junction}$ takes ~ 0.1 ms to reach 63 % of its steady-state level (see Eqn. 2.8, Fig. 2.2A). Thus, for LTCC openings that last < ~ 0.3 *ms*, $[Ca^{2+}]_{junction}$ does not reach steady-state, which implies that short LTCC openings should not be as effective in triggering SR Ca^{2+} release. In connection to this point, the decay of $[Ca^{2+}]_{junction}$ has a rapid initial component, followed by a slow late component (Soeller and Cannell, 1997). This persistent low level of $[Ca^{2+}]_{junction}$ following LTCC closure may mean that subsequent openings in this period may be more effective in triggering SR Ca^{2+} release, if they were required. This complexity precludes an analytical

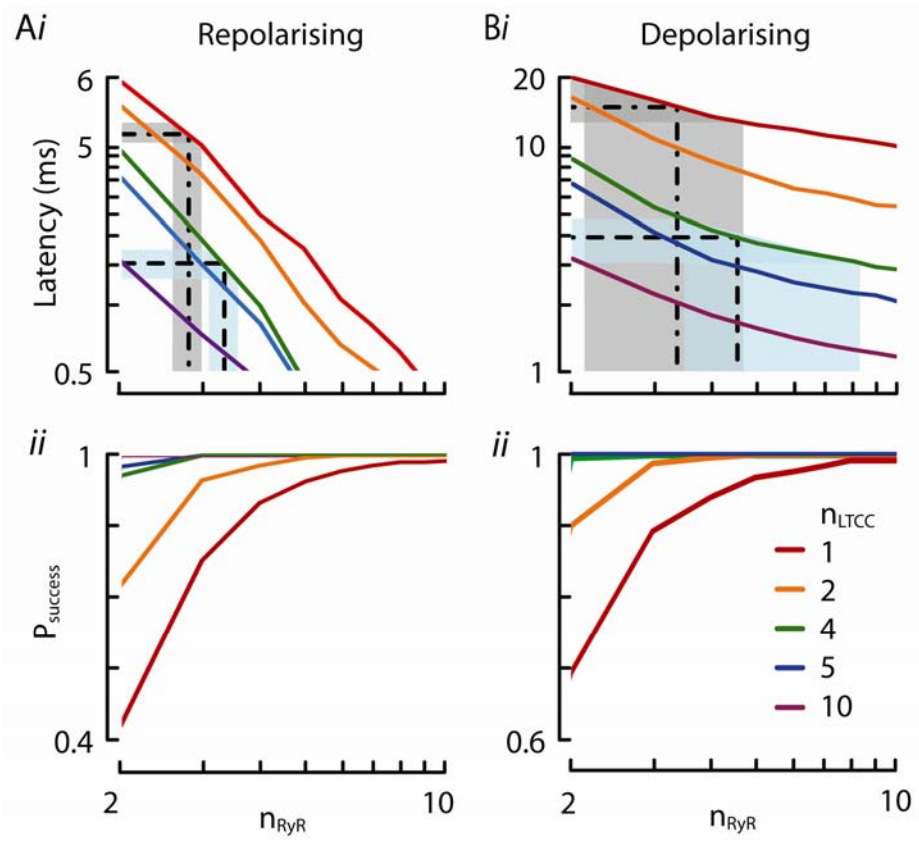

Figure 2.11 Computer simulations of the latency of SR Ca^{2+} release at – 15 *mV*. Simulations of repolarising **(A**, initial $P_{O,LTCC}$ = 0.29, Josephson, et al., 2010b**)** and depolarising **(B)** step activation of a CRU comprised of n_{RyR} by n_{LCC}. The top panels **(i)** show the calculated latencies and the bottom panels **(ii)** show the probability of successfully activating a CRU during a sweep ($P_{success}$, calculated from 500 sweeps, 45 *ms* per sweep). The observed latencies for Ca^{2+} sparks (grey) and Ca^{2+} transients (light blue) are shown with the shaded area representing the range.

analysis of waiting times. The CRU response to $[Ca^{2+}]_{junction}$ is shown for one (red lines, Fig. 2.10C) and three (green lines) RyR channels within a CRU that are able to sense $[Ca^{2+}]_{junction}$.

Since LTCC activation kinetics and i_{Ca} are voltage-sensitive, computer simulations were performed at several step potentials to examine how they affect CICR latency within a single couplon. Fig. 2.11i and ii show the latencies and probabilities of CRU activation ($P_{success}$) calculated at (Fig. 2.11A) V_{REPOL} and (Fig. 2.11B) V_{DEPOL} = - 15 *mV* at various n_{RyR} and n_{LTCC}. As expected, as n_{LTCC} and n_{RyR} increased, $P_{success}$ increased. For those sweeps that were successful, the calculated latencies matched those from experiments (dashed lines, Fig. 2.11i) at n_{RyR} = 3 - 4 and n_{LTCC}/couplon = 1 and 4 for Ca^{2+} sparks and Ca^{2+} transients, respectively. This was achieved at three different potentials (Fig. 2.12A).

To determine the extent with which LTCC activation contributes to CICR latency, the mean duration LTCC(s) spent in the open state prior to CRU activation ('trigger integral', as defined as the product of the number of LTCCs open and the time that they are open) was recorded. At V_{DEPOL} = - 15 *mV*, the probability that an average LTCC opening activated a CRU or the fraction of LTCC openings that do trigger a Ca^{2+} spark ($P_{CPL,\tau O}$, Wang, *et al.*, 2001) was 1.0 and meant that the latency of CRU activation is due to waiting for ~ 1 LTCC opening. At – 35 and 5 *mV*, $P_{CPL,\tau O}$ = 0.64, 0.38, respectively. When n_{LTCC} = 4, the trend was similar, with $P_{CPL,\tau O}$ = 0.6, 1.0, 0.7 at – 35, - 15 and 5 *mV*, respectively. This behaviour is also observed when using $\tau_{act,LTCC}$ (Eqn. 2.3) and measured ΔL (for when n_{LTCC} is 1) to infer the average number of trigger openings (as defined in Cheng and Lederer, 2008), *e.g.* at – 15 and 5 *mV*, $\tau_{C,LTCC}$ was 0.83 and 0.59 of *ΔL*, respectively.

This high coupling fidelity implies a large Ca^{2+} spark to LTCC flux ratio (or coupling 'gain', see *e.g.* Cannell, *et al.*, 1995). If the average Ca^{2+} spark flux is ~ 3 *pA* for 10 *ms* (see Cheng, *et al.*, 1993; Cheng and Lederer, 2008), the ratio of flux integrals between the evoked Ca^{2+} spark and the trigger integral (γ_L) can be estimated. At – 15 and 5 mV, γ_L were ~ 220 and ~ 120, respectively, when n_{LTCC} = 1 and ~ 220 and ~ 200, respectively, when n_{LTCC} = 4. However, at the macroscopic level, I_{Ca} cannot be separated from that preceding and that during/following local SR Ca^{2+} release (see Fig. 2.12B). To estimate how this reduces apparent gain, the flux integral ratio was calculated including LTCC flux 10 *ms* (to approximate Ca^{2+} spark flux duration) after the time of CRU activation. In this scenario,

apparent gain (γ_{L+S}) at – 15 *mV* becomes ~ 75 when $n_{LTCC} = 1$ and ~ 30 when $n_{LTCC} = 4$. Thus, it is clear that gain is greatly reduced when LTCC openings after CRU activation are included. However, at 0 *mV*, these data are consistent with a requirement of 1 - 2 LTCC openings to trigger a Ca^{2+} spark, which means that a simple comparison of macroscopic and microscopic gain will not yield a correct estimate of the number of LTCC openings that are redundant to CICR.

Fig. 2.12B shows the computer simulated I_{Ca} during a depolarising step pulse when n_{LTCC} was 1 or 4. The portion of the I_{Ca} current that occurred prior to CRU activation are highlighted (bold coloured lines, Fig. 2.12B) and illustrate that a significant proportion of I_{Ca} is not involved with CICR. Although inactivation of LTCCs was not modelled here, comparison of the trigger current with recorded I_{Ca} over the 20 *ms* duration shown (*e.g.*

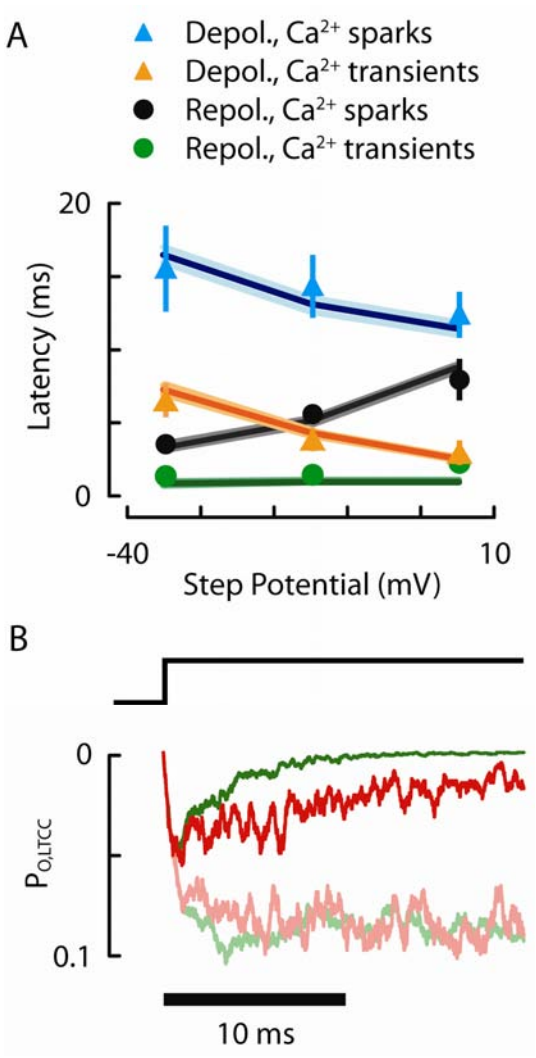

Figure 2.12 Summary of results from computer simulations. (A) Computer simulated latency of SR Ca^{2+} release at various step potentials for depolarising and repolarising steps. The measured latencies are shown as data points, while the computer simulated latencies are shown by lines, where the dark-coloured line is the mean and the light-coloured lines indicate one S.E.M. The parameters that enabled these latencies were $n_{RyR} = 4$ and $n_{LTCC} = 1$ for Ca^{2+} sparks and $n_{LTCC} = 4$ for Ca^{2+} transients. $n_{RyR} = 3$ was used for repolarising step Ca^{2+} spark latencies. **(B)** Computer simulated $P_{O,LTCC}$ at – 15 mV (1000 sweeps) when one (red lines) or four (green lines) LTCCs are available. The light-coloured lines are averaged total $P_{O,LTCC}$, while the bright-coloured lines are averaged trigger $P_{O,LTCC}$ (i.e. prior to CRU activation).

McDonald, *et al.*, 1994; Josephson, *et al.*, 2010a) is still consistent with this idea.

2.4. Discussion

[Ca^{2+}]-dependence of CRU activation

The delay from sarcolemmal depolarisation to SR Ca^{2+} release during EC coupling involves the progression of several processes, namely: *(1)* LTCC activation; *(2)* influx through LTCCs and diffusion of Ca^{2+} to the CRU; *(3)* CRU activation and *(4)* SR Ca^{2+} release and diffusion of Ca^{2+} out of the junction.

The basis of the data analyses presented here begins with the simple rationale that *(1)* during a depolarising step, LTCCs are initially closed and begin to open when the depolarising step is made and *(2)* during a repolarising step, LTCCs are already opened (to maximum $P_{O,LTCC}$) by the pre-pulse to ~ 100 *mV*, but are unable to conduct Ca^{2+} until the driving force for Ca^{2+} entry is increased by repolarisation. The simplest interpretation is that for a given repolarising step, the SR Ca^{2+} release latency is a measure of the average time it takes for that i_{Ca} at that potential to activate a CRU, while the difference (ΔL) is a measure of the latency to the first LTCC opening, $\tau_{act,LTCC}$ (Eqn. 2.3). Depending on the number of LTCC openings required to activate CICR, the voltage-dependence of repolarising step latency could follow the estimated voltage([Ca^{2+}])-dependence of the rate of RyR activation closely, or be made more shallow due to some remaining dependence on LTCC activation.

In these studies, both Ca^{2+} transient and Ca^{2+} spark latencies during repolarising steps revealed a near linear dependence on i_{Ca} (Fig. 2.7C), which is slightly steeper than that of Ca^{2+} spikes at V_{REPOL} of – 120 to - 40 *mV* (Poláková, *et al.*, 2008, but see Altamirano and Bers, 2007b and Inoue and Bridge, 2005 who observed much longer latencies). However, several studies suggest a steeper [Ca^{2+}]-dependence of RyR channel activation (Zahradníková, *et al.*, 1999; Zahradníková, *et al.*, 2004; Laver and Honen, 2008). One possible explanation is that, at the very negative potentials shown here (e.g. – 120 *mV*, associated with very large i_{Ca}), steady-state $[Ca^{2+}]_{junction}$ is within the linear range of the [Ca^{2+}]-dependence (*i.e.* near and above the K_D ~ 40 μM for RyR activation, see for example, Fig. 2.2B). At more positive potentials and in the presence of nifedipine, where $[Ca^{2+}]_{junction}$ during an LTCC opening is small, the repolarising step latencies measured here

may be steeper (see filled circles at i_{Ca}/i_{Ca} at $0\,mV < 1$, Fig. 2.7C), though further measurements at potentials above $0\,mV$ for a longer observation duration would be necessary.

Previous work modelling Ca^{2+} influx into a junction suggested that steady-state $[Ca^{2+}]_{junction}$ might be $\sim 65\,\mu M$ in the centre of a junction with a $0.2\,pA$ influx, with steady-state $[Ca^{2+}]_{junction}$ being proportional to i_{Ca} (Soeller and Cannell, 1997). At $0\,mV$, i_{Ca} is estimated to be $0.06 - 0.12\,pA$ (Guia, *et al.*, 2001), which gives an estimated $[Ca^{2+}]_{junction}$ $\sim 20 - 40\,\mu M$, which is near the K_D for the $[Ca^{2+}]$ activation of RyR channels. At the K_D, $dP_{O,RyR}/d[Ca^{2+}]$ is ~ 25 % of the Hill coefficient (Cannell and Thomas, 1994), which means the slope of the on rate would be near linear despite a higher Hill coefficient for the underlying process. When nifedipine is absent, Ca^{2+} entering the junction is much larger, which would lead to operation in the highly sub-linear range of RyR channel activation (see blue squares, Fig. 2.7C).

Apart from i_{Ca}, $\tau_{O,LTCC}$ also affects the ability of an LTCC opening to trigger SR Ca^{2+} release, for example, a $0.03\,ms$ opening raises $[Ca^{2+}]_{junction}$ to only half that of a $0.3\,ms$ opening at the same potential (see asterisks in Fig. 2.10 and Fig. 2.2A). This becomes increasingly important with decreasing V_m as $\tau_{O,LTCC}$ decreases (Josephson, *et al.*, 2010b) and LTCC openings are no longer faithfully reflected by $[Ca^{2+}]_{junction}$. While CRUs that do not fire initially may be activated by subsequent LTCC openings at V_{REPOL} within the window current (and thereby increase mean latency), LTCC re-openings are highly unlikely at very negative V_{REPOL} (McDonald, *et al.*, 1994; Poláková, *et al.*, 2008). Thus, only CRUs that are activated during the initial repolarisation contributed to latency (which was short at very negative potentials, Fig. 2.7), while the remaining failed sites contribute to a reduced P_{spark}, or Ca^{2+} transient maximum rate of rise. As i_{Ca} increased (with decreasing V_{REPOL}), the maximum rate of rise of Ca^{2+} transients increased with an approximately square dependence from $+ 20\,mV$ ($[Ca^{2+}]_{junction} \sim 15\,\mu M$) until $- 40\,mV$, where the maximum rate of rise began to decrease again (Fig. 2.8C). A similar result was obtained in an early study that measured Ca^{2+} transient amplitude as a function of V_{REPOL} (Fan and Palade, 1999). The initial increase in SR Ca^{2+} release can be explained by the effect of $[Ca^{2+}]_{junction}$ on $P_{O,RyR}$ (Laver and Honen, 2008). The fitted relationship between maximum rate of rise of Ca^{2+} transients and i_{Ca} (see Fig. 2.8C) is in agreement with two (e.g. Fabiato, 1985b; Cannell, *et al.*, 1994; Santana, *et al.*, 1996) or 3 (e.g. Laver, 2009) occupied binding sites (but not one,

e.g. López-López, *et al.*, 1995; Fan and Palade, 1999 or four, e.g. Zahradníková, *et al.*, 2004; Zahradníková, *et al.*, 2007).

However, the decrease in maximum rate of rise at very negative V_{REPOL} (and high i_{Ca}) is problematic. For example, at – 135 *mV*, $[Ca^{2+}]_{junction}$ is expected to reach ~ 200 *μM* at steady-state. Though this is now within the range where RyR $[Ca^{2+}]$-inactivation is thought to occur (Gyorke and Fill, 1993; Schiefer, *et al.*, 1995; Sitsapesan, *et al.*, 1995; Valdivia, *et al.*, 1995; Gyorke, 1999, but see Chu, *et al.*, 1993), another possible explanation is that CICR is now limited by $\tau_{O,LTCC}$, since it decreases with decreasing step voltage (McDonald, *et al.*, 1994). A recent study of rat LTCCs using on-cell single-channel recording has shown that $\tau_{O,LTCC}$ decreases to ~ 0.44 *ms* (dead-time subtracted, Josephson, *et al.*, 2010a; Josephson, *et al.*, 2010b) at – 30 *mV* from ~ 1 *ms* at 0 *mV*. These data suggest that at much more negative potentials, $\tau_{O,LTCC}$ is likely much shorter than the time required for $[Ca^{2+}]_{junction}$ to reach steady-state (Soeller and Cannell, 1997), which would reduce the ability of an LTCC opening to trigger SR Ca^{2+} release. At – 135 *mV*, $\tau_{O,LTCC}$ can be estimated to be ~ 2 *μs* (see Methods). In this time, $[Ca^{2+}]_{junction}$ might only reach ~ 20 % of that attained in 0.3 *ms* (Fig. 2.2A). Although LTCC gating kinetics at such negative potentials have not been reported, the idea that $\tau_{O,LTCC}$ limits coupling fidelity is supported by some preliminary experiments with FPL (white squares, Fig. 2.8C), which prolongs $\tau_{O,LTCC}$. FPL appeared to remove the decrease in Ca^{2+} transient maximum rate of rise at very negative potentials. This observation also rules out RyR $[Ca^{2+}]$-dependent inactivation since $[Ca^{2+}]_{junction}$ should be even higher in this scenario. Polakova, *et al.* (2008) also reported an increase in Ca^{2+} spike probability at – 120 *mV* upon the addition of BayK-8644, another LTCC agonist known to prolong $\tau_{O,LTCC}$. However, BayK-8644 also prolongs $\tau_{C,LTCC}$ and in combination with its inability to be washed out (to check for run-down effects, Bechem, 1993, McDonald, 1994), mean that the increase in Ca^{2+} spike latencies in BayK-8644 is problematic. It should be noted that although these data do not exclude the possibility of RyR $[Ca^{2+}]$-inactivation, RyR inactivation is thought to be much slower than the time-course of CICR (Schiefer, *et al.*, 1995).

Repolarising step latencies at more positive potentials could be reproduced when n_{LTCC} was 1 and n_{RyR} was 3 when nifedipine was present (black lines, Fig. 2.12A). When nifedipine was absent, recorded latencies during repolarising steps could be reproduced when n_{RyR} was 4 and n_{LTCC} was 4 (green lines, Fig. 2.12A). This four-fold increase in the number of

LTCCs available is consistent with the decrease in I_{Ca} amplitude due to nifedipine (Fig. 2.4A) and lends support to the idea that the model stoichiometry may be approximately correct. At more negative potentials, the predicted latency was very short. For example, at – 135 *mV*, the expected latency from the computer model was ~ 0.60 ± 0.01 *ms*, which is similar to that measured here (Fig. 2.7C) and by Polakova, *et al.* (2008) using Ca^{2+} spikes (~ 0.7 *ms*). That is, despite relatively similar data, the interpretations are different because Polakova, *et al.* (2008) could not correctly measure the expected short $\tau_{O,LTCC}$ at very negative potentials and did not take into account the voltage-dependence of $\tau_{O,LTCC}$ when extrapolating coupling fidelity to 0 *mV*.

Latency of SR Ca^{2+} release due to LTCC activation

The measured latencies of Ca^{2+} transients during depolarising steps (Fig. 2.6C) are similar to those reported in previous studies, which also showed that latency decreased as step potential increased (Cleemann and Morad, 1991; Isenberg and Han, 1994; Sham, *et al.*, 1998, but see Altamirano and Bers, 2007b). Similarly, the Ca^{2+} spark latencies were similar to those reported elsewhere (López-López, *et al.*, 1995; Collier, *et al.*, 1999; Inoue and Bridge, 2005), although at + 50 *mV*, Collier, *et al.* (1999) observed a wide distribution of Ca^{2+} spark latencies in the absence of an LTCC antagonist.

As test potential increased, latency decreased approximately e-fold every 40 *mV*. The steepness of this relationship is consistent with the voltage-dependence of $\tau_{C,LTCC}$ estimated from the work of Josephson, *et al.* (2010b) and Rose, *et al.* (1992), combined with slower CRU activation at more positive potentials. When latencies during repolarising steps to the same potentials were subtracted, ΔL (Fig. 2.9A) revealed a steeper dependence on voltage that was closer to the voltage-dependence of $\tau_{C,LTCC}$.

At $n_{RyR} = 4$, the computer model presented here produced CRU activation latencies that are in general agreement with both Ca^{2+} transient (using $n_{LTCC} = 4$) and Ca^{2+} spark ($n_{LTCC} = 1$) latencies observed during depolarising steps (Fig. 2.11B). These values are approximations that have not included the likely important spatial gradients within a junction that would mean four RyR channels are unlikely to sense the same [Ca^{2+}] produced from the opening of one or few LTCCs, nor does it consider any spatial gradients that may develop as a result of channel gating within the CRU (*e.g.* the possibility of a single RyR channel openings that fail to initiate a Ca^{2+} spark, but nevertheless contribute to $[Ca^{2+}]_{junction}$, Sato and Bers,

2011). To address the former issue, Cannell and Soeller (1997) showed that in various RyR channel arrangements (~ 4 – 9 RyR channels with respect to one open LTCC), CRU activation was most affected by whether an RyR was directly opposed to the open LTCC, rather than the number of extra RyR channels surrounding the one closest to the LTCC. That is, although the modelling here suggests that 4 RyR channels can explain the observed CICR latencies, this is only a lower limit for the number of RyRs that are present within a CRU. Another point to consider is that as n_{LTCC} increases, the number of RyR channels that sense the trigger Ca^{2+} should increase, which should make the voltage/[Ca^{2+}]-dependence of RyR activation appear more shallow. Nevertheless, the agreement between the simulated and measured latencies support the idea that a small number (*e.g.* ~ 1 - 2) of LTCC openings functionally trigger SR Ca^{2+} release during EC coupling and that activation of the first RyR channel is then sufficient to activate the entire CRU to produce a Ca^{2+} spark.

The computer model also allowed estimation of the number of LTCC openings that occurred prior to CRU activation, which allowed the calculation of $P_{CPL,\tau O}$. When $n_{LTCC} = 1$ and $V_{DEPOL} = -15$ *mV*, $P_{CPL,\tau O}$ was 1.0. At more negative potentials, $P_{CPL,\tau O}$ decreased due to the reduction in $\tau_{O,LTCC}$ (as discussed earlier) and also at more positive potentials due to a reduction in i_{Ca}. These coupling fidelities are substantially higher than those estimated by Polakova, *et al.* (2008), who recorded Ca^{2+} spike latencies at $V_{REPOL} = -120$ *mV* to estimate P_{CPL} at 0 *mV*. Even in the presence of cAMP, P_{CPL} was only ~ 0.15. When extrapolated to 0 *mV*, P_{CPL} reduced to ~ 0.04, which implies a large LTCC density to produce the short latencies observed (*e.g.* 20 – 60 n_{LTCC}/couplon). As noted above, in the computer simulations presented here, $P_{CPL,\tau O}$ at very negative potentials was very small due to the inability of the short open times to raise $[Ca^{2+}]_{junction}$ sufficiently. This means that extrapolating P_{CPL} by an exponential function from – 120 to 0 *mV* is inappropriate, since P_{CPL} should increase, then decrease with voltage as a function of both increasing $\tau_{O,LTCC}$ and decreasing i_{Ca} (see Gómez, *et al.*, 1997). At very negative potentials, Polakova, *et al.* (2008) may have over-estimated $[Ca^{2+}]_{junction}$ due to the assumption of steady-state and over-estimation of $\tau_{O,LTCC}$ due to the inability of the whole-cell voltage-clamp to step instantaneously from + 50 to – 120 *mV*. Single-channel studies will be useful to confirm $\tau_{O,LTCC}$ at such negative potentials, particularly following a pre-pulse to a very positive potential. Another concern for previous analysis was that $\tau_{O,LTCC}$ was assumed to be voltage-independent, while i_{Ca} was assumed to decrease linearly with voltage. This is in contrast to a clear increase in the time-constant of recovery for measured tail currents from

– 120 to – 40 *mV* (Poláková, *et al.*, 2008, consistent with a previous study, Fan and Palade, 1999) and increased I_{Ca} integral from – 120 to – 40 *mV*, which is consistent with a $\tau_{O,LTCC}$ that increases with voltage, even if i_{Ca} decreases near-linearly. Though it is unclear what current-voltage relationship was used, they reported a ~ 0.1 fmol of carried charge for one LTCC opening of 0.52 *ms* at – 120 *mV*, which is equivalent to an i_{Ca} of ~ 4 pA. This is much larger than the current calculated in this computer model (1.13 *pA*, based on Rose, *et al.*, 1992; Guia, *et al.*, 2001 and Eqn. 2.2) and linear extrapolation using previously reported slopes (Rose, *et al.*, 1992; Guia, *et al.*, 2001) would lead to a very large i_{Ca} at 0 *mV* (*i.e.* ~ 0.9 *pA*), which would lead to an under-estimation of P_{CPL}.

When Ca^{2+} sparklets and Ca^{2+} sparks were evoked in cells under loose-seal patch clamp, the estimated P_{CPL} was ~ 0.7 for a step pulse to ~ 0 *mV* for one LTCC and the mean delay between Ca^{2+} sparklet and Ca^{2+} spark activation was ~ 6.7 ms (Wang, *et al.*, 2001). Though these values are similar to those measured here, Ca^{2+} sparklet measurements were made in the presence of 10 *μM* FPL and 20 *mM* $[Ca^{2+}]_O$, which should have increased $\tau_{O,LTCC}$ and i_{Ca} (Wang, *et al.*, 2001; Cheng and Lederer, 2008). Extrapolation to more physiological conditions (*e.g.* 1 *mM* $[Ca^{2+}]_O$ in the absence of FPL) yielded a P_{CPL} of ~ 0.006 at 0 *mV*, or 1 in ~ 170 LTCC openings. By another method, comparison of the estimated microscopic (γ ~ 600, by the ratio of estimated Ca^{2+} spark flux integral, 3 *pA* for 10 *ms*, to one open LTCC flux integral, 0.1 *pA* for 0.5 *ms*) and measured macroscopic (G ~ 10) gains, Cheng and Lederer (2008) calculated that only 1 in ~ 60 LTCC openings activated a Ca^{2+} spark. Thus, their conclusion was that P_{CPL} was extremely low, even at 0 *mV*. This conclusion may be erroneous due to the lack of consideration for LTCC re-openings (i.e. $\tau_{C,LTCC}$), which may be significant at 0 *mV* (McDonald, *et al.*, 1994; Josephson, *et al.*, 2010a). Macroscopic gain does not distinguish between LTCC openings before and after CRU activation and as such, the majority of the 60 openings could occur after CRU activation in the whole-cell. That is, LTCC openings that are involved in CRU activation are only a small fraction of the total current (Fig. 2.12B, see also Fabiato, 1985b; Fabiato, 1985a; Eisner and Trafford, 2009). Furthermore, incorporation of LTCC re-openings into the analysis would predict that FPL should reduce the latency of SR Ca^{2+} release if P_{CPL} is < 1, rather than increase it, as calculated by Cheng and Lederer (2008). In connection with this point, the relatively long measured Ca^{2+} spark-sparklet latency of ~ 7 *ms* in FPL may have resulted from Ca^{2+} sparklets arising in a different region of the cell from the couplon that generated the spark. This might result from geometric distortion of the junction by the patch pipette or reflect

non-junctional LTCC in the surface membrane as it is unknown whether LTCCs exist only in couplons (Kawai, *et al.*, 1999; Scriven, *et al.*, 2000).

To test whether Ca^{2+} sparklets can be observed without the presence of a patch pipette, Ca^{2+} sparks evoked in the presence of 10 μM FPL were compared to those evoked without trigger augmentation (Fig. 2.13). In the presence of FPL, an increase in fluorescence at the foot of the Ca^{2+} spark was not observed in 63 events, even when aligned by their maximum rates of rise and averaged to improve signal-to-noise ratio. When these Ca^{2+} sparks were compared to spontaneous release events, no difference could be observed at the foot of fluorescence increase (Fig. 2.13B), which suggests that Ca^{2+} sparklets do not normally occur.

A minimal computer model presented by Sobie, *et al.* (2009) appeared to agree with a low coupling gain and fidelity, in contrast to the data and interpretation shown here. The model of Sobie, *et al.* (2009) assumed *(1)* $[Ca^{2+}]_{junction}$ was proportional to $\tau_{O,LTCC}$ during an LTCC opening (in contrast to the results of Soeller and Cannell, 1997), *(2)* that LTCCs only opened once during a test pulse (which unlikely to be true within the window current, McDonald, *et al.*, 1994), *(3)* LTCCs that opened did so at the same time (*i.e.* not a stochastic process, as modelled here), *(4)* $\tau_{O,LTCC}$ was voltage-independent (in contrast to the results of Josephson, *et al.*, 2010b) and *(5)* i_{Ca} was linear with voltage (Hille, 2001). As

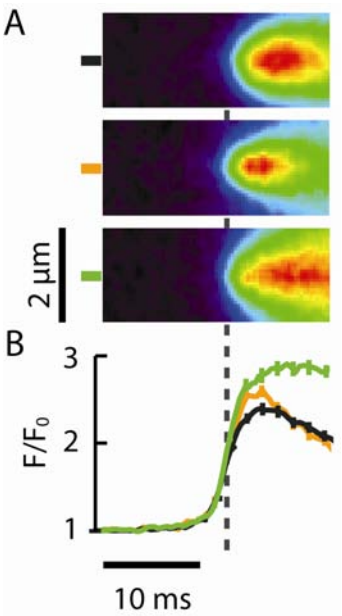

Figure 2.13 Ca^{2+} sparks aligned by maximum rate of rise. ***(A)*** Spontaneous (*black*, *n = 75*) and AP-evoked (current-clamp, where pipette solution was similar to that for voltage-clamp, but with K^+ instead of Cs^+) events without (*orange*, *n = 30*) and with (*green*, *n = 63*) FPL show comparable time-courses ***(B)*** and rates of rise, with no evidence of a 'foot' or Ca^{2+} sparklet. Ca^{2+} sparks in FPL appear wider due events being less-well separated. When ryanodine and thapsigargin were added, 'local' increases in fluorescence were not observed along scan-lines that had previously shown Ca^{2+} sparks.

explained above, these considerations are important when extrapolating measurements from a different potential (*e.g.* Poláková, *et al.*, 2008) and/or from conditions where LTCC gating has been altered (*e.g.* Wang, *et al.*, 2001).

Number of LTCCs in a junction

These data and the accompanying computer simulations are consistent with n_{LTCC}/couplon = 1 and 4 in the presence and absence of nifedipine, respectively. Although this 4-fold difference in LTCC availability is consistent with the measured reduction in I_{Ca} (Fig. 2.4A), it is important to compare this value to other reports. If 4 LTCCs are available in a couplon under physiological conditions, assuming ~ 30,000 CRUs per cell (Soeller, *et al.*, 2007), i_{Ca} = 0.06 – 0.12 *pA* (*Guia, et al., 2001*) and $P_{O,LTCC}$ = 0.1 - 0.2 (Rose, *et al.*, 1992; Josephson, *et al.*, 2010b) at 0 *mV* then whole-cell I_{Ca} is ~ 1.8 *nA/cell* or 8.7 *pA/pF* for a 207 *pF* cell (3 month old rat, Bers, 2001), which is similar to that measured in intact myocytes (*e.g.* Yuan, *et al.*, 1996). This is in contrast to previous binding studies and measurement of surface charge movement, which suggested much larger LTCC density (*e.g.* 300,000 per cell, Bers and Stiffel, 1993), but consistent with previous electrophysiological estimates (*e.g.* McDonald, *et al.*, 1986). The discrepancy may be due to the presence of LTCCs that are not available to contribute to the trigger for CICR (*e.g.* those in inactive or low availability states).

Latency during an action potential

The Ca^{2+} transient latencies in response to the AP measured in this study (Fig. 2.3B) are similar to those measured previously in rabbit myocytes (2 to 6 *ms* after peak of AP, Inoue and Bridge, 2003), with minor differences possibly due to the species-differences in AP shape. The Ca^{2+} spark latencies reported here (Fig. 2.5B) are also similar to latencies measured in isolated myocytes that were electrically field-stimulated (Kong and Cannell, 2010). An earlier study in field-stimulated myocytes that compared the fluorescence signals due to the Ca^{2+} transient in the absence and presence of ryanodine and thapsigargin (to reveal the trigger) showed no detectable latency between them (Cannell, *et al.*, 1994). This suggested that the latency between trigger influx and SR Ca^{2+} release was within ~ 2 - 4 *ms* (two lines in the line-scan image) during an AP (although the shape of the AP at later times is likely to have changed by the loss of SR Ca^{2+} release, Cannell, *et al.*, 1994). This is

similar to the latencies reported here and supports the idea that most of the waiting time during CICR is due to LTCC activation.

To test whether the LTCC waiting times could explain the latencies in Ca^{2+} sparks during the changes in i_{Ca} and LTCC gating parameters during an AP, ΔL was used to compute an expected latency by converting it from a function of voltage (Fig. 2.9A) to a function of time (since the AP profile is the transform between voltage and time). Fig. 2.9B shows the resulting estimates of LTCC waiting time during an AP for Ca^{2+} transients and Ca^{2+} sparks, which are similar to the measured values in Fig. 2.3B and Fig. 2.5B, respectively. The agreement is poor at high I_{Ca} (during Ca^{2+} transients) at later times possibly due to the lack of LTCC Ca^{2+}- and time-dependent inactivation in these calculations (Josephson, *et al.*, 2010a). Nevertheless, the general trend seems to support the conclusions from the analysis of the depolarising and repolarising step latencies: that during an AP, waiting for a ~ single LTCC opening from a pool of ~ 4 available LTCCs in a couplon can explain the observed latency in SR Ca^{2+} release. When nifedipine is used to reduce LTCC availability so that on average less than 1 is available per couplon, Ca^{2+} spark latency increases ~ 4-fold due to Eqn. 2.3. This is in reasonable agreement with the requirement of three available LTCCs concluded by Inoue and Bridge (2003) and with the conclusions of Altamirano and Bers (2007b), who also suggested that one LTCC opening is sufficient to activate SR Ca^{2+} release at 0 *mV*.

Estimating the time-course of Ca^{2+} spark production from a Ca^{2+} transient

Even though the results of Ca^{2+} transients and Ca^{2+} sparks are in general agreement, the application of nifedipine may have unknown effects on CICR. The purpose of using nifedipine was to increase signal contrast by reducing P_{spark}. If P_{spark} or SR Ca^{2+} release flux (*e.g.* Sipido and Wier, 1991) can be measured or calculated directly from Ca^{2+} transients, then use of nifedipine (or any other perturbation to physiological CICR) can be avoided. Deconvolution was used in an attempt to restore P_{spark} from Ca^{2+} transients measured at high time resolution (Fig. 2.3, see also Tanaka, *et al.*, 1998). Fig. 2.14B shows an example of deconvolving a Ca^{2+} transient (Fig. 2.3) with a Ca^{2+} spark (Fig. 2.14A). Discrete sites of release can be seen, which are likely the in- and out-of-focus active release sites within the confocal scan volume, but restricted to sarcomeric periodicity. When the signal profiles at each local region was aligned and averaged (blue line, Fig. 2.14D), the duration of release is shorter than suggested by the first derivative of the Ca^{2+} transient (red line, Fig. 2.14D,

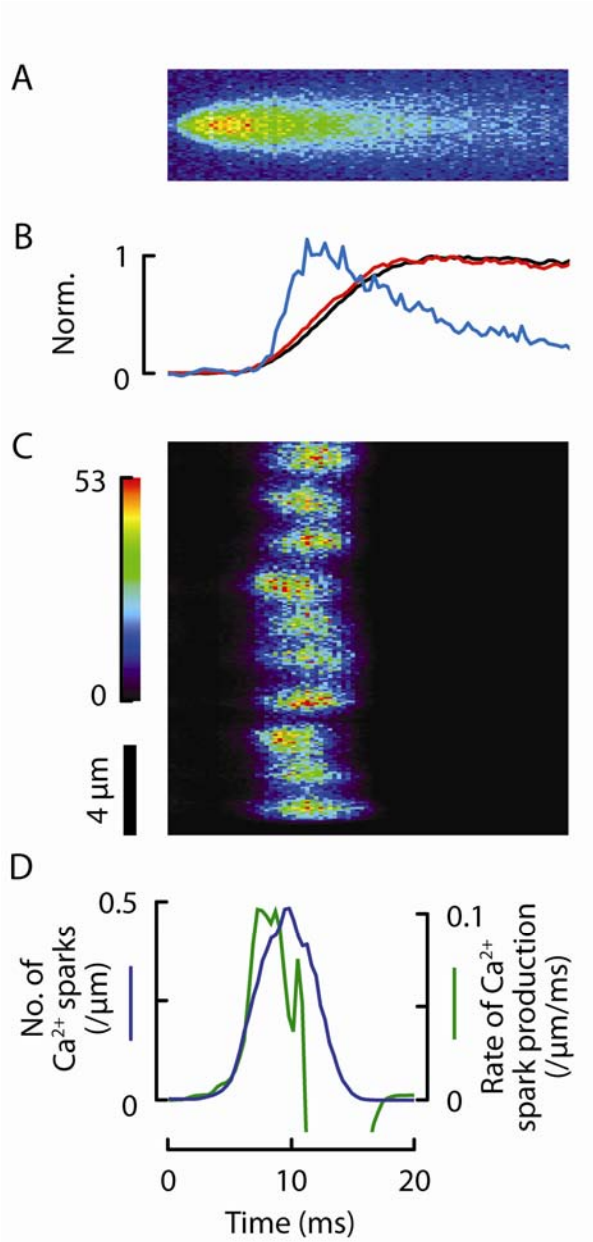

Figure 2.14 Using de-convolution to estimate Ca^{2+} spark production during a Ca^{2+} transient. (A) A high signal-to-noise spontaneous Ca^{2+} spark used as the point-spread function. It was scaled so that its total signal mass was unity. **(B)** shows the time-course of a Ca^{2+} spark (blue line) and Ca^{2+} transient (red line, 1.8 μm periodic regions and black line, whole image average, from Fig. 2.3). **(C)** Result of deconvolving a Ca^{2+} transient (shown in Fig. 2.3) with the Ca^{2+} spark shown above by a Richardson-Lucy method (150 iterations). **(D)** The time profiles of the periodic, discrete regions were aligned in time and averaged to give the average number of Ca^{2+} sparks occurring through time (blue line). This is shown with the first derivative of the Ca^{2+} transient (red line, from Fig. 2.3). The calibration assumes an average Ca^{2+} spark amplitude of $\Delta F/F_0 = 0.5$.

from Fig. 2.3B) or Ca^{2+} spark measurements. This may be a manifestation of Ca^{2+}- and time-dependent LTCC activation (McDonald, *et al.*, 1994; Josephson, *et al.*, 2010a) and a refractory period of the CRU (Brochet, *et al.*, 2005; Sobie, *et al.*, 2005; Ramay, *et al.*, 2011), which would be more pronounced during normal I_{Ca} compared to in the presence of nifedipine.

Limitations

The underlying assumption in the computer model and interpretations presented here is that the number of available LTCCs during depolarising and repolarising step protocols are the same. Though both protocols used a holding potential $-80\ mV$, the depolarising step

protocol included a slow (550 *ms*) ramp to - 40 *mV* immediately before the test pulse to inactivate the Na^+ channels. This may have reduced LTCC availability, athough McDonald, *et al.* (1994) suggests that this effect would be < 0.2 n_{LTCC}). Another uncertainty is that of LTCC gating parameters. For example, $\tau_{O,LTCC}$ at 0 *mV* has been reported to be as low as ~ 0.2 *ms* (Rose, *et al.*, 1992) and up to 1 *ms* (Josephson, *et al.*, 2010b). Further clarification would be important in determining coupling fidelity and gain. However, if $P_{O,LTCC}$ was much lower, then the kinetics of the other processes (e.g. RyR channel gating) would have to be much faster to be consistent with the latencies presented here, though it is possible that LTCCs could be coupled (e.g. Navedo, *et al.*, 2010, though this has yet to be verified by another method.

2.5. Summary

These results suggest that only a few (~ 4) LTCCs are needed in a junction to allow even fewer openings to trigger a Ca^{2+} spark (~ 1 at - 15 *mV* and ~ 2 at 0 *mV*). The majority of the EC coupling latency during depolarising steps appears to be due to the kinetics of LTCC activation. During repolarisation, SR Ca^{2+} release is consistent with the $[Ca^{2+}]_i$-dependence of RyR activation kinetics measured in bilayers when the LTCC:RyR stoichiometry is 1:4. At negative step potentials, the reduction in $\tau_{O,LTCC}$, is not compensable by the increase in i_{Ca}, so that $[Ca^{2+}]_{junction}$ during an LTCC opening decreases which can explain the observed reduction in SR Ca^{2+} release during repolarising steps and the previously-reported low coupling fidelity (Poláková, *et al.*, 2008). During the rat AP, latencies are longer than those measured during repolarising steps, but shorter than those measured during depolarising steps. This supports the idea that during an AP, most of the latency in SR Ca^{2+} release is due to waiting for LTCCs to open, but that this rate of activation is maximised during the rapid upstroke to very positive potentials. The initial repolarisation phase increases the driving force for Ca^{2+} entry, but at a much slower rate than that achieved by a repolarising step. These data are consistent with the idea (e.g. Inoue and Bridge, 2003) that the majority of LTCCs serve to reduce waiting time for LTCC openings and that a significant fraction of I_{Ca} does not participate in CICR, but may serve a different purpose (*e.g.* regulate $[Ca^{2+}]_{SR,}$ Fabiato, 1985a). This highlights a potential problem in the concept of EC coupling 'gain'. The relationship between the time-dependence of I_{Ca} and SR Ca^{2+} release is complex and non-unique so that it is possible to under-estimate the true amplification factor between the LTCC opening(s) responsible for triggering CICR and the Ca^{2+} spark that results. That is, at

any given potential, the proportion of LTCC openings that directly contribute to CICR depends on i_{Ca}, open and closed times.

3. Local SR Ca^{2+} Release and Termination

3.1. Background

Once a CRU is activated, a Ca^{2+} spark is thought to progress independently of the trigger due to regenerative CICR within a junction (Cannell, *et al.*, 1995). Despite this positive-feedback, Ca^{2+} sparks exhibit a distinct time-course, which indicates that local SR Ca^{2+} release terminates robustly (*e.g.* Cheng, *et al.*, 1993). To date, the mechanism(s) responsible for the control of termination remain unclear, although several ideas have been proposed, including regulatory mechanisms that are intrinsic to the single RyR channel (e.g. inactivation, Schiefer, *et al.*, 1995), as well as mechanisms that are the product of either the arrangement of RyR channels within a CRU (e.g. coupled gating, Marx, *et al.*, 2001) and/or their location at a terminal SR cistern. The proposed ideas include: *(1)* $[Ca^{2+}]_i$-dependent inactivation and/or adaptation of the RyR channel, although the time-course of this mechanism is several-fold slower than the calculated release flux duration (Gyorke and Fill, 1993; Schiefer, *et al.*, 1995; Sitsapesan, *et al.*, 1995; Valdivia, *et al.*, 1995; Gyorke, 1999, but see Chu, *et al.*, 1993), so may not be relevant during a Ca^{2+} spark. *(2)* Stochastic attrition and *(3)* local SR Ca^{2+} depletion.

Stochastic attrition describes the probabilistic occurrence that all (n) RyR channels within a CRU are closed at the same time (Stern, 1992b). However, this phenomenon becomes increasingly unlikely as n_{RyR} increases, which means the time constant to reach that state (τ_{att}) becomes exceedingly long (Eqn. 3.1, Stern and Cheng, 2004).

$$\tau_{att} = \frac{\tau_O \cdot (1 - (1 - P_O)^n)}{n \cdot P_O \cdot (1 - P_O)^{n-1}} \qquad \textbf{Eqn. 3.1}$$

For example, if *n* is 200 (Franzini-Armstrong, *et al.*, 1999; Soeller, *et al.*, 2007) and each RyR channel exhibited a mean open probability (P_O) and open time (τ_O) of 0.5 and 2 *ms*, respectively (Copello, *et al.*, 1997; Laver and Honen, 2008, see also Chapter 2.2), then τ_{att} would be ~ 10^{55} seconds, which is clearly not possible. Even if *n* was much smaller (e.g. 14, as observed for peripheral CRU, Baddeley, *et al.*, 2009), τ_{att} would be over 2 *s*, which is still much longer than the observed Ca^{2+} spark duration. The likelihood of stochastic attrition may be improved if the RyR channels within a CRU exhibit coupled gating, wherein the gating of one RyR in a cluster is affected by the gating of a neighbour (Stern,

1992b; Sobie, *et al.*, 2002; Stern and Cheng, 2004). Though this would cause a CRU to behave as if there were fewer RyRs in the cluster, the role of coupled gating (Marx, *et al.*, 2001) in release termination remains controversial (see Fill and Copello, 2002; Cheng and Lederer, 2008).

Local SR Ca^{2+} depletion is a possible candidate because a reduction in release flux may be able to reduce $[Ca^{2+}]_{junction}$ to de-activate the CRU. However, the extent of depletion may not be sufficient to terminate CICR (e.g. Zima, *et al.*, 2008b; Ramay, *et al.*, 2011) and may require a $[Ca^{2+}]_{JSR}$-dependent mechanism to increase the sensitivity of RyR channel gating to SR luminal $[Ca^{2+}]$ (*e.g.* Sobie, *et al.*, 2002; Terentyev, *et al.*, 2002). It has been proposed that CSQ may be the luminal Ca^{2+}-sensor and regulator of RyR function (Ikemoto, *et al.*, 1989; Lukyanenko, *et al.*, 1996; Terentyev, *et al.*, 2003; Gyorke, *et al.*, 2004).

To determine which mechanism(s) terminate local SR Ca^{2+} release, it has been useful to investigate which factors effect release duration. In the presence of tetracaine, which reduces RyR P_O (Laver and van Helden, 2011 and similar to the effects of procaine, see Györke, *et al.*, 1997 and references therein), a proportion of CRUs exhibited long-lasting SR Ca^{2+} release events (LLEs, Zima, *et al.*, 2008a). Like Ca^{2+} sparks, LLEs were spatially-localised, but unlike Ca^{2+} sparks, LLEs were associated with an increase in fluorescence that was sustained for up to several seconds before returning to baseline (Zima, *et al.*, 2008a). The plateau in fluorescence suggested that $[Ca^{2+}]$ in the Ca^{2+} spark volume (and by inference, $[Ca^{2+}]_{junction}$) must have reached a pseudo steady-state. For this to be possible, Zima, *et al.* (2008a) proposed that Ca^{2+} efflux from the JSR had been reduced to match Ca^{2+} diffusion from the network SR, perhaps at sites where the network and JSR were already well-connected (Zima, *et al.*, 2008a). However, the details of this scheme are unclear, since the rates of diffusion of Ca^{2+} within the SR and into a particular JSR are not known (e.g. Swietach, *et al.*, 2008; Picht, *et al.*, 2011). In any case, the conclusions of their study combined with observations of an apparent $[Ca^{2+}]_{SR}$ termination 'threshold' implied that under normal circumstances, $[Ca^{2+}]_{JSR}$ depletion is important in the termination of Ca^{2+} sparks (Zima, *et al.*, 2008a; Zima, *et al.*, 2008b). On the other hand, the eventual termination of LLEs showed that another slower (unknown) mechanism was able to stop local SR Ca^{2+} release (Zima, *et al.*, 2008a; Zima, *et al.*, 2008b).

Ca^{2+} sparks that were repeatedly activated from (apparently) the same CRU has shown that Ca^{2+} spark amplitude decreased with decreasing interval between activations (*Δt*). At short *Δt* (~ 50 *ms*), Sobie, *et al.* (2005) showed that Ca^{2+} spark amplitude was as small as ~ 10 *%* of the Ca^{2+} spark amplitude at infinite *Δt*, which strongly supported the idea that $[Ca^{2+}]_{JSR}$ depletion was significant. The time constant for Ca^{2+} spark amplitude restitution was ~ 100 *ms* (Sobie, *et al.*, 2005; Ramay, *et al.*, 2011), although this value appears variable between groups (see Brochet, *et al.*, 2005). When *Δt* was shorter than 50 *ms*, no Ca^{2+} sparks were observed. This observation and the idea that CRU activation should exhibit an exponentially-distributed closed time (*Δt*) led Sobie, *et al.* (2005) to suggest that an additional mechanism (*e.g.* that includes an inactivated state) may be required to explain the apparent refractory period. However, since $[Ca^{2+}]_{JSR}$ was severely depleted at *Δt* below 50 *ms* (i.e. not clamped), it is difficult to determine the cause of the apparent refractory period. Although the authors attempted to correct for missed events in detection of very small amplitude events, the effects of $[Ca^{2+}]_{JSR}$ and release flux on the propagation of CICR within a CRU is unknown. Therefore, whether CRUs require any inactivation mechanism to terminate release remains unclear.

To clarify the mechanism(s) responsible for the termination of CICR, spontaneous local Ca^{2+} release events were recorded in the absence and presence of tetracaine to reduce $n{\cdot}P_O$. The idea behind these experiments was that if termination is purely time-dependent, a reduction in RyR P_O should have no effect on the time-course of Ca^{2+} sparks. If termination is primarily due to stochastic attrition, then local Ca^{2+} release duration should decrease with $n{\cdot}P_O$ (Eqn. 3.1) and/or release flux should decrease if i_{RyR} is constant (which would be the case if $[Ca^{2+}]_{JSR}$ is the same in events). On the other hand, if CICR termination is primarily Ca^{2+}-dependent ($[Ca^{2+}]_i$-inactivation or $[Ca^{2+}]_{SR}$ depletion/desensitisation), then the duration of SR Ca^{2+} release should increase with decreased release flux. Detailed analyses of LLEs and active release sites should, therefore, help clarify the underlying flux regulation and number of RyR channels involved in local SR Ca^{2+} release.

3.2. Methods

Preparation of ventricular myocytes and Ca^{2+} imaging

Rat cardiac ventricular myocytes were enzymatically isolated and prepared for fluorescence imaging as previously described (see Methods, Chapter 2.2). When required, 1 *mM* Ca^{2+}-

Tyrode's solution containing 100 *μM* tetracaine (Sigma-Aldrich) made from a 0.5 *mM* stock in MilliQ water was used.

During imaging, cells were perfused with 1 *mM* Ca^{2+}-Tyrode's solution at room temperature with either of the systems previously described (Methods, Chapter 2.2). Line-scan images of spontaneous Ca^{2+} sparks were obtained using a Zeiss (Germany) laser-scanning confocal microscope *LSM*710 with an LD C-Apochromat 40 x 1.1 N.A. water-immersion objective. Line-scan images of spontaneous Ca^{2+} sparks were oriented along the longitudinal axis of the cell (defined here as *x*). The pixel (*px*) size of recorded images were between 53 – 200 *nm/px* and the time resolution was 0.35 - 1 *ms/line* for 512 *px* and 10,000 – 20,000 lines were recorded.

Curve-fitting and measurement of Ca^{2+} sparks

Image analysis was performed using custom routines written in IDL. Line-scan images were normalized to F/F_0 as previously described (Methods, Chapter 2.2) and spontaneous Ca^{2+} sparks were detected and located using the Matched Filter Detection Algorithm (Kong, *et al.*, 2008). Time profiles of Ca^{2+} sparks were calculated by averaging over 0.3 *μm* on either side of the centroid and fitted to a continuous, biphasic function (Eqn. 3.2), where the rising phase is asymmetric (rising more slowly at the beginning and reaching the peak more rapidly). The rate of rise is determined by τ_{rise} and the rate of decay by τ_{decay}. *S* is the scaling factor and *u* determines the shift in time. For some rapidly-reactiviting release sites observed in the presence of tetracaine, the number of fluctuations (*nf*) was determined by eye prior to fitting.

The fitted result was used to numerically measure Ca^{2+} spark parameters, such as peak fluorescence (F/F_0), amplitude ($\Delta F/F_0$) and time to peak. The start of each fluctuation was defined as the time where the fitted fluorescence exceeded 0.1·maximum rate of rise + F_0, similar to the method described in Chapter 2.2 (Eqn. 2.5). The maximum rate of rise was corrected by subtracting the rate of decay to produce a better estimate of release flux (using rate of decay as an approximation of the rate of Ca^{2+} removal from the junctional space, e.g. Sipido and Wier, 1991). This produced corrected maximum rates of rise measurements that were typically 35 % greater than the measured maximum rates of rise.

$$\frac{F}{F_0}(t) = \sum_{i=1}^{nf} S \cdot e^{-a_i - b_i} + F_0$$ **Eqn. 3.2**

where,

$$a_i = e^{-\frac{(t-u_i)}{\tau_{rise,i}}}$$

$$b_i = \frac{(t-u_i)}{\tau_{decay,i}}$$

The spatial width of a release event was measured at its peak by fitting to a one-dimensional Gaussian function (Eqn. 3.3), where x_0 is the spatial translation (of the centre of the peak) and σ is the width of the curve (related to FWHM as defined).

$$\frac{\Delta F}{F_0}(x) = A \cdot e^{\frac{(x-x_0)^2}{2 \cdot \sigma^2}}$$ **Eqn. 3.3**

where,

$$FWHM = 2 \cdot \sigma \cdot \sqrt{2 \cdot \ln(2)}$$

LLEs exhibited behaviour that was not easily fitted to such simple functions. To obtain measurements from LLEs, time profiles were obtained by spatial averaging across to 0.2 *μm* either side of the centroid and smoothed in time by a Savitzy-Golay filter that was 6 *ms* long. This data was used to obtain maximum rates of rise, peak and time to peak. The start of an event was usually obtained by the fitting the early phase with a Sigmoid function and defining start as where the fitted fluorescence exceeded 0.1·maximum rate of rise + F_0 (see above). Start times of intermediate fluctuations were all determined by eye. The maximum rate of rise and rate of decay for initial and intermediate fluctuations were determined by fitting of a straight line to manually-selected regions of the rising and decaying phases and checking against raw and smoothed data by eye. The maximum rate of rise was corrected as described above. The peak fluorescence was measured by the time profiles and the amplitudes calculated by subtracting the fluorescence at the time of start of the fluctuation from peak fluorescence. Since LLEs exhibited a complex time-course, the event duration was defined by the time for the event to decay by 25, 50 and 80 % of the peak amplitude (t_{25}, t_{50} and t_{80}, respectively). Because these durations were relatively long, time profiles that were further processed by a median (15 *ms*), box car filter (6 *ms*) to

prevent erroneous measurement due to excess noise/fluctuations. This extra filtering step was not used to measure the properties of the shorter rising phase or the peak amplitude. The time interval (*Δt*) between consecutive events/fluctuations was measured from the time of peak of the first event to the start time of the second and is defined as the delay to the second event.

Noise analysis of long-lasting SR Ca^{2+} release

Power spectra of the plateau region LLEs were calculated using the discrete fast Fourier transform (FFT). First, a time profile of the event was taken from one line of pixels through the centre of the event. The mean was subtracted, data-set zero-padded to 2 *s* (if required), then multiplied by a Hanning window that was the same length as the time profile (see Press, *et al.*, 1992). The power spectrum was calculated as the square of the absolute FFT magnitude. The mean duration of these regions was 1.6 ± 0.2 *s*.

To determine the power spectra of a fluorescence profile in the absence of SR Ca^{2+} release, regions nearby the LLEs that contained no apparent release events were analysed. These lines were typically from a period immediately preceding the LLE, but if this region was not long enough to match the length of the corresponding LLE plateau, then an adjacent line would be used. The data processing and FFT calculation was then the same as that for LLE plateaus, as stated above.

For transitions between two states (i.e. open and closed), the power spectrum should follow a single Lorentzian function (Eqn. 3.4, e.g. Larsson, *et al.*, 1996), where k_+ and k_- are the rate constants for the forward and back reactions, respectively, P_{zero} is the power at 0th frequency and f_C is the corner-frequency (i.e. frequency at which P_{zero} is halved).

$$\mathrm{Power(f)} = \frac{P_{zero}}{1 + \left(\frac{2 \cdot \pi \cdot f}{f_C}\right)^2} \qquad \textbf{Eqn. 3.4}$$

where,

$$f_C = \frac{k_+ + k_-}{2 \cdot \pi}$$

Monte Carlo simulations of long-lasting local SR Ca^{2+} release events

To examine whether a decreased RyR P_O (due to tetracaine) and/or increased rate of $[Ca^{2+}]_{JSR}$ refilling are able to affect release duration, a simple computer model was constructed (Fig. 3.1). Free Ca^{2+} was able to move between the network SR, JSR, junctional space, a Ca^{2+} spark volume and the bulk cytosol (Fig. 3.1). Free $[Ca^{2+}]$ in the network SR and cytosol were fixed to 1 *mM* (Shannon, 1997) and 100 *nM* (Cannell, *et al.*, 1987b), respectively. The rate of Ca^{2+} diffusion between the network and JSR was determined by the concentration gradient and k_1, which was set to give a half time of $[Ca^{2+}]_{JSR}$ recovery of ~ 250 *ms* (Brochet, *et al.*, 2005; Zima, *et al.*, 2008b; Picht, *et al.*, 2011; Ramay, *et al.*, 2011) following a local SR Ca^{2+} release.

Ca^{2+} movement from the JSR to junctional space was determined by RyR channel $n{\cdot}P_O$ and i_{RyR}. Eqn. 3.5 describes the linear dependence of i_{RyR} on the JSR-junction $[Ca^{2+}]$ gradient (Mejia-Alvarez, *et al.*, 1999), where *z* is the valence of Ca^{2+} and *F* is Faraday's Constant.

$$i_{RyR} = \frac{0.4\ \mathrm{pA} \cdot ([Ca^{2+}]_{JSR} - [Ca^{2+}]_{junction})}{1\mathrm{mM} \cdot z \cdot F} \qquad \textbf{Eqn. 3.5}$$

RyR $n{\cdot}P_O$ was determined by Monte Carlo simulation of a two-state process (open and

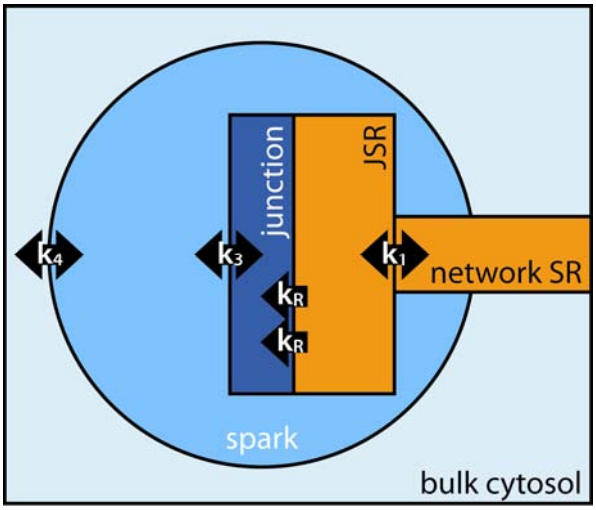

Figure 3.1 Schematic of model used to test the effect of $[Ca^{2+}]_{JSR}$ refilling and reduced RyR P_O on release duration. The compartments of free $[Ca^{2+}]$ were: network SR, JSR, junctional space, Ca^{2+} spark volume and bulk cytosol. Ca^{2+} diffusion between these compartments was determined by the concentration gradient and rate constant (denoted by *k*). See text for details.

Parameter	Value	Notes and References
Time step, dt (μs)	10	
Number of RyR channels	28	See Discussion (section 3.4)
JSR volume, V_{JSR} (aL)	5.03	Cylindrical volume of radius: 200 *nm* and height: 40 *nm*, Brochet, et al., 2005; Knollmann, et al., 2006
Junction volume, V_J (aL)	1.88	Cylindrical volume of radius: 200 *nm* and height: 15 *nm*, Franzini-Armstrong, et al., 1999
Spark volume, V_S (fL)	4.19	Spherical volume of radius: 1 μm, Cheng, et al., 1993
k_1 (/ms)	1×10^{-18}	See text
RyR mean closed time (ms)	Eqn. 2.9	See Chapter 2.2
RyR mean open time (ms)	2	See Chapter 2.2
k_3 ($/ms$)	3.2×10^{-17}	See text
k_4 ($/ms$)	7.4×10^{-14}	See text

Table 3.1 Parameters for simulating long-lasting local SR Ca^{2+} release events in tetracaine. For details, see text.

closed), where the closing and opening rate constants were the inverse of RyR open time and closed time, respectively (see Fig. 2.2B in Chapter 2.2). The rate of Ca^{2+} diffusion between the junction and Ca^{2+} spark volume (to estimate observed free [Ca^{2+}]) and between the Ca^{2+} spark volume and bulk cytosol was determined by their corresponding concentration gradients and k_3 and k_4, respectively. k_3 and k_4 were set so that [Ca^{2+}] in the Ca^{2+} spark volume matched a typical Ca^{2+} spark time-course. Ca^{2+} buffers within each compartment were instantaneous and had capacities of 60 (primarily from CSQ, Murphy, *et al.*, 2011), 25 and 100 (estimated from Shannon, 1997) for the JSR, junction and bulk cytosol, respectively. The parameters used are given in Table 3.1. Flux equations are given below (Eqn. 3.6, Eqn. 3.7 and Eqn. 3.8), where the calculated flux was a quantity per time. This flux was multiplied by the time step (dt) and divided by the respective volume to yield the change in concentration. All calculations were performed in units of μmol and ms. The frequency of oscillations was also calculated as described above and compared to noise analysis of experimentally recorded LLEs.

$$\frac{dCa^{2+}_{JSR}}{dt} = \left(\left[k_1 \cdot ([Ca^{2+}]_{network} - [Ca^{2+}]_{JSR}) - n \cdot P_O \cdot i_{Ca}\right]\right)$$ **Eqn. 3.6**

$$\frac{dCa^{2+}_{junction}}{dt} = \left(n \cdot P_O \cdot i_{Ca} - k_3 \cdot ([Ca^{2+}]_{junction} - [Ca^{2+}]_{spark})\right)$$ **Eqn. 3.7**

$$\frac{dCa^{2+}_{spark}}{dt} = k_3 \cdot ([Ca^{2+}]_{junction} - [Ca^{2+}]_{spark}) + k_4 \cdot ([Ca^{2+}]_{spark} - [Ca^{2+}]_i)$$ **Eqn. 3.8**

Statistics

Statistical significance was determined using non-parametric tests. The Chi-square test for two-samples was used to test the null hypothesis (H_0) that two sample distributions are the same. The Chi-squared test statistic (χ^2) was compared to the Chi-square distribution and the probability of obtaining that value or greater if the H_0 was true (*P*) is given. The method and code for calculating χ^2, the degrees of freedom (*df*, the number of non-zero bins in one group) and associated P-value was modified from Fortran 77 routines published by Press, *et al.* (1992). Where the count within any one bin of the histogram was below five, adjacent bins were accumulated (for both samples). If H_0 was rejected ($P < 0.05$), the Wilcoxon Rank-Sum test was used to test a second hypothesis of whether the two means of distributions were the same. The Rank-Sum test statistic (*Z*) is approximately normally-distributed for sample sizes larger than ten and the two-tailed P-values reported accordingly, where $P < 0.05$ was defined as statistically significant.

3.3. Results

Spontaneous Ca^{2+} sparks in the presence of tetracaine

To examine the effect of tetracaine on local SR Ca^{2+} release, spontaneous Ca^{2+} sparks were recorded in the absence and presence of tetracaine (Fig. 3.2 and Fig. 3.3). These examples were selected to highlight the polymorphisms that are present in Ca^{2+} release events under

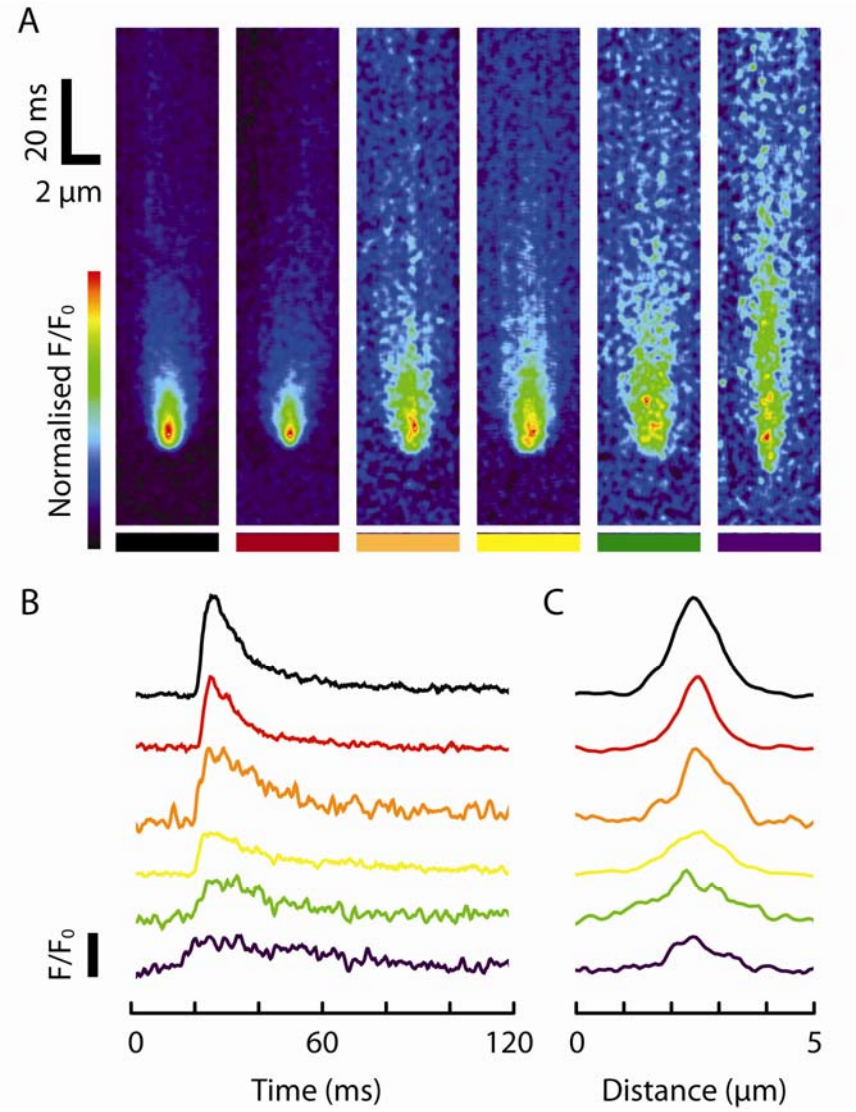

Figure 3.2 Examples of spontaneous Ca^{2+} sparks in the absence of tetracaine. (A) Line-scan images of six Ca^{2+} sparks are shown to illustrate the range of morphology exhibited across different cells and SR Ca^{2+} release sites. More frequent and typical Ca^{2+} sparks are marked by black, red, orange or yellow bars, while rare, unusual events are marked by green or purple bars. The colour table was scaled to each image to highlight their shapes. **(B)** show the corresponding time profiles of the Ca^{2+} sparks shown in *(A)*, coloured in accordance with the aforementioned coloured bars. The profiles are offset for clarity, but all had an initial F/F_0 of one. The vertical scale bar shows one F/F_0. **(C)** shows the corresponding spatial profiles at time of peak.

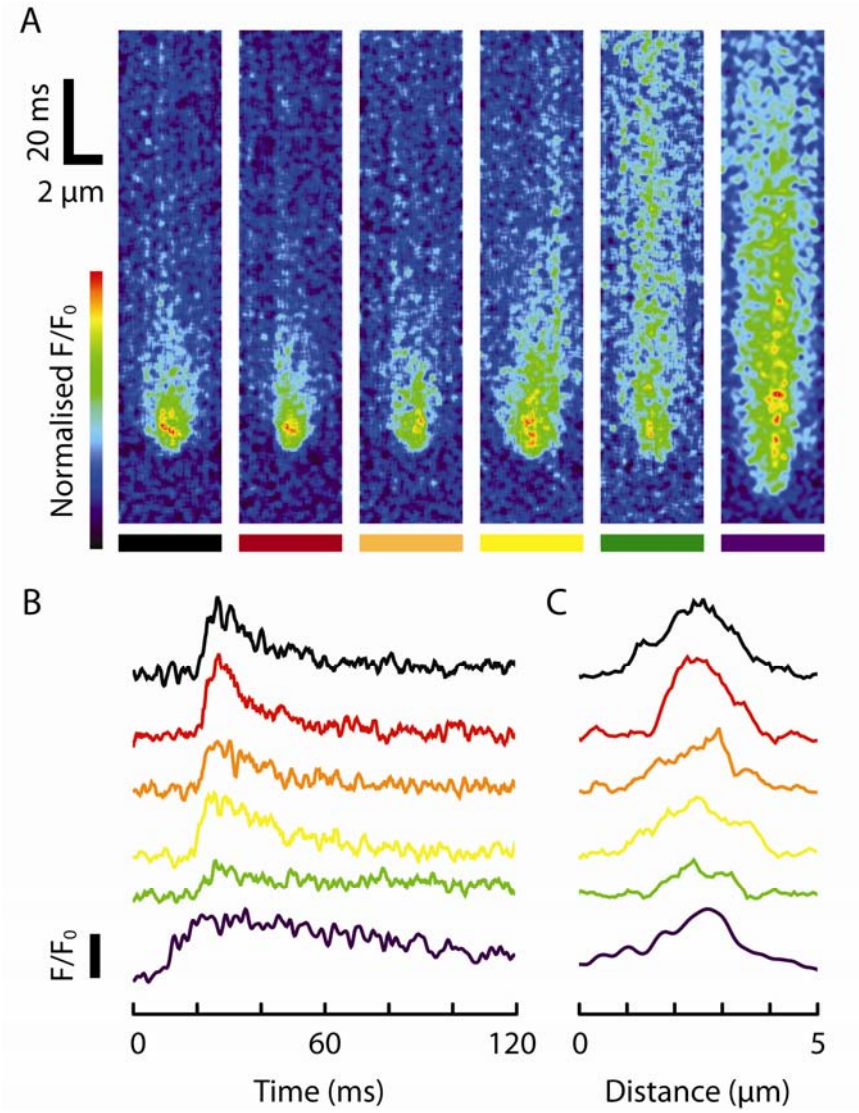

Figure 3.3 Examples of spontaneous Ca^{2+} sparks in the presence of 100 *µM* tetracaine. (A) Line-scan images of six Ca^{2+} sparks in tetracaine to illustrate the range of morphology exhibited across different cells and SR Ca^{2+} release sites. A higher proportion of events are slightly longer (e.g. yellow), while some events were long-lasting (green or purple). The colour table was scaled for each event to highlight the different morphologies. **(B)** The corresponding time profiles of Ca^{2+} sparks coloured as shown in (A). The profiles are offset for clarity, but all had an initial F/F_0 of one. The vertical scale bar shows one F/F_0. **(C)** shows the corresponding spatial profiles of Ca^{2+} sparks at time of peak.

control conditions (see also Shen, *et al.*, 2004). The line-scan images of control Ca^{2+} sparks (Fig. 3.2A) show a high amplitude event (marked in black) alongside a range of typical Ca^{2+} sparks (red, orange, yellow) and unusual events that were longer (green, purple) and/or more narrow (purple). Unusual events ($t_{50} > 50$ *ms*) comprised < 0.4 % of all measured control events. Fig. 3.2B shows the time profiles of these events, where it is clear that the amplitudes are higher for the more typical events.

Following the application of 100 μM tetracaine, Ca^{2+} sparks had smaller amplitudes (Fig. 3.3B), while some events had markedly longer durations than any event observed in control (Fig. 3.3A, marked in green or purple). Approximately 16 % of events observed in tetracaine had a t_{50} that exceeded 50 *ms* (or ~ 40 % of fluctuations were observed at release sites that also exhibited LLEs). Note that there was not a strong correlation between event amplitude and duration (see Fig. 3.6).

The properties of spontaneous Ca^{2+} sparks recorded in cells with and without application of tetracaine are summarised in Fig. 3.4 and Table 3.2. Events that exhibited a plateau before returning to baseline were excluded from these measurements and are presented later. In the presence of tetracaine (blue bars, Fig. 3.4A), the distribution and mean of Ca^{2+} spark peak fluorescence were significantly different to that of control (black bars, Fig. 3.4A), however the magnitude of this difference was small (see Table 3.2). The FWHM of events did not change (Fig. 3.4B), which might be expected as this property is mainly driven by diffusion and microscope blurring. Tetracaine was associated with a ~ 20 % reduction in the maximum rate of rise (Fig. 3.4C), while the time to peak of events was increased by ~ 40 % (Fig. 3.4D).

The decay time-course was also prolonged, where t_{25} was ~ 3 *ms* longer in tetracaine (Fig. 3.4E) and t_{50} (Fig. 3.4F) and t_{80} (not shown) was also prolonged. This difference was due to a prolongation of the time to peak and t_{25} (i.e. associated with release flux) as there was no change in decay times, $t_{50} - t_{25}$ (Fig. 3.4F inset) and $t_{80} - t_{50}$ (Fig. 3.4G). The integral of event fluorescence greater than half maximum amplitude was smaller in tetracaine (median $F/F_0 \cdot ms$ ~ 9.0 compared to ~ 10.3 in control, Fig. 3.4H). Overall, the most pronounced changes in the spark-like Ca^{2+} sparks in tetracaine were decreased maximum rate of rise and prolonged time-course in the early phases (time to peak and t_{25}).

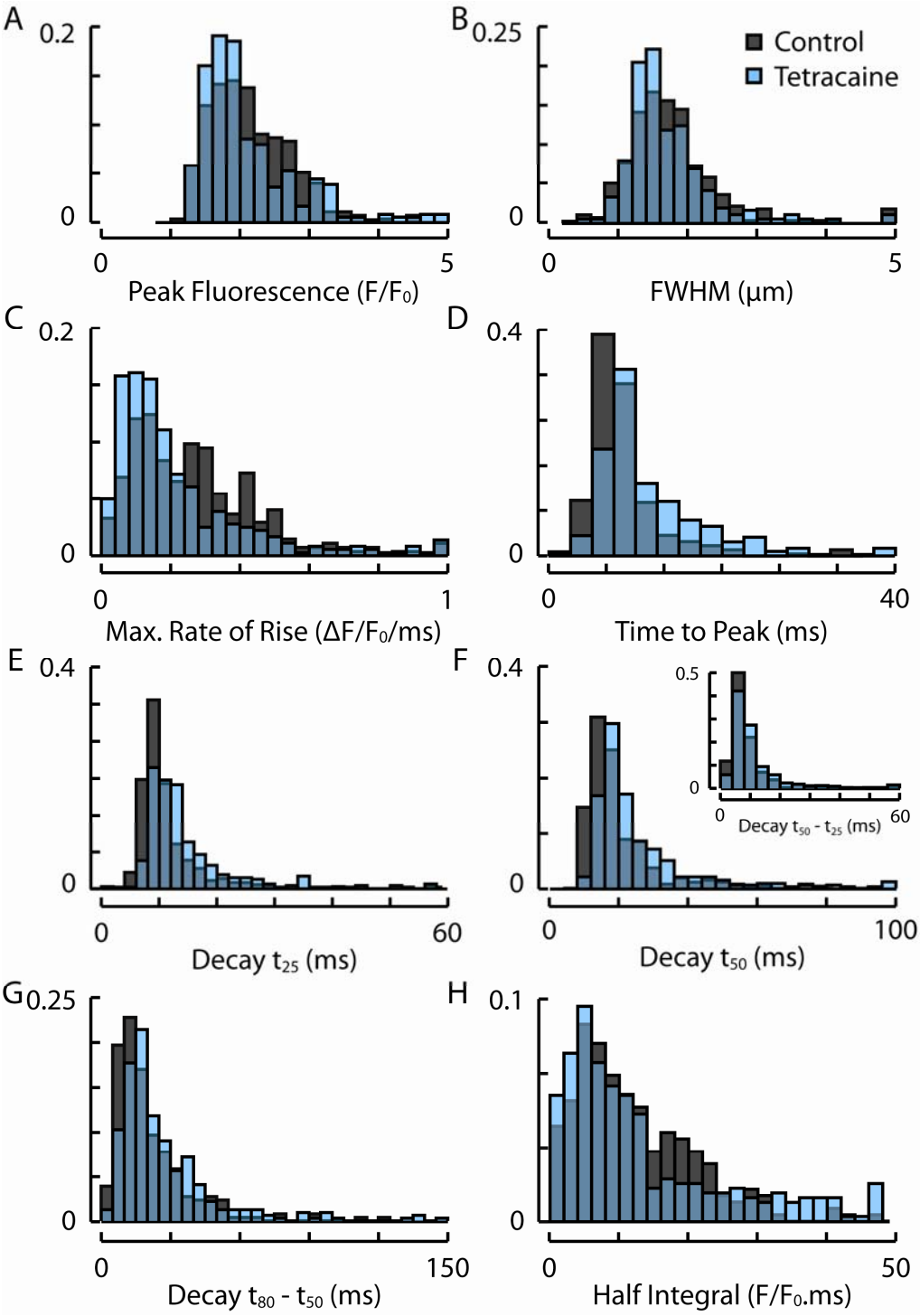

Figure 3.4 Properties of spontaneous Ca^{2+} sparks recorded in the absence (black, n = 234, 14 cells) and presence of tetracaine (blue, n = 325, 6 cells). In tetracaine, **(A)** peak fluorescence and **(B)** FWHM were not changed, **(C)** the maximum rate of rise was reduced and **(D)** the time to peak was prolonged. The time taken for fluorescence to decay was also prolonged in tetracaine **(E, F),** though this occurred predominantly during the early phase of decline. That is, $t_{50} - t_{25}$ (*inset, F*) and $t_{80} - t_{50}$ **(G)** showed no difference. **(H)** The integral of release above half maximum amplitude showed a different distribution in tetracaine.

	Control		Tetracaine		Distributions (Chi-Square Two Sample Test)				Means (R.S. Test)	
Property	$\bar{x}$	**S.E.**	$\bar{x}$	**S.E.**	**Bin**	**df**	χ^2	***P***	**Z**	**P**
Peak Fluorescence (F/F_0)	2.09	0.04	2.07	0.04	0.2	11	22	*0.01	-1.8	*0.04
FWHM (μm)	1.81	0.06	1.72	0.04	0.2	12	11	0.5	-	-
Max. Rate of Rise ($\Delta F/F_0/ms$)	0.27	0.01	0.22	0.01	0.04	16	40	*8 x 10^{-4}	-4.7	*0.0
Time to Peak (ms)	8.4	0.3	11.7	0.4	2.5	8	66	*4 x 10^{-11}	7.7	*0.0
t_{25} (ms)	10.6	0.3	13.5	0.4	2	10	162	*1 x 10^{-29}	6.8	*0.0
t_{50} (ms)	18.8	0.7	23.2	0.9	4	11	143	*4 x 10^{-25}	5.1	*0.0
t_{50} - t_{25} (ms)	8.5	0.5	12.1	0.7	4	7	7	0.4	-	-
t_{80} - t_{50} (ms)	19.6	1	22.2	1	5	12	14	0.3	-	-
Half Integral ($F/F_0 \cdot ms$)	12.3	0.6	15	1	2	15	31	*0.01	-0.72	0.2

Table 3.2 Properties of Ca^{2+} sparks in the presence and absence of tetracaine. The means and standard errors of means (S.E.) are shown for all events within control and tetracaine groups. To test whether the data were likely sampled from the same distribution, the Chi-square test for two samples was used. As this test is sensitive to the bin sizes of the histogram, they are shown (same units as the property) alongside the degrees of freedom (df) used, which was calculated as the number of bins (per group). The Chi-square test statistic (χ^2) is shown alongside the calculated P, where asterisks indicate statistical significance. To test whether the means of distributions were significantly different, the Wilcoxon Rank-Sum test was used. The test statistic (Z) is shown alongside the calculated P, where asterisks indicate statistical significance.

Long-lasting SR Ca^{2+} release events

Despite the relatively small changes in the time course in the majority of Ca^{2+} sparks in tetracaine, a subset of release sites exhibited LLEs that continued for up to several seconds. Release sites that produced LLEs exhibited a continuum of behaviour, as illustrated in Fig. 3.5. Panel A shows an example where a relatively large and rapid increase in fluorescence was followed by a rapid decline, then a sustained plateau (~ 70 % of the initial peak fluorescence) with few obvious fluctuations (though see asterisks, Fig. 3.5A). A second example is shown in Fig. 3.5B, where a relatively modest and slow increase in fluorescence was followed by clear fluctuations. Occasionally, fluorescence would decline to baseline only to increase again within tens of *ms*, suggestive of rapid re-activation of the CRU. A third example is shown in Fig. 3.5C, where the release site produced a large number of Ca^{2+} sparks, where the second event occurred before the previous event had declined back to baseline (asterisks, Fig. 3.5C). LLEs also occurred at this site and are suggestive of Ca^{2+} release events that were superimposed due to a short Δt (triangles, Fig. 3.5C). Note that over 7 *s*, the peak fluorescence of the release events remained remarkably constant, which suggests that release is being activated from the same CRU.

To clarify whether LLE sites were different to those sites that did not show LLEs, the relationships between different Ca^{2+} spark properties that are related to release flux were examined. Fig. 3.6 shows the measured properties of recorded events in control (black dots) and tetracaine (spark-like: blue dots; all fluctuations of at LLE sites: orange dots; initial fluctuation of an LLE event: red dots). For clarity, the inset shows the means and one S.E.M. for the three populations. There was a positive relationship between the maximum rate of rise and peak amplitude for all fluctuations, with a slope of 0.35 on the $\log_{10}$-$\log_{10}$ scale (Fig. 3.6A), which suggests amplitude increased with the 3rd power of the maximum rate of rise. Fluctuations at LLE sites appeared to belong to the same population, albeit with generally much lower values for both amplitude and maximum rate of rise, whereas the initial fluctuations at LLE sites appeared to be scattered in this relationship. The mean maximum rate of rise ($\Delta F/F_0/ms$) for all and initial fluctuations at LLE sites were 0.05 ± 0.01 and 0.11 ± 0.02 ($Z = 3.3$, $P = 5 \times 10^{-4}$), respectively. These values are much smaller (25 and 50 %) than that measured of spark-like events in tetracaine (see Fig. 1.4C and Table 2). The mean amplitudes ($\Delta F/F_0$) for all and initial fluctuations at LLE sites were 0.44 ± 0.03 and 0.89 ± 0.07 ($Z = 5.4$, $P = 6 \times 10^{-8}$), respectively. Note that the mean

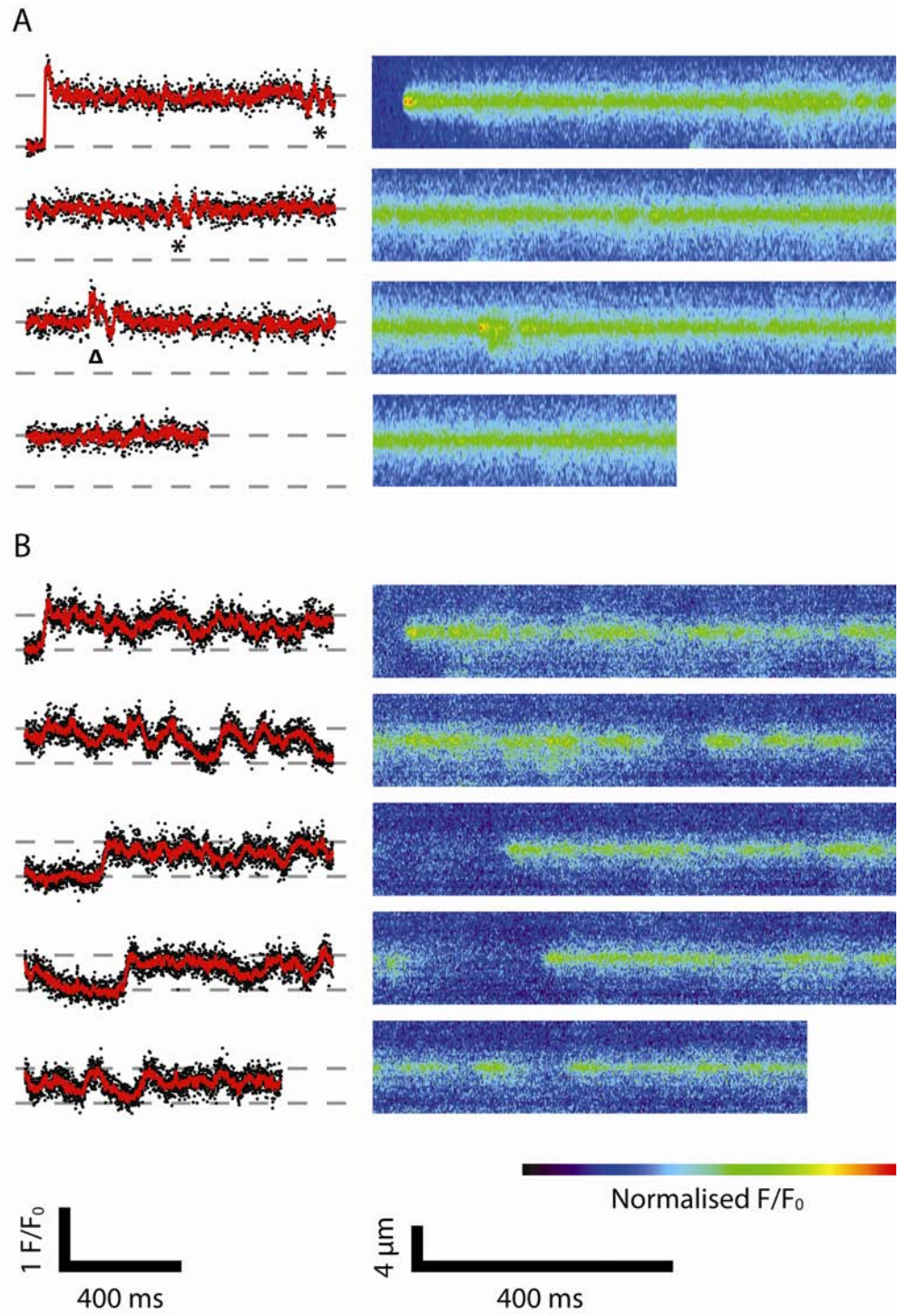

Figure 3.5 LLEs in the presence of tetracaine. Three examples from different cells are shown, each chosen to show the variation observed. The left panels show time profiles through the centroid of the events, which was obtained by averaging across 0.4 μm about the centroid (black dots), then smoothed in time with a 6 ms wide Savitzy-Golay filter (red lines). The resting F/F_0 value was one and the peak or plateau

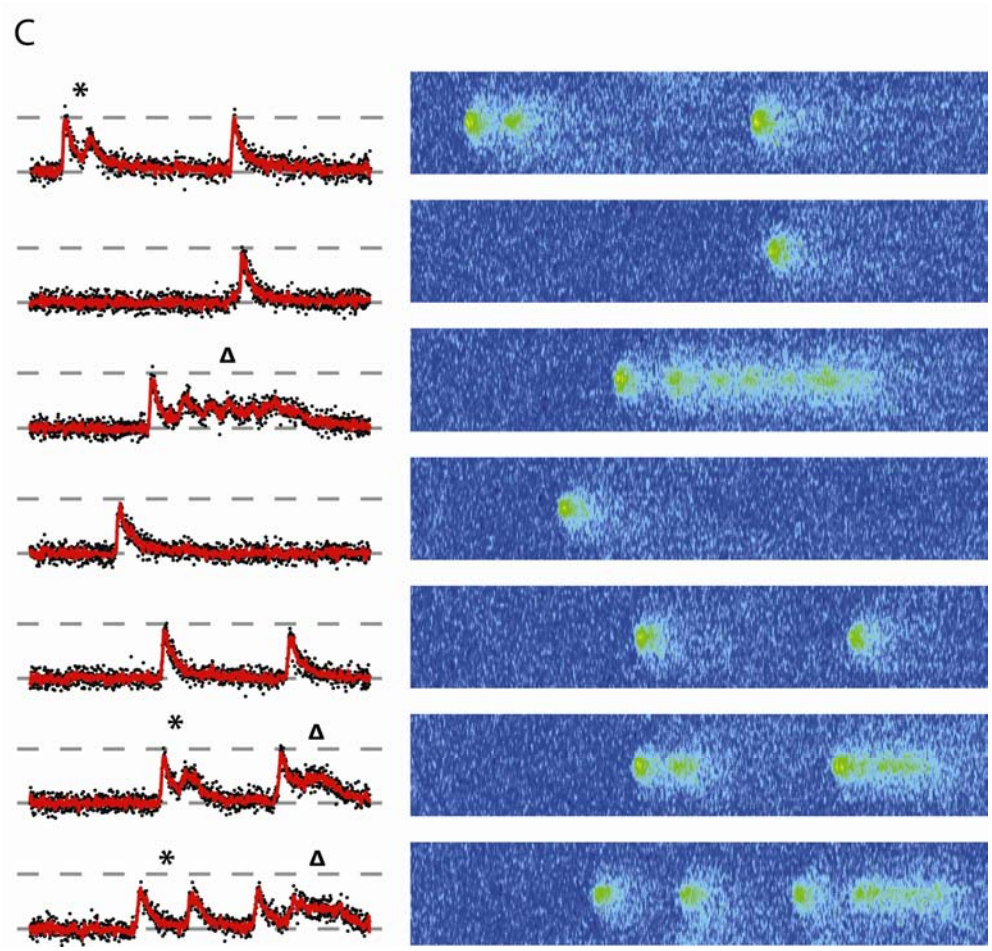

fluorescence for each separate release site is marked in each segment (*grey, dashed lines*). The right panels show the corresponding line-scan images in 1 *s* segments, where the images for each release site has been scaled to the range of the colour table. The images have been scaled differently for each of the three apparent release sites. **(A)** shows release that began with a relatively high amplitude, which then decayed to an intermediate level that was sustained for seconds. Note that small fluctuations are present (asterisks), though some may be due to contribution from a nearby release site (triangle). **(B)** shows a low amplitude, slow release that is sustained, but fluctuates dramatically about this plateau level over a long period of time. **(C)** shows an apparent release site with a high probability of Ca^{2+} spark activation. This site exhibited events that had regular and long durations (triangles). Often, a second release event would occur before a previous event had returned to baseline (asterisks, first triangle). Note that throughout the ~ 7 *s* of recording, the Ca^{2+} spark amplitude remained remarkably constant.

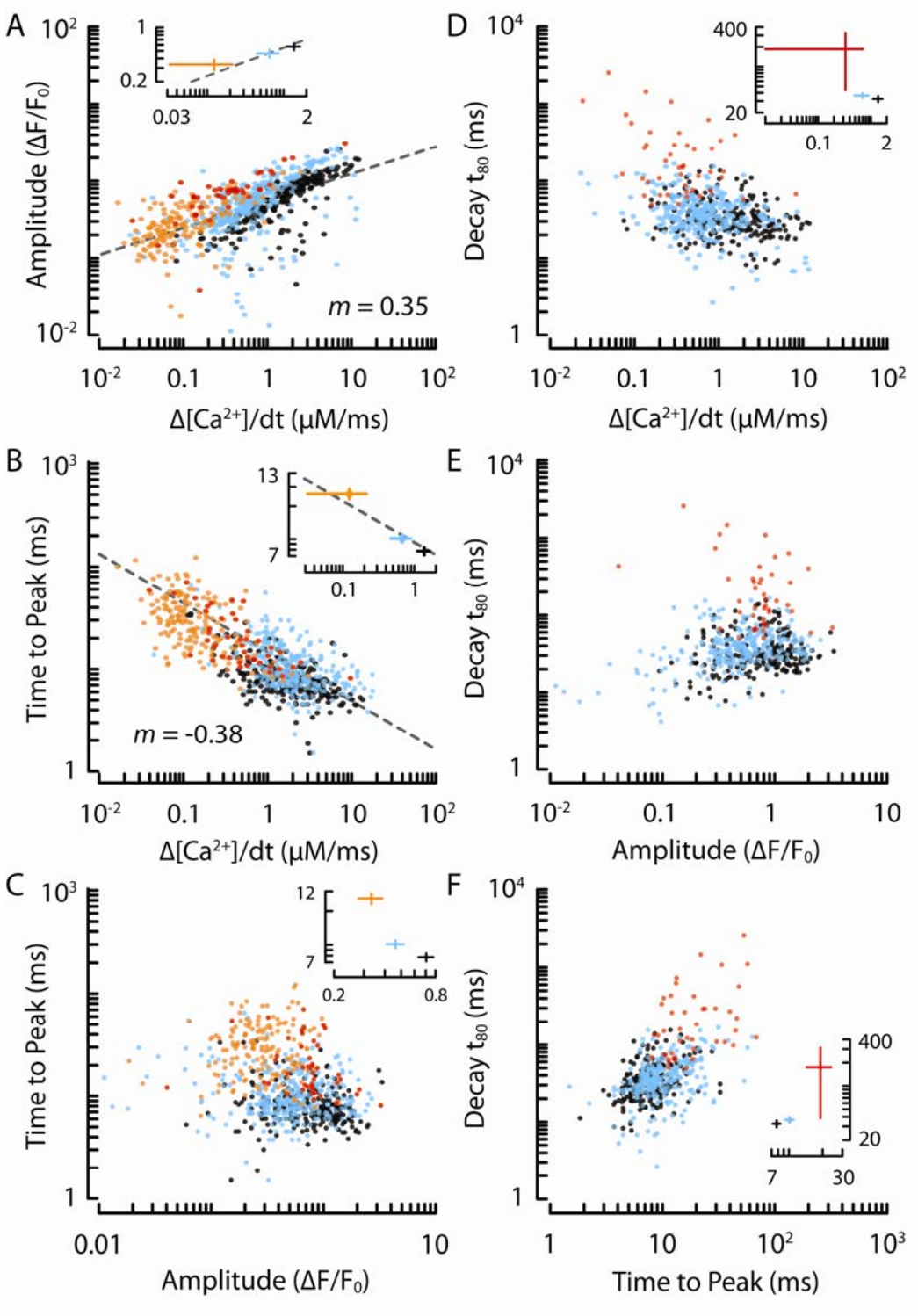

Figure 3.6 Properties of local SR Ca^{2+} release events at LLE sites in comparison to Ca^{2+} sparks. The properties of Ca^{2+} sparks in the absence (black dots, $n = 234$) and presence (blue dots,$n = 325$) of tetracaine from Fig. 3.4 compared to similar measurements of SR Ca^{2+} release events that occurred at LLE sites (tetracaine). The effects of tetracaine on Fluo-4 fluorescence and $[Ca^{2+}]_{SR}$ have been taken into account, although it should be noted that this causes very little change in the results (see text). Orange dots show measurements made from all fluctuations at the site ($n = 208$), while red dots are a subset (initial fluctuations, $n = 46$). The insets show

amplitude of the initial fluctuations was similar to that of spark-like events in tetracaine (Fig. 3.4A, Table 3.2), but only ~ half for all fluctuations. This is due to increased fluorescence at the beginning of the fluctuation, since the absolute peak fluorescence of events at LLE sites was similar to other events (mean F/F_0 of 1.73 ± 0.03, not shown). In contrast, the time to peak of fluctuations was inversely related to the maximum rate of rise (Fig. 3.6B) for all events, where time to peak was approximately *inversely* proportional to the 0.4^{th} power of maximum rate of rise. The time to peak was longer at LLE sites (30 ± 1 and 24 ± 3 *ms* for all and initial fluctuations, respectively, Fig. 3.6B, vertical axis), consistent with their reduced maximum rate of rise. Since amplitude and time to peak appeared to show opposite relationships to the maximum rate of rise, the relationship between amplitude and time to peak was examined. Interestingly, fluctuation amplitude and time to peak showed only a weak inverse relationship (Fig. 3.6C).

Event duration (t_{80}) were also examined and are shown in Fig. 3.6 (right panels). The mean t_{80} was 315 ± 65 *ms*. Note that four events were omitted from analysis due to their duration exceeding the length of the image. Fig. 3.6D shows that as the maximum rate of rise increased, t_{80} decreased. Comparison of spark-like and LLEs suggests that for a given maximum rate of rise, t_{80} at LLE sites were disproportionately longer than would be expected by extrapolating from the spark-like population. A similar difference was found for amplitude (Fig. 3.6E). In contrast, the time to peak was positively related to t_{80}, where all fluctuations appeared to follow the same trend. Together, these data suggest that all sites in the absence and presence of tetracaine have similar underlying properties, but that some (unknown) factor allows LLE sites to produce a plateau in fluorescence.

---

the calculated means of each population and the error bars show one S.E.M. **(A)** shows a positive relationship between the maximum rate of rise and amplitude. Fluctuations at LLE sites showed generally smaller amplitudes and rates of rise. **(B)** shows a negative relationship between maximum rate of rise and time to peak, where the slope is – 0.38. **(C)** shows the relationship between peak fluorescence and time to peak, where the time to peak at LLE sites was higher than that expected from regular-duratio n sites. Trends were similar when $\Delta F/F_0$ was used (very small negative slope of ~ -0.05 for spark-like events and similar trend of longer time to peak for a given $\Delta F/F_0$, not shown). **(D)-(F)** show relationships between maximum rate of rise, peak fluorescence or time to peak with t_{80}.

Effect of interval on repeated events

For highly active release sites that exhibited LLEs, the fluctuations could be analysed on the time delay (interval, *Δt*) between consecutive CRU activations to examine the restitution of various parameters. Fig. 3.7A and B show two examples of release sites where repeated events occurred. The first event (from Fig. 3.5C) showed little decrease in peak fluorescence (orange circles, left panel), amplitude (blue crosses) or maximum rate of rise (green triangles) over ~ 8 *s*, except during fluctuations that occurred at short Δt (e.g. just before 3 *s*, or the first *triangle* LLE shown in Fig. 3.5C). When these measures were evaluated against *Δt*, all measures declined as *Δt* declined (Fig. 3.7A, right panel). At the shortest *Δt* (~ 10 *ms*), F/F_0 was reduced by ~ 30 *%*, while $\Delta F/F_0$ was reduced to less than 10 *%* of the initial amplitude and recovered to 63 *%* when *Δt* ~ 160 *ms*. The maximum rate of rise recovered even more slowly and was not restored even when amplitudes (and peak fluorescence) had recovered. Fig. 3.7B shows another release site that showed a slight decrease in peak fluorescence over 6 s (~ 15 %, left panel). $\Delta F/F_0$ at this release site were more variable, but was suggestive of a ~ 180 *ms* time constant of recovery. For this event, rate of rise followed a similar trend to amplitude. Summaries of all fluctuations occurring at LLE sites (*n* = 27) are shown in Fig. 3.7C. Again, peak fluorescence shows little change with *Δt*, however, the time constant of recovery for $\Delta F/F_0$ was ~ 250 *ms*.

The *Δt* distribution is shown in Fig. 3.7D, which shows that Ca^{2+} release events occurred when *Δt* < 50 *ms.* The minimum *Δt* measured was ~ 10 *ms*, so in these conditions there did not appear to be a ~ 50 ms absolute refractory period in activation of local SR Ca^{2+} release, as described by Sobie, *et al.* (2005).

Figure 3.7 The dependence of Ca^{2+} spark properties on interval. Peak fluorescence (orange circles), peak amplitude (blue crosses) and maximum rate of rise (green triangles) of release events at LLE sites are shown. **(A)** shows an example of an active release site (from Fig. 3.5*C*), where local SR Ca^{2+} release events occurred repeatedly over ~ 8 *s* of recording. The left panel shows that the absolute peak fluorescence of the events did not vary a lot over this time (normalised to the first fluctuation, which had a peak F/F_0 = 1.82 and maximum rate of rise $\Delta F/F_0$/ms = 0.17), except for some clusters of fluctuations. When these measurements were sorted by delay (Δt), it became apparent that as Δt decreased, amplitude decreased. For this release site, the time constant for $\Delta F/F_0$ recovery was ~ 157 *ms*. Absolute peak F/F_0

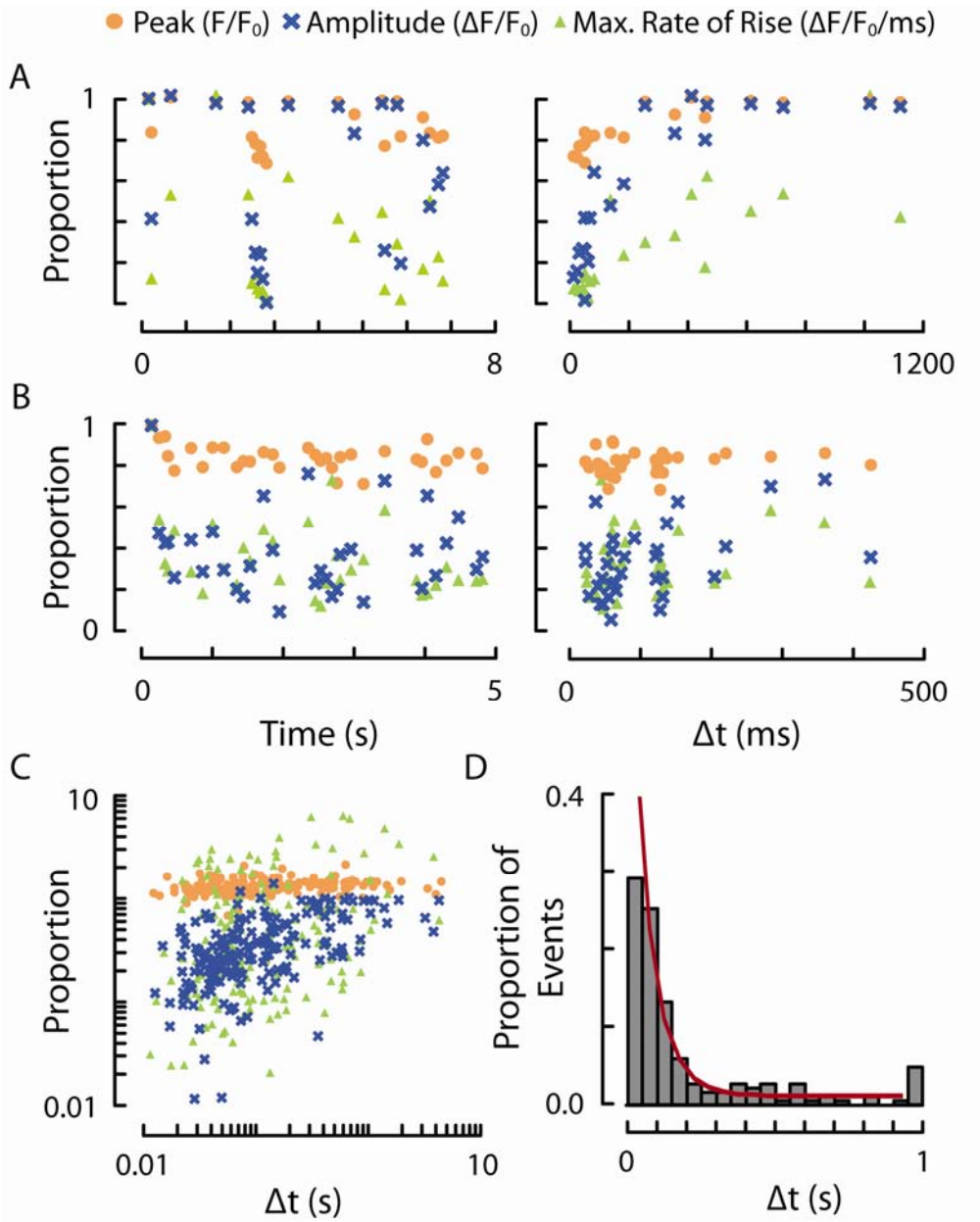

did not show a dramatic decline with decreased Δt.As expected, the rate of rise also increased as Δt increased, but at a slower rate than $\Delta F/F_0$. **(B)** shows an example of another release site that showed more variable data. There was a small reduction in absolute peak fluorescence (initial peak $F/F_0 = 1.82$ and maximum rate of rise $\Delta F/F_0/ms = 0.06$) and amplitude over time (left panel). The $\Delta F/F_0$ time constant of recovery may be slightly longer at ~ 176 *ms*. **(C)** is a summary of all fluctuations at LLE sites (*n* = 27 sites). Overall, the average recovery time for $\Delta F/F_0$ appears to be ~ 250 *ms*, although this is variable (~ 70 to 650 *ms*). Absolute amplitude appears to be independent of *Δt* (at least, for *Δt* > 10 *ms*). **(D)** is the distribution of release event delay (Δt) as a proportion of the total number of events (*i.e.* the 27 initial events with unknown *Δt* are not shown). There did not appear to be an absolute refractory period in release activation, at least in the presence of tetracaine. The red curve is an exponential function with a time constant of 65 *ms*.

Fluctuation noise analysis

Even though it is likely that LLE plateaus occur because release flux is equal to the rate of $[Ca^{2+}]_{JSR}$ recovery (Zima, *et al.*, 2008a), this idea has not been fully explored. It seems reasonable to assume that during several *seconds* of approximately steady fluorescence, the underlying RyR channels would be stochastically gating (given *ms* open and closed times, Copello, *et al.*, 1997; Laver and Honen, 2008). To examine whether any excess noise could be detected and whether this could help quantify the underlying fluxes, spectral analysis of the plateau phases of LLEs was performed.

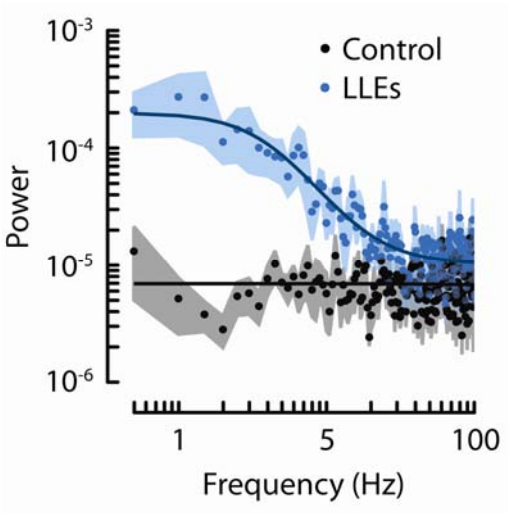

Figure 3.8 Power spectra of LLE plateaus. The power spectra (arbitrary units) of long-lasting SR Ca^{2+} release events with durations longer than 1000 lines (n = 11, blue) and nearby regions in the same image with no apparent SR Ca^{2+} release activity (n = 11, black) were calculated, then averaged. f_C for LLEs was 4.1 *Hz*, with an offset of 1.0 x 10^{-5} *a.u.* The mean power of control regions was 6.9 x 10^{-6} *a.u.* Shaded areas represent S.E.M. of data.

The average power spectrum of the control regions corresponding to measured LLEs showed a uniform distribution of power across all frequencies measured (black circles, Fig. 3.8). In contrast, the average power spectrum of the plateau periods of long LLEs showed more power at low frequencies and this decreased monotonically with increasing frequency (blue circles, Fig. 3.8). A Lorentzian function (Eqn. 3.4) was fitted to these data, with parameters, P_0 = 1.9 x 10^{-4}, f_C = 4.1 Hz, offset = 1.0 x 10^{-5}.

3.4. Discussion

Reduced release flux in tetracaine

The presence of tetracaine was associated with Ca^{2+} sparks that had decreased amplitude, maximum rate of rise and increased duration. These changes are qualitatively similar to the changes observed by Zima, *et al.* (2008a), although Ca^{2+} sparks in this study had higher amplitudes (~ 124 %) and shorter time to peak durations (~ 52 %) than they reported. Ca^{2+}

spark probability decreased by 35 *%* in tetracaine (5.3 ± 1.2 */s/100 µm*, *n* = 6 cells, compared to control: 8.1 ± 1.6 */s/100 µm*, *n* = 14 cells), which is similar to observations made by Gyorke, *et al.* (1997) and Zima, *et al.* (2008a) at 100 and 750 *µM* tetracaine, respectively and consistent with the extent of inhibition observed in lipid bilayer studies (IC_{50} ~ 200 *µM*, Zahradnikova and Palade, 1993; Györke, *et al.*, 1997; Zima, *et al.*, 2008a; Laver and van Helden, 2011). Single-channel data suggests that tetracaine reduces RyR channel P_O by increasing closed times, but not decreasing open times (Laver and van Helden, 2011).

However, the effect of tetracaine on RyR function *in situ* is more complex, as a reduction in $P_{O,RyR}$ may reduce diastolic SR Ca^{2+} release ('leak', e.g. Shannon, *et al.*, 2002; Santiago, *et al.*, 2010), which would increase $[Ca^{2+}]_{SR}$ and increase RyR unitary current (i_{RyR}). Previous studies have have shown a variable effect of tetracaine on $[Ca^{2+}]_{SR}$. In un-stimulated rat myocytes, which shows rest potentiation, that $[Ca^{2+}]_{SR}$ increased to 170 % (3 *min* after application of 100 *µM* tetracaine, Overend, *et al.*, 1997). However, other studies have reported more modest increases in $[Ca^{2+}]_{SR}$ in the presence of high dose of (0.75 *mM*) tetracaine, which should abolish SR Ca^{2+} release (Györke, *et al.*, 1997). For example, in paced and permeabilised rabbit myocytes $[Ca^{2+}]_{SR}$ increased by ~ 20 *%* (Shannon, *et al.*, 2002; Zima, *et al.*, 2008b). In rat myocytes, Gyorke, *et al.* (1997) found a similar increase in $[Ca^{2+}]_{SR}$ (~ 15 *%* after 2 *min* and ~ 55 *%* after 5 *min*), while Lukyanenko, *et al.*(2001) found a 30 *%* increase after 5 min in 100 *µM* tetracaine. In the presence of 1 *µM* isoprenaline and a high [tetracaine] for 6 *min* $[Ca^{2+}]_{SR}$ in permeabilised cat myocytes increased to 180 *%* (Zima, *et al.*, 2008a).

In this study, changes in $[Ca^{2+}]_{SR}$ were estimated using the corrected maximum rates of rise as a measure of initial Ca^{2+} spark release flux (I_{spark}). Since I_{spark} decreased by ~ 24 *%* in the presence tetracaine (Fig. 3.4A) and $n \cdot P_O$ was reduced by 35 *%* (from the reduction in P_{spark} in the presence of tetracaine), i_{RyR} should have increased to 112 *%* (see Eqn. 3.9, modified from Eqn. 1.2):

$$I_{spark} = i_{RyR} \cdot n \cdot P_O \qquad \textbf{Eqn. 3.9}$$

Eqn. 3.9 states that I_{spark} is the product of i_{RyR}, the number of RyR channels in a CRU, *n* and the open probability of each channel, P_O, assuming independence. In this range, unitary flux

is approximately proportional to $[Ca^{2+}]_{SR}$ (Mejia-Alvarez, *et al.*, 1999). Though a 12 % increase in $[Ca^{2+}]_{SR}$ is within the range reported by others, it is likely that tetracaine causes quenching of Fluo-4 fluorescence since tetracaine has been shown to cause a ~ 5 % decrease in fluorescence of Fluo-3 (*in vitro* calibrations, Shannon, *et al.*, 2003b). If this is true for Fluo-4, then the measured F/F_0 in tetracaine needs to be corrected. For example, the peak fluorescence in control (F/F_0 of 2.09, Table 3.2) would correspond to 238 *nM* if using a K_D of 0.9 *μM* (Baylor and Hollingworth, 1998; Baylor and Hollingworth, 2000; Wang, *et al.*, 2001; Woodruff, *et al.*, 2002) and resting $[Ca^{2+}]_i$ of 100 *nM* (Cannell, *et al.*, 1987b) using Eqn. 3.10 (*Cheng, et al., 1993*).

$$[Ca^{2+}] = \frac{K_D \cdot F/F_0}{F_{max} - F/F_0} \qquad \textbf{Eqn. 3.10}$$

where,

$$F_{max} = \frac{K_D}{[Ca^{2+}]_{i,rest}} + 1$$

When a 5 % quench in dye signal was taken into account (so that quenched F_{max} is $0.95 \cdot F_{max}$), an F/F_0 of 2.07 in tetracaine (Table 3.2) would correspond to 251 *nM* (which would correspond to F/F_0 of 2.18 if there was no dye quenching). However, resting $[Ca^{2+}]_i$ has been shown to be decreased in the presence of tetracaine (~ 25 % in rabbit, Shannon, *et al.*, 2002), which would alter the pseudo-ratio calibration of Fluo-4, as well as have a minor effect on i_{RyR}. Therefore, if $[Ca^{2+}]_{i,rest}$ is 75 *nM*, then a measured F/F_0 of 2.07 in tetracaine would correspond to a $[Ca^{2+}]$ of 181 *nM*. The overall result of these two opposing effects mean that in the presence of tetracaine, the maximum rate of rise (used to approximate I_{spark}) was reduced by ~ 28 %, which is similar to that calculated from the original measured values and that $[Ca^{2+}]_{SR}$ had increased to 144 %.

Release termination of Ca^{2+} sparks

The majority of Ca^{2+} sparks measured in the presence of tetracaine showed little change from those measured in control conditions. In this population of 'spark-like' release events, time to peak and t_{25} (but not $t_{50} - t_{25}$ or $t_{80} - t_{50}$) were prolonged in tetracaine (~ 140 and 130 % of control, respectively, see Table 3.2). Since only the early phase of Ca^{2+} spark time-course was prolonged, this result suggests that the SR release flux was sustained for a

longer duration when $n \cdot P_O$ and I_{spark} were reduced. Certainly, in all recorded events, I_{spark} was inversely proportional to time to peak (Fig. 3.6B), which is inconsistent with stochastic attrition being the primary termination mechanism. Stochastic attrition would predict that release duration (or τ_{att}) would increase with I_{spark}, since I_{spark} is proportional to $n \cdot P_O$ (with the assumption that $[Ca^{2+}]_{SR}$ is relatively constant, at least in cells in the same conditions, Eqn. 3.9). On the other hand, release duration would be expected to *decrease* with I_{spark} for release flux or Ca^{2+}-dependent termination mechanisms, such as $[Ca^{2+}]_i$-inactivation, $[Ca^{2+}]_{JSR}$ depletion and/or sensitisation, because a larger I_{spark} would lead to faster $[Ca^{2+}]_i$-inactivation and/or $[Ca^{2+}]_{JSR}$ depletion.

Examination of the relationship between time to peak (as an estimate of release duration) and maximum rate of rise (as an estimate of release flux) revealed that release duration was inversely proportional to the 0.4^{th} power of release flux (Fig. 3.6B; Shen, *et al.*, 2004, see also Lukyanenko, *et al.*, 1998). This is also consistent with previous studies that showed Ca^{2+} sparks had smaller amplitudes and durations in thapsigargin (reduced $[Ca^{2+}]_{SR}$, Song, *et al.*, 1997) and longer durations at increased SR Ca^{2+} buffering (*e.g.* Zima, *et al.*, 2008a, although see Jones, *et al.*, 1998; Wang, *et al.*, 2000). If termination of local SR Ca^{2+} release was simply due to the local $[Ca^{2+}]_{JSR}$ emptying, then release flux would be inversely proportional to the release duration. Instead, the observed dependence suggests that $[Ca^{2+}]_{JSR}$ depletion does not directly determine release duration. A 3rd power dependence is seen between RyR closed time and $[Ca^{2+}]_i$ (*e.g.* Laver and Honen, 2008), as well as between the frequency of spontaneous SR Ca^{2+} release and $[Ca^{2+}]_{SR}$ (Díaz, *et al.*, 1997, although see Song, *et al.*, 1997). However, the steepness of the relationship is critically dependent on where the RyRs are operating in terms of their Ca^{2+} response curve. Therefore, a weak dependence may result when RyRs are near saturating in Ca^{2+} in the junctional space as may occur during Ca^{2+} release (see section 2). Since release flux is proportional to $[Ca^{2+}]_{junction}$ over the time scale of a Ca^{2+} spark (Soeller and Cannell, 1997) and release duration is CRU open time, the inverse relationship between release flux and duration can be explained by $[Ca^{2+}]_i$-dependence of RyR channel activation alone. In other words, termination of CICR within a CRU involves $[Ca^{2+}]_{JSR}$ depletion, the subsequent reduction in $[Ca^{2+}]_{junction}$ and RyR channel de-activation. Note that when $[Ca^{2+}]_{SR}$-dependent regulation of RyR P_O was incorporated into a model of Ca^{2+} spark termination (i.e. P_O set to be linearly-dependent on $[Ca^{2+}]_{JSR}$), the relationship between release flux and duration was steeper than that observed in these data (Sobie, *et al.*, 2002). Furthermore,

Sobie's model could not produce the increased event duration at increased $[Ca^{2+}]_{SR,}$ as observed by Zima, *et al.*, 2008a, which suggests that the negative control invoked was too strong (i.e. termination was more robust or dependence too steep) than observed data. The presence of repeated SR Ca^{2+} release during sustained levels of relatively high $[Ca^{2+}]_{junction}$ during LLEs also suggest that $[Ca^{2+}]_i$-inactivation cannot be occurring within the time-course of these LLE events (although it is possible tetracaine may have had an effect on $[Ca^{2+}]$i-inactivation, this is unlikely since it has not been reported that tetracaine has any effect on RyR channel availability, Laver and van Helden, 2011).

Nevertheless, it is possible that $[Ca^{2+}]_i$-dependent inactivation becomes more important during CRU re-activation due to refractoriness. Thus, the ability of CRU to re-activate at short Δt was investigated. The analysis of highly active sites in the presence of tetracaine showed that ~ 25 *%* (Fig. 3.7D) of Ca^{2+} sparks were evoked within Δt ~ 50 *ms*. This result is different to that of Sobie, *et al.* (2005), who reported a distinctly biphasic Δt distribution, with a mode at 240 *ms*. This discrepancy may due to differences in methods used to increase P_{spark} (tetracaine vs. low concentration of ryanodine). It is unclear whether ryanodine may have altered resting $[Ca^{2+}]_i$ and $[Ca^{2+}]_{SR}$ during the 10 *min* of recording (given that it had increased P_O and may have induced sub-conductance states, *e.g.* Cheng, *et al.*, 1993 to increase spontaneous SR Ca^{2+} release and reduce $[Ca^{2+}]_{SR}$), which may reduce event amplitude and their ability to be detected. Further, the induction of sub-conductance states (*e.g.* Cheng, *et al.*, 1993) may have reduced the ability of a spontaneous RyR opening to trigger a Ca^{2+} spark. The observation of high P_{spark} sites is paradoxical since tetracaine reduced RyR channel P_O. It is possible that some sites exhibit relatively low $n \cdot P_O$ (note the Binomial nature of block and variation in CRU sizes) in combination with a highly connected JSR that enables relatively fast $[Ca^{2+}]_{JSR}$ refilling and therefore, release flux to be matched (Zima, *et al.*, 2008b).

Certainly, at sites that exhibited high P_{spark}, secondary release events occurred even before the fluorescence due to a previous event had returned to baseline. It is possible that at these junctions, the available $[Ca^{2+}]_{junction}$ was still high enough to cause regenerative CICR when $[Ca^{2+}]_{JSR}$ was partially restored. On the other hand, at the majority of junctions where spark-like events occurred in tetracaine, the network and JSR connectivity was insufficient to allow the time-courses of JSR restoration and Ca^{2+} spark decay to match. This meant that release duration was just prolonged enough to deplete $[Ca^{2+}]_{JSR}$, reduce release flux and de-

activate the CRU. A continuum of behaviour would result from differences in the rate of $[Ca^{2+}]_{JSR}$ replenishment. The effect is this variation is enhanced when $n{\cdot}P_O$ is low and CRU behaviour is largely influenced by the stochastic gating of the few RyR channels available. This means that when tetracaine is absent, $n{\cdot}P_O$ and release flux is much higher during CRU activation and is able to deplete the $[Ca^{2+}]_{JSR}$ over a range of Ca^{2+} buffering and refilling capacities. Supporting evidence for this idea has come from the measurement of Ca^{2+} blinks. Where LLEs occur, some Ca^{2+} blink data suggest that $[Ca^{2+}]_{JSR}$ is maintained at some steady-state during the long release (Zima, *et al.*, 2008b), which suggests $[Ca^{2+}]_{JSR}$ had initially reduced, but not depleted entirely to prevent release.

Though these lines of evidence support a major role of $[Ca^{2+}]_{JSR}$ in the termination of CICR, the extent of its depletion has been reported to be 'only' ~ 30 - 40 *%* of the caffeine-sensitive store (Brochet, *et al.*, 2005; Zima, *et al.*, 2008b), where caffeine reduced the SR Fluo-5N signal by 50 *%* (Brochet, *et al.*, 2005). Calibration of these pseudo-ratio measurements yielded a minimum $[Ca^{2+}]_{SR}$ ~ 200 μM during caffeine-induced SR Ca^{2+} release and ~ 500 μM during spontaneous Ca^{2+} blinks (Shannon, *et al.*, 2003a). However, it is not clear whether the minimum fluorescence of Ca^{2+} blinks correctly reflects $[Ca^{2+}]_{JSR}$. The minimum $[Ca^{2+}]_{JSR}$ reached during a Ca^{2+} spark could be much lower than previously suggested because *(1)* neighbouring network and JSR are not reduced to the same extent (Picht, *et al.*, 2011), *(2)* the caffeine-insensitive fluorescence, which was assumed to be irrelevant to SR Ca^{2+} release (*e.g.* in fluorescence arisng from mitochondria, which comprise a substantial ~ 30 *%* of the cell cytoplasm compared to 0.6 *%* by the JSR, *Bers, 2001*), would together *(3)* contribute to the Ca^{2+} blink signal in a non-linear manner due to their (unknown) changes relative to $[Ca^{2+}]_{JSR}$ and the limited optical resolution of a confocal microscope (see Chapter 4). In this study, measurement of Ca^{2+} sparks at short Δt showed that amplitude could be as small as ~ 10 *%* of the initial event (Fig. 3.7C and Sobie, *et al.*, 2005). This suggests that the initial Ca^{2+} spark had released *at least* 90 *%* of the releasable content, under the reasonable assumption that maximum $n{\cdot}P_O$ during CRU activation at the same site had not changed. Further, the restitution of Ca^{2+} spark amplitude required a long period of time (relative to the time-course of a Ca^{2+} spark), which further supports the likelihood of $[Ca^{2+}]_{JSR}$ depletion. Similar to a previous study, the recovery time at different release sites showed considerable heterogeneity (Zima, *et al.*, 2008b), although it was not possible within this study to examine the variability of recovery within a given release site. The average amplitude recovery time was ~ 250 *ms*, which is similar to that

measured by Brochet, *et al.* (2005), but ~ double that measured in the presence of 50 *nM* ryanodine alone or including tetracaine (Sobie, *et al.*, 2005; Ramay, *et al.*, 2011). The reason for this discrepancy is unclear, but may be due to an overall higher $[Ca^{2+}]_{SR}$ in the presence of tetracaine. That is, even though higher $[Ca^{2+}]_{JSR}$ can auto-regulate Ca^{2+} spark duration by $[Ca^{2+}]_{JSR}$ depletion, replenishment of the highly-buffered JSR will be dependent on $[Ca^{2+}]$ in the network SR as well as SERCA activity. The latter would be reduced at high $[Ca^{2+}]_{SR}$. Nevertheless, the recovery time of Ca^{2+} blinks have also been measured as being longer ~ 150 – 180 *ms* (Zima, *et al.*, 2008b; Picht, *et al.*, 2011, although see Brochet, *et al.*, 2005).

It has also been suggested that tetracaine may change the 'threshold' of $[Ca^{2+}]_{JSR}$ that terminates release (Zima, *et al.*, 2008b). This was based on observations of Ca^{2+} blinks that had more variable minimum fluorescence levels compared to control events, which had relatively constant minima. However, the interpretation of Fluo-5N data obtained in tetracaine is complex because of the associated increase in $[Ca^{2+}]_{SR}$ and ~ 15 *%* reduction in fluorescence (Shannon, *et al.*, 2003a). The increased $[Ca^{2+}]_{SR}$ could mean that the Ca^{2+} blink further under-estimates $[Ca^{2+}]_{JSR}$ depletion due to increased contribution of out-of-focus network or adjacent JSR $[Ca^{2+}]$ to fluorescence. This effect would not be controlled by measuring fluorescence during a caffeine-induced release, because this manoeuvre depletes global $[Ca^{2+}]_{SR}$, making a proportion of the out-of-focus contamination caffeine-sensitive. Examination of the release amplitudes and integrals of spark-like events (after taking into account quenching of Fluo-4, see Fig. 3.4A, G and text) and the relationship between release flux and time to peak for all events (Fig. 3.6B) would suggest that a similar amount of Ca^{2+} is being released between control and tetracaine groups. The duration of release (time to peak) decreased with a similar steepness with release flux, consistent with the dependence of RyR channel (de)-activation with $[Ca^{2+}]$. When release flux is reduced substantially (at some sites in tetracaine), the rate of $[Ca^{2+}]_{JSR}$ depletion is such that it can be restored within the time of Ca^{2+} spark decay and gives rise to LLEs. Nevertheless, LLEs eventually terminate, so another mechanism must exist for this to occur.

Note that the 2D histograms presented here (and by Shen, *et al.*, 2004) are dissimilar to those presented by Shkryl, *et al.* (2012), who used 4D confocal imaging to select for 'in-focus' Ca^{2+} sparks. This discrepancy may be explained by the technique itself, which forfeits significant temporal resolution in order to improve spatial resolution. Their 5.6 *ms*

per 3 slice z-stack compared to an expected ~ 10 *ms* time to peak of a Ca^{2+} spark is insufficient to correctly capture the peak and its associated parameters (*e.g.* time to peak, peak amplitude, FWHM, maximum rate of rise). Furthermore, given that Ca^{2+} spark FWHM is 1.2 - 2 *µm* (Cheng, *et al.*, 1993; Shen, *et al.*, 2004), it is unclear how useful z-stacks taken 1 *µm* apart would be in selecting for the focus of release given junctions are ~ 200 – 400 *nm* wide and 0.6 *µm* apart (Soeller and Cannell, 2004).

Sustained release and termination during long-lasting events

Since LLEs produced a prolonged period of elevated $[Ca^{2+}]_{junction}$ with no apparent $[Ca^{2+}]$ or flux dependence, its termination must depend on other factors. One possibility is stochastic attrition. Though this is thought to play only a minor role under physiological conditions due to the large number of RyR channels within a cluster (*e.g.* Stern and Cheng, 2004; Cannell and Kong, 2012, see Eqn. 3.1), stochastic attrition may be unmasked in the presence of tetracaine due to reduced $n{\cdot}P_O$ and reduction of $[Ca^{2+}]_{JSR}$ depletion during LLEs. To investigate whether this could be possible, the number of available RyR channels during LLE events was estimated from the events' maximum rate of rise and then τ_{att} was calculated. If maximum RyR P_O under normal conditions is ~ 0.5 (see Fig. 2.2B), then P_O during spark-like events in tetracaine would be ~ 0.33 (35 % blockade, estimated by the reduction in P_{spark}, see above). Since the mean duration of LLEs was ~ 320 *ms* (equivalent to τ_{att}), using τ_O = 2 *ms* (see Chapter 2.2) in Eqn. 3.1 yields ~ 18 available RyR channels per CRU at LLE sites. Since there is no *a priori* reason to believe that tetracaine blockade or $[Ca^{2+}]_{JSR}$ at steady-state is different across CRUs, the average number of RyR channels available during spark-like events should also be 18, which would correspond to 28 being available under control conditions. This value is compatible to peripheral CRU sizes (Wang, *et al.*, 2004; Baddeley, *et al.*, 2009) when the different diffusion geometry is taken into account (Kong & Cannell 2011). However, this estimate is smaller than earlier studies examining internal CRUs using diffraction-limited confocal (Chen-Izu, *et al.*, 2006; Soeller, *et al.*, 2007) and thin-section electron (Franzini-Armstrong, *et al.*, 1999) microscopy (~ 200 in rat). As discussed in Chapter 1.2, this discrepancy may be due to the inability of de-convolution to accurately back-calculate CRU sizes in confocal images and sampling bias towards larger CRUs during thin section selection in electron microscopy.

However, this does not explain why some CRUs in tetracaine exhibit LLEs. It has been previously suggested that LLEs occur at CRUs where the rate of JSR efflux and refilling

are matched (Zima, *et al.*, 2008a). Since LLEs do not occur under normal conditions and only comprise a small subset of the Ca^{2+} release events that occur in tetracaine, it seems reasonable to suggest that LLEs occur at CRUs where both release flux is decreased and JSR to network SR connectivity is relatively large (Zima, *et al.*, 2008a). At a maintained, low level release flux, stochastic gating of RyR channels should be observed. The average power spectrum of LLE plateaus resembled a Lorentzian curve (blue line, Fig. 3.8), with as offset of energy across all energies (1.5×10^{-5} a.u.). The power in this offset was ~ 1.7-fold greater than the uniform power in noise during control periods (8.9×10^{-6} a.u., black line, Fig. 3.8), which is consistent with photon noise, where variance is proportional to the mean signal (mean peak fluorescence of all fluctuations during LLEs was $F/F_0 \sim 1.7$, compared to in control, by definition $F/F_0 = 1$). The f_C of ~ 4 *Hz* corresponds to a time constant of ~ 40 *ms* (Eqn. 3.4). This time constant is due to a process that is much slower than the stochastic gating of a single RyR channel, given $\tau_O = 2$ *ms* and at $P_O = 0.5$, τ_C would be ~ 2 *ms* and f_C would be ~ 160 *Hz* (Eqn. 3.4). Similarly, though the Fluo-4 dye should reduce the observed frequency of stochastic gating, this effect does not explain the observations. For example, if the on rate constant of Fluo-4 is approximately diffusion-limited (3.1×10^8 */M/s*, Baylor, *et al.*, 2002) and K_D is 900 *μM* (Baylor and Hollingworth, 1998; Baylor and Hollingworth, 2000; Wang, *et al.*, 2001; Woodruff, *et al.*, 2002), then the off rate would be 140 */s* and at $[Ca^{2+}] = 200$ *nM*, the expected f_C would be ~ 65 *Hz* (Eqn. 3.4). Even at a lower $[Ca^{2+}]_i$ of 150 *nM*, which might be the case during LLEs, f_C would still be ~ 50 Hz. However, if repeated activation of a CRU is primarily dependent on $[Ca^{2+}]_{JSR}$ refilling, then a slow frequency may be explained. Given that during CRU activation, release duration is ~ 30 *ms* (estimated from the time to peak of spark-like and long-lasting events) and refilling takes ~ 150 *ms*, the calculated f_C would be ~ 6 *Hz*. Thus, the oscillations may be due to effect of $[Ca^{2+}]_{JSR}$ cycling (de- and repletion) on CRU activation through $[Ca^{2+}]_{junction}$.

To test the effect of $[Ca^{2+}]_{JSR}$ refilling on CRU activation and local SR Ca^{2+} release during reduced release flux (*i.e.* in tetracaine), a simple five compartment computer model was constructed (Fig. 3.1). During simulations of control conditions ($n = 28$, maximum $P_O = 0.5$), local SR Ca^{2+} release resembled a Ca^{2+} spark. That is, $[Ca^{2+}]$ in the Ca^{2+} spark volume increased to a maximum of ~ 240 *nM* in ~ 10 *ms* and decayed to half of this value in ~ 25 *ms*. Termination of the Ca^{2+} spark occurred due to depletion of the $[Ca^{2+}]_{JSR}$, reaching a minimum of ~ 90 *μM*, which recovered with a half time of ~ 250 ms (Fig. 3.7C,

see also Sobie, *et al.*, 2002; Sobie, *et al.*, 2005; Zima, *et al.*, 2008b). $[Ca^{2+}]_{JSR}$ depletion reduced release flux, which dramatically reduced RyR channel P_O due to its steep dependence on $[Ca^{2+}]_{junction}$ (*e.g.* Laver and Honen, 2008). To simulate the effect of tetracaine, maximum P_O was reduced by decreasing the RyR on rate (35 % reduction in P_O was associated with a 73 % reduction in on rate, see Eqn. 1.1 and Laver and van Helden, 2011). In these conditions, Ca^{2+} sparks had slightly longer time to peak and t_{50}, similar to spark-like events in tetracaine (Fig. 3.4), but were not long-lasting until the Ca^{2+} diffusion rate between the JSR and network SR was increased. This is consistent with a previous study which showed that a decrease in release flux or increase in $[Ca^{2+}]_{SR}$ alone were insufficient to cause LLEs (Zima, *et al.*, 2008). Fig. 3.9*A* shows stochastic RyR channel gating that resulted from an initial spontaneous 2 *ms* RyR opening. Fig. 3.9*B* shows the

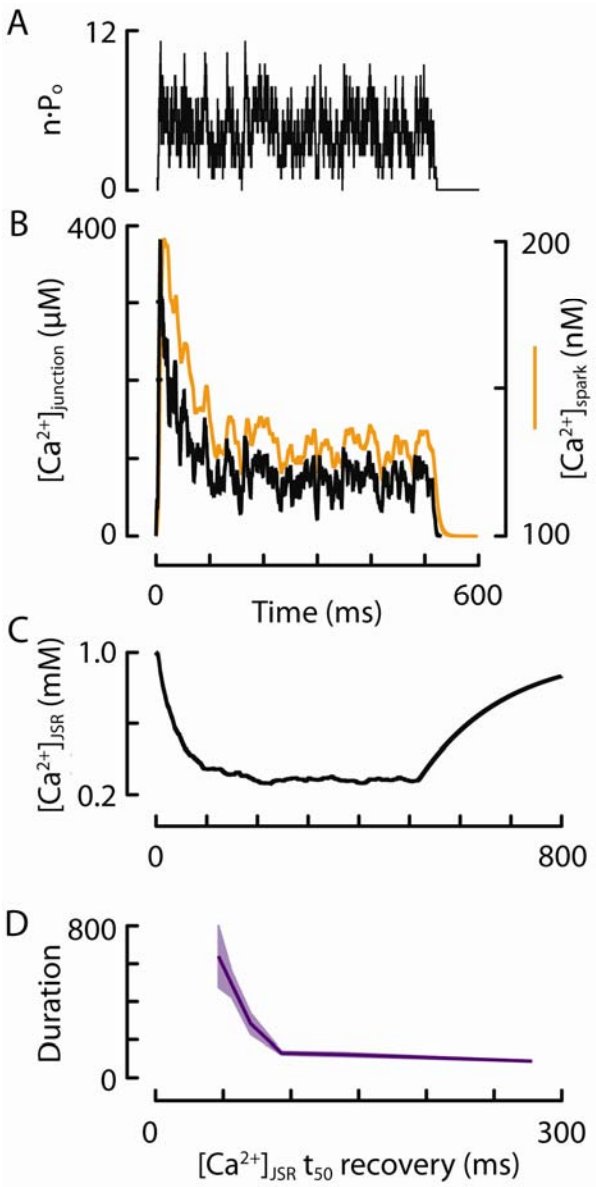

Figure 3.9 Simulation of LLEs by reducing release flux and increasing rate of $[Ca^{2+}]_{JSR}$ restoration. An example simulation is shown, where SR Ca^{2+} release was initiated by an initial 2 *ms* RyR channel opening. **(A)** shows RyR $n{\cdot}P_O$. Initially, it rapidly increased from 1 to 11 due to regenerative CICR, which resulted in a relatively large release flux. This increased $[Ca^{2+}]_{junction}$ **(B**, black line**)** and decreased $[Ca^{2+}]_{JSR}$ **(C)** dramatically. The $[Ca^{2+}]$ in the Ca^{2+} spark volume is also shown **(B**, orange line**)**. Due to the rapid rate of $[Ca^{2+}]_{JSR}$ refilling (see end of C, where $[Ca^{2+}]_{JSR}$ is restored to 50 % of the released fraction in ~ 100 *ms*), $[Ca^{2+}]_{JSR}$ is able to continue release Ca^{2+} into the junction, which plateaus and shows fluctuations similar to those observed experimentally. **(D)** shows the event duration (as defined when $n{\cdot}P_O$ becomes zero) as a function of $[Ca^{2+}]_{JSR}$ recovery time. The shaded area shows one S.E.M. (25 simulations).

corresponding increase in $[Ca^{2+}]_{junction}$ (black line) and $[Ca^{2+}]$ in the Ca^{2+} spark volume (orange line) that persisted for a long duration. During this event, $[Ca^{2+}]_{JSR}$ declined to ~ 260 *μM*, which was not as low as that during a Ca^{2+} spark due to faster recovery (~ 100 *ms* half time by increasing k_1 3.5-fold, Fig. 3.9C). This appeared to be enough to sustain a low level of $[Ca^{2+}]_{junction}$ for ~ 500 *ms*. The eventual termination of the event occurred due to low average RyR P_O (Fig. 3.9A) and subsequent stochastic attrition (Eqn. 3.4). The duration of events increased as JSR recovery increased (Fig. 3.9D, see also Zima, *et al.*, 2008a). This simple model demonstrates that decreased RyR P_O and increased $[Ca^{2+}]_{JSR}$ refilling is able to dramatically prolong release duration. However, the oscillations in $[Ca^{2+}]_i$ did not occur at the frequency shown in Fig. 3.8. The frequency of oscillations are not likely to be reproduced in this simplified scheme because the complex spatio-temporal $[Ca^{2+}]_{junction}$ gradients were not considered. That is, buffering and electrostatic effects on Ca^{2+} would dampen the $[Ca^{2+}]_{junction}$ oscilliations (*e.g.* Soeller and Cannell, 1997), while the spatial distribution of RyR channels relative to release flux would increase the time delay during CICR due to physical distances and closed times. Although this model does not explicitly rule out a $[Ca^{2+}]_{JSR}$-dependent desensitisation during $[Ca^{2+}]_{JSR}$ depletion, it demonstrated that several characteristics of local SR Ca^{2+} release (Ca^{2+} spark termination, release prolongation and termination in the presence of tetracaine) could be reproduced without invoking an additional termination mechanism. It would of interest in future studies to examine whether $n \cdot P_O$ and release duration during an LLE follow Eqn. 3.4. However, a good estimate would require a measure of $[Ca^{2+}]_{JSR}$ during the time-course of release (*e.g.* concurrent recordings of Ca^{2+} blinks).

Quantal local SR Ca^{2+} release flux

Despite some agreement between these data and those presented by Shen, *et al.* (2004, by loose-seal patch clamp), for example, the inverse relationship between rate for rise and time to peak (Fig. 3.6B) and a weak relationship between event amplitude and time to peak (Fig. 3.6C), this study did not find the same wide variation in amplitude (see Table 3.2). The previously observed variance in amplitude has led others to suggest that the number of RyR channels that are active in a CRU during a Ca^{2+} spark is variable (Shen, *et al.*, 2004) and later, quantal (Wang, *et al.*, 2004). Although this seems counter-intuitive under local control, wherein the inherent regenerative property of CICR is contained within a CRU, it may be possible in light of recent data showing ‘sub-clusters’ of RyR channels within a putative CRU (Baddeley, *et al.*, 2009; Xie, *et al.*, 2010). However, quantal Ca^{2+} sparks have

yet to be observed using another method that does not potentially alter the junctional structure (as discussed in Chapters 1 and 2.4) and the clear reduction in the number of quanta observed in the presence of tetracaine (Wang, *et al.*, 2004) seems unlikely due to tetracaine's complex effects on $[Ca^{2+}]_{SR}$, $[Ca^{2+}]_i$ and fluorescence (see above). Although when spontaneous Ca^{2+} sparks were measured in the presence of tetracaine, the maximum rate of rise was reduced (see above and also Zima, *et al.*, 2008a), which is consistent with the RyR blocking effect of tetracaine, it does not provide further support for quantal release fluxes without a large change in the spread of data. The distribution of maximum rates of rise during LLEs did not show detectable quantized rates of rise (not shown). Further, it is unclear how RyR channels within a CRU (or at least, a confocal volume) can release Ca^{2+} without activating nearby RyRs (Wang, *et al.*, 2004, see Niggli, 1999; Sato and Bers, 2011).

3.5. Summary

Once initiated, it is thought that SR Ca^{2+} release locally regenerates and as such, continues until it is terminated by some robust, yet undetermined mechanism. It has been proposed that the mechanism(s) responsible for terminating CICR could be: *(1)* stochastic attrition; *(2)* $[Ca^{2+}]_i$-dependent inactivation; or *(3)* $[Ca^{2+}]_{JSR}$ depletion and/or $[Ca^{2+}]_{JSR}$-dependent de-sesnsitisation of the RyR channels.

The observation of Ca^{2+} sparks that occurred repeatedly at the same CRU at short Δt and in sometimes elevated $[Ca^{2+}]_i$ argues strongly against a $[Ca^{2+}]_i$-inactivated state, while the measurement of a long (relative to the duration of Ca^{2+} spark) Ca^{2+} amplitude restitution time and small Ca^{2+} spark amplitudes at short Δt support significant $[Ca^{2+}]_{JSR}$ depletion. At the same time, measurement of spontaneous Ca^{2+} spark properties in the presence and absence of tetracaine revealed that release duration was inversely proportional to release flux in a manner that can be explained by $[Ca^{2+}]_{JSR}$ depletion and subsequent $[Ca^{2+}]_i$-dependent RyR (de)-activation. Computer modelling using a simplified scheme was able to demonstrate this possibility. When release flux was reduced by tetracaine, release duration was substantially increased to produce LLEs, which is consistent with the idea that $[Ca^{2+}]_{JSR}$ efflux is matched with influx. The remaining small number of available RyR channels then gate stochastically to produce fluctuations during an LLE and their eventual termination appear to be $[Ca^{2+}]_i$-independent. This mechanism is likely to be stochastic attrition. When $n \cdot P_O$ was reduced (by increasing channel closed time) and $[Ca^{2+}]_{JSR}$ influx

was increased in the computer model, LLEs occurred. Termination occurred within a time-course estimated is stochastic attrition was primarily responsible, with no requirement for additional mechanisms.

4. Numerical Analysis of Ca^{2+} Spark Formation

4.1. Background

Despite intensive research, the factors that control Ca^{2+} spark morphology remain unclear. The formation of a Ca^{2+} spark involves the *(1)* activation of a CRU, *(2)* SR Ca^{2+} release and diffusion and *(3)* CRU closure. As discussed in Chapter 3 the mechanism(s) that underlie the termination of CICR remains unclear. Although local SR [Ca^{2+}] depletion appears to be a strong candidate, attempts at measuring $[Ca^{2+}]_{JSR}$ have shown that during a Ca^{2+} spark, SR Ca^{2+} signals (Ca^{2+} scraps or blinks) only decreased to ~ half of that during a caffeine-induced release (Shannon, *et al.*, 2003a; Brochet, *et al.*, 2005; Zima, *et al.*, 2008b; Picht, *et al.*, 2011). It has been suggested that this lack of decrease in $[Ca^{2+}]_{JSR}$ is due to *fast* intra-SR Ca^{2+} diffusion (*e.g.* Picht, *et al.*, 2011), however this quantity has proven difficult to measure directly (see the large discrepancy between Swietach, *et al.*, 2008; Picht, *et al.*, 2011) and is inconsistent with other data. For example, measurements of Ca^{2+} spark amplitude restitution have suggested that $[Ca^{2+}]_{JSR}$ refilling is *slow* (half time of recovery ~ 100 – 250 ms, Fig. 3.7, Brochet, *et al.*, 2005; Picht, *et al.*, 2011; Ramay, *et al.*, 2011, see also Cheng, *et al.*, 1996), taking longer than the duration of a Ca^{2+} spark. This agrees with Ca^{2+} blink measurements, which recover with a time constant of ~ 180 *ms*, but vary between release sites (Zima, *et al.*, 2008b, although see Brochet, *et al.*, 2005). Another possible reason to explain the lack of [Ca2+]JSR depletion is that $[Ca^{2+}]_{JSR}$ is well-buffered. However, the extent of this buffering remains unclear (e.g. Shannon, 1997; Shannon, *et al.*, 2000). In connection with this point, it has been recently shown that [CSQ] may be much higher than previously thought (Murphy, *et al.*, 2011). Thus, it will be useful to understand whether the current interpretation of Ca^{2+} blink signals is correct. An under-estimation is possible because the fluorescent Ca^{2+} dye used to measure Ca^{2+} blinks is highly non-linear over the large range that $[Ca^{2+}]_{JSR}$ may go through during release. Further, the JSR volume is small relative to that of the confocal point-spread function (PSF), which would mean that any decrease in signal would be diminished by the relatively bright signal from neighbouring network SR. Though some calibration of the Fluo-5N binding kinetics have been made (see Shannon, *et al.*, 2003a; Brochet, *et al.*, 2005), the effect of the microscope blurring on Ca^{2+} blinks has not been considered and is expected to be different to that on Ca^{2+} sparks.

Consideration of dye kinetics and optical blurring is also important when calculating local SR Ca^{2+} release flux from Ca^{2+} spark recordings. It has been shown that sampling of Ca^{2+} sparks with a confocal microscope leads to a monotonically decaying Ca^{2+} spark amplitude distribution due to out-of-focus events, regardless of the true underlying distribution (Pratusevich and Balke, 1996; Cheng, *et al.*, 1999). However, it is unclear how an *actual* confocal PSF affects *in-focus* Ca^{2+} spark and Ca^{2+} blink amplitude, width and time-course. The correct calculation of local release flux is important in estimating a number of uncertainties in CICR, such as the number of RyRs that are required to be open during a Ca^{2+} spark and as discussed above, whether this release flux is able to deplete $[Ca^{2+}]_{JSR}$.

While the previous chapters have focussed primarily on single-cell experimental approaches to clarify the generation of Ca^{2+} sparks, this chapter will focus on the construction of a more detailed computer model to simulate Ca^{2+} release at a single junction and Ca^{2+} movement in the nearby micro-domain, including the JSR, connected network SR and major Ca^{2+} buffers, including ATP. During Ca^{2+} spark recording, the true release flux or change in $[Ca^{2+}]$ is altered by processes necessary to the experiment, namely, Ca^{2+} dye binding and optical blurring by a confocal microscope. The effect of these processes on the recorded Ca^{2+} spark and Ca^{2+} blink was examined. Lastly, the computer model was used to fit experimentally recorded Ca^{2+} sparks to calculate the underlying release flux and examine its primary determinants during CRU activation and termination.

4.2. Methods

Preparation of single ventricular myocytes and Ca^{2+} spark imaging

Single ventricular myocytes were obtained from Wistar rat hearts by enzymatic dissociation and prepared for fluorescence imaging as previously described (see Chapter 2.2). Spontaneous Ca^{2+} sparks were imaged as described in Chapter 3.2.

The microscope PSF was measured by imaging *z*-stacks of 100 *nm* diameter yellow-green Fluorospheres (Invitrogen, see Fig. 4.1). Beads resting on the glass cover-slip of the perfusion bath (Fig. 4.1i) and on top of live myocytes (Fig. 4.1ii,iii) were recorded and measured. For those resting on cells, care was taken to avoid Ca^{2+} waves and fast, but

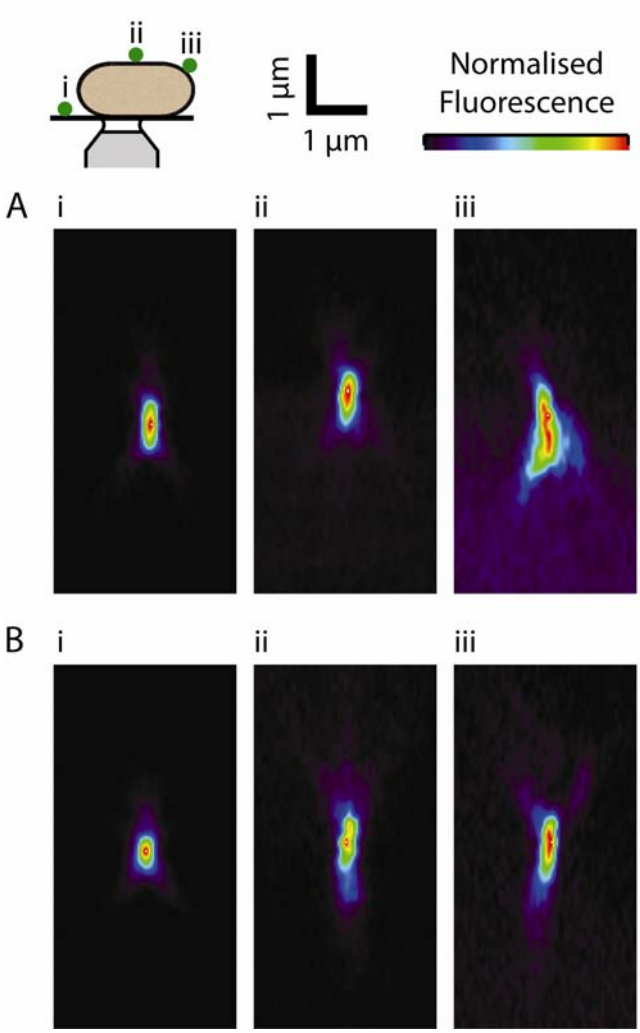

Figure 4.1 Measurement of the confocal microscope PSF on the cover-slip and on top of live myocytes. Representative *x-z* images of 100 *nm* yellow-green Fluorospheres, as recorded by a water- **(A)** or oil-**(B)** immersion objective. Each bead was measured at a different location (indicated by ***i***, ***ii*** and ***iii***, corresponding to the top left schematic of looking down the longitudinal axis of a myocyte resting on a coverslip located above an inverted objective). To highlight the changes in shape of the PSF, image intensities have been scaled. Large aberrations are seen when the bead is resting on the curved edge of the cell (iii) and is primarily due to astigmatism. The intensity drop with increasing distance from the coverslip was significant, but difficult to measure, as the same microscope settings could not capture distant beads (10 – 20 μm above the coverslip, measured from z-stacks) without saturating proximal beads. Note that the refractive indices for glass, water and muscle cytoplasm are 1.52, 1.33 and ~ 1.38 (Huxley and Niedergerke, 1958; Curl, et al., 2005), respectively.

low-resolution z-stacks were used to obtain its height (z) above the cover-slip and its location on the curve of the cell surface. In these experiments, perfusion was stopped during scans to avoid washing away the beads. This process was performed for both the water-immersion objective (stated above) and a Plan-Apochromat 63 x 1.4 N.A. oil-immersion objective, typical of objective types used in most Ca^{2+} spark studies. As shown in Fig. 4.1, significant changes to the PSF is observed when the bead is situated on top of the myocyte, with the most prominent distortion of the PSF occurring when the bead is resting on a curved edge. The measured dimensions of the PSFs are given in Table 4.1.

	FWHM (*μm*)			
	x	**y**	**z**	**n**
Water immersion				
Coverslip	0.38 ± 0.03	0.35 ± 0.02	1.7 ± 0.2	6
Cell	0.34 ± 003	0.36 ± 0.03	1.5 ± 0.1	5
Oil immersion				
Coverslip	0.29 ± 0.01	0.22 ± 0.02	0.61 ± 0.04	4
Cell	0.32 ± 0.01	0.32 ± 0.02	1.19 ± 0.06	5

Table 4.1 Measurement of confocal point-spread functions (PSFs) using yellow-green Fluorospheres. Two objectives were investigated, with PSFS measured from the cell-top and coverslip positions. Beads recorded on a very curved surface of the cell (see Fig. 4.1iii) were not measured due to their complex shapes.

Image analysis

Image analysis was performed using custom routines written in IDL. Spontaneous Ca^{2+} sparks were detected by a Matched Filter Detection Algorithm (Kong, *et al.*, 2008). Since the distortion of the true Ca^{2+} spark amplitude distribution by confocal sampling has been well-defined by others (Pratusevich and Balke, 1996; Izu, *et al.*, 1998; Shirokova, *et al.*, 1999), a simple method to back-calculate the underlying amplitude distribution was performed. First, the expected distribution from confocal sampling of a stereotypic event was calculated by convolution with a measured PSF in three dimensions (3D, 10 *nm/px* grid). A 3D Gaussian function with FWHM of 0.35 *μm* in the focal plane (*x*, *y*) and 1 *μm*

along the optical axis (*z*) was also used to approximate the measured PSF (from the average PSF measured by an oil immersion objective at the cell-top, Table 4.1). Next, these expected distributions were used as the PSF in a Richardson-Lucy deconvolution method to obtain the underlying Ca^{2+} spark amplitude distribution. Those Ca^{2+} sparks with moderately high amplitudes (and therefore more likely to be in-focus) were chosen for analysis.

Model parameters and diffusion equations

The Ca^{2+} spark computer model equations were solved numerically by FACSIMILE (Flow and Chemistry Simulator, U.K. Atomic Energy Authority, 1987). Unless otherwise stated, FACSIMILE solutions were then read into IDL for further analysis. Where appropriate, the start of a function (*e.g.* $n \cdot P_O$) was defined as where the function first exceeded 110 % of the baseline.

The computer model consisted of cytosolic and SR compartments, each containing Ca^{2+} buffers that had unique binding kinetics and mobility (Fig. 4.2). Diffusion within the cytosol was approximated using equations that describe diffusion in a spherical volume (Crank, 1979). The radius was set to 4 *μm* and divided into 40 equally spaced elements. The volume of each cytosolic element (*Vi*) was calculated using Eqn. 4.1, where *r* is the distance between the centre of the ith element to the centre of the 0th element.

$$V_i = \frac{4}{3} \cdot \pi({r_i}^3 - {r_{i-1}}^3) \qquad \textbf{Eqn. 4.1}$$

The range of *i* is therefore, $0 \leq i \leq 39$, where 0 is the first element closest to the centre of the sphere.

The volumes of the SR elements were calculated as 3.2% of total cell volume (assuming the cytosolic volume is 60% of total cell volume, Bers, 2001), with the exception of the first element, which was set to 5 *aL* to represent the JSR. This volume was a compromise between estimates obtained by two methods. *(1)* If 0.3 % of total cell volume is JSR and cell volume is ~ 30 *pL* (rat, Bers, 2001), then the volume of one JSR is ~ 3 *aL*, assuming that couplons occur at 1.01 $/\mu m^3$ cell (rat, Soeller, *et al.*, 2007). This compares to *(2)* measurements from electron microscopy data, which yield ~ 8 *aL* (by approximating

the junction as a cylinder of radius = 296 *nm* and height = 30 *nm*, Brochet, *et al.*, 2005). Since tissue prepared for electron micrographs suffer shrinkage artefacts and data collection from thin sections preferentially selects for larger junctions, the EM data was considered the upper limit. On the other hand, immuno-fluorescence localisation of RyR channels may over-estimate the number of junctions or CRUs due to rogue receptors, which would under-estimate the size of the average junction. Therefore, an intermediate volume of 5 *aL* was chosen for the jSR.

The area of diffusion (*Ai*) between any two given elements along the radius of the sphere was calculated using Eqn. 4.2, while the rate of diffusion was calculated using Eqn. 4.3

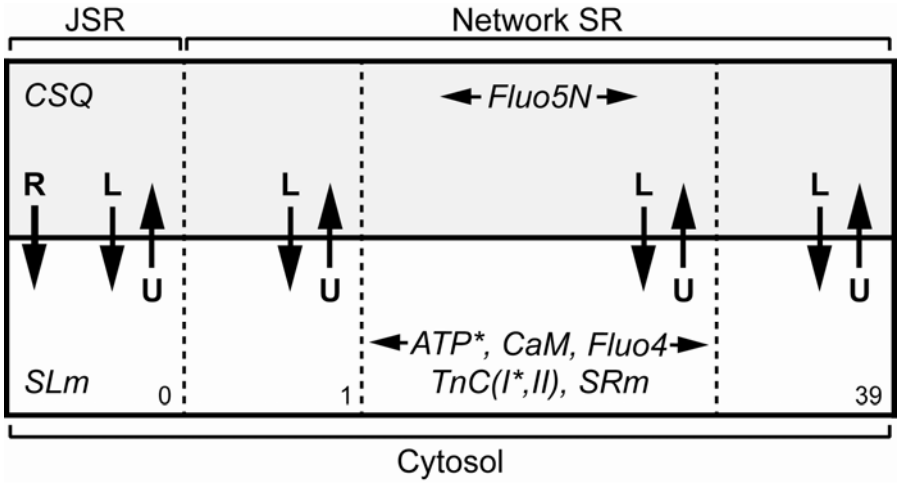

Figure 4.2 Schematic of Ca^{2+} movements and binding sites in Ca^{2+} spark model. The radial axis of the spherical model begins at element, *i* = 0 on the left to *i* = 39 on the right. Each element is shown as a square box and a dashed boundary marks an area (Eqn. 4.2) through which Ca^{2+} and mobile buffers (*e.g.* ATP or Fluo-5N) can diffuse. The bottom row represents the cytosol, which contains ATP, troponin-C (both I and II binding sites), sarcolemmal (SL) and SR membrane (SRm) binding sites, calmodulin (CaM) and Fluo-4. Both ATP and TnC(I) (asterisked) are able to bind Mg^{2+}. Ca^{2+} uptake (U) into the SR is able to occur across the entire radius and is opposed by a leak (L) flux. The top row represents the SR: the 0th element is junctional (JSR), contains calsequestrin (CSQ) and is able to release SR Ca^{2+} into the 0th cytosol element. The remaining network SR elements contain Fluo-5F.

(Crank, 1979), where *D* is the diffusion coefficient of a given species, *A* is given by Eqn. 4.2 and *Δx* is the distance between the centres of the two adjacent elements (100 *nm*).

$$A_i = 4\pi r_i^2$$ **Eqn. 4.2**

$$Q = -D \cdot A \cdot \frac{\Delta[Ca^{2+}]}{\Delta x}$$ **Eqn. 4.3**

As shown in Fig. 4.2, only the JSR element contained CSQ and was able to release Ca^{2+} ('R') into the first cytosolic element. All SR elements were able to re-uptake ('U') and leak ('L') Ca^{2+} from and into the corresponding cytosolic element, respectively. The kinetics of re-uptake were set so that when $[Ca^{2+}]_i$ was transiently increased to 10 *mM*, return to rest occurred in a half-time of ~ 160 *ms* (V_{max} = 300 *μM/s*, K_m = 0.3 *μM*, stoichiometry = 2, Bers, 2001), while the leak flux was set so that $[Ca^{2+}]_i$ at steady-state was 100 *nM*. Within the SR, the only other buffer included was Fluo-5N. In the cytosol, buffers included ATP, CaM, Fluo-4, SL and SR membrane binding sites (SL_m and SR_m, respectively) and troponin-C (both high and low affinity sites, $TnC_{I,II}$). Simple one-to-one binding reactions were used for all buffers.

A summary of the concentrations, diffusion coefficients and rate constants used for these buffers are given in Table 4.2. The diffusion coefficient for ATP (D_{ATP}) was found to be 1.4 x 10^{-8} dm^2/s at 16 ºC (Baylor and Hollingworth, 2000). Since this work is at room temperature, D_{ATP} at 24 ºC was estimated by two methods: *(1)* if the diffusion of ATP has a Q_{10} of 1.4, then D_{ATP} at 24 ºC would be 1.9 x 10^{-8} dm^2/s (see also Sidell and Hazel, 1987; Hubley, *et al.*, 1996). *(2)* Given that the molecular mass of ATP is 507.18 *g/mol* and assuming a globular structure, D_{ATP} was estimated to be 1.4 x 10^{-8} dm^2/s (Stoke-Einstein equation), so an intermediate value was used.

D_{CaM} was estimated also from its Stoke's radius (Sorensen and Shea, 1996) and was 4.5 x 10^{-9} dm^2/s. The on and off rates of Fluo-4 were also estimated from the data of Baylor and Hollingworth (2000) obtained at 16 ºC using a Q_{10} of 2. $K_{D,Fluo\text{-}4}$ *in vivo* was estimated to be 0.9 *μM* from various in vitro calibrations that yielded 0.8 *μM* (Woodruff, *et al.*, 2002; Yasuda, *et al.*, 2004) and 1.1 *μM* (Fluo-3, Wang, *et al.*, 2001). Likewise, $K_{D,Fluo\text{-}5F}$ was taken from Woodruff, *et al.* (2002), but has also been reported at 1.6 *μM* at

24 ºC (Yasuda, *et al.*, 2004). [Mg^{2+}] was set to 1 *mM* in all compartments (Gupta, *et al.*, 1984, though see Blatter and McGuigan, 1986; Quamme, 1990).

D_{Ca} in the SR was estimated to be 50-fold less than that in the cytosol, a value that was chosen to include the effect of tortuosity and Ca^{2+} binding sites within the SR. If the SR lattice is simplified as diffusion within a flat sheet, with staggered blocks as barriers, then the effective diffusion coefficient can be calculated from the ratio between the size of and distance between the blocks (see Fig. 12.8 in Crank, 1979). Since SR tubules are ~ 40 *nm* in diameter and the 'holes' in the SR network between adjacent tubules are ~ 160 *nm* wide (*e.g.* Ogata and Yamasaki, 1990), then the effective diffusion coefficient would be ~ 0.3 of that in free solution.

In addition, binding to buffers would also reduce the rate of diffusion proportional to the number of binding sites present. It is thought that ~ 60 % of Ca^{2+} buffers in the network SR is SERCA (for a review, see Tada and Toyofuku, 2011). It has been estimated that there is ~ 1.7 $mmol/L_{SR}$ of SERCA in rat (Hove-Madsen and Bers, 1993). Assuming each SERCA has two binding sites for Ca^{2+}, free $[Ca^{2+}]_{SR}$ is 1 *mM* (*e.g.* Chen, *et al.*, 1996; Shannon, 1997) and the other buffers have 1:1 reactions with Ca^{2+}, then the concentration of binding sites would be ~ 2.8 $mmol/L_{SR}$ and diffusion would be reduced by ~ 65 %. Thus, the overall effect of tortuosity and Ca^{2+} binding is a ~ 90 % reduction in $D_{Ca,SR}$. Further, local Ca^{2+} flux into a JSR is likely to be further reduced due to reduced connectivity (by only one or two tubules, Brochet, *et al.*, 2005). In this model, the area for diffusion between the first (JSR) and second SR elements is larger than that of a single tubule leading into the JSR. If there was only one tubule of 40 *nm* diameter connecting the two, then the rate of diffusion between them would be reduced by ~ 95 % (Eqn. 4.2).

Note that this was able to reproduce the time-course of previously reported Ca^{2+} blinks (Zima, *et al.*, 2008b; Picht, *et al.*, 2011, see below) and consistent with slow Ca^{2+} diffusion in the SR (Swietach, *et al.*, 2008). Diffusion of Fluo-5N within the SR was set to one fifth that of Fluo-4 in the cytoplasm, a value within the range estimated by Picht, *et al.*, 2011) using fluorescence recovery after photobleaching.

x x	[x] (µM)	D (10^{-8} dm^2/s)	K_{on} (/µM/s)	K_{off} (/s)	K_D (µM)	References and Notes
Cytosol						
Ca^{2+}_{free}	0.1	3.0	-	-	-	Sidell and Hazel, 1987; Wier, *et al.*, 1987; Cheung, *et al.*, 1989; Ward, *et al.*, 2003
ATP	4000	1.5	13.64	30000	2200	See text. $K_{on,Mg}$ = 3.3 x 10^{-4} */µM/s*, $K_{off,Mg}$ = 3 /s, Fabiato, 1983; Baylor and Hollingworth, 1998
CaM	9(4)	0.45	100	31	0.31	4 binding sites, Fabiato, 1983; Sorensen and Shea, 1996; Smith, *et al.*, 1998; Maier, *et al.*, 2006
Fluo-4	100	0.75	307	276.7	0.9	Baylor and Hollingworth, 1998; 2000; Wang, *et al.*, 2001; Woodruff, *et al.*, 2002
Fluo-5F	100	0.75	307	451.9	1.47	Woodruff, *et al.*, 2002; Yasuda, *et al.*, 2004
$TnC_{I,hi}$	70(2)	-	100	7.1	0.071	2 binding sites, with affinity for Mg^{2+}: $K_{on,Mg}$ = 0.03 /µM/s, $K_{off,Mg}$ = 1.11 /s, Holroyde, *et al.*, 1980; Pan and Solaro, 1987
$TnC_{II,lo}$	70	-	125	500	4	Holroyde, *et al.*, 1980; Fabiato, 1983; Pan and Solaro, 1987
SL_m	86	-	125	1625	13	Page, *et al.*, 1971; Fabiato, 1983; Post and Langer, 1992; Soeller and Cannell, 1997
SR_m	47	-	115	100	0.87	Fabiato, 1983; Smith, *et al.*, 1998
SR						
Ca^{2+}_{free}	1000	*	-	-	-	1 – 1.5 *mM*, Shannon, *et al.*, 2003a, *see text for diffusion constant
CSQ	120000	-	100	600000	600	From a binding capacity of 30 – 40 Ca^{2+} per CSQ, Murphy, *et al.*, 2011, see also Cala and Jones, 1999, Campbell, *et al.*, 1983a and Ginsburg and Bers, 2004
Fluo-5N	50	*	307	122956	400	*See text

Table 4.2 Parameters of Ca^{2+} and related buffers used to generate Ca^{2+} sparks and Ca^{2+} blinks Parameters shown include: concentration expressed per litre of respective volume, [x]; diffusion coefficient, *D*; on (K_{on}) and off (K_{off}) binding rates and dissociation constant, K_D for each species are given. Abbreviations: ATP, adenosine-3',5'-triphosphate; CaM, calmodulin; TnC, troponin-C, which has high (I) and low (II) affinity binding sites; SL_m, sarcolemmal Ca^{2+} binding sites; SR_m, sarco-endoplasmic reticulum (SR) membrane Ca^{2+} binding sites accessible by cytosolic Ca^{2+}; CSQ, calsequestrin. Note that a major cytosolic Ca^{2+} buffer, ATP, can also bind Mg^{2+}. This means that at rest, ~ 99 % of ATP is Mg^{2+}-bound. 24 °*C* estimated.

Generation of a Ca^{2+} release function

Ca^{2+} release as a function of time , *CR(t)*, was defined by a continuous function (Eqn. 4.4), where k_{on} and k_{off} were rate constants (*/ms*) for the rising and decay phases, respectively, while *S* was a scaling factor for magnitude (*/ms*) and t_0 (*ms*) was a shift in time. These four parameters were varied during curve-fitting to recorded Ca^{2+} sparks. Curve-fitting was performed in two-dimensions using a non-linear least-squares method coded in IDL (Markwardt, 2009). This involved executing FACSCIMILE code within an IDL function to generate a Ca^{2+} spark for minimisation. The accuracy of this fitting method was tested using synthetic datasets with Poisson noise.

$$\mathrm{CR(t)} = \mathrm{S} \cdot \mathrm{rise} \cdot \mathrm{decay} \qquad \textbf{Eqn. 4.4}$$

where,

$$\mathrm{rise} = \mathrm{TANH}\big(\mathrm{k_{on}} \cdot (\mathrm{t} - \mathrm{t_0})\big) + \mathrm{TANH}(\mathrm{k_{on}} \cdot \mathrm{t_0})$$

$$\mathrm{decay} = \mathrm{e}^{-\mathrm{k_{off}} \cdot (\mathrm{t} - \mathrm{t_0})}$$

The product of *CR(t)* and the concentration gradient between the JSR and first cytosolic element produced Ca^{2+} release flux in *μM/ms*, which was then used to estimate $n \cdot P_O$ of the CRU. During SR Ca^{2+} release, the dependence of i_{RyR} on SR [Ca^{2+}] was estimated from the work of Mejia-Alvarez and colleagues (1999, see Eqn. 4.5). The maximum unitary RyR channel current was ($i_{RyR,max}$) set to 2 *pA* and half maximal conductance ($K_{m,RyR}$) at $[Ca^{2+}]_{JSR}$ = 2 *mM*, which gives i_{RyR} ~ 0.6 *pA* when $[Ca^{2+}]_{JSR}$ is 1 *mM*. i_{RyR} was then divided from the release flux (*M/s*) to give $n \cdot P_O$, as shown by Eqn. 4.5, where $V_{cyt,0}$ is the volume of

the first cytosolic element (4.18 *aL*), *z* is the valence of Ca^{2+} and *F* is Faraday's constant. Using a maximum $P_{O,RyR}$ of ~ 0.5 (see Chapter 2.2), a lower limit for the number of RyR channels required in the cluster (*n*) was estimated.

$$n \cdot P_O = \frac{\text{release flux} \cdot V_{cyt,0} \cdot z \cdot F}{i_{RyR}} \qquad \textbf{Eqn. 4.5}$$

where,

$$i_{RyR} = \frac{i_{RyR,max}}{(1 + \frac{K_{m,RyR}}{[Ca^{2+}]_{JSR}})}$$

Simulation of optical blurring of Ca^{2+} sparks during confocal imaging

The Ca^{2+}-bound Fluo-4 signal was blurred spatially at each time-point to simulate an experimentally recorded Ca^{2+} spark in a line-scan image. A 3D Gaussian function (see above) was used as the PSF (weighting function), where the total energy was set to unity. Due to the spherical geometry of this model, the asymmetric PSF had to be re-calculated, where the PSF weights had to be mapped from its original position in 3D (relative to a sphere) to a corresponding position along the radius of the sphere (see Fig. 4.3). To do this, a sphere with 40 shells (corresponding to the elements in the computer model) and the 3D Gaussian PSF were generated.

At each iteration, the contribution of signal from each shell to the blurred signal was calculated. This was the volume of the shell that overlapped the PSF and could be calculated by setting the values of the current shell to one, then multiplying with the PSF in 3D space (*e.g.* blue PSF, Fig. 4.3). This contribution was projected (by summation) to a radial position. Before the contribution of the next shell is calculated, the current shell was restored to zero. After the contribution sums from each of the 40 shells have been calculated (see Fig. 4.3B) and stored, the next iteration could begin. For the next iteration, the PSF was displaced radially by one shell/element relative to the sphere (green PSF, Fig. 4.3). This process was continued until all of the energy from the original Gaussian PSF had been accounted for in the new weighting function, which was a 40 x 40 array with the contribution of all 40 shells at 40 displacements.

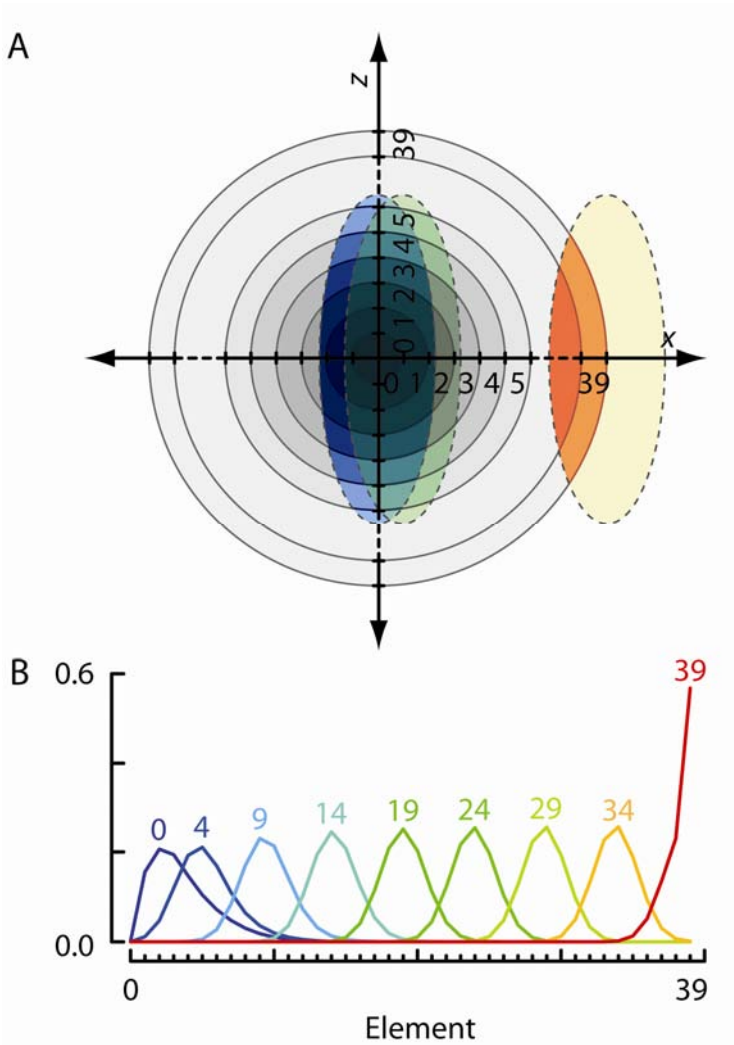

Figure 4.3 Transformation of a 3D PSF into a radial weighting function for blurring Ca^{2+} sparks. (A) shows an *x-z* cross-section of the asymmetric 3D Gaussian function (PSF) and the spherical model space divided into 40 shells and how the PSF is displaced with respect to the shells to calculate the radial weighting function. See text for details. **(B)** shows the calculated weighting function across the elements at various displacements (noted above in colour above its corresponding function). The colours correspond (roughly) to the colours shown in (A), where blue and red are zero and maximum displacements, respectively.

The weights at each displacement equalled unity, except for when displacement of the PSF caused it to lose energy outside of the computational volume. In this case, the weight was placed into the last element/shell because the computer model (r = 4.0 μm) is sufficiently large that the last element is representative of the space beyond. In addition, the weighting of the first element was reduced by 91 % (and this weight placed into the last element to conserve energy) to mimic the reduced volume in the junction compared to the spherical computational element (*i.e.* if the junctional space is a cylinder of height 12 *nm*, with a diameter equal to the width of the first element, its volume would be 9 % that of the element). To avoid errors due to digitisation, calculations of the PSF were performed at 10 *nm* spacing, giving < 0.001% error.

The weighting function was multiplied with the Ca^{2+}-bound Fluo-4 signal at each displacement and accumulated, as occurs in convolution in the spatial domain. This entire process was repeated at each time-point to generate the blurred signal. The weighting function was read into FACSIMILE and employed using a loop to control displacement.

Simulation of optical blurring of Ca^{2+} blinks during confocal imaging

The optical blurring that the Ca^{2+}-bound Fluo-5N signal undergoes to form a Ca^{2+} blink is not the same as that for a Ca^{2+} spark due to different geometry of the SR relative to the size and shape of the PSF and likely significant contribution of out-of-focus signal from nearby network SR and/or JSR (*i.e.* volume(s) of high [Ca^{2+}] within the confocal volume that is not depleted and will contribute to the Ca^{2+} blink). From the JSR, the network SR extends transversely at the *z*-line and wraps around the myofilaments (Fig. 4.4A). In this stylisation, the myofilaments are packed together, with the network SR curving around their perimeter. This network SR feeds a JSR located at the centre of the cross-section (white solid line). Depending on the orientation of this arrangement with respect to the PSF in grey (Fig. 4.4A vs. B), contamination of the true JSR signal by the network SR can differ from the ‘worst’ (Fig. 4.4A, C) to the ‘best’ (Fig. 4.4B, D) case scenario. The difference in calculated Ca^{2+} blink amplitude between these two cases was ~ 30 % (not shown).

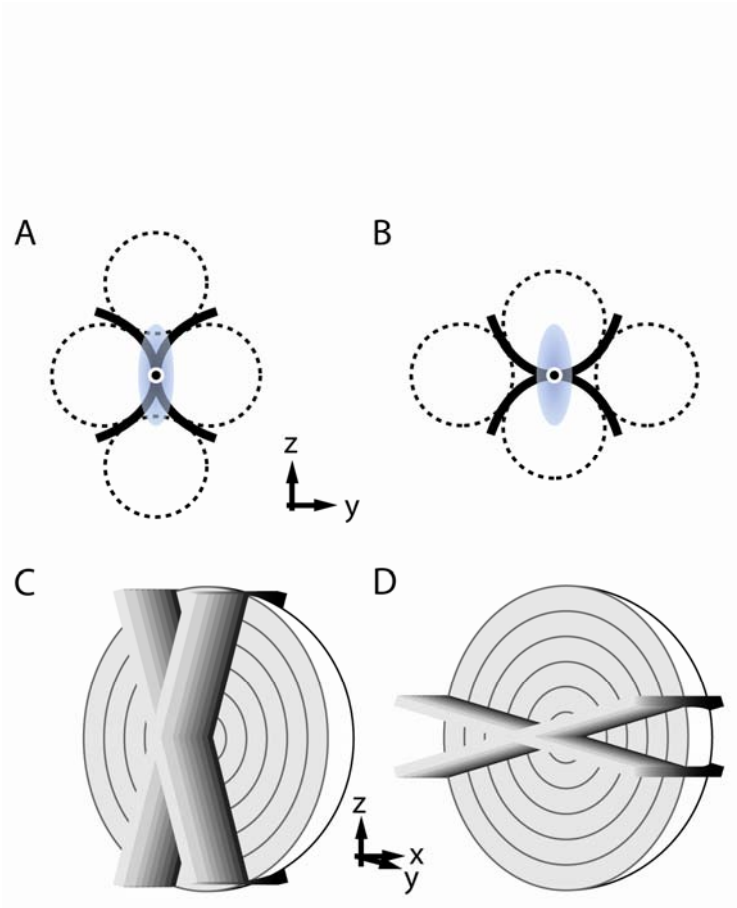

Figure 4.4 Generation of a weighting function for blurring Ca^{2+} blinks. (A) shows a stylised drawing of a region of a myocyte transverse (y-z) cross-section at the z-line. Myofilament bundles (dotted circles) have a diameter of 1 μm (Ham, A.W. & Cormack, D.H., 1979), are packed closely together and surrounded by network SR (black curved x) with tubules of 40 nm diameter. Where the network SR tubules cross is a proposed JSR (white circle). The Gaussian PSF is shown in relative size. Note that the PSF has a volume of ~ 100-fold larger than the JSR. **(B)** shows this same cross-section rotated at 90 ° with respect to the PSF. (A) is the 'worst' case scenario, where network SR contribute extensively to the blurred Ca^{2+} blink, while (B) is the 'best' case scenario, where network SR contribution is minimised. In the model, (A) and (B) were simplified as an 'x' that extended into the longitudinal (x) axis of the spherical model (grey shells). These are shown in **(C)** and **(D)** for the worst and best cases, respectively. Note that in reality, the network SR in *x* is grid-like.

Parameter sensitivity of the computer model

Analysis of release flux may be highly-sensitive to changes in parameters that were predefined, which is problematic for parameters that exhibit large variability in the literature. Therefore, parameters were independently-altered and the resultant Ca^{2+} spark measured and compared to a 'standard'. This was defined using Eqn. 4.4 (K_{on} = 800, K_{off} = 400, S = 15000, t_0 = 0.02 *s*), which resulted in a Ca^{2+} spark that reached a maximum F/F_0 of 2.2 in 6.5 *ms*, exhibited a time to half decay of 31 *ms* and a FWHM of 1.1 *µm*.

4.3. Results

Formation of a Ca^{2+} spark

The computer model described was able to reproduce the general spatio-temporal profile of a Ca^{2+} spark, where the Ca^{2+} release function (*CR(t)*, Eqn. 4.4) was able to be adjusted to match recorded Ca^{2+} sparks. This is demonstrated using a recorded event that was chosen for its high signal-to-noise ratio and amplitude (Fig. 4.5A). The corresponding simulated Ca^{2+} spark is shown in panel B. The quality of the fit can be appreciated by examining the absolute difference between recorded and simulated events (shown in panel C), where the mean was approximately zero (– 0.07) and the residual sum of squares was small (0.1). The quality of the fit can also be appreciated by examining the time (Fig. 4.5D) and spatial (Fig. 4.5E) profiles of the recorded and computer-generated Ca^{2+} sparks through the centroid and at some distance (or time) away from the centroid.

The recorded Ca^{2+} spark is usually formed by blurring of the Ca^{2+}-bound Fluo-4 signal by a confocal microscope PSF. This was achieved in the model by blurring the computed Ca^{2+}-bound Fluo-4 signal by the described in-focus confocal PSF weighting function. The effect of this blurring procedure is shown in Fig. 4.6. The simulated event from Fig. 4.5A is shown in Fig. 4.6A, above the Ca^{2+}-bound Fluo-4 signal prior to microscope blurring (Fig. 4.6B). Blurring by the confocal PSF reduced the amplitude of the Ca^{2+} spark by more than half and delayed the time of peak amplitude by ~ 1.5 *ms* (compare blue solid and red dashed lines, Fig. 4.6D). In contrast, the FWHM was almost doubled (compare blue solid and red dashed lines, Fig. 4.6D). That is, even for an *in-focus* Ca^{2+} spark, its amplitude and spatial extent are dramatically altered by microscope blurring, with moderate effects on time-course.

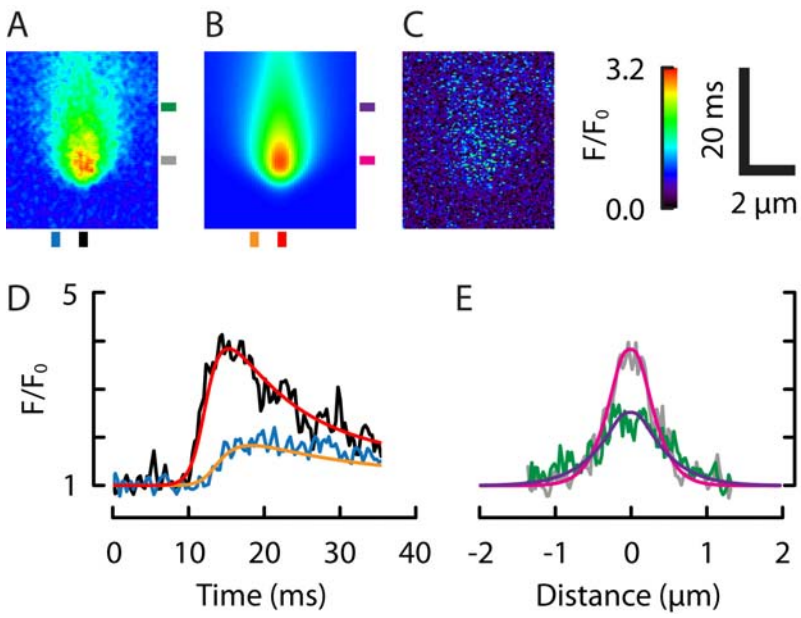

Figure 4.5 Computer simulation of a Ca^{2+} spark by fitting to recorded event. (A) shows a measured spontaneous Ca^{2+} spark. **(B)** shows the corresponding simulated Ca^{2+} spark, where *CR(t)* was varied to minimise the residuals. Both of these events have been displayed scaled to the same colour table (shown on right). **(C)** shows the absolute difference between (A) and (B), which has been scaled to the whole colour table range. It had a mean F/F_0 of 0.09 and the residual sum of squares was 0.1. **(D)** shows time profiles through the centroid of the recorded (black line) and simulated (red line) Ca^{2+} sparks. The time profiles at 1 *µm* away from the centre are also shown for the measured (blue line) and simulated (orange line) events. The locations of these are also marked in panels (A) and (B). **(E)** shows spatial profiles through the centre of the recorded (grey line) and simulated (magenta line) Ca^{2+} sparks. The spatial profiles are also shown 10 *ms* after the peak for recorded (green line) and simulated (purple line) events. The time of these are also marked in panels (A) and (B).

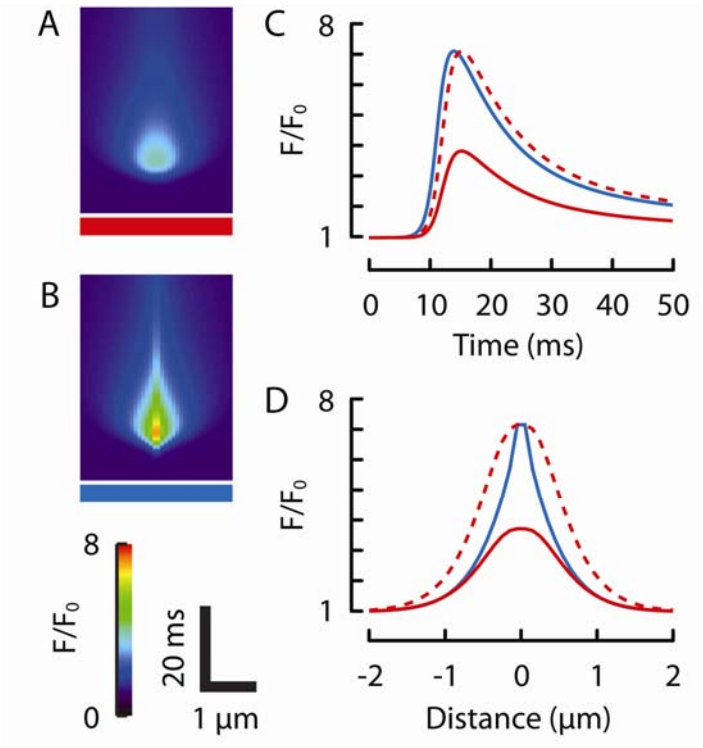

Figure 4.6 The effect of optical blurring on the observed Ca^{2+} spark. **(A)** shows the simulated Ca^{2+} spark from Fig. 4.5B in a different colour table for comparison here. **(B)** shows the same simulated event prior to blurring by the microscope PSF (*i.e.* the direct Ca^{2+}-bound Fluo-4 signal). The temporal **(C)** and spatial **(D)** profiles of the Ca^{2+} spark signal before (blue line) and after (red line) microscope blurring are also shown. The peak fluorescence was ~ halved. When scaled to the sample peak fluorescence as the non-blurred event, the blurred event (red dashed line) showed a slightly prolonged time-course, where the peak fluorescence occurred 1.1 *ms* after the peak of the Ca^{2+}-Fluo-4 signal. Note that this is ~ 1.9 *ms* after the peak of $[Ca^{2+}]_{junction}$ (see Fig. 4.8A). The width of the event had ~ doubled (214 %) due to microscope blurring.

Formation of a Ca^{2+} blink

Changes [Ca^{2+}] within the SR compartment during this Ca^{2+} spark was also calculated. Fig. 4.7A, B and C show simulated line-scan images of $[Ca^{2+}]_{SR}$, Ca^{2+}-bound Fluo-5N signal before and after optical blurring, respectively. The latter corresponds to a recorded Ca^{2+} blink without noise. $[Ca^{2+}]_{JSR}$ decreased by ~ 93 *%* to 70 *μM* (Fig. 4.7D). However, due to its K_D, the Ca^{2+}-Fluo-5N signal only decreased by ~ 80 *%* (blue solid line, Fig. 4.7D). However, this effect was not as large as that due to optical blurring. The calculated Ca^{2+} blink severely under-estimated the extent of Ca^{2+} depletion by showing a mere ~ 33 *%* maximum decrease in signal (red solid line, Fig. 4.7D). In contrast, the under-estimation of $[Ca^{2+}]_{JSR}$ depletion and refilling was mostly due to Fluo-5N kinetics (Fig. 4.7D). The Ca^{2+} blink over-estimated the spatial extent of SR Ca^{2+} depletion by ~ 57 % and this effect was mainly due to microscope blurring (compare red dashed and black solid lines, Fig. 4.7E).

Local Ca^{2+} release flux

The underlying release flux was able to be estimated from this model. The development of [Ca^{2+}] in the first cytosolic element ($[Ca^{2+}]_{junction}$) is shown in Fig. 4.8A (black line). $[Ca^{2+}]_{junction}$ increased from 150 *nM* to a maximum of ~ 31 *μM* in ~ 7.1 *ms* and declined to half of that value in ~ 3.6 *ms*. Peak $[Ca^{2+}]_{junction}$ occurred ~ 2 *ms* earlier than the peak of the Ca^{2+} spark (from Fig. 4.6B, scaled to $[Ca^{2+}]_{junction}$, red dashed line, Fig. 4.8A). From $[Ca^{2+}]_{junction}$, release flux was estimated using the volume of the first element (black line, Fig. 4.8B). This reached ~ 13 *pA*, which was equivalent to ~ 33 open RyR channels (see Methods) and are both lower estimates given the lack of resolution within the junction. Note that release flux began to decline before $n{\cdot}P_O$ declined. This is because release flux is the product of $n{\cdot}P_O$ and $i_{RyR,}$ which is ~ proportional to the [Ca^{2+}] gradient. As shown in Fig. 4.8*C*, $[Ca^{2+}]_{JSR}$ (black solid line) declined as Ca^{2+} release progressed beyond its maximum, where the effect of decreasing $[Ca^{2+}]_{JSR}$ outweighed the increase in $n{\cdot}P_O$. The [Ca^{2+}] gradient across the junctional membrane ($[Ca^{2+}]_{JSR} - [Ca^{2+}]_{junction}$, green dashed line, Fig. 4.8*C*) is similar to $[Ca^{2+}]_{JSR}$ because even though peak $[Ca^{2+}]_{junction}$ was 31 *μM*, this occurred when $[Ca^{2+}]_{JSR}$ was still ~ 490 *μM* and when $[Ca^{2+}]_{JSR}$ was at its minimum (85 *μM*), $[Ca^{2+}]_{junction}$ had already declined to ~ 3 *μM*.

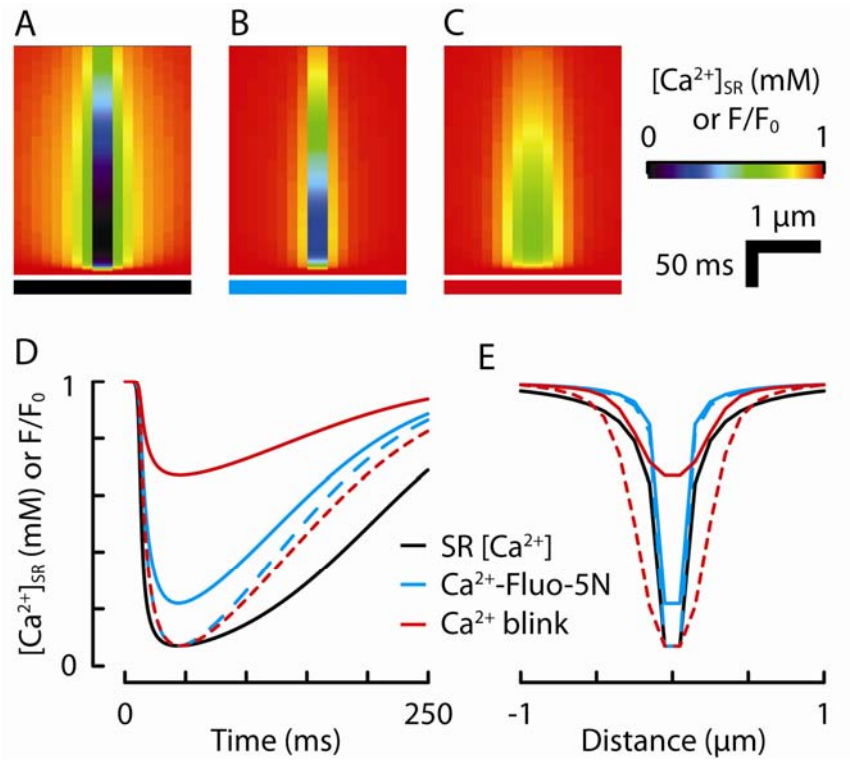

Figure 4.7 SR [Ca^{2+}] and Ca^{2+} blink during a Ca^{2+} spark. (A) shows a simulated line-scan image of $[Ca^{2+}]_{SR}$ during the Ca^{2+} spark shown in Fig. 4.5. The corresponding Ca^{2+}-bound Fluo-5N signal before **(B)** and after **(**Ca^{2+} blink**, C)** microscope blurring are also shown. **(D)** shows the time profiles of $[Ca^{2+}]_{JSR}$ (black line, in *mM*), the Ca^{2+}-Fluo-5N (blue line, in F/F_0) and Ca^{2+} blink signals (red line, in F/F_0). $[Ca^{2+}]_{JSR}$ reached a minimum of ~ 70 *µM* at 44 *ms*, with a half recovery time of ~ 167 *ms*. To compare alterations in time-course, the Ca^{2+}-Fluo-5N (blue dashed line) and Ca^{2+} blink (red dashed line) were scaled to the amplitude of $[Ca^{2+}]_{JSR}$. These scaled profiles show that both Fluo-5N signals under-estimate the rate of $[Ca^{2+}]_{JSR}$ depletion, prolongs time to reach minimum (by ~ 1 *ms*) and time of recovery. Here, the Ca^{2+} blink recovered with a half time of ~ 121 *ms*. **(E)** shows the spatial profiles of $[Ca^{2+}]_{SR}$ (black line), Ca^{2+}-Fluo-5N (blue line) and Ca^{2+} blink (red line) at the time of minimum fluorescence of the Ca^{2+} blink. There was a steep [Ca^{2+}] gradient across the SR elements that was under-estimated in the Ca^{2+} blink signal. Microscope blurring also meant that the spatial extent of SR [Ca^{2+}] depletion was over-estimated by ~ 57 *%* (FWHM ~ 0.7 *µm*),

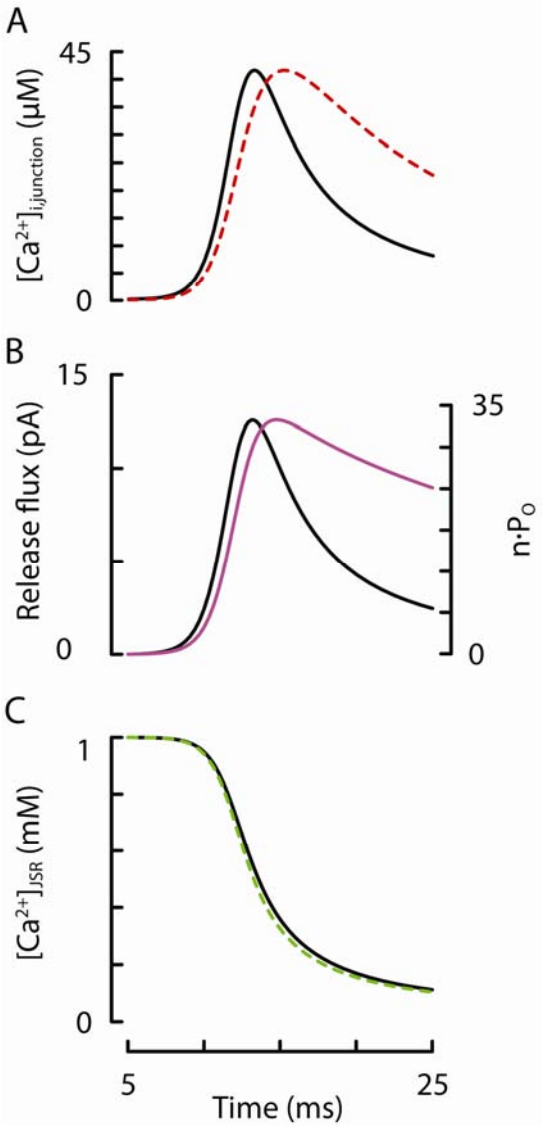

Figure 4.8 Release flux calculated by the computer model. (A) shows the development of $[Ca^{2+}]$ in the first element of the cytosol (junction; black line) associated with the Ca^{2+} spark shown in Fig. 4.5B (red dashed line), scaled to shown its relatively slow time-course. For this Ca^{2+} spark of $F/F_0 \sim 3.8$, the maximum $[Ca^{2+}]_{junction}$ was ~ 41.5 μM **(B)** shows the associated release flux (black line), which followed a similar time-course to $[Ca^{2+}]_{junction}$ in (A) and had a maximum value of ~ 12.6 pA. The calculated $n \cdot P_O$ (see Methods) is also shown (purple line), which continues to increase to a maximum of ~ 33, even after release flux has peaked. **(C)** shows $[Ca^{2+}]_{JSR}$ (black line), which declined monotonically. This decrease in $[Ca^{2+}]_{JSR}$ is responsible for the decrease in release flux prior to a decrease in $n \cdot P_O$ through the Ca^{2+} gradient across the JSR (green dashed line).

Selection of in-focus Ca^{2+} sparks for analysis

A number of experimental Ca^{2+} sparks that were recorded in-focus and with high signal-to-noise ratio were required to test the function of this computer model in curve-fitting and analysis. A criteria for choosing in-focus Ca^{2+} sparks for analysis was developed in an attempt to overcome the problem that the majority of events recorded in a confocal system are out-of-focus (Pratusevich and Balke, 1996; Cheng, *et al.*, 1999). The effect of de-focus along (z) and orthogonal (in-plane, y) to the optical axis on the recorded signal amplitude is shown in Fig. 4.9A for both measured (blue contours) and Gaussian (orange contours) PSFs. The in-plane Gaussian PSF profile was very similar to that of the measured PSF. However, along the optical axis, the measured PSF showed a poorer quality, with ~ 10 % of

energy spread to ~ 2.5 μm from the focal point. If CRUs are ~ 0.7 μm apart inside a cell (Soeller, *et al.*, 2007), then the furthest a focal point will be from a release site is only 0.35 μm. This is considerably less than the z-resolution of the microscope and suggests that the highest amplitude sparks are essentially in-focus. From Fig. 4.9A, this would lead to a ~ 20 - 30 % reduction in the calculated average Ca^{2+} spark amplitude compared to an in-focus event (note that that even in-focus events suffer from the effects of blurring (see Fig. 4.6). These PSF functions were then used to generate expected Ca^{2+} spark amplitude histograms if the underlying event was stereotypic ($\Delta F/F_0$ ~ 2). The histogram constructed from the measured (blue line, Fig. 4.9B) and Gaussian (orange line, Fig. 4.9B) PSFs are shown on top of the measured Ca^{2+} spark amplitude histogram (black line, Fig. 4.9B). The expected amplitude histograms were multiplied with the detection function of the Matched

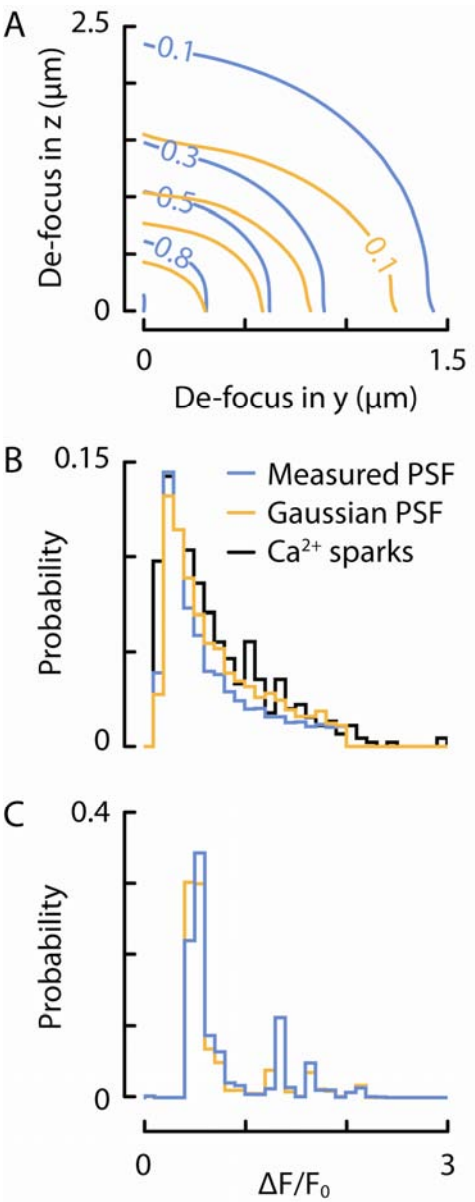

Figure 4.9 Amplitude distribution of Ca^{2+} sparks. The effect of de-focus on signal amplitude is shown in **(A)**, as a proportion of the in-focus amplitude. *y* corresponds to the in-plane direction that is perpendicular to scan-line direction (that is, assuming that Ca^{2+} sparks occurring along the scan-line will be captured by the scan eventually and z is along the optical axis. An in-focus laser-scanning confocal microscope PSF is shown (blue lines), as well as its Gaussian approximation, which was used in generating the weighting function for the computer model (yellow lines). This shows that a measured PSF dissipates energy further out than compared to a Gaussian, which is expected. **(B)** shows the measured amplitude histogram of 512 Ca^{2+} sparks, as detected by the Matched Filter Detection Algorithm, where the last bin includes events $\Delta F/F_0 > 3$. Histograms of (A) are also plotted scaled to a maximum $\Delta F/F_0$ of 2. Comparison of these distributions (deconvolution, 40 iterations; **C)** show that the remaining distribution is modal with a mean of $\Delta F/F_0$ ~ 0.5, regardless of which PSF is used, although the likelihood of observing higher amplitude, in-focus events is reduced for a measured PSF.

Filter Detection Algorithm (positive predictive value as a function of $\Delta F/F_0$, as calculated using synthetic data, see Kong, *et al.*, 2008), then scaled to the third bin of the measured amplitude histogram. To estimate the true underling Ca^{2+} spark amplitude distribution, the expected amplitude histograms were used to deconvolve the measured distribution. The resulting histograms of estimated true Ca^{2+} spark amplitude (Fig. 4.9C) for both PSFs have a mean of $\Delta F/F_0 \sim 0.5$, as measured from their cumulative sum.

Ca^{2+} release during Ca^{2+} sparks

Three examples of selected Ca^{2+} sparks are shown (Fig. 4.10Ai) above their associated simulated event (Fig. 4.10Aii, marked by green, blue and orange bars). A Ca^{2+} spark with average amplitude ($\Delta F/F_0 \sim 1$) is also shown to the same colour table for comparison (red bar, Fig. 4.10A). It is apparent that Ca^{2+} sparks exhibited varied time-courses and amplitudes (Fig. 4.10B, Bi), but fairly consistent FWHM (Fig. 4.10B, Bii). The duration (measured as when it first reached 10 % of peak flux to when it decayed to 50 % of peak flux) and amplitude of the associated release fluxes are shown (Fig. 4.10C). For small events, release flux was mainly controlled by $n \cdot P_O$ (Fig. 4.10D), while for large events, release flux was mainly controlled by $[Ca^{2+}]_{JSR}$ (solid lines, Fig. 4.10E). The $[Ca^{2+}]_{SR}$ signals are shown with their corresponding Ca^{2+} blinks (Fig. 4.10E), which consistently under-estimate the magnitude of $[Ca^{2+}]_{JSR}$ depletion, while over-estimating its spatial extent.

A summary of measurements made from fitted Ca^{2+} sparks measured using Fluo-4 or -5F are shown in Fig. 4.11. The fitted Ca^{2+} spark amplitude showed a non-linear relationship with the calculated change in $[Ca^{2+}]_{junction}$, which could be explained by dye non-linearity (Fig. 4.11A). The relationship between $[Ca^{2+}]$ and F/F_0 derived using the pseudo-ratio method (Cheng, *et al.*, 1993) is shown (solid lines, Fig. 4.11A), where the calculated $[Ca^{2+}]$ was scaled to match $[Ca^{2+}]_{junction}$. A similar non-linearity was found between Ca^{2+} blink amplitude and change in $[Ca^{2+}]_{JSR}$ (Fig. 4.11B), although some of this curvature could not be predicted by dye non-linearity (not shown), likely due to refilling of the JSR. Importantly, even when $[Ca^{2+}]_{JSR}$ had decreased by ~ 1 *mM*, Ca^{2+} blink amplitude was only $\Delta F/F_0 \sim 0.4$. Flux durations ranged from 13 ± 0.6 *ms*, with peak values of 6.3 ± 0.6 *pA*, which is equivalent to an estimated $n \cdot P_O$ of 15.7 ± 2.6. The time to halve $[Ca^{2+}]_{JSR}$ (where it did halve) was positively associated with flux duration (Fig. 4.11C), where the longer the release flux, the further $[Ca^{2+}]_{JSR}$ depleted and took longer to refill (note that the rate of

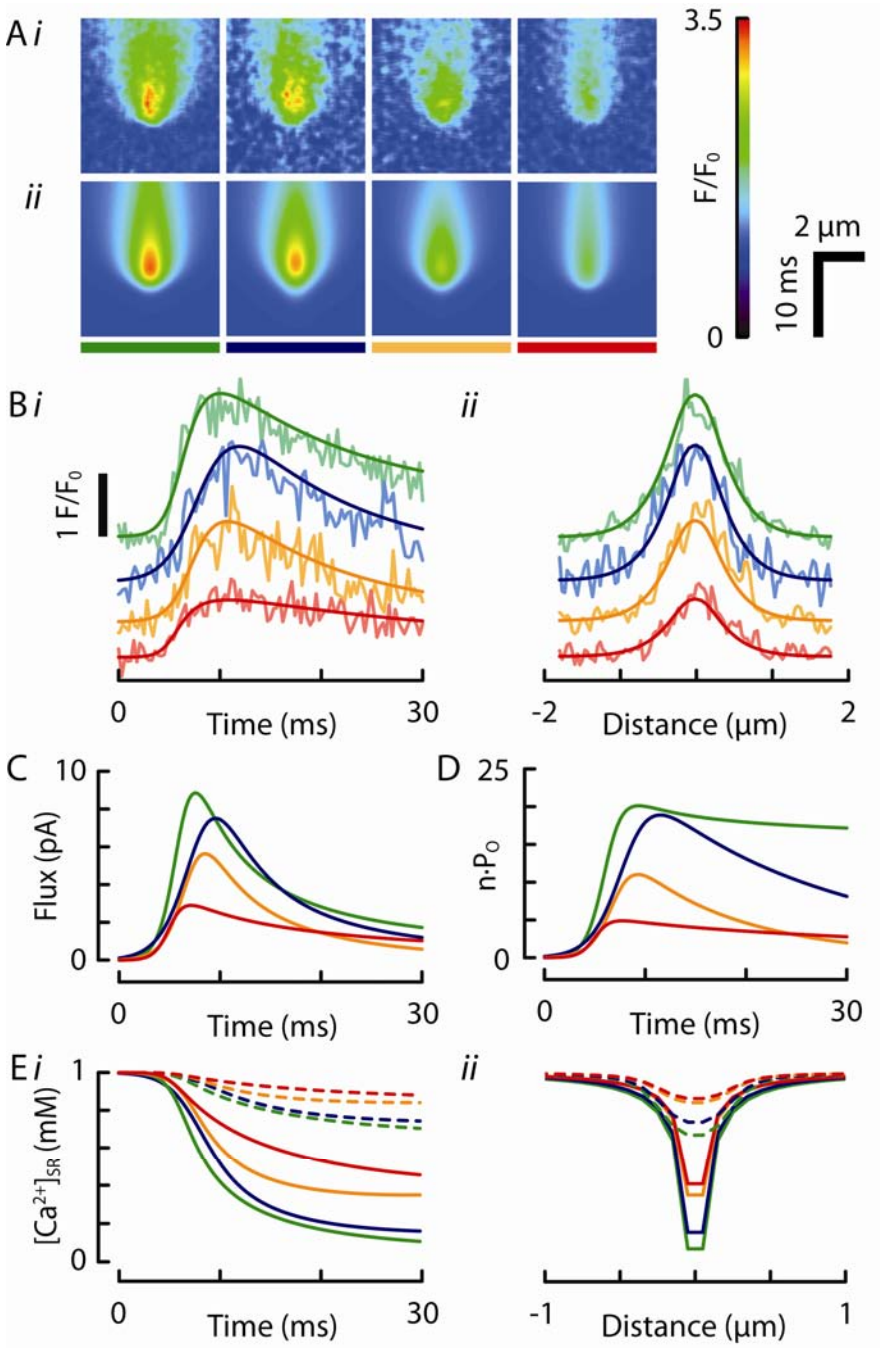

Figure 4.10 Numeric analysis of in-focus Ca^{2+} sparks. (Ai) shows three recorded Ca^{2+} sparks of high ($F/F_0 \geq 2.8$, marked by green, blue, orange lines) and one of 'average' amplitude ($F/F_0 \sim 2$, red lines), with their corresponding simulated events in ***(ii)***. The goodness of fit can be visually examined in the temporal **(Bi)** and spatial **(ii)** profiles through the peak. The events have been offset for clarity. Despite their variability in amplitude, their FWHM were very similar. **(C)** shows the corresponding estimated Ca^{2+} release flux. **(D)** shows estimated $n \cdot P_O$. Temporal **(Ei)** and spatial **(ii)** profiles of $[Ca^{2+}]_{JSR}$ (solid lines) and Ca^{2+} blinks (dashed lines) are also shown.

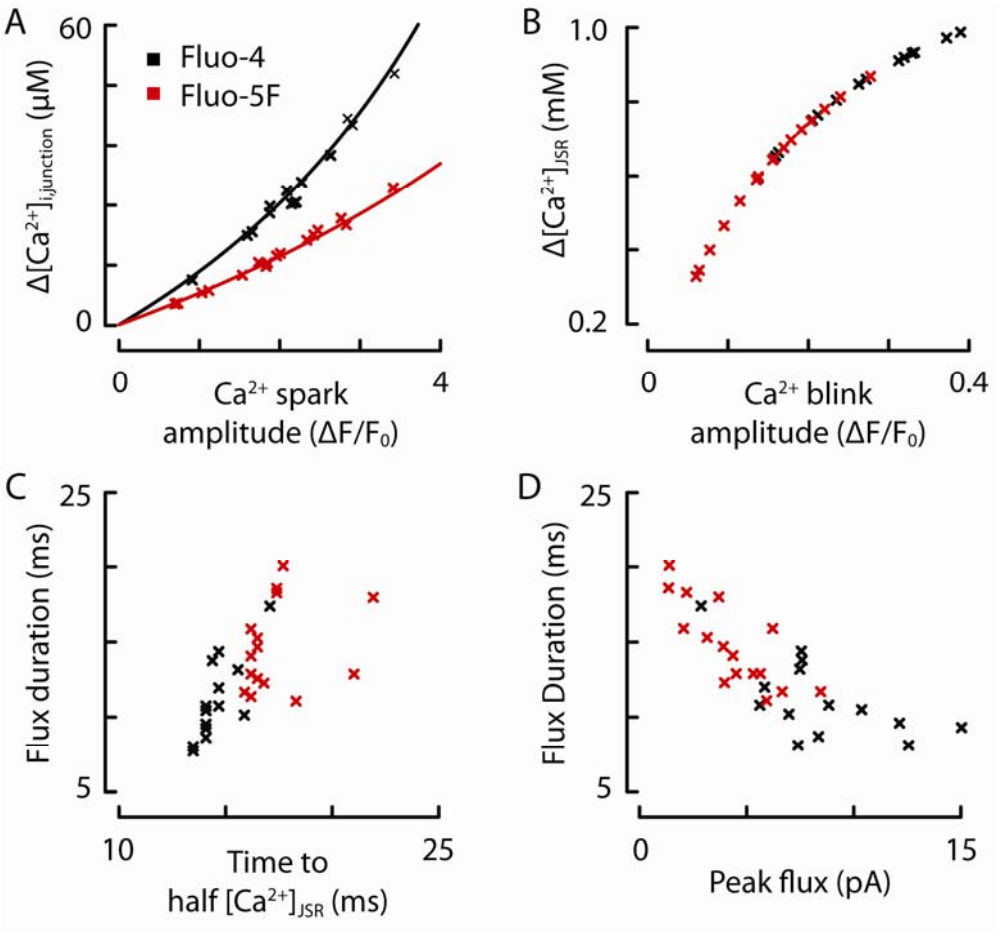

Figure 4.11 Properties of Ca^{2+} sparks measured using Fluo-4/AM (n = 14) and Fluo-5/AM (n = 16). (A) shows the change in $[Ca^{2+}]_{junction}$ for a given Ca^{2+} spark amplitude. As expected, this non-linear relationship was primarily due to dye non-linearity. The curves show the expected relationship calculated from the dye K_D, resting $[Ca^{2+}]_i$ of 100 *nM* and Eqn. 3.10 (Cheng, et al., 1993), where a scaling factor for $[Ca^{2+}]$ was determined manually-to scale to the data-points. **(B)** shows the change in $[Ca^{2+}]_{JSR}$ for a given Ca^{2+} blink amplitude. The curvature in this relationship did not exactly follow that calculated from the dye K_D and is possibly due to the non-linear under-estimation of $\Delta[Ca^{2+}]_{JSR}$ due to microscope blurring and also time effects (e.g. SR refilling) on $\Delta[Ca^{2+}]_{JSR}$. **(C)** shows that the time for $[Ca^{2+}]_{JSR}$ to reach half its minimum value is positively associated ($R^2 = 0.47$) with release flux duration (measured as when it first reached 10 % of peak flux to when it decayed to 50 % of peak flux). **(D)** shows that peak flux is negatively associated with flux duration ($R^2 = 0.6$).

refilling was not altered between events during analysis, unlike simulations shown in Fig. 3.9 in Chapter 3.4). Peak flux was negatively associated with flux duration (Fig. 4.11D) in a relationship consistent with that previously shown in (note the much smaller range on flux durations versus time to peaks in Fig. 3.6).

4.4. Discussion

Computer simulations of local Ca^{2+} signals

This relatively simple spherical model of a micro-domain was able to reproduce the basic spatio-temporal characteristics of Ca^{2+} sparks (Fig. 4.5 and Fig. 4.10) and Ca^{2+} blinks (Fig. 4.7, Zima, *et al.*, 2008b; Picht, *et al.*, 2011, although see Brochet, *et al.*, 2005). The spatial extent of the simulated Ca^{2+} sparks fitted well to the spatial profiles of recorded events (Fig. 4.5E and Fig. 4.10Bii). The experimentally recorded Ca^{2+} sparks exhibited a slightly smaller FWHM than the ~ 2 μm reported by some studies (Cheng, *et al.*, 1993; Izu, *et al.*, 2001), but closer to the 1.2 – 1.5 μm range reported by others (Shen, *et al.*, 2004; Shkryl, *et al.*, 2012). This is likely due to improved microscope resolution and selection of in-focus events, rather than physical differences in cells, as suggested by their regular sarcomeric spacing of 1.8 μm (not shown, measured from stationary dye staining).

The effect of microscope blurring in the generation of Ca^{2+} sparks

One of the main issues this model was built to address was the effect of in-focus confocal microscope blurring on recorded Ca^{2+} signals and by connection, to develop a method to select for in-focus Ca^{2+} sparks from images, so that they can be analysed using the computer model. Since a line-scan is near-randomly placed with respect to the location of CRUs in a cell (apart from scanning roughly perpendicular to the *z*-lines), most recorded Ca^{2+} sparks are likely to be out-of-focus events. Further, since these recorded events have been shown to exhibit a monotonically-declining amplitude distribution (Pratusevich and Balke, 1996; Izu, *et al.*, 1998; Cheng, *et al.*, 1999), the events with large F/F_0 are more likely to be in-focus. To estimate the proportion of events that are out-of-focus, the measured and Gaussian PSFs were used to generate the expected distributions of detected events (Fig. 4.9B). When either of these were used to deconvolve the recorded Ca^{2+} spark amplitude distribution, the estimated true underlying Ca^{2+} spark amplitude was widely distributed and had a mean of $\Delta F/F_0 \sim 0.5$ (Fig. 4.9A). This value is consistent with initial

Ca^{2+} spark observations (Cheng, *et al.*, 1993) and recent studies using 4D confocal imaging (Shkryl, *et al.*, 2012, although see Shen, *et al.*, 2004). The mean of the original distribution was $\Delta F/F_0 = 0.7 \pm 0.5$, which is consistent with previous reports that did not correct for out-of-focus events (e.g. see Song, *et al.*, 1997; Cheng, *et al.*, 1999 who also show amplitude histograms).

However, once in-focus, recorded events are still distorted by the confocal PSF due to integration of fluorescence from relatively distant locations that are at resting $[Ca^{2+}]_i$. This distortion should depend on the volume of the true Ca^{2+}-bound Fluo-4 signal relative to that of the PSF, which means that optical blurring is most important during the early phase of the Ca^{2+} spark, where the spatially-restricted rise in fluorescence seen in Fig. 4.6B was lost in Fig. 4.6A. At the time of peak amplitude, microscope blurring halved Ca^{2+} spark amplitude itself and doubled its width (Smith, *et al.*, 1998; Izu, *et al.*, 2001). Surprisingly, Ca^{2+} spark time-course was only modestly affected by in-focus blurring (Fig. 4.6), which is in contrast to a previous computer study by Smith, *et al.* (1998). The effect of a real PSF on in-focus Ca^{2+} sparks is expected to be more dramatic, as PSFs measured under experimental conditions suffered from additional optical aberrations (Fig. 4.1), due to light passing through media of different refractive indices (glass cover-slip to bath solution and through the intracellular milieu).

For a Ca^{2+} blink, the effect of optical blurring was large. A near ~ 100 % depletion of $[Ca^{2+}]_{JSR}$ resulted in a mere 40 % decrease in Ca^{2+} blink amplitude, supporting the idea that Ca^{2+} blink measurements are insufficient to reject the hypothesis of extensive $[Ca^{2+}]_{JSR}$ depletion. Further, the under-estimation of the time-course of depletion by Fluo-5N means that JSR refilling may be even slower than currently estimated by Ca^{2+} blinks (~ 180 ms, Zima, *et al.*, 2008b) and may agree with slower Ca^{2+} spark amplitude restitution (i.e. Brochet, *et al.*, 2005, rather than Sobie, *et al.*, 2005; Ramay, *et al.*, 2011). Estimation of the extent of $[Ca^{2+}]_{JSR}$ depletion and rate of $[Ca^{2+}]_{JSR}$ repletion are important because small changes in $[Ca^{2+}]_{JSR}$ (and release flux) will have large effects on RyR P_O due to its steep dependence on $[Ca^{2+}]_i$.

Other factors that contribute to Ca^{2+} spark shape

Although microscope blurring is likely to cause significant changes to the shape of a recorded Ca^{2+} spark, diffusive and stationary Ca^{2+} buffers should alter the observed change

in $[Ca^{2+}]_i$. To examine how these buffers contribute to Ca^{2+} spark morphology, their properties (*e.g.* concentration or rate of diffusion) were altered and the resulting Ca^{2+} spark compared to a 'standard' (see Methods).

The main factors that contributed to Ca^{2+} spark amplitude were: *(1)* the amplitude, *S*, of *CR(t)* (as might be expected), *(2)* [ATP], *(3)* [Fluo-4], *(4)* [CSQ] and *(5)* V_{JSR}. As the

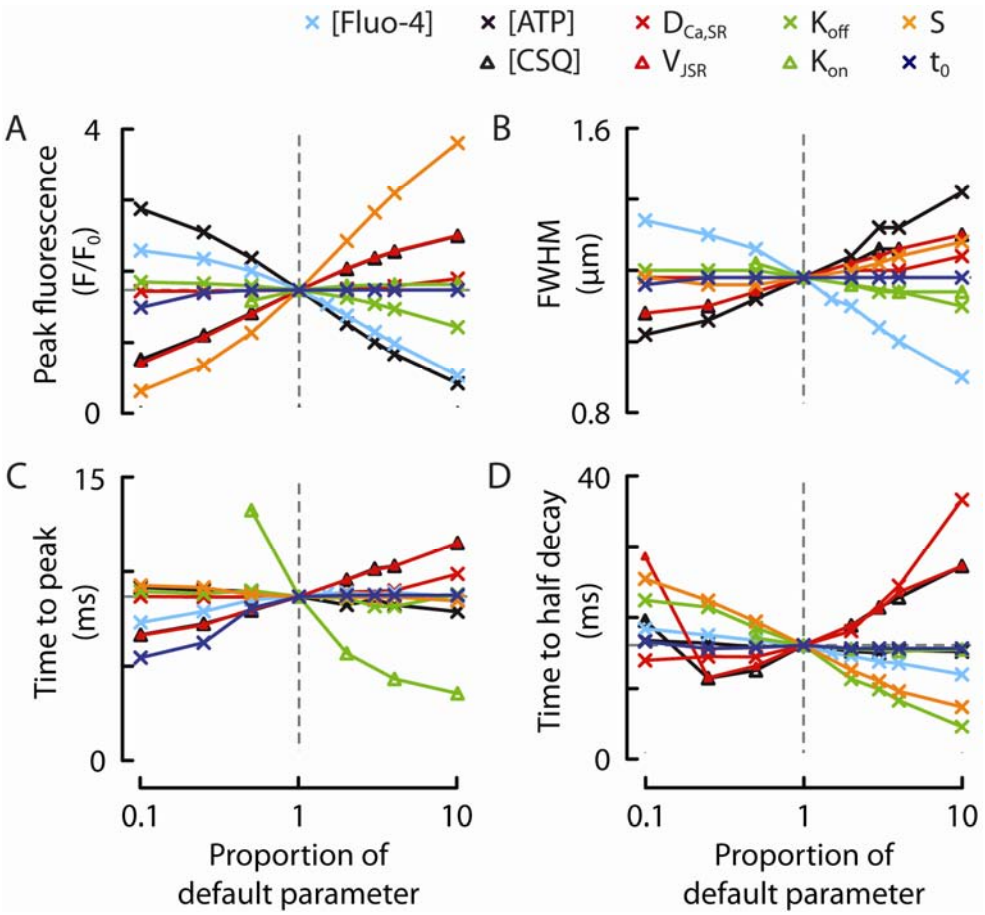

Figure 4.12 Sensitivity of Ca^{2+} spark computer model to parameter values. Ca^{2+} spark properties, **(A)** peak amplitude, **(B)** FWHM, **(C)** time to peak and **(D)** time to half decay were measured to quantify how the simulated Ca^{2+} spark changes with various changes in default parameter values (Table 4.1). The parameters that were tested are shown in the key on the top right. *[ATP]* = concentration of adenosine-3',5'-triphosphate in the cytosol; *[CSQ]* = concentration of calsequestrin in the JSR; $D_{Ca,SR}$ = diffusion coefficient of Ca^{2+} in the SR; *[Fluo-4]* = concentration of Fluo-4 in the cytosol; V_{JSR} = JSR volume; and parameters for the release function, *CR(t)* (Eqn. 4.4): K_{on} = 'rise' rate constant; K_{off} = 'decay' rate constant; *S* = amplitude scaling factor; t_0 = shift in time. See text for details.

concentration of ATP or Fluo-4 increased, the peak fluorescence decreased (Fig. 4.12A). ATP acted as a mobile Ca^{2+} buffer that carried Ca^{2+} away from the site of release to decrease peak fluorescence and increase FWHM, with little effect on the event time-course (black crosses, Fig. 4.12). Conversely, increasing [Fluo-4] decreased fluorescence, but at the same time decreased FWHM (due to its relatively low diffusion coefficient), which may be important during the course of an experiment, as Fluo-4 is removed from the cell. The effects of [CSQ] and V_{JSR} were very similar for all Ca^{2+} spark parameters and suggests that serve a similar purpose. This idea is in qualitative agreement with recent observations that knockout of CSQ was associated with larger V_{JSR} (Knollmann, *et al.*, 2006). Increasing the local SR [Ca^{2+}] store (by increasing [CSQ] or V_{JSR}) increased peak fluorescence, FWHM and time-course because more Ca^{2+} was being released. Note that in this model, increasing $D_{Ca,SR}$ increased Ca^{2+} spark time to peak and half decay.

Ca^{2+} release during a Ca^{2+} spark

Analysis of Ca^{2+} sparks (mean $F/F_0 = 3.0 \pm 0.1$, Fig. 4.11A) suggested that release flux increased to a maximum of 6.3 ± 0.3 *pA* in 6.4 ± 0.3 ms (time to peak, measured from 10 *%* of peak), with an overall duration of 13.1 ± 0.6 *ms* (measured from 10 *%* of peak to when current had decayed to 50 *%* of peak). This is similar to previous analyses. Cheng, *et al.* (1993) estimated that a release event of $F/F_0 = 2$ would require a constant flux of ~ 4 *pA* for 10 *ms*, although a range of Ca^{2+} spark amplitudes and estimated peak fluxes have been reported, from low (F/F_0 ~ 1.35 when simultaneously recorded with Ca^{2+} blinks, Brochet, *et al.*, 2005) to moderate (1.2 - 8.7 *pA*; *Wang, et al., 2001*) to large (F/F_0 ~ 6, corresponding to peak ~ 20 *pA*; Izu, *et al.*, 2001). This variation highlights a number of factors that influence calculations of release flux (e.g. out-of-focus events, buffering scheme).

The maximum peak $[Ca^{2+}]_{junction}$ calculated from all events analysed was 50 *μM* (mean = 20 ± 2 *μM*, Fig. 4.11). This value appears small compared to a previously calculated $[Ca^{2+}]_{junction}$ of ~ 70 μM for a 0.2 pA Ca^{2+} flux (see Fig. 2.2A and Soeller and Cannell, 1997). Given that the average peak flux was ~ 6 pA over ~ 13 ms, this gives an average flux of ~ 0.5 pA, which should have increased $[Ca^{2+}]_{junction}$ to at least 175 μM, which is much larger than that calculated The reason for this under-estimation in the model is due to the volume of the first element, which was 4.18 aL. Since fluxes were calculated in μmol/ms, concentrations were obtained by dividing by the element volumes, which over-estimated the volume of the junctional space, due to the limit in the number of elements that

could be described in the solver. If a junction is 0.8 aL (cylinder of 150 nm radius and 12 nm height, Franzini-Armstrong, *et al.*, 1999), then $[Ca^{2+}]_{junction}$ would be closer to ~ 260 µM. This value is above the $[Ca^{2+}]$ required to maximally activate RyR channels (see Fig. 2.2B, Schiefer, *et al.*, 1995; Copello, *et al.*, 1997; Laver and Honen, 2008) and also suggests that the driving force for Ca^{2+} release becomes quite small toward the end of the release event. The mean maximum $n \cdot P_O$ was ~ 16 ± 3. If the maximum P_O of RyR channels is ~ 0.5 (Chapter 2.2), then this equates to ~ 32 functional RyR channels within a CRU, although this value depends on the precision to which the i_{RyR} is known (Mejia-Alvarez, *et al.*, 1999). For example, the number of RyRs in a CRU would be ~ 50 if i_{RyR} was 0.4 pA at 1 mM $[Ca^{2+}]_{SR}$ (see Chapter 3.2). Again, this CRU size is smaller than those reported by immuno-fluorescence and EM studies (Franzini-Armstrong, *et al.*, 1999; Soeller, *et al.*, 2007), but larger than the size reported by single-molecule detection studies on peripheral couplings (see earlier discussion in Chapter 3.4). The calculated range of CRU sizes is consistent with the idea that during EM studies, large CRUs may be selected.

Local depletion of Ca^{2+} in the SR

The extent of JSR Ca^{2+} depletion depends on the balance between JSR Ca^{2+} efflux (through the CRU) and influx (primarily through diffusion of Ca^{2+} from the network SR). In this model, the reduction in $[Ca^{2+}]_{JSR}$ was approximately linear with the corresponding increase in $[Ca^{2+}]_i$ in the first element of the cytosol because the rate of intra-SR diffusion was relatively low (Fig. 4.10Eii). Even with this low intra-SR diffusion rate, Ca^{2+} sparks could be reproduced with the amount of Ca^{2+} available within the JSR. A large JSR Ca^{2+} buffering capacity, combined with slow intra-SR Ca^{2+} diffusion is consistent with the relatively large and fast Ca^{2+} release required to reproduce a Ca^{2+} spark. A small JSR buffering capacity cannot be compensated for by fast intra-SR diffusion, unless this rate is similar to release flux, which seems unlikely.

The decrease in $[Ca^{2+}]_{JSR}$ during a Ca^{2+} spark reduced release flux. For large release fluxes, $[Ca^{2+}]_{JSR}$ depletion was sufficient to terminate a Ca^{2+} spark, even when $n \cdot P_O$ remained persistently high (Fig. 4.10D). It is unclear whether another termination mechanism exists for Ca^{2+} sparks that have small amplitudes/release fluxes (e.g. red line, Fig. 4.10), but it is possible that the distributions of CRU size (e.g. exponential, Baddeley, *et al.*, 2009), V_{JSR} and $[CSQ]_{JSR}$ (both unknown) may be able to explain Ca^{2+} sparks that differ between (Shen, *et al.*, 2004), but not within release sites (Bridge, *et al.*, 1999; Zima, *et al.*, 2008b).

Note that the variability in these parameters does not need to be as large as the variability in Ca^{2+} spark amplitude due to the steep dependence of RyR open probability on $[Ca^{2+}]_i$ and therefore, release flux and the $[Ca^{2+}]$ gradient (controlled primarily by CRU size, V_{JSR} and $[CSQ]_{JSR}$).

The time-course of recovery of simulated Ca^{2+} blinks were highly variable (not shown), with a mean of 83 ± 4 ms, which is similar to those reported (Zima, *et al.*, 2008; Picht, *et al.*, 2011, although see Brochet, *et al.*, 2005) and is in reasonable agreement with Ca^{2+} spark amplitude restitution studies (see Chapter 3.3, also Brochet, *et al.*, 2005; Sobie, *et al.*, 2005; Picht, *et al.*, 2011). This was dependent primarily on the rate of intra-SR diffusion, which was low (e.g. Swietach, *et al.*, 2008, although see Picht, *et al.*, 2011). The mean time to peak of simulated Ca^{2+} blinks (for examples, see Fig. 4.10Ei) was 34 ± 2 ms, which is similar to one study (Brochet, *et al.*, 2005), but not others (Zima, *et al.*, 2008b; Picht, *et al.*, 2011). The discrepancy may be due to the size of the confocal pinhole, which may have been increased to improve signal-to-noise.

Zima, *et al.* (2008b) also showed that Ca^{2+} blinks always decreased to the same minimum regardless of the amplitude of the corresponding Ca^{2+} spark (Zima, *et al.*, 2008b). The simulated Ca^{2+} blinks in this study showed relatively more variable amplitude (mean of $\Delta F/F_0 = 0.21 \pm 0.02$), however, this could be due to a real variation in V_{JSR} that was constant in the model. That is, if V_{JSR} and its Ca^{2+} capacity varied, then the differences in local SR $[Ca^{2+}]$ depletion would be minimised, which would also likely reduce the contribution of model $n \cdot P_O$, but increase that of the $[Ca^{2+}]$ gradient on release termination. It is expected that this would support the $[Ca^{2+}]_{JSR}$ depletion hypothesis for the termination of CICR, however, it would require further detail on the variability of V_{JSR} and its Ca^{2+} buffering capacity/ Ideally, the computer model should be modified to include $[Ca^{2+}]_i$-dependent RyR channel gating parameters to replace CR(t). The release function used here (Eqn. 4.4) was used because it was asymmetric and flexible and provided the relatively low rate of rise at the beginning of release compared to the more rapid approach to the peak. This shape is consistent with the steep $[Ca^{2+}]_i$-dependence of RyR activation (Laver and Honen, 2008). However, it is likely that local gradients within a junction (i.e. spatially asymmetric model) would be important in determining the actual CRU response to Ca^{2+} release during a Ca^{2+} spark.

4.5. Summary

The recorded Ca^{2+} spark is shaped by many factors, including the underlying CRU Ca^{2+} release flux, which is a result of $n \cdot P_O$ and the $[Ca^{2+}]$ gradient across the JSR membrane. This release flux changes $[Ca^{2+}]_{junction}$, which is buffered in a non-linear manner and affected in a complex way by electrostatic effects. The free Ca^{2+} that then diffuses out of the junction, into the surrounding micro-domain is dependent on mobile Ca^{2+} buffers, the most important being ATP, which was able to significantly increase Ca^{2+} spark width. The non-linear kinetics of the Ca^{2+} indicator slowed the apparent change in $[Ca^{2+}]$ in the junction and micro-domain. This Ca^{2+}-sensitive fluorescence signal is then usually detected by a line-scan confocal microscope, which introduces optical blurring. In-focus microscope blur is significant and reduces Ca^{2+} spark amplitude and increases spatial width, while out-of-focus increases the extent of these effects.

For Ca^{2+} blinks, the signal is shaped by similar factors, where a reduction in $[Ca^{2+}]_{JSR}$ drives the fluorescence depletion signal. The extent of $[Ca^{2+}]_{JSR}$ reduction depends on the balance of Ca^{2+} efflux (CRU release flux) and influx (diffusion of Ca^{2+} from the network SR). However, the reduction in the Ca^{2+} blink signal is largely contaminated by out-of-focus signal from relatively high $[Ca^{2+}]$ in the network SR and likely, another JSR given measured inter-CRU distances and the volume of a PSF. Even for a full depletion, the corresponding Ca^{2+} blink only reduced by 40 %. This suggests that recorded small Ca^{2+} blink amplitudes are insufficient to determine $[Ca^{2+}]_{JSR}$. When real PSFs were measured through live cardiac myocytes, optical aberrations and the reduction in resolution were evident, likely due to change in refractive indices and the curvature of the cell surface. This suggests that optical blurring by real PSFs would be even larger than that applied using the Gaussian PSF shown here due to complex PSF shapes.

Analysis of Ca^{2+} spark amplitudes suggested that most of the distribution could be accounted for by out-of-focus events and that the underlying in-focus Ca^{2+} spark amplitude distribution was modal at $\Delta F/F_0 \sim 1$. Analysis of in-focus Ca^{2+} sparks suggested that local SR Ca^{2+} release flux was ~ 3 - 15 pA. During a Ca^{2+} spark, $[Ca^{2+}]_{JSR}$ decreased, which in turn decreased release flux, which is consistent with the hypothesis that $[Ca^{2+}]_{JSR}$ depletion is able to terminate CICR.

5. Conclusions

Though CICR was described in cardiac muscle some ~ 40 years ago (Fabiato and Fabiato, 1973; Fabiato, 1983), the details of its operation remain unclear.

The measurement of Ca^{2+} transient and spark latency during AP-clamp and voltage-clamp steps in Chapter 2 suggested that the triggering of Ca^{2+} sparks during a rat action potential can be explained by the activation of 1 – 2 LTCCs (at ~ 0 *mV*). In order to provide these openings at a short latency, ~ 4 LTCCs must be available per CRU. However, the implied discrepancy between the number of functional LTCCs and DHP binding sites (Lew, *et al.*, 1991) remains unresolved, although it is possible that not all LTCCs are located in couplons (see Crossman, *et al.*, 2011) and/or there may be excess DHP binding sites which are not activated (*e.g.* a small fraction of LTCCs are available for activation). This differential regulation remains unclear, although β-adrenergic pathways may be linked (Chase, *et al.*, 2010).

The high CICR fidelity measured here would support the idea that CICR 'gain' is large (e.g. Inoue and Bridge, 2003; Altamirano and Bers, 2007b, in contrast to the conclusions of Cheng and Lederer, 2008; Poláková, *et al.*, 2008). In the model presented in Chapter 2, the LTCC current required to trigger a Ca^{2+} spark is small compared to Ca^{2+} spark flux. For the majority of Ca^{2+} sparks that occur during an AP (between – 15 and 10 *mV*), latency appears to be due to both LTCC and RyR activation making an equal contribution. This strategy may stabilise LTCC-RyR coupling from small changes in the function of either protein. Any LTCC current beyond that associated with the triggering event would reduce apparent gain at the macroscopic level, as well as at the microscopic level due to a decrease in 'digital' or time-dependent gain (Cannell, *et al.*, 1995). As suggested by Fabiato (1985b), this excess LTCC current may serve to regulate SR Ca^{2+} content. This is an interesting idea because large SR Ca^{2+} release can, in turn, regulate I_{Ca} through Ca^{2+}-dependent inactivation. Though these studies suggest that I_{Ca} is an efficient trigger of CICR, further experiments with Na^{+} in the patch pipette should allow for the contribution of reverse-mode NCX to be evaluated. It has been suggested that reverse-mode NCX facilitates CICR by 'priming' the junction with Ca^{2+} (e.g. Torres, *et al.*, 2010), which would aid short LTCC openings in triggering Ca^{2+} release (Grantham and Cannell, 1996). Further, clarification of LTCC gating properties in physiological conditions (particularly, its maximum P_O and the

voltage-dependence of its closing rate, see Josephson, *et al.*, 2010b and Rose, *et al.*, 1992) will be important in clarifying LTCC:RyR coupling fidelity.

Analysis of Ca^{2+} sparks using the computer model described in Chapter 4 suggested that once activated, the local SR Ca^{2+} release flux takes ~ 6 *ms* to maximally-activate and continues for another ~ 10 *ms*. Therefore, the duration of the release flux is longer than the Ca^{2+} spark time to peak and influences its early phase of decline (t_{25}, Chapter 2). The analysis of CRU [Ca^{2+}] sensitivity in Chapter 2 suggested that the minimum number of RyR channels required was ~ 4, but given ~ 4 LTCCs were required and a 1:7 LTCC:RyR ratio (Bers and Stiffel, 1993), ~ 28 RyR channels would need to be in a CRU. This estimate is in accord with analysis of long-lasting and spark-like events seen in the presence of tetracaine (Chapter 3). Although this is somewhat smaller than the number (36 – 50) suggested by the computer modelling in Chapter 4, this is likely due to selection of Ca^{2+} sparks with larger amplitudes and signal-to-noise for curve-fitting. With so many RyRs being involved in Ca^{2+} spark production it is hard to explain the observation of quantized release fluxes (Wang, *et al.*, 2004). Future studies that use an imaging modality with higher axial resolution (e.g. Navedo, *et al.*, 2006) and without loose-seal patch-clamping should be useful in clarifying whether quantal release fluxes are possible, as well as provide an opportunity to observe 'Ca^{2+} sparklets' (Wang, *et al.*, 2001; Navedo, *et al.*, 2006) and any functional differences between peripheral and internal CRUs. Nevertheless, the number of RyRs in a CRU may affect its sensitivity to activation by open LTCCs (depending on their relative locations) and will affect how rapidly the local $[Ca^{2+}]_{JSR}$ is depleted, which seems to be crucial in the termination of local SR Ca^{2+} release. However, it should be noted that for both activation and regeneration of CICR, the physical arrangement of the RyRs will also be important for sensing local [Ca^{2+}] gradients within the junction.

The computer simulations suggested that during a Ca^{2+} spark, $[Ca^{2+}]_{JSR}$ is heavily depleted (Chapter 4). Thus, the larger the initial release flux, the shorter the release duration, which is consistent with a mechanism where faster $[Ca^{2+}]_{JSR}$ depletion leads to a reduction in release flux and $[Ca^{2+}]_{junction}$, then CRU de-activation (Chapters 3 and 4). This idea is supported by the steep $[Ca^{2+}]_i$-dependence of RyR channel gating and slow Ca^{2+} spark amplitude restitution, which are locally controlled by the restricted cytosolic junctional space, as well as the restricted SR junction. This is consistent with the reduced amplitude and duration of Ca^{2+} sparks during moderate inhibition of SERCA (Song, *et al.*, 1997) and

the inverse when SR [Ca^{2+}] buffering was increased (Zima, *et al.*, 2008a). By having $[Ca^{2+}]_{JSR}$ depletion as a primary factor in CICR termination, having large numbers of RyRs in a CRU does not increase the amount released, providing resilience to biological variation in CRU composition. A second benefit is that changes in $[Ca^{2+}]_{SR}$ simply alter Ca^{2+} spark amplitude without large increases in Ca^{2+} spark duration. On the other hand, having a large $[Ca^{2+}]_{JSR}$ store with few RyRs to cause depletion (as may occur in tetracaine or ryanodine) will cause an LLE. This suggests that during CRU assembly/dis-assembly, some other factors may be involved in keeping the ratio of RyR to JSR Ca^{2+} capacity within some limited range. This could be provided by accessory proteins, such as triadin and junctophillin (e.g. Zhang, *et al.*, 1997; Gyorke, *et al.*, 2004).

Although previous experimental studies have not shown profound $[Ca^{2+}]_{JSR}$ depletion, the computer model suggests that optical blurring of a local depletion signal is a serious confounding problem for such measurements. Furthermore, use of a caffeine-induced Ca^{2+} transient (i.e. a global depletion signal) is unlikely to reveal the correct ‘background’ to use for Ca^{2+} blink calibration. Given these uncertainties, even small Ca^{2+} blink amplitudes cannot be used to eliminate the possibility of profound $[Ca^{2+}]_{JSR}$ depletion. Future studies that use another method to measure local SR Ca^{2+} will be important in demonstrating the extent of $[Ca^{2+}]_{JSR}$ depletion and its time-course of recovery. One approach could be to develop and use a mutated form of CSQ that fluoresces when bound to Ca^{2+}. This could be made possible by expressing two different CSQ mutants with different fluorochromes of a fluorescence resonance energy transfer (FRET) pair. Polymerisation of CSQ upon Ca^{2+} binding would allow fluorescence to report $[Ca^{2+}]_{JSR}$. The primary benefit of this technique would be its specificity to the JSR, which would reduce out-of-focus fluorescence. In connection to this, the effect of $[Ca^{2+}]_{JSR}$ depletion on CRU gating could be tested by incorporating a $[Ca^{2+}]_i$-dependent RyR gating scheme into the computer model presented in Chapter 4. However, a stochastic model as simple as that described in Chapter 3 would increase complexity drastically and was not feasible in FACSIMILE.

The work presented here made extensive use of computer models to help create and test hypotheses for how CICR might be regulated. The utility of this approach can be seen where I have concluded that CICR is relatively high fidelity and gain, which is in contrast to the conclusions of Polakova, *et al.* (2008) despite reasonably close agreement between our experimental data. Certainly, it seems that the complexity of local control and

microscopic Ca^{2+} signalling in heart muscle is beyond intuitive analysis and guidance by experimental evidence is limited (*e.g.* by resolution) at this point. In this regard, mathematical modelling has been invaluable in testing concrete hypotheses in known physical and chemical conditions and will be crucial to future understanding.

6. References

Allen, DG and Kurihara, S. The effects of muscle length on intracellular calcium transients in mammalian cardiac muscle. *J Physiol*. 1982;**327**(1):79-94.

Altamirano, J and Bers, DM. Effect of intracellular Ca^{2+} and action potential duration on L-type Ca^{2+} channel inactivation and recovery from inactivation in rabbit cardiac myocytes. *Am J Physiol Heart Circ Physiol*. 2007a;**293**(1).

Altamirano, J and Bers, DM. Voltage dependence of cardiac excitation-contraction coupling: unitary Ca^{2+} current amplitude and open channel probability. *Circ Res*. 2007b;**101**(6):590-7.

Baddeley, D, Jayasinghe, ID, Lam, L, Rossberger, S, Cannell, MB, Soeller, C. Optical single-channel resolution imaging of the ryanodine receptor distribution in rat cardiac myocytes. *Proc Natl Acad Sci U S A*. 2009;**106**(52):22275-80.

Balke, CW, Rose, WC, Marban, E, Wier, WG. Macroscopic and unitary properties of physiological ion flux through T-type Ca^{2+} channels in guinea-pig heart cells. *J Physiol*. 1992;**456**:247-65.

Balke, CW and Goldman, L. Excitation contraction coupling in cardiac muscle: is there a purely voltage-dependent component? *J Gen Physiol*. 2003;**121**(5):349-52.

Banyasz, T, Chen-Izu, Y, William, Izu, L. A new approach to the detection and classification of Ca^{2+} sparks. *Biophys J*. 2007;**92**(12):4458-65.

Barcenas-Ruiz, L and Wier, WG. Voltage dependence of intracellular $[Ca^{2+}]_i$ transients in guinea pig ventricular myocytes. *Circ Res*. 1987;**61**(1):148-54.

Barry, P. JPCalc, a software package for calculating liquid junction potential corrections in patch-clamp, intracellular, epithelial and bilayer measurements and for correcting junction potential measurements. *J Neurosci Methods*. 1994;**51**(1):107-16.

Bassani, JW, Yuan, W, Bers, DM. Fractional SR Ca release is regulated by trigger Ca and SR Ca content in cardiac myocytes. *Am J Physiol*. 1995;**268**(5 Pt 1):C1313-9.

Bassani, R and Bers, DM. Rate of diastolic Ca release from the sarcoplasmic reticulum of intact rabbit and rat ventricular myocytes. *Biophys J*. 1995;**68**(5):2015-22.

Baylor, S and Hollingworth, S. Measurement and interpretation of cytoplasmic $[Ca^{2+}]$ signals from calcium-indicator dyes. *News in the Physiological Sciences*. 2000;**15**:19-26.

Baylor, SM and Hollingworth, S. Model of sarcomeric Ca^{2+} movements, including ATP Ca^{2+} binding and diffusion, during activation of frog skeletal muscle. *J Gen Physiol*. 1998;**112**(3):297-316.

Baylor, SM, Hollingworth, S, Chandler, WK. Comparison of simulated and measured calcium sparks in intact skeletal muscle fibers of the frog. *J Gen Physiol*. 2002;**120**(3):349-68.

Beeler, GW, Jr. and Reuter, H. Membrane calcium current in ventricular myocardial fibres. *J Physiol*. 1970a;**207**(1):191-209.

Beeler, GW, Jr. and Reuter, H. The relation between membrane potential, membrane currents and activation of contraction in ventricular myocardial fibres. *J Physiol*. 1970b;**207**(1):211-29.

Beeler, GW, Jr. and Reuter, H. Voltage clamp experiments on ventricular myocarial fibres. *J Physiol*. 1970c;**207**(1):165-90.

Berlin, J, Bassani, J, Bers, D. Intrinsic cytosolic calcium buffering properties of single rat cardiac myocytes. *Biophys J*. 1994;**67**(4):1775-87.

Berlin, JR, Cannell, MB, Lederer, WJ. Cellular origins of the transient inward current in cardiac myocytes. Role of fluctuations and waves of elevated intracellular calcium. *Circ Res*. 1989;**65**(1):115-26.

Berridge, M, Bootman, M, Lipp, P. Calcium - a life and death signal. *Nature*. 1998;**395**(6703):645-8.

Bers, DM and Stiffel, VM. Ratio of ryanodine to dihydropyridine receptors in cardiac and skeletal muscle and implications for E-C coupling. *Am J Physiol*. 1993;**264**(6 Pt 1):C1587-93.

Bers, DM. *Excitation-Contraction Coupling and Cardiac Contractile Force*. 2nd ed.: Kluwer Academic Publishers; 2001.

Beuckelmann, DJ and Wier, WG. Mechanism of release of calcium from sarcoplasmic reticulum of guinea-pig cardiac cells. *J Physiol*. 1988;**405**(1):233-55.

Bkaily, G, Sperelakis, N, Doane, J. A new method for preparation of isolated single adult myocytes. *Am J Physiol*. 1984;**247**(6 Pt 2):H1018-26.

Blatter, LA and McGuigan, JA. Free intracellular magnesium concentration in ferret ventricular muscle measured with ion selective micro-electrodes. *Q J Exp Physiol*. 1986;**71**(3):467-73.

Bozler, E. Relaxation in extracted muscle fibers. *J Gen Physiol*. 1954;**38**(2):149-59.

Brette, F and Orchard, C. T-tubule function in mammalian cardiac myocytes. *Circ Res*. 2003;**92**(11):1182-92.

Bridge, JHB, Ershler, PR, Cannell, MB. Properties of Ca^{2+} sparks evoked by action potentials in mouse ventricular myocytes. *The Journal of Physiology*. 1999;**518**(2):469-78.

Brochet, D, Yang, D, Maio, A, Lederer, J, Franzini-Armstrong, C, Cheng, H. Ca^{2+} blinks: Rapid nanoscopic store calcium signaling. *Proc Natl Acad Sci U S A*. 2005;**102**(8):3099-104.

Brown, E and Macleod, J. Extracellular calcium sensing and extracellular calcium signaling. *Physiol Rev*. 2001;**81**(1):239-97.

Callewaert, G. Excitation-contraction coupling in mammalian cardiac cells. *Cardiovasc Res*. 1992;**26**(10):923-32.

Campbell, KP, MacLennan, DH, Jorgensen, AO, Mintzer, MC. Purification and characterization of calsequestrin from canine cardiac sarcoplasmic reticulum and identification of the 53,000 dalton glycoprotein. *J Biol Chem*. 1983a;**258**(2):1197-204.

Campbell, KP, MacLennan, DH, Jorgensen, AO. Staining of the Ca^{2+}-binding proteins, calsequestrin, calmodulin, troponin C, and S-100, with the cationic carbocyanine dye "Stains-all". *J Biol Chem*. 1983b;**258**(18):11267-73.

Cannell, MB and Lederer, WJ. The arrhythmogenic current I_{TI} in the absence of electrogenic sodium-calcium exchange in sheep cardiac Purkinje fibres. *J Physiol*. 1986a;**374**:201-19.

Cannell, MB and Lederer, WJ. A novel experimental chamber for single-cell voltage-clamp and patch-clamp applications with low electrical noise and excellent temperature and flow control. *Pflügers Arch*. 1986b;**406**(5):536-9.

Cannell, MB, Berlin, JR, Lederer, WJ. Effect of membrane potential changes on the calcium transient in single rat cardiac muscle cells. *Science*. 1987a;**238**(4832):1419-23.

Cannell, MB, Berlin, JR, Lederer, WJ. Intracellular calcium in cardiac myocytes: calcium transients measured using fluorescence imaging. *Soc Gen Physiol Ser*. 1987b;**42**:201-14.

Cannell, MB and Thomas, MV. Intracellular ion measurement with fluorescent indicators. *In*: Ogden DC, editor. *Microelectrode Techniques: The Plymouth Workshop Handbook*. 2nd. ed: Company of Biologists; 1994.

Cannell, MB, Cheng, H, Lederer, WJ. Spatial non-uniformities in $[Ca^{2+}]_i$ during excitation-contraction coupling in cardiac myocytes. *Biophys J*. 1994;**67**(5):1942-56.

Cannell, MB, Cheng, H, Lederer, WJ. The control of calcium release in heart muscle. *Science*. 1995;**268**(5213):1045-9.

Cannell, MB and Soeller, C. Numerical analysis of ryanodine receptor activation by L-type channel activity in the cardiac muscle diad. *Biophys J*. 1997;**73**(1):112-22.

Cannell, MB, Crossman, DJ, Soeller, C. Effect of changes in action potential spike configuration, junctional sarcoplasmic reticulum micro-architecture and altered t-tubule structure in human heart failure. *J Muscle Res Cell Motil*. 2006;**27**(5-7):297-306.

Cannell, MB and Kong, CH. Local control in cardiac E-C coupling. *J Mol Cell Cardiol*. 2012;**52**(2):298-303.

Carl, S, Felix, K, Caswell, A, Brandt, N, Ball, W, Vaghy, P, *et al.* Immunolocalization of sarcolemmal dihydropyridine receptor and sarcoplasmic reticular triadin and ryanodine receptor in rabbit ventricle and atrium. *J Cell Biol*. 1995;**129**(3):673-82.

Cavalie, A, Ochi, R, Pelzer, D, Trautwein, W. Elementary currents through Ca^{2+} channels in guinea pig myocytes. *Pflügers Arch*. 1983;**398**(4):284-97.

Cavalié, A, Pelzer, D, Trautwein, W. Fast and slow gating behaviour of single calcium channels in cardiac cells. *Pflügers Arch*. 1986;**406**(3):241-58.

Chase, A, Colyer, J, Orchard, CH. Localised Ca channel phosphorylation modulates the distribution of L-type Ca current in cardiac myocytes. *J Mol Cell Cardiol*. 2010;**49**(1):121-31.

Chen-Izu, Y, McCulle, S, Ward, C, Soeller, C, Allen, B, Rabang, C, *et al.* Three-dimensional distribution of ryanodine receptor clusters in cardiac myocytes. *Biophys J*. 2006;**91**(1):1-13.

Chen, W, Steenbergen, C, Levy, L, Vance, J, London, R, Murphy, E. Measurement of free Ca in sarcoplasmic reticulum in perfused rabbit heart loaded with 1,2-Bis(2-amino-5,6-difluorophenoxy)ethane-N,N,Na',Na'-tetraacetic acid by $_{19}F$ NMR. *J Biol Chem*. 1996;**271**(13):7398-403.

Cheng, H, Lederer, WJ, Cannell, MB. Calcium sparks: elementary events underlying excitation-contraction coupling in heart muscle. *Science*. 1993;**262**(5134):740-4.

Cheng, H, Cannell, MB, Lederer, WJ. Propagation of excitation-contraction coupling into ventricular myocytes. *Pflügers Arch*. 1994;**428**(3):415-7.

Cheng, H, Cannell, MB, Lederer, WJ. Partial inhibition of Ca^{2+} current by methoxyverapamil (D600) reveals spatial nonuniformities in $[Ca^{2+}]_i$ during excitation-contraction coupling in cardiac myocytes. *Circ Res*. 1995;**76**(2):236-41.

Cheng, H, Lederer, MR, Lederer, WJ, Cannell, MB. Calcium sparks and $[Ca^{2+}]_i$ waves in cardiac myocytes. *Am J Physiol*. 1996;**270**(1 Pt 1):C148-59.

Cheng, H, Song, LS, Shirokova, N, González, A, Lakatta, EG, Ríos, E, *et al*. Amplitude distribution of calcium sparks in confocal images: theory and studies with an automatic detection method. *Biophys J*. 1999;**76**(2):606-17.

Cheng, H and Lederer, WJ. Calcium sparks. *Physiol Rev*. 2008;**88**(4):1491-545.

Cheung, JY, Tillotson, DL, Yelamarty, RV, Scaduto, RC. Cytosolic free calcium concentration in individual cardiac myocytes in primary culture. *Am J Physiol Cell Physiol*. 1989;**256**(6):C1120-30.

Ching, L, Williams, A, Sitsapesan, R. Evidence for Ca^{2+} activation and inactivation sites on the luminal side of the cardiac ryanodine receptor complex. *Circ Res*. 2000;**87**(3):201-6.

Chu, A, Fill, M, Stefani, E, Entman, ML. Cytoplasmic Ca^{2+} does not inhibit the cardiac muscle sarcoplasmic reticulum ryanodine receptor Ca^{2+} channel, although Ca^{2+}-induced Ca^{2+} inactivation of Ca^{2+} release is observed in native vesicles. *J Membr Biol*. 1993;**135**(1):49-59.

Cleemann, L and Morad, M. Role of Ca^{2+} channel in cardiac excitation-contraction coupling in the rat: evidence from Ca^{2+} transients and contraction. *J Physiol*. 1991;**432**(1):283-312.

Cleemann, L, Wang, W, Morad, M. Two-dimensional confocal images of organization, density, and gating of focal Ca^{2+} release sites in rat cardiac myocytes. *Proc Natl Acad Sci U S A*. 1998;**95**(18):10984-9.

Collier, M, Thomas, A, Berlin, J. Relationship between L-type Ca^{2+} current and unitary sarcoplasmic reticulum Ca^{2+} release events in rat ventricular myocytes. *J Physiol*. 1999;**516**(1):117-28.

Colquhoun, D and Hawkes, AG. The principles of the stochastic interpretation of ion-channel mechanisms. *In*: Sakmann B, Neher E, editors. *Single-Channel Recording*. 2nd ed: Plenum Press; 1983. p. 397-479.

Cooper, PJ, Soeller, C, Cannell, MB. Excitation-contraction coupling in human heart failure examined by action potential clamp in rat cardiac myocytes. *J Mol Cell Cardiol*. 2010;**49**(6):911-7.

Copello, JA, Barg, S, Onoue, H, Fleischer, S. Heterogeneity of Ca^{2+} gating of skeletal muscle and cardiac ryanodine receptors. *Biophys J*. 1997;**73**(1):141-56.

Crank, J. *The Mathematics of Diffusion*. 2nd ed.: Oxford University Press, Oxford; 1979.

Crespo, LM, Grantham, CJ, Cannell, MB. Kinetics, stoichiometry and role of the Na-Ca exchange mechanism in isolated cardiac myocytes. *Nature*. 1990;**345**(6276):618-21.

Crossman, DJ, Ruygrok, PN, Soeller, C, Cannell, MB. Changes in the organization of excitation-contraction coupling structures in failing human heart. *PLoS One*. 2011;**6**(3):e17901.

Curl, C, Bellair, C, Harris, T, Allman, B, Harris, P, Stewart, A, *et al*. Refractive index measurement in viable cells using quantitative phase-amplitude microscopy and confocal microscopy. *Cytometry Part A*. 2005;**65**(1):88-92.

Curtis, BM and Catterall, WA. Purification of the calcium antagonist receptor of the voltage-sensitive calcium channel from skeletal muscle transverse tubules. *Biochemistry (Mosc)*. 1984;**23**(10):2113-8.

Delbridge, LM, Bassani, JW, Bers, DM. Steady-state twitch Ca^{2+} fluxes and cytosolic Ca^{2+} buffering in rabbit ventricular myocytes. *Am J Physiol Cell Physiol*. 1996;**270**(1):C192-9.

DelPrincipe, F, Egger, M, Niggli, E. Calcium signalling in cardiac muscle: refractoriness revealed by coherent activation. *Nat Cell Biol*. 1999;**1**(6):323-9.

Denk, W. Two-photon scanning photochemical microscopy: mapping ligand-gated ion channel distributions. *Proc Natl Acad Sci U S A*. 1994;**91**(14):6629-33.

Diaz, ME, Trafford, AW, O'Neill, SC, Eisner, DA. A measurable reduction of S.R. Ca content follows spontaneous Ca release in rat ventricular myocytes. *Pflügers Archiv: Eur J Physiol*. 1997;**434**(6):852-4.

Díaz, ME, Trafford, AW, O'Neill, SC, Eisner, DA. Measurement of sarcoplasmic reticulum Ca^{2+} content and sarcolemmal Ca^{2+} fluxes in isolated rat ventricular myocytes during spontaneous Ca^{2+} release. *J Physiol*. 1997;**501 (Pt 1)**:3-16.

Ebashi, S. The Croonian lecture, 1979: regulation of muscle contraction. *Proc Roy Soc Lond B Biol Sci*. 1980;**207**(1168):259-86.

Eckert, R and Chad, JE. Inactivation of Ca channels. *Prog Biophys Mol Biol*. 1984;**44**(3):215-67.

Eisner, DA and Trafford, AW. What is the purpose of the large sarcolemmal calcium flux on each heartbeat? *Am J Physiol Heart Circ Physiol*. 2009;**297**(2):H493-4.

Ellis-Davies, G and Barsotti, R. Tuning caged calcium: photolabile analogues of EGTA with improved optical and chelation properties. *Cell Calcium*. 2006;**39**(1):75-83.

Ellis-Davies, GC, Kaplan, JH, Barsotti, RJ. Laser photolysis of caged calcium: rates of calcium release by nitrophenyl-EGTA and DM-nitrophen. *Biophys J*. 1996;**70**(2):1006-16.

Endo, M, Tanaka, M, Ogawa, Y. Calcium induced release of calcium from the sarcoplasmic reticulum of skinned skeletal muscle fibres. *Nature*. 1970;**228**(5266):34-6.

Engel, J, Fechner, M, Sowerby, AJ, Finch, SA, Stier, A. Anisotropic propagation of Ca^{2+} waves in isolated cardiomyocytes. *Biophys J*. 1994;**66**(6):1756-62.

Engelhardt, WA and Ljubimowa, MN. Myosine and adenosinetriphosphatase. *Nature*. 1939;**144**:668-9.

Erdös, T. Rigor, contracture and ATP. *Stud Inst Med Chem Univ Szeged*. 1943;**3**:51-6.

Evans, AM and Cannell, MB. The role of L-type Ca^{2+} current and Na^{+} current-stimulated Na/Ca exchange in triggering SR calcium release in guinea-pig cardiac ventricular myocytes. *Cardiovasc Res*. 1997;**35**(2):294-302.

Faas, GC, Karacs, K, Vergara, JL, Mody, I. Kinetic properties of DM-nitrophen binding to calcium and magnesium. *Biophys J*. 2005;**88**(6):4421-33.

Fabiato, A and Fabiato, F. Activation of skinned cardiac cells. Subcellular effects of cardioactive drugs. *Eur J Cardiol*. 1973;**1**(2):143-55.

Fabiato, A and Fabiato, F. Calcium release from the sarcoplasmic reticulum. *Circ Res*. 1977;**40**(2):119-29.

Fabiato, A. Calcium-induced release of calcium from the cardiac sarcoplasmic reticulum. *Am J Physiol*. 1983;**245**(1):C1-14.

Fabiato, A. Simulated calcium current can both cause calcium loading in and trigger calcium release from the sarcoplasmic reticulum of a skinned canine cardiac Purkinje cell. *J Gen Physiol*. 1985a;**85**(2):291-320.

Fabiato, A. Time and calcium dependence of activation and inactivation of calcium-induced release of calcium from the sarcoplasmic reticulum of a skinned canine cardiac Purkinje cell. *J Gen Physiol*. 1985b;**85**(2):247-89.

Fan, J-S and Palade, P. One calcium ion may suffice to open the tetrameric cardiac ryanodine receptor in rat ventricular myocytes. *J Physiol*. 1999;**516**(3):769-80.

Fanburg, B, Finkel, RM, Martonosi, A. The role of calcium in the mechanism of relaxation of cardiac muscle. *J Biol Chem*. 1964;**239**:2298-305.

Fawcett, DW and McNutt, NS. The ultrastructure of the cat myocardium. I. Ventricular papillary muscle. *J Cell Biol*. 1969;**42**(1):1-45.

Ferrier, GR and Howlett, SE. Cardiac excitation-contraction coupling: role of membrane potential in regulation of contraction. *Am J Physiol Heart Circ Physiol*. 2001;**280**(5):H1928-44.

Fill, M and Copello, JA. Ryanodine receptor calcium release channels. *Physiol Rev*. 2002;**82**(4):893-922.

Forbes, MS and Sperelakis, N. A labyrinthine structure formed from a transverse tubule of mouse ventricular myocardium. *J Cell Biol*. 1973;**56**(3):865-9.

Ford, LE and Podolsky, RJ. Regenerative calcium release within muscle cells. *Science*. 1970;**167**(914):58-9.

Franzini-Armstrong, C, Protasi, F, Ramesh, V. Comparative ultrastructure of Ca^{2+} release units in skeletal and cardiac muscle. *Ann N Y Acad Sci*. 1998;**853**:20-30.

Franzini-Armstrong, C, Protasi, F, Ramesh, V. Shape, size, and distribution of Ca^{2+} release units and couplons in skeletal and cardiac muscles. *Biophys J*. 1999;**77**(3):1528-39.

Franzini-Armstrong, C, Protasi, F, Tijskens, P. The assembly of calcium release units in cardiac muscle. *Ann N Y Acad Sci*. 2005;**1047**:76-85.

Gee, KR, Brown, KA, Chen, WNU, Bishop-Stewart, J, Gray, D, Johnson, I. Chemical and physiological characterization of fluo-4 Ca^{2+}-indicator dyes. *Cell Calcium*. 2000;**27**(2):97-106.

Ginsburg, K and Bers, D. Modulation of excitation–contraction coupling by isoproterenol in cardiomyocytes with controlled SR Ca^{2+} load and Ca^{2+} current trigger. *J Physiol*. 2004;**556**(2):463-80.

Goldhaber, JI, Lamp, ST, Walter, DO, Garfinkel, A, Fukumoto, GH, Weiss, JN. Local regulation of the threshold for calcium sparks in rat ventricular myocytes: role of sodium-calcium exchange. *J Physiol*. 1999;**520 Pt 2**:431-8.

Gomez, A, Schuster, I, Fauconnier, J, Prestle, J, Hasenfuss, G, Richard, S. FKBP12.6 overexpression decreases Ca^{2+} spark amplitude but enhances $[Ca^{2+}]_i$ transient in rat cardiac myocytes. *Am J Physiol Heart Circ Physiol*. 2004;**287**(5):H1987-93.

Gómez, AM, Cheng, H, Lederer, WJ, Bers, DM. Ca^{2+} diffusion and sarcoplasmic reticulum transport both contribute to $[Ca^{2+}]_i$ decline during Ca^{2+} sparks in rat ventricular myocytes. *J Physiol*. 1996;**496 (Pt 2)**:575-81.

Gómez, AM, Valdivia, HH, Cheng, H, Lederer, MR, Santana, LF, Cannell, MB, *et al.* Defective excitation-contraction coupling in experimental cardiac hypertrophy and heart failure. *Science*. 1997;**276**(5313):800-6.

Grantham, CJ and Cannell, MB. Ca^{2+} influx during the cardiac action potential in guinea pig ventricular myocytes. *Circ Res*. 1996;**79**(2):194-200.

Griffiths, H and MacLeod, KT. The voltage-sensitive release mechanism of excitation contraction coupling in rabbit cardiac muscle is explained by calcium-induced calcium release. *J Gen Physiol*. 2003;**121**(5):353-73.

Gu, Y, Gorelik, J, Spohr, HA, Shevchuk, A, Lab, MJ, Harding, SE, *et al.* High-resolution scanning patch-clamp: new insights into cell function. *FASEB J*. 2002;**16**(7):748-50.

Guia, A, Stern, M, Lakatta, E, Josephson, I. Ion concentration-dependence of rat cardiac unitary L-type calcium channel conductance. *Biophys J*. 2001;**80**(6):2742-50.

Gupta, RK, Gupta, P, Moore, RD. NMR studies of intracellular metal ions in intact cells and tissues. *Annu Rev Biophys Bioeng*. 1984;**13**(1):221-46.

Gyorke, I, Hester, N, Jones, LR, Gyorke, S. The role of calsequestrin, triadin, and junctin in conferring cardiac ryanodine receptor responsiveness to luminal calcium. *Biophys J*. 2004;**86**(4):2121-8.

Györke, I and Györke, S. Regulation of the cardiac ryanodine receptor channel by luminal Ca^{2+} involves luminal Ca^{2+} sensing sites. *Biophys J*. 1998;**75**(6):2801-10.

Gyorke, S and Fill, M. Ryanodine receptor adaptation: control mechanism of Ca^{2+}-induced Ca^{2+} release in heart. *Science*. 1993;**260**(5109):807-9.

Gyorke, S. Ca^{2+} spark termination: inactivation and adaptation may be manifestations of the same mechanism. *J Gen Physiol*. 1999;**114**(1):163-6.

Györke, S, Lukyanenko, V, Györke, I. Dual effects of tetracaine on spontaneous calcium release in rat ventricular myocytes. *J Physiol*. 1997;**500**(Pt 2):297-309.

Hadley, RW and Hume, JR. An intrinsic potential-dependent inactivation mechanism associated with calcium channels in guinea-pig myocytes. *J Physiol*. 1987;**389**(1):205-22.

Hamill, OP, Marty, A, Neher, E, Sakmann, B, Sigworth, FJ. Improved patch-clamp techniques for high-resolution current recording from cells and cell-free membrane patches. *Pflügers Arch*. 1981;**391**(2):85-100.

Han, S, Schiefer, A, Isenberg, G. Ca^{2+} load of guinea-pig ventricular myocytes determines efficacy of brief Ca^{2+} currents as trigger for Ca^{2+} release. *J Physiol*. 1994;**480**(Pt 3):411-21.

Hancox, JC and Levi, AJ. Calcium transients which accompany the activation of sodium current in rat ventricular myocytes at 37 degrees C: a trigger role for reverse Na-Ca exchange activated by membrane potential? *Pflügers Arch*. 1995;**430**(6):887-93.

Hasselbach, W. Structural and enzymatic properties of the calcium transporting membranes of the sarcoplasmic reticulum. *Ann N Y Acad Sci*. 1966;**137**(Biological Membranes: Recent Progress):1041-8.

Heilbrunn, LV and Wiercinski, FJ. The action of various cations on muscle protoplasm. *J Cell Physiol*. 1947;**29**(1):15-32.

Hess, P, Lansman, J, Tsien, R. Different modes of Ca channel gating behaviour favoured by dihydropyridine Ca agonists and antagonists. *Nature*. 1984;**311**(5986):538-44.

Hess, P and Tsien, R. Mechanism of ion permeation through calcium channels. *Nature*. 1984;**309**(5967):453-6.

Hill, AV. The abrupt transition from rest to activity in muscle. *Proc Roy Soc Lond B Biol Sci*. 1949;**136**(884):399-420.

Hille, B. *Ion Channels of Excitable Membranes*. 3rd ed.: Sinauer Associates; 2001.

Hobai, IA, Howarth, FC, Pabbathi, VK, Dalton, GR, Hancox, JC, Zhu, JQ, *et al.* "Voltage-activated Ca release" in rabbit, rat and guinea-pig cardiac myocytes, and modulation by internal cAMP. *Pflügers Arch*. 1997;**435**(1):164-73.

Hodgkin, AL, Huxley, AF, Katz, B. Measurement of current-voltage relations in the membrane of the giant axon of Loligo. *J Physiol*. 1952;**116**(4):424-48.

Hohl, C, Ansel, A, Altschuld, R, Brierley, GP. Contracture of isolated rat heart cells on anaerobic to aerobic transition. *Am J Physiol Heart Circ Physiol*. 1982;**242**(6):H1022-30.

Holroyde, MJ, Robertson, SP, Johnson, JD, Solaro, RJ, Potter, JD. The calcium and magnesium binding sites on cardiac troponin and their role in the regulation of myofibrillar adenosine triphosphatase. *J Biol Chem*. 1980;**255**(24):11688-93.

Hove-Madsen, L and Bers, DM. Sarcoplasmic reticulum Ca^{2+} uptake and thapsigargin sensitivity in permeabilized rabbit and rat ventricular myocytes. *Circ Res*. 1993;**73**(5):820-8.

Hubley, MJ, Locke, BR, Moerland, TS. The effects of temperature, pH, and magnesium on the diffusion coefficient of ATP in solutions of physiological ionic strength. *Biochim Biophys Acta*. 1996;**1291**(2):115-21.

Huxley, AF and Niedergerke, R. Measurement of the striations of isolated muscle fibres with the interference microscope. *J Physiol*. 1958;**144**(3):403-25.

Huxley, AF. The Croonian Lecture, 1967: The activation of striated muscle and its mechanical response. *Proc Roy Soc Lond B Biol Sci*. 1971;**178**(50):1-27.

Ibrahim, M, Gorelik, J, Yacoub, MH, Terracciano, CM. The structure and function of cardiac t-tubules in health and disease. *Proc Biol Sci*. 2011;**278**(1719):2714-23.

Ikemoto, N, Ronjat, M, Meszaros, LG, Koshita, M. Postulated role of calsequestrin in the regulation of calcium release from sarcoplasmic reticulum. *Biochemistry Moscow*. 1989;**28**(16):6764-71.

Imredy, JP and Yue, DT. Mechanism of Ca^{2+}-sensitive inactivation of L-type Ca^{2+} channels. *Neuron*. 1994;**12**(6):1301-18.

Inoue, M and Bridge, JHB. Ca^{2+} sparks in rabbit ventricular myocytes evoked by action potentials: involvement of clusters of L-type Ca^{2+} channels. *Circ Res*. 2003;**92**(5):532-8.

Inoue, M and Bridge, JH. Variability in couplon size in rabbit ventricular myocytes. *Biophys J*. 2005;**89**(5):3102-10.

Inui, M, Saito, A, Fleischer, S. Purification of the ryanodine receptor and identity with feet structures of junctional terminal cisternae of sarcoplasmic reticulum from fast skeletal muscle. *J Biol Chem*. 1987;**262**(4):1740-7.

Isenberg, G and Han, S. Gradation of Ca^{2+}-induced Ca^{2+} release by voltage-clamp pulse duration in potentiated guinea-pig ventricular myocytes. *J Physiol*. 1994;**480 (Pt 3)**:423-38.

Ishide, N, Urayama, T, Inoue, K, Komaru, T, Takishima, T. Propagation and collision characteristics of calcium waves in rat myocytes. *Am J Physiol*. 1990;**259**(3 Pt 2):H940-50.

Izu, L, Wier, G, Balke, W. Theoretical analysis of the Ca^{2+} spark amplitude distribution. *Biophys J*. 1998;**75**(3):1144-62.

Izu, L, Mauban, J, Balke, CW, Wier, G. Large currents generate cardiac Ca^{2+} sparks. *Biophys J*. 2001;**80**(1):88-102.

Jafri, MS, Rice, JJ, Winslow, RL. Cardiac Ca^{2+} dynamics: the roles of ryanodine receptor adaptation and sarcoplasmic reticulum load. *Biophys J*. 1998;**74**(3):1149-68.

Janczewski, AM, Spurgeon, HA, Stern, MD, Lakatta, EG. Effects of sarcoplasmic reticulum Ca^{2+} load on the gain function of Ca^{2+} release by Ca^{2+} current in cardiac cells. *Am J Physiol*. 1995;**268**(2 Pt 2):H916-20.

Jayasinghe, ID, Cannell, MB, Soeller, C. Organization of ryanodine receptors, transverse tubules, and sodium-calcium exchanger in rat myocytes. *Biophys J*. 2009;**97**(10):2664-73.

Jayasinghe, ID, Baddeley, D, Kong, CH, Wehrens, XH, Cannell, MB, Soeller, C. Nanoscale organization of junctophilin-2 and ryanodine receptors within peripheral Couplings of rat ventricular cardiomyocytes. *Biophys J*. 2012;**102**(5):L19-21.

Jewett, PH, Leonard, SD, Sommer, JR. Chicken cardiac muscle: its elusive extended junctional sarcoplasmic reticulum and sarcoplasmic reticulum fenestrations. *J Cell Biol*. 1973;**56**(2):595-600.

Jiang, D, Xiao, B, Yang, D, Wang, R, Choi, P, Zhang, L, *et al.* RyR2 mutations linked to ventricular tachycardia and sudden death reduce the threshold for store-overload-induced Ca^{2+} release (SOICR). *Proc Natl Acad Sci U S A*. 2004;**101**(35):13062-7.

Jones, LR, Suzuki, YJ, Wang, W, Kobayashi, YM, Ramesh, V, Franzini-Armstrong, C, *et al.* Regulation of Ca^{2+} signaling in transgenic mouse cardiac myocytes overexpressing calsequestrin. *J Clin Invest*. 1998;**101**(7):1385-93.

Jorgensen, AO and Campbell, KP. Evidence for the presence of calsequestrin in two structurally different regions of myocardial sarcoplasmic reticulum. *J Cell Biol*. 1984;**98**(4):1597-602.

Jorgensen, AO, Shen, AC, Campbell, KP. Ultrastructural localization of calsequestrin in adult rat atrial and ventricular muscle cells. *J Cell Biol*. 1985;**101**(1):257-68.

Jorgensen, AO, Shen, AC, Arnold, W, McPherson, PS, Campbell, KP. The Ca^{2+}-release channel/ryanodine receptor is localized in junctional and corbular sarcoplasmic reticulum in cardiac muscle. *J Cell Biol*. 1993;**120**(4):969-80.

Josephson, I, Guia, A, Lakatta, E, Stern, M. Modulation of the conductance of unitary cardiac L-type Ca^{2+} channels by conditioning voltage and divalent ions. *Biophys J*. 2002a;**83**(5):2587-94.

Josephson, I, Guia, A, Lakatta, E, Stern, M. Modulation of the gating of unitary cardiac L-type Ca^{2+} channels by conditioning voltage and divalent ions. *Biophys J*. 2002b;**83**(5):2575-86.

Josephson, I, Guia, A, Lakatta, E, Lederer, J, Stern, M. Ca^{2+}-dependent components of inactivation of unitary cardiac L-type Ca^{2+} channels. *J Physiol*. 2010a;**588**(Pt 1):213-23.

Josephson, I, Guia, A, Sobie, E, Lederer, J, Lakatta, E, Stern, M. Physiologic gating properties of unitary cardiac L-type Ca^{2+} channels. *Biochem Biophys Res Commun*. 2010b;**396**(3):763-6.

Junker, J, Sommer, JR, Sar, M, Meissner, G. Extended junctional sarcoplasmic reticulum of avian cardiac muscle contains functional ryanodine receptors. *J Biol Chem*. 1994;**269**(3):1627-34.

Kaftan, E, Marks, A, Ehrlich, B. Effects of rapamycin on ryanodine receptor/Ca^{2+}-release channels from cardiac muscle. *Circ Res*. 1996;**78**(6):990-7.

Kass, RS, Lederer, WJ, Tsien, RW, Weingart, R. Role of calcium ions in transient inward currents and aftercontractions induced by strophanthidin in cardiac Purkinje fibres. *J Physiol*. 1978;**281**(1):187-208.

Kawai, M, Hussain, M, Orchard, C. Excitation-contraction coupling in rat ventricular myocytes after formamide-induced detubulation. *Am J Physiol Heart Circ Physiol*. 1999;**277**(2):H603-9.

Kielley, WW and Meyerhof, O. Studies on adenosinetriphosphatase of muscle; a new magnesium-activated a denosinetriphosphatase. *J Biol Chem*. 1948;**176**(2):591-601.

Kim, N, Cannell, MB, Hunter, PJ. Changes in the calcium current among different transmural regions contributes to action potential heterogeneity in rat heart. *Prog Biophys Mol Biol*. 2010;**103**(1):28-34.

Knollmann, BC, Chopra, N, Hlaing, T, Akin, B, Yang, T, Ettensohn, K, *et al*. Casq2 deletion causes sarcoplasmic reticulum volume increase, premature Ca^{2+} release, and catecholaminergic polymorphic ventricular tachycardia. *J Clin Invest*. 2006;**116**(9):2510-20.

Kong, CHT, Soeller, C, Cannell, MB. Increasing sensitivity of Ca^{2+} spark detection in noisy images by application of a matched-filter object detection algorithm. *Biophys J*. 2008;**95**(12):6016-24.

Kong, CHT and Cannell, MB. Looking at the trigger for CICR during rat cardiac action potentials. *Biophys J*. 2010;**98**(3, Suppl 1):104a.

Lacerda, AE and Brown, AM. Nonmodal gating of cardiac calcium channels as revealed by dihydropyridines. *J Gen Physiol*. 1989;**93**(6):1243-73.

Lai, FA, Anderson, K, Rousseau, E, Liu, QY, Meissner, G. Evidence for a Ca^{2+} channel within the ryanodine receptor complex from cardiac sarcoplasmic reticulum. *Biochem Biophys Res Commun*. 1988;**151**(1):441-9.

Lamb, GD. Ryanodine receptor 'adaptation': a flash in the pan? *J Muscle Res Cell Motil*. 1997;**18**(6):611-6.

Lamb, GD, Laver, DR, Stephenson, DG. Questions about adaptation in ryanodine receptors. *J Gen Physiol*. 2000;**116**(6):883-90.

Langer, GA and Brady, AJ. Calcium flux in the mammalian ventricular myocardium. *J Gen Physiol*. 1963;**46**:703-19.

Langer, GA and Peskoff, A. Calcium concentration and movement in the diadic cleft space of the cardiac ventricular cell. *Biophys J*. 1996;**70**(3):1169-82.

Larbig, R, Torres, N, Bridge, JH, Goldhaber, JI, Philipson, KD. Activation of reverse Na^+-Ca^{2+} exchange by the Na^+ current augments the cardiac Ca^{2+} transient: evidence from NCX knockout mice. *J Physiol*. 2010;**588**(Pt 17):3267-76.

Larsson, HP, Picaud, SA, Werblin, FS, Lecar, H. Noise analysis of the glutamate-activated current in photoreceptors. *Biophys J*. 1996;**70**(2):733-42.

Lauven, M, Handrock, R, Müller, A, Hofmann, F, Herzig, S. Interaction of three structurally distinct Ca^{2+} channel activators with single L-type Ca^{2+} channels. *Naunyn Schmiedebergs Arch Pharmacol*. 1999;**360**(2):122-8.

Laver, D. Ca^{2+} stores regulate ryanodine receptor Ca^{2+} release channels via luminal and cytosolic Ca^{2+} sites. *Clin Exp Pharmacol Physiol*. 2007;**34**(9):889-96.

Laver, D and Honen, B. Luminal Mg^{2+}, a key factor controlling RYR2-mediated Ca^{2+} release: cytoplasmic and luminal regulation modeled in a tetrameric channel. *J Gen Physiol*. 2008;**132**(4):429-46.

Laver, D. Luminal Ca^{2+} activation of cardiac ryanodine receptors by luminal and cytoplasmic domains. *Eur Biophys J*. 2009;**39**(1):19-26.

Laver, D and van Helden, D. Three independent mechanisms contribute to tetracaine inhibition of cardiac calcium release channels. *J Mol Cell Cardiol*. 2011;**51**(3):357-69.

Laver, DR, Roden, LD, Ahern, GP, Eager, KR, Junankar, PR, Dulhunty, AF. Cytoplasmic Ca^{2+} inhibits the ryanodine receptor from cardiac muscle. *J Membr Biol*. 1995;**147**(1):7-22.

Leblanc, N and Hume, JR. Sodium current-induced release of calcium from cardiac sarcoplasmic reticulum. *Science*. 1990;**248**(4953):372-6.

Lederer, WJ and Tsien, RW. Transient inward current underlying arrhythmogenic effects of cardiotonic steroids in Purkinje fibres. *J Physiol*. 1976;**263**(2):73-100.

Lederer, WJ, Niggli, E, Hadley, RW. Sodium-calcium exchange in excitable cells: fuzzy space. *Science*. 1990;**248**(4953):283.

Lee, K, Akaike, N, Brown, A. The suction pipette method for internal perfusion and voltage clamp of small excitable cells. *J Neurosci Methods*. 1980;**2**(1):51-78.

Lee, KS and Tsien, RW. High selectivity of calcium channels in single dialysed heart cells of the guinea-pig. *J Physiol*. 1984;**354**:253-72.

Levi, AJ, Spitzer, KW, Kohmoto, O, Bridge, JH. Depolarization-induced Ca entry via Na-Ca exchange triggers SR release in guinea pig cardiac myocytes. *Am J Physiol*. 1994;**266**(4 Pt 2):H1422-33.

Lew, WY, Hryshko, LV, Bers, DM. Dihydropyridine receptors are primarily functional L-type calcium channels in rabbit ventricular myocytes. *Circ Res*. 1991;**69**(4):1139-45.

Lipp, P and Niggli, E. Microscopic spiral waves reveal positive feedback in subcellular calcium signaling. *Biophys J*. 1993;**65**(6):2272-6.

Lipp, P and Niggli, E. Sodium current-induced calcium signals in isolated guinea-pig ventricular myocytes. *J Physiol*. 1994;**474**(3):439-46.

Lipp, P and Niggli, E. Submicroscopic calcium signals as fundamental events of excitation-contraction coupling in guinea-pig cardiac myocytes. *J Physiol*. 1996;**492**(Pt 1):31-8.

Lipp, P and Niggli, E. Fundamental calcium release events revealed by two-photon excitation photolysis of caged calcium in guinea-pig cardiac myocytes. *J Physiol*. 1998;**508**(3):801-9.

Litwin, SE, Zhang, D, Bridge, JH. Dyssynchronous Ca^{2+} sparks in myocytes from infarcted hearts. *Circ Res*. 2000;**87**(11):1040-7.

Liu, Y, Porta, M, Qin, J, Ramos, J, Nani, A, Shannon, TR, *et al.* Flux regulation of cardiac ryanodine receptor channels. *J Gen Physiol*. 2010;**135**(1):15-27.

López-López, JR, Shacklock, PS, Balke, CW, Wier, WG. Local, stochastic release of Ca^{2+} in voltage-clamped rat heart cells: visualization with confocal microscopy. *J Physiol*. 1994;**480 (Pt 1)**:21-9.

López-López, JR, Shacklock, PS, Balke, CW, Wier, WG. Local calcium transients triggered by single L-type calcium channel currents in cardiac cells. *Science*. 1995;**268**(5213):1042-5.

Louch, WE, Bito, V, Heinzel, FR, Macianskiene, R, Vanhaecke, J, Flameng, W, *et al.* Reduced synchrony of Ca^{2+} release with loss of T-tubules-a comparison to Ca^{2+} release in human failing cardiomyocytes. *Cardiovasc Res*. 2004;**62**(1):63-73.

Loughrey, CM, Seidler, T, Miller, SLW, Prestle, J, Maceachern, KE, Reynolds, DF, *et al.* Over-expression of FK506-binding protein FKBP12.6 alters excitation-contraction coupling in adult rabbit cardiomyocytes. *J Physiol*. 2004;**556**(3):919-34.

Lukyanenko, V, Gyorke, I, Gyorke, S. Regulation of calcium release by calcium inside the sarcoplasmic reticulum in ventricular myocytes. *Pflügers Arch*. 1996;**432**(6):1047-54.

Lukyanenko, V, Wiesner, TF, Györke, S. Termination of Ca^{2+} release during Ca^{2+} sparks in rat ventricular myocytes. *J Physiol*. 1998;**507 (Pt 3)**:667-77.

Lukyanenko, V and Gyorke, S. Ca^{2+} sparks and Ca^{2+} waves in saponin-permeabilized rat ventricular myocytes. *J Physiol*. 1999;**521(Pt 3)**:575-85.

Lukyanenko, V, Viatchenko-Karpinski, S, Smirnov, A, Wiesner, TF, Györke, S. Dynamic regulation of sarcoplasmic reticulum Ca^{2+} content and release by luminal Ca^{2+}-sensitive leak in rat ventricular myocytes. *Biophys J*. 2001;**81**(2):785-98.

Maclennan, D. Purification and properties of an adenosine triphosphatase from sarcoplasmic reticulum. *J Biol Chem*. 1970;**245**(17):4508-18.

MacLennan, DH and Wong, PT. Isolation of a calcium-sequestering protein from sarcoplasmic reticulum. *Proc Natl Acad Sci U S A*. 1971;**68**(6):1231-5.

Maier, L, Ziolo, M, Bossuyt, J, Persechini, A, Mestril, R, Bers, D. Dynamic changes in free Ca-calmodulin levels in adult cardiac myocytes. *J Mol Cell Cardiol*. 2006;**41**(3):451-8.

Markwardt, CB. Non-linear Least-squares Fitting in IDL with MPFIT. *ASP Conf Ser*. 2009;**411**.

Marsh, BB. A factor modifying muscle fibre synaeresis. *Nature*. 1951;**167**(4261):1065-6.

Marx, S, Ondrias, K, Marks, A. Coupled gating between individual skeletal muscle Ca^{2+} release channels (ryanodine receptors). *Science*. 1998;**281**(5378):818-21.

Marx, SO, Gaburjakova, J, Gaburjakova, M, Henrikson, C, Ondrias, K, Marks, AR. Coupled gating between cardiac calcium release channels (ryanodine receptors). *Circ Res*. 2001;**88**(11):1151-8.

McDonald, T, Cavalié, A, Trautwein, W, Pelzer, D. Voltage-dependent properties of macroscopic and elementary calcium channel currents in guinea pig ventricular myocytes. *Pflügers Arch*. 1986;**406**(5):437-48.

McDonald, TF, Pelzer, S, Trautwein, W, Pelzer, DJ. Regulation and modulation of calcium channels in cardiac, skeletal, and smooth muscle cells. *Physiol Rev*. 1994;**74**(2):365-507.

Meissner, G and McKinley, D. Permeability of canine cardiac sarcoplasmic reticulum vesicles to K^+, Na^+, H^+, and Cl. *J Biol Chem*. 1982;**257**(13):7704-11.

Meissner, G and Henderson, JS. Rapid calcium release from cardiac sarcoplasmic reticulum vesicles is dependent on Ca^{2+} and is modulated by Mg^{2+}, adenine nucleotide, and calmodulin. *J Biol Chem*. 1987;**262**(7):3065-73.

Mejia-Alvarez, R, Kettlun, C, Rios, E, Stern, M, Fill, M. Unitary Ca^{2+} current through cardiac ryanodine receptor channels under quasi-physiological ionic conditions. *J Gen Physiol*. 1999;**113**(2):177-86.

Mines, GR. On functional analysis by the action of electrolytes. *J Physiol*. 1913;**46**(3):188-235.

Mitra, R and Morad, M. A uniform enzymatic method for dissociation of myocytes from hearts and stomachs of vertebrates. *Am J Physiol*. 1985;**249**(5 Pt 2):H1056-60.

Moré, J. The Levenberg-Marquardt algorithm: implementation and theory. *In*: Watson GA, editor. *Numerical Analysis: Proceedings of the Bienniel Conference Held at Dundee*. Berlin: Springer-Verlag; 1978. p. 199.

Murphy, RM, Mollica, JP, Beard, NA, Knollmann, BC, Lamb, GD. Quantification of calsequestrin 2 (CSQ2) in sheep cardiac muscle and Ca^{2+}-binding protein changes in CSQ2 knockout mice. *Am J Physiol Heart Circ Physiol*. 2011;**300**(2):H595-604.

Näbauer, M, Callewaert, G, Cleemann, L, Morad, M. Regulation of calcium release is gated by calcium current, not gating charge, in cardiac myocytes. *Science*. 1989;**244**(4906):800-3.

Navedo, M, Amberg, G, Nieves, M, Molkentin, J, Santana, L. Mechanisms underlying heterogeneous Ca^{2+} sparklet activity in arterial smooth muscle. *J Gen Physiol*. 2006;**127**(6):611-22.

Navedo, MF, Cheng, EP, Yuan, C, Votaw, S, Molkentin, JD, Scott, JD, *et al.* Increased coupled gating of L-type Ca^{2+} channels during hypertension and Timothy syndrome. *Circ Res*. 2010;**106**(4):748-56.

Neco, P, Rose, B, Huynh, N, Zhang, R, Bridge, JH, Philipson, KD, *et al.* Sodium-calcium exchange is essential for effective triggering of calcium release in mouse heart. *Biophys J*. 2010;**99**(3):755-64.

Niggli, E and Lederer, WJ. Voltage-independent calcium release in heart muscle. *Science*. 1990;**250**(4980):565-8.

Niggli, E. Localized intracellular calcium signaling in muscle: calcium sparks and calcium quarks. *Annu Rev Physiol*. 1999;**61**:311-35.

Nilius, B, Hess, P, Lansman, JB, Tsien, RW. A novel type of cardiac calcium channel in ventricular cells. *Nature*. 1985;**316**(6027):443-6.

Nowycky, MC, Fox, AP, Tsien, RW. Three types of neuronal calcium channel with different calcium agonist sensitivity. *Nature*. 1985;**316**(6027):440-3.

Ogata, T and Yamasaki, Y. High-resolution scanning electron microscopic studies on the three-dimensional structure of the transverse-axial tubular system, sarcoplasmic reticulum and intercalated disc of the rat myocardium. *Anat Rec*. 1990;**228**(3):277-87.

Overend, CL, Eisner, DA, O'Neill, SC. The effect of tetracaine on supontaneous Ca^{2+} release and sarcoplasmic reticulum calcium content in rat ventricular myocytes. *J Physiol*. 1997;**502**(3):471-9.

Page, E, McCallister, LP, Power, B. Stereological measurements of cardiac ultrastructures implicated in excitation-contraction coupling. *Proc Natl Acad Sci U S A*. 1971;**68**(7):1465-6.

Page, E and Surdyk-Droske, M. Distribution, surface density, and membrane area of diadic junctional contacts between plasma membrane and terminal cisterns in mammalian ventricle. *Circ Res*. 1979;**45**(2):260-7.

Pan, BS and Solaro, RJ. Calcium-binding properties of troponin C in detergent-skinned heart muscle fibers. *J Biol Chem*. 1987;**262**(16):7839-49.

Parker, I, Zang, WJ, Wier, WG. Ca^{2+} sparks involving multiple Ca^{2+} release sites along Z-lines in rat heart cells. *J Physiol*. 1996;**497 (Pt 1)**:31-8.

Peachey, L. The sarcoplasmic reticulum and transverse tubules of the frog's sartorius. *J Cell Biol*. 1965;**25**(3):209-31.

Piacentino, V, 3rd, Gaughan, JP, Houser, SR. L-type Ca^{2+} currents overlapping threshold Na^{+} currents: could they be responsible for the "slip-mode" phenomenon in cardiac myocytes? *Circ Res*. 2002;**90**(4):435-42.

Picht, E, Zima, AV, Shannon, TR, Duncan, AM, Blatter, LA, Bers, DM. Dynamic calcium movement inside cardiac sarcoplasmic reticulum during release. *Circ Res*. 2011;**108**(7):847-56.

Pietrobon, D and Hess, P. Novel mechanism of voltage-dependent gating in L-type calcium channels. *Nature*. 1990;**346**(6285):651-5.

Poláková, E, Zahradníková, Pavelková, J, Zahradník, I, Zahradníková, A. Local calcium release activation by DHPR calcium channel openings in rat cardiac myocytes. *J Physiol*. 2008;**586**(16):3839-54.

Porta, M, Zima, A, Nani, A, Diaz-Sylvester, P, Copello, J, Ramos-Franco, J, *et al.* Single ryanodine receptor channel Basis of caffeine's action on Ca^{2+} sparks. *Biophys J*. 2011;**100**(4):931-8.

Porter, K and Palade, G. Studies on the endoplasmic reticulum: III. Its form and distribution in striated muscle cells. *J Cell Biol*. 1957;**3**(2):269-300.

Post, JA and Langer, GA. Sarcolemmal calcium binding sites in heart: I. Molecular origin in "gas-dissected" sarcolemma. *J Membr Biol*. 1992;**129**(1):49-57.

Powell, T and Twist, VW. A rapid technique for the isolation and purification of adult cardiac muscle cells having respiratory control and a tolerance to calcium. *Biochem Biophys Res Commun*. 1976;**72**(1):327-33.

Pratusevich, VR and Balke, CW. Factors shaping the confocal image of the calcium spark in cardiac muscle cells. *Biophys J*. 1996;**71**(6):2942-57.

Press, W, Flannery, B, Teukolsky, S, Vetterling, W. *Numerical Recipes in Fortran 77: The Art of Scientific Computing, Second Edition*. Cambridge University Press; 1992.

Puglisi, J, Yuan, W, Bassani, J, Bers, DM. Ca^{2+} influx through Ca^{2+} channels in rabbit ventricular myocytes during action potential clamp: influence of temperature. *Circ Res*. 1999;**85**(6):e7-16.

Qin, J, Valle, G, Nani, A, Nori, A, Rizzi, N, Priori, SG, *et al.* Luminal Ca^{2+} regulation of single cardiac ryanodine receptors: insights provided by calsequestrin and its mutants. *J Gen Physiol*. 2008;**131**(4):325-34.

Quamme, G. Cytosolic free magnesium in cardiac myocytes: identification of a Mg^{2+} influx pathway. *Biochem Biophys Res Commun*. 1990;**167**(3):1406-12.

Radermacher, M, Rao, V, Grassucci, R, Frank, J, Timerman, AP, Fleischer, S, *et al.* Cryo-electron microscopy and three-dimensional reconstruction of the calcium release channel/ryanodine receptor from skeletal muscle. *J Cell Biol*. 1994;**127**(2):411-23.

Ramay, HR, Liu, OZ, Sobie, EA. Recovery of cardiac calcium release is controlled by sarcoplasmic reticulum refilling and ryanodine receptor sensitivity. *Cardiovasc Res*. 2011;**91**(4):598-605.

Rampe, D and Lacerda, AE. A new site for the activation of cardiac calcium channels defined by the nondihydropyridine FPL 64176. *J Pharmacol Exp Ther*. 1991;**259**(3):982-7.

Rardon, DP, Cefali, DC, Mitchell, RD, Seiler, SM, Jones, LR. High molecular weight proteins purified from cardiac junctional sarcoplasmic reticulum vesicles are ryanodine-sensitive calcium channels. *Circ Res*. 1989;**64**(4):779-89.

Reuter, H and Seitz, N. The dependence of calcium efflux from cardiac muscle on temperature and external ion composition. *J Physiol*. 1968;**195**(2):451-70.

Reuter, H and Scholz, H. A study of the ion selectivity and the kinetic properties of the calcium dependent slow inward current in mammalian cardiac muscle. *J Physiol*. 1977;**264**(1):17-47.

Reuter, H, Stevens, CF, Tsien, RW, Yellen, G. Properties of single calcium channels in cardiac cell culture. *Nature*. 1982;**297**(5866):501-4.

Ringer, S. A further contribution regarding the influence of the different constituents of the blood on the contraction of the heart. *J Physiol*. 1883;**4**(1):29-42.3.

Roberts, WM and Almers, W. Patch voltage clamping with low-resistance seals: Loose patch clamp. *Methods Enzymol*. 1992;**207**:155-76.

Rose, WC, Balke, CW, Wier, WG, Marban, E. Macroscopic and unitary properties of physiological ion flux through L-type Ca^{2+} channels in guinea-pig heart cells. *J Physiol*. 1992;**456**:267-84.

Rousseau, E, Smith, JS, Meissner, G. Ryanodine modifies conductance and gating behavior of single Ca^{2+} release channel. *Am J Physiol*. 1987;**253**(3 Pt 1):C364-8.

Sah, R, Ramirez, RJ, Kaprielian, R, Backx, PH. Alterations in action potential profile enhance excitation-contraction coupling in rat cardiac myocytes. *J Physiol*. 2001;**533**(Pt 1):201-14.

Sah, R, Ramirez, R, Backx, P. Modulation of Ca^{2+} release in cardiac myocytes by changes in repolarization rate: role of phase-1 action potential repolarization in excitation-contraction coupling. *Circ Res*. 2002;**90**(2):165-73.

Sandow, A. Excitation-contraction coupling in muscular response. *Yale J Biol Med*. 1952;**25**(3):176-201.

Santana, LF, Cheng, H, Gomez, AM, Cannell, MB, Lederer, WJ. Relation between the sarcolemmal Ca^{2+} current and Ca^{2+} sparks and local control theories for cardiac excitation-contraction coupling. *Circ Res*. 1996;**78**(1):166-71.

Santana, LF, Gomez, AM, Lederer, WJ. Ca^{2+} flux through promiscuous cardiac Na^{+} channels: Slip-mode conductance. *Science*. 1998;**279**(5353):1027-33.

Santiago, D, Curran, J, Bers, D, Lederer, WJ, Stern, M, Ríos, E, *et al.* Ca sparks do not explain all ryanodine receptor-mediated SR Ca leak in mouse ventricular myocytes. *Biophys J*. 2010;**98**(10):2111-20.

Saris, NEL and Carafoli, E. A historical review of cellular calcium handling, with emphasis on mitochondria. *Biochemistry Moscow*. 2005;**70**(2):187-94.

Sato, D and Bers, DM. How does stochastic ryanodine receptor-mediated Ca leak fail to initiate a Ca spark? *Biophys J*. 2011;**101**(10):2370-9.

Satoh, H, Blatter, LA, Bers, DM. Effects of $[Ca^{2+}]_i$, SR Ca^{2+} load, and rest on Ca^{2+} spark frequency in ventricular myocytes. *Am J Physiol*. 1997;**272**(2 Pt 2):H657-68.

Schiefer, A, Meissner, G, Isenberg, G. Ca^{2+} activation and Ca^{2+} inactivation of canine reconstituted cardiac sarcoplasmic reticulum Ca^{2+}-release channels. *J Physiol*. 1995;**489**(Pt 2):337-48.

Schuetze, SM. The discovery of the action potential. *Trends Neurosci*. 1983;**6**:164-8.

Scriven, D, Dan, P, Moore, E. Distribution of proteins implicated in excitation-contraction coupling in rat ventricular myocytes. *Biophys J*. 2000;**79**(5):2682-91.

Sedarat, F, Xu, L, Moore, E, Tibbits, G. Colocalization of dihydropyridine and ryanodine receptors in neonate rabbit heart using confocal microscopy. *Am J Physiol Heart Circ Physiol*. 2000;**279**(1):H202-9.

Sham, JS, Cleemann, L, Morad, M. Gating of the cardiac Ca^{2+} release channel: The role of Na^{+} current and Na^{+}-Ca^{2+} exchange. *Science*. 1992;**255**(5046):850-3.

Sham, JS, Cleemann, L, Morad, M. Functional coupling of Ca^{2+} channels and ryanodine receptors in cardiac myocytes. *Proc Natl Acad Sci U S A*. 1995a;**92**(1):121-5.

Sham, JS, Hatem, SN, Morad, M. Species differences in the activity of the Na^{+}-Ca^{2+} exchanger in mammalian cardiac myocytes. *J Physiol*. 1995b;**488 (Pt 3)**:623-31.

Sham, JS, Song, LS, Chen, Y, Deng, LH, Stern, MD, Lakatta, EG, *et al.* Termination of Ca^{2+} release by a local inactivation of ryanodine receptors in cardiac myocytes. *Proc Natl Acad Sci U S A*. 1998;**95**(25):15096-101.

Shannon, T. Assessment of intra-SR free [Ca] and buffering in rat heart. *Biophys J*. 1997;**73**(3):1524-31.

Shannon, T, Guo, T, Bers, DM. Ca^{2+} scraps: local depletions of free $[Ca^{2+}]$ in cardiac sarcoplasmic reticulum during contractions leave substantial Ca^{2+} reserve. *Circ Res*. 2003a;**93**(1):40-5.

Shannon, TR, Ginsburg, KS, Bers, DM. Potentiation of fractional sarcoplasmic reticulum calcium release by total and free intra-sarcoplasmic reticulum calcium concentration. *Biophys J*. 2000;**78**(1):334-43.

Shannon, TR, Ginsburg, KS, Bers, DM. Quantitative assessment of the SR Ca^{2+} leak-load relationship. *Circ Res*. 2002;**91**(7):594-600.

Shannon, TR, Pogwizd, SM, Bers, DM. Elevated sarcoplasmic reticulum Ca^{2+} leak in intact ventricular myocytes from rabbits in heart failure. *Circ Res*. 2003b;**93**(7):592-4.

Shen, JX, Wang, S, Song, LS, Han, T, Cheng, H. Polymorphism of Ca^{2+} sparks evoked from in-focus Ca^{2+} release units in cardiac myocytes. *Biophys J*. 2004;**86**(1 Pt 1):182-90.

Shirokova, N, González, A, Kirsch, WG, Ríos, E, Pizarro, G, Stern, MD, *et al.* Calcium sparks: release packets of uncertain origin and fundamental role. *J Gen Physiol*. 1999;**113**(3):377-84.

Shkryl, VM, Blatter, LA, Rios, E. Properties of Ca^{2+} sparks revealed by four-dimensional confocal imaging of cardiac muscle. *J Gen Physiol*. 2012;**139**(3):189-207.

Shorofsky, SR and January, CT. L- and T-type Ca^{2+} channels in canine cardiac Purkinje cells. Single- channel demonstration of L-type Ca^{2+} window current. *Circ Res*. 1992;**70**(3):456-64.

Sidell, BD and Hazel, JR. Temperature affects the diffusion of small molecules through cytosol of fish muscle. *J Exp Biol*. 1987;**129**:191-203.

Simmerman, HK and Jones, LR. Phospholamban: protein structure, mechanism of action, and role in cardiac function. *Physiol Rev*. 1998;**78**(4):921-47.

Sipido, KR and Wier, WG. Flux of Ca^{2+} across the sarcoplasmic reticulum of guinea-pig cardiac cells during excitation-contraction coupling. *J Physiol*. 1991;**435**(1):605-30.

Sipido, KR, Carmeliet, E, Pappano, A. Na^{+} current and Ca^{2+} release from the sarcoplasmic reticulum during action potentials in guinea-pig ventricular myocytes. *J Physiol*. 1995;**489 (Pt 1)**:1-17.

Sipido, KR. Efficiency of L-type Ca^{2+} current compared to reverse mode Na/Ca exchange or T-type Ca^{2+} current as trigger for Ca^{2+} release from the sarcoplasmic reticulum. *Ann N Y Acad Sci*. 1998;**853**:357-60.

Sipido, KR, Carmeliet, E, Van de Werf, F. T-type Ca^{2+} current as a trigger for Ca^{2+} release from the sarcoplasmic reticulum in guinea-pig ventricular myocytes. *J Physiol*. 1998;**508 (Pt 2)**:439-51.

Sitsapesan, R and Williams, AJ. Regulation of the gating of the sheep cardiac sarcoplasmic reticulum Ca^{2+}-release channel by luminal Ca^{2+}. *J Membr Biol*. 1994;**137**(3):215-26.

Sitsapesan, R, Montgomery, R, Williams, A. New insights into the gating mechanisms of cardiac ryanodine receptors revealed by rapid changes in ligand concentration. *Circ Res*. 1995;**77**(4):765-72.

Sitsapesan, R and Williams, AJ. Regulation of current flow through ryanodine receptors by luminal Ca^{2+}. *J Membr Biol*. 1997;**159**(3):179-85.

Sitsapesan, R and Williams, A. Do inactivation mechanisms rather than adaptation hold the key to understanding ryanodine receptor channel gating? *J Gen Physiol*. 2000;**116**(6):867-72.

Smith, GD, Keizer, JE, Stern, MD, Lederer, WJ, Cheng, H. A simple numerical model of calcium spark formation and detection in cardiac myocytes. *Biophys J*. 1998;**75**(1):15-32.

Sobie, E, Song, L-S, Lederer, WJ. Local recovery of Ca^{2+} release in rat ventricular myocytes. *J Physiol*. 2005;**565**(Pt 2):441-7.

Sobie, E and Ramay, H. Excitation-contraction coupling gain in ventricular myocytes: insights from a parsimonious model. *J Physiol*. 2009;**587**(6):1293-9.

Sobie, EA, Dilly, KW, dos Santos Cruz, J, Lederer, WJ, Jafri, MS. Termination of cardiac Ca^{2+} sparks: an investigative mathematical model of calcium-induced calcium release. *Biophys J*. 2002;**83**(1):59-78.

Sobie, EA, Guatimosim, S, Gómez-Viquez, L, Song, LS, Hartmann, H, Saleet Jafri, M, *et al*. The Ca^{2+} leak paradox and rogue ryanodine receptors: SR Ca^{2+} efflux theory and practice. *Prog Biophys Mol Biol*. 2006;**90**(1-3):172-85.

Sobie, EA, Cannell, MB, Bridge, JH. Allosteric activation of Na^{+}-Ca^{2+} exchange by L-type Ca^{2+} current augments the trigger flux for SR Ca^{2+} release in ventricular myocytes. *Biophys J*. 2008;**94**(7):L54-6.

Soeller, C and Cannell, MB. Numerical simulation of local calcium movements during L-type calcium channel gating in the cardiac diad. *Biophys J*. 1997;**73**(1):97-111.

Soeller, C and Cannell, MB. Two-photon microscopy: imaging in scattering samples and three-dimensionally resolved flash photolysis. *Microsc Res Tech*. 1999;**47**(3):182-95.

Soeller, C and Cannell, MB. Analysing cardiac excitation-contraction coupling with mathematical models of local control. *Prog Biophys Mol Biol*. 2004;**85**(2-3):141-62.

Soeller, C, Crossman, DJ, Gilbert, R, Cannell, MB. Analysis of ryanodine receptor clusters in rat and human cardiac myocytes. *Proc Natl Acad Sci U S A*. 2007:14958-63.

Somlyo, AV, Gonzalez-Serratos, HG, Shuman, H, McClellan, G, Somlyo, AP. Calcium release and ionic changes in the sarcoplasmic reticulum of tetanized muscle: an electron-probe study. *J Cell Biol*. 1981;**90**(3):577-94.

Sommer, JR and Waugh, RA. The ultrastructure of the mammalian cardiac muscle cell--with special emphasis on the tubular membrane systems. A review. *Am J Pathol*. 1976;**82**(1):192-232.

Song, LS, Stern, MD, Lakatta, EG, Cheng, H. Partial depletion of sarcoplasmic reticulum calcium does not prevent calcium sparks in rat ventricular myocytes. *J Physiol*. 1997;**505 (Pt 3)**:665-75.

Sorensen, BR and Shea, MA. Calcium binding decreases the stokes radius of calmodulin and mutants R74A, R90A, and R90G. *Biophys J*. 1996;**71**(6):3407-20.

Stern, M, Pizarro, G, Rios, E. Local control model of excitation-contraction coupling in skeletal muscle. *J Gen Physiol*. 1997;**110**(4):415-40.

Stern, MD. Buffering of calcium in the vicinity of a channel pore. *Cell calcium*. 1992a;**13**(3):183-92.

Stern, MD. Theory of excitation-contraction coupling in cardiac muscle. *Biophys J*. 1992b;**63**(2):497-517.

Stern, MD, Song, LS, Cheng, H, Sham, JS, Yang, HT, Boheler, KR, *et al.* Local control models of cardiac excitation-contraction coupling. A possible role for allosteric interactions between ryanodine receptors. *J Gen Physiol*. 1999;**113**(3):469-89.

Stern, MD and Cheng, H. Putting out the fire: What terminates calcium-induced calcium release in cardiac muscle? *Cell Calcium*. 2004;**35**(6):591-601.

Subramanian, S, Viatchenko-Karpinski, S, Lukyanenko, V, Györke, S, Wiesner, T. Underlying mechanisms of symmetric calcium wave propagation in rat ventricular myocytes. *Biophys J*. 2001;**80**(1):1-11.

Sun, X, Protasi, F, Takahashi, M, Takeshima, H, Ferguson, D, Franzini-Armstrong, C. Molecular architecture of membranes involved in excitation-contraction coupling of cardiac muscle. *J Cell Biol*. 1995;**129**(3):659-71.

Swietach, P, Spitzer, K, Vaughan-Jones, R. Ca^{2+}-mobility in the sarcoplasmic reticulum of ventricular myocytes is low. *Biophys J*. 2008;**95**(3):1412-27.

Szent-Gyorgi, A. The contraction of myosin threads. *Stud Inst Med Chem Univ Szeged*. 1942a;**1**:17-26.

Szent-Gyorgi, A. The reversibility of the contraction of myosin threads. *Stud Inst Med Chem Univ Szeged*. 1942b;**2**:25-6.

Tada, M and Toyofuku, T. Cardiac sarcoplasmic reticulum Ca^{2+}-ATPase. *In*: Terjung R, editor. *Comprehensive Physiology*: John Wiley & Sons, Inc.; 2011. p. 301-34.

Takamatsu, T and Wier, WG. Calcium waves in mammalian heart: quantification of origin, magnitude, waveform, and velocity. *FASEB J*. 1990;**4**(5):1519-25.

Takeda, Y, Tohse, N, Nakaya, H, Kanno, M. Voltage-dependence of Ca^{2+} agonist effect of YC-170 on cardiac L-type Ca^{2+} channels. *Br J Pharmacol*. 1995;**116**(3):2134-40.

Tan, W, Fu, C, Fu, C, Xie, W, Cheng, H. An anomalous subdiffusion model for calcium spark in cardiac myocytes. *Applied Physics Letters*. 2007;**91**(18):183901.

Tanaka, H, Sekine, T, Kawanishi, T, Nakamura, R, Shigenobu, K. Intrasarcomere [Ca^{2+}] gradients and their spatio-temporal relation to Ca^{2+} sparks in rat cardiomyocytes. *J Physiol*. 1998;**508**(1):145-52.

Ter Keurs, HE, Wakayama, Y, Miura, M, Stuyvers, BD, Boyden, PA, Landesberg, A. Spatial nonuniformity of contraction causes arrhythmogenic Ca^{2+} waves in rat cardiac muscle. *Ann N Y Acad Sci*. 2005;**1047**:345-65.

Terentyev, D, Viatchenko-Karpinski, S, Valdivia, H, Escobar, A, Gyorke, S. Luminal Ca^{2+} controls termination and refractory behavior of Ca^{2+}-induced Ca^{2+} release in cardiac myocytes. *Circ Res*. 2002;**91**(5):414-20.

Terentyev, D, Viatchenko-Karpinski, S, Györke, I, Volpe, P, Williams, S, Györke, S. Calsequestrin determines the functional size and stability of cardiac intracellular calcium stores: Mechanism for hereditary arrhythmia. *PNAS*. 2003;**100**(20):11759-64.

Torres, NS, Larbig, R, Rock, A, Goldhaber, JI, Bridge, JH. Na^{+} currents are required for efficient excitation-contraction coupling in rabbit ventricular myocytes: a possible contribution of neuronal Na^{+} channels. *J Physiol*. 2010;**588**(Pt 21):4249-60.

Trafford, AW and Eisner, DA. No role for a voltage sensitive release mechanism in cardiac muscle. *J Mol Cell Cardiol*. 2003;**35**(2):145-51.

Tripathy, A and Meissner, G. Sarcoplasmic reticulum lumenal Ca^{2+} has access to cytosolic activation and inactivation sites of skeletal muscle Ca^{2+} release channel. *Biophys J*. 1996;**70**(6):2600-15.

Tseng, GN. Calcium current restitution in mammalian ventricular myocytes is modulated by intracellular calcium. *Circ Res*. 1988;**63**(2):468-82.

Tsien, RW, Bean, BP, Hess, P, Lansman, JB, Nilius, B, Nowycky, MC. Mechanisms of calcium channel modulation by beta-adrenergic agents and dihydropyridine calcium agonists. *J Mol Cell Cardiol*. 1986;**18**(7):691-710.

Valdivia, HH, Kaplan, JH, Ellis-Davies, GC, Lederer, WJ. Rapid adaptation of cardiac ryanodine receptors: modulation by Mg^{2+} and phosphorylation. *Science*. 1995;**267**(5206):1997-2000.

Valent, I, Zahradnikova, A, Pavelkova, J, Zahradnik, I. Spatial and temporal Ca^{2+}, Mg^{2+}, and ATP^{2-} dynamics in cardiac dyads during calcium release. *Biochim Biophys Acta*. 2007;**1768**(1):155-66.

Vendelin, M and Birkedal, R. Anisotropic diffusion of fluorescently labeled ATP in rat cardiomyocytes determined by raster image correlation spectroscopy. *Am J Physiol Cell Physiol*. 2008;**295**(5):C1302-15.

Wagenknecht, T and Samsó, M. Three-dimensional reconstruction of ryanodine receptors. *Front Biosci*. 2002;**7**:d1464-74.

Wang, S-Q, Song, L-S, Lakatta, E, Cheng, H. Ca^{2+} signalling between single L-type Ca^{2+} channels and ryanodine receptors in heart cells. *Nature*. 2001;**410**(6828):592-6.

Wang, SQ, Stern, MD, Ríos, E, Cheng, H. The quantal nature of Ca^{2+} sparks and in situ operation of the ryanodine receptor array in cardiac cells. *Proc Natl Acad Sci U S A*. 2004;**101**(11):3979-84.

Wang, W, Cleemann, L, Jones, LR, Morad, M. Modulation of focal and global Ca^{2+} release in calsequestrin-overexpressing mouse cardiomyocytes. *J Physiol*. 2000;**524 Pt 2**:399-414.

Ward, M-L, Pope, A, Loiselle, D, Cannell, M. Reduced contraction strength with increased intracellular $[Ca^{2+}]$ in left ventricular trabeculae from failing rat hearts. *J Physiol*. 2003;**546**(Pt 2):537-50.

Weber, A. On the role of calcium in the activity of adenosine 5'-triphosphate hydrolysis by actomyosin. *J Biol Chem*. 1959;**234**:2764-9.

Wibo, M, Bravo, G, Godfraind, T. Postnatal maturation of excitation-contraction coupling in rat ventricle in relation to the subcellular localization and surface density of 1,4-dihydropyridine and ryanodine receptors. *Circ Res*. 1991;**68**(3):662-73.

Wier, WG, Cannell, MB, Berlin, JR, Marban, E, Lederer, WJ. Cellular and subcellular heterogeneity of $[Ca^{2+}]_i$ in single heart cells revealed by fura-2. *Science*. 1987;**235**(4786):325-8.

Wier, WG, Egan, TM, López-López, JR, Balke, CW. Local control of excitation-contraction coupling in rat heart cells. *J Physiol*. 1994;**474**(3):463-71.

Williams, A, West, D, Sitsapesan, R. Light at the end of the Ca^{2+}-release channel tunnel: structures and mechanisms involved in ion translocation in ryanodine receptor channels. *Q Rev Biophys*. 2001;**34**(01):61-104.

Woodruff, M, Sampath, AP, Matthews, H, Krasnoperova, NV, Lem, J, Fain, G. Measurement of cytoplasmic calcium concentration in the rods of wild-type and transducin knock-out mice. *The Journal of Physiology*. 2002;**542**(3):843-54.

Wu, X and Bers, DM. Sarcoplasmic reticulum and nuclear envelope are one highly interconnected Ca^{2+} store throughout cardiac myocyte. *Circ Res*. 2006;**99**(3):283-91.

Xie, W, Brochet, DX, Wei, S, Wang, X, Cheng, H. Deciphering ryanodine receptor array operation in cardiac myocytes. *J Gen Physiol*. 2010;**136**(2):129-33.

Xu, L, Mann, G, Meissner, G. Regulation of cardiac Ca^{2+} release channel (ryanodine receptor) by Ca^{2+}, H^{+}, Mg^{2+}, and adenine nucleotides under normal and simulated ischemic conditions. *Circ Res*. 1996;**79**(6):1100-9.

Xu, L and Meissner, G. Regulation of cardiac muscle Ca2+ release channel by sarcoplasmic reticulum lumenal Ca2+. *Biophys J*. 1998;**75**(5):2302-12.

Yasuda, R, Nimchinsky, E, Scheuss, V, Pologruto, T, Oertner, T, Sabatini, B, *et al.* Imaging calcium concentration dynamics in small neuronal compartments. *Sci STKE*. 2004;**2004**(219):pl5.

Yasui, K, Palade, P, Gyorke, S. Negative control mechanism with features of adaptation controls Ca^{2+} release in cardiac myocytes. *Biophys J*. 1994;**67**(1):457-60.

Yin, C and Lai, A. Intrinsic lattice formation by the ryanodine receptor calcium-release channel. *Nat Cell Biol*. 2000;**2**:669-71.

Yin, C, Han, H, Wei, R, Lai, F. Two-dimensional crystallization of the ryanodine receptor Ca release channel on lipid membranes. *J Struct Biol*. 2005;**149**(2):219-24.

Yuan, W, Ginsburg, KS, Bers, DM. Comparison of sarcolemmal calcium channel current in rabbit and rat ventricular myocytes. *J Physiol*. 1996;**493 (Pt 3)**:733-46.

Yue, DT, Herzig, S, Marban, E. Beta-adrenergic stimulation of calcium channels occurs by potentiation of high-activity gating modes. *Proc Natl Acad Sci U S A*. 1990;**87**(2):753-7.

Zahradníková, Poláková, E, Zahradník, I, Zahradníková, A. Kinetics of calcium spikes in rat cardiac myocytes. *J Physiol*. 2007;**578**(3):677-91.

Zahradnikova, A, Gaburjakova, M, Bridge, JH, Zahradnik, I. Challenging quantal calcium signaling in cardiac myocytes. *J Gen Physiol*. 2010;**136**(5):581-3.

Zahradníková, A, Zahradník, I, Györke, I, Györke, S. Rapid activation of the cardiac ryanodine receptor by submillisecond calcium stimuli. *J Gen Physiol*. 1999;**114**(6):787-98.

Zahradníková, A, Kubalová, Z, Pavelková, J, Györke, S, Zahradník, I. Activation of calcium release assessed by calcium release-induced inactivation of calcium current in rat cardiac myocytes. *Am J Physiol Cell Physiol*. 2004;**286**(2):C330-C41.

Zhang, L, Kelley, J, Schmeisser, G, Kobayashi, YM, Jones, LR. Complex formation between junctin, triadin, calsequestrin, and the ryanodine receptor. Proteins of the cardiac junctional sarcoplasmic reticulum membrane. *J Biol Chem*. 1997;**272**(37):23389-97.

Zhou, Y-Y, Cheng, H, Song, L-S, Wang, D, Lakatta, E, Xiao, R-P. Spontaneous beta 2-adrenergic signaling fails to modulate L-type Ca^{2+} current in mouse ventricular myocytes. *Mol Pharmacol*. 1999;**56**(3):485-93.

Zhou, Z and Bers, DM. Ca^{2+} influx via the L-type Ca^{2+} channel during tail current and above current reversal potential in ferret ventricular myocytes. *J Physiol*. 2000;**523**(1):57-66.

Zima, A, Picht, E, Bers, DM, Blatter, L. Partial inhibition of sarcoplasmic reticulum Ca release evokes long-lasting Ca release events in ventricular myocytes: Role of luminal Ca in termination of Ca release. *Biophys J*. 2008a;**94**(5):1867-79.

Zima, AV, Picht, E, Bers, DM, Blatter, LA. Termination of cardiac Ca^{2+} sparks: Role of intra-SR [Ca^{2+}], release flux, and intra-SR Ca^{2+} diffusion. *Circ Res*. 2008b;**103**(8):e110-e5.

Zima, AV, Bovo, E, Bers, DM, Blatter, LA. Ca^{2+} spark-dependent and -independent sarcoplasmic reticulum Ca^{2+} leak in normal and failing rabbit ventricular myocytes. *J Physiol*. 2010;**588**(Pt 23):4743-57.

Zucker, RS. The calcium concentration clamp: spikes and reversible pulses using the photolabile chelator DM-nitrophen. *Cell Calcium*. 1993;**14**(2):87-100.